Author:
Meredith-Smith, Aimee

Title:
The effect of galvanic interactions between sulphide mineral pairs during seafloor mining and the environmental impact.

The effect of galvanic interactions between sulphide mineral pairs during seafloor mining and the environmental impact.

By Aimee Meredith-Smith

A dissertation submitted to the University of Bristol in accordance with the requirements for award of the degree of Masters by Research in the Faculty of Earth Sciences May 2021.

Word Count: 25 696

Abstract

Seafloor massive sulphide (SMS) mining is becoming an attractive solution to meet increasing demands for metal commodities, necessitating further research on the effects of mining on hydrothermal environments and ecosystems. This thesis is focused on material generated through SMS extraction, processing and return waste to the seafloor, specifically accelerated dissolution through galvanic interactions between sulphide mineral pairs. Galvanic cell formation is investigated by comparing sulphide mixtures, mechanical and naturally intergrown contacts.

Monomineralic and polymineralic sulphide oxidative dissolution semi batch experiments were run with artificial seawater, to assess the effect of mineral pairs on metal leachate using ICP-OES. Experiments were conducted with stock sulphides and SMS, 18-25°C, pH ~8.1, air equilibrated; representative of processing at ocean surface and/or return waste. 50°C experiments were representative of return waste deposited near active vents.

Surface area and temperature were dominant controls on dissolution. Increases in metal leachate in polymineralic experiments, attributed to galvanic interactions, were observed. Most significant stock-sulphide pairings were: pyrite-galena, with a ~10% increase in Pb and pyrite-chalcopyrite-sulphide-mix, with a ~33% increase in Cu; pyrite being cathodically protected in both. Logatchev polymineralic (chalcopyrite-secondary-Cu-sulphide) saw sustained Cu and the absence of Fe leaching, with ~75% and ~63% reductions in Zn and Ni when compared to monomineralic Logatchev (chalcopyrite). 50°C experiments saw higher metal leachate than 18-25°C experiments, ~6-84x and ~2-4x for Fe and Pb respectively. Cu, Zn and Pb were identified as major toxicants released from sulphide pairs in this study. Cu and Zn were higher in natural SMS experiments, resulting in much higher concentrations than guidelines recommend for seawater systems (AZMECC/ARMCANZ, 2000), ~7.4x104x higher for Cu in the extreme case.

Accelerated metal leaching through galvanic cells could pose a threat to vent species through metal toxicity, worsening where mine waste settles near active vents. Natural vent samples were found to be more representative of leachate concentrations in these environments, favouring the use of natural samples when assessing the environmental impact of SMS mining.

Acknowledgements

I would like to thank my supervisors Emily and Richard for their constant help and support throughout this project. Thank you both for believing in me to take on this project and building my confidence in making my own decisions when it comes to conducting experiments and research. Especially thank you Emily for trusting me with all your samples and showing me the ways around all the many labs! Richard, thank you for looking out for me throughout all the COVID lockdowns and working so hard to get me back in the labs.

I would like to say a huge thank you to Adam McAleer, firstly for allowing me to take up so much space in your lab and getting me back in so soon with all the new COVID safety guidelines; but also for all the time you dedicated to teaching me the necessary lab skills to conduct my experiments and allowing me to bombard the ICP-OES torch with so much sodium!

Finally, I am so thankful for my family and friends, my parents Carole and Phil for supporting me through university and always encouraging me to take on new challenges; but also my friends, Ellie, Hugh, Kati and Cindy for all the laughs and much needed distractions over the last 2 years.

COVID-19 Impact Statement

National lockdowns for the COVID-19 pandemic, beginning in early 2020, put a restriction on laboratory access for the experimental portion of this Master's project. Approximately 3 months of laboratory time was lost to the first national lockdown that was unable to be made up, resulting in there not being enough time to complete repeat experiments for this study. Reduced access to laboratory's from July-August meant that experiment runs had to be prioritised and ICP-OES analyses rushed to be completed. Furthermore, it put major time restrictions on the sample preparation portion of this Masters, especially for sample grain picking. EMPA and XRD analyses were unable to be carried out for certain samples due to lack of access and time constraints. Later national lockdowns further impacted access to the University buildings, preventing post-experiment sample EMPA analyses for samples: sphalerite-1 and chalcopyrite.

Overall time lost to national lockdowns and access restrictions thereafter has greatly impacted this Master's thesis, both in reducing the experimental portion of the project that had been planned for and in the analyses of material.

Author Declaration

I declare that the work in this dissertation was carried out in accordance with the requirements of the University's Regulations and Code of Practice for Research Degree Programmes and that it has not been submitted for any other academic award. Except where indicated by specific reference in the text, the work is the candidate's own work. Work done in collaboration with, or with the assistance of, others, is indicated as such. Any views expressed in the dissertation are those of the author.

SIGNED: *A. Meredith-Smith* DATE: 24th May 2021

Table of Contents

List of Figures

List of Tables

1.0 Introduction

1.1 Background

Seafloor massive sulphide (SMS) deposits are hydrothermal ore grade features which form as metal sulphides precipitate and accumulate over time on the seafloor and the sub-seafloor, sometimes resulting in the famous smoker chimneys (Herzig, 1999; Boschen *et al.*, 2013). SMS deposits generally form in association with oceanic plate divergence, precipitating out from hydrothermal fluids that are related to magmatic systems. This can create massive sulphides on the seafloor and/or networks of stock-work and replacement sulphides in the sub-seafloor (Herzig, 1999; Boschen *et al.*, 2013). SMS deposits are characterised by high proportions of base metals and sulphide, making them a potential mineral resource and as a result, have attracted interest from mining companies for a number of decades (Boschen *et al.*, 2013).

Emerging economies such as China, Brazil, and India have increasing demands for commodities e.g. Cu, Ni, Pb, etc. to support their growth. This coupled with the movement towards a greener future, is resulting in the global demand for metals to rise (*Standard Definitions*, 2012; Petersen *et al.*, 2016). This global requirement is also predicted to increase in correlation with population growth over the next few decades (Petersen *et al.*, 2016). As terrestrial mineral resources are becoming increasingly expensive and difficult to discover/mine, seafloor mining is becoming a feasible option when it comes to meeting global demands (Beaulieu *et al.*, 2017). The technology required for SMS exploration and mining will largely be adapted from offshore gas and petroleum industries, and this could provide an opportunity for mining companies to transfer current impact assessments and apply these to environmental hazards associated with these new mining techniques (Birney *et al.*, 2008). SMS deposits are often very high grade (e.g. Cu, Zn, Au and Ag) with concentration in a smaller volume than their alternative counterparts, such as terrestrial resources and manganese nodules, and as a result, their mining footprint is also comparatively reduced (Beaulieu *et al*., 2017).

As societal and political demands push towards a low-carbon future, renewable energy resources are expected to overtake their non-renewable counterparts (Vidal *et al*., 2013). The unintended consequence of this will be a rise in the demand for raw materials required for renewable energy facilities such as solar, wind and battery technology (Vidal *et al*., 2013). The world wide fund for nature (WWF) has predicted an annual increase of 5-18% in global production for ferrous, base and minor metals, if solar and wind energy is to increase to 25000 TWh by 2050: with ~$40x10^6$ tonnes of copper needed to build these facilities (Vidal *et al*., 2013). Although, SMS mining is not always seen as a commercial viable option currently, it may eventually become a necessity in the face of a greener future, given the high grades of base metals such as Fe, Cu, Zn, and Pb (Hoagland *et al.*, 2010; Vidal *et al*., 2013).

Global interest in deep-sea mining for both SMS deposits, ferromanganese crusts and polymetallic nodules is already gaining momentum, with companies from China, UK, Belgium, Germany, France and Japan all being awarded exploration contracts for these resources (Miller *et al*,. 2018). Furthermore, many governments and countries across the world have been granted exploration contracts for polymetallic sulphides, according to the International Seabed Authority (*Isa.org.jm*,. 2019). Up to 2019, contracts had been granted to Poland, India, Germany, France, Korea, Russia and China (*Isa.org.jm.*, 2019).

1.1.2 The Nature of SMS Deposits:

SMS deposits are concentrated along tectonic plate margins including mid ocean spreading ridges, back-arc basins, and submarine volcanic arcs, Figure 1 (Hannington *et al*., 2015). In 2005 <5% of these environments had been explored, with <25 identified sites of hydrothermal seafloor activity with associated mineralisation (Herzig and Hannington, 1995). By 2015, there were >500 identified sites, with a median tonnage of sulphide minerals at 50,000-100,000 tonnes (Hannington *et al*., 2015). The number of identified sites will grow with continued exploration; with total tonnage of sulphides predicted to be within the order of $600x10^6$ tonnes, and total metals ~$30x10^6$ tonnes. These estimates are competitive with terrestrial Cenozoic volcanic-hosted SMS deposits (Hannington *et al*., 2015). These statistics highlight the huge economic potential of SMS mining, future work will undoubtedly include further exploration of the seafloor, and the identification of new SMS deposits (NOAA, 2017).

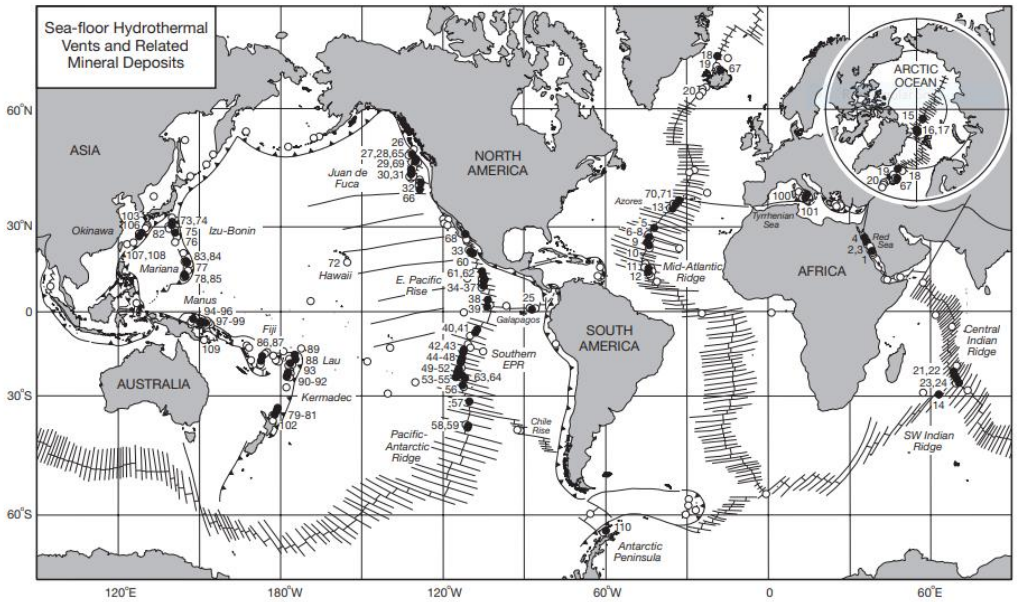

Figure 1*:* Locations of identified hydrothermal vents and associated mineral deposits; Infilled circles represent high-temperature hydrothermal vents and polymetallic sulphide deposits, whilst open circles represent low-temperature hydrothermal vents, including Fe-Mn crusts and metalliferous sediments (Hannington et al., 2005).

SMS deposit formation was first discussed in 1979 in relation to the 'black smokers' on the East Pacific Rise (see review in Romano, 2012). SMS deposits form as cool seawater seeps down into oceanic crust through cracks and fissures in areas of crustal divergence or rifting to meet hot magmatic systems. In these 'sub-volcanic' systems, seawater is heated by a nearby magma source, becoming more acidic and dissolving a variety of elements as it percolates through and reacts with the oceanic crust. This hydrothermal fluid can reach temperatures in excess of 400 °C, being transported back up through the crust via convective circulation cells, until it is re-introduced back out into cold seawater (see Herzig *et al*., 2002). Here, temperature differences between hydrothermal fluids and seawater force dissolved elements to quickly precipitate out as fine grained particulate (black smokers), depositing sulphide minerals rich in base metals across the seafloor (Figure 2).

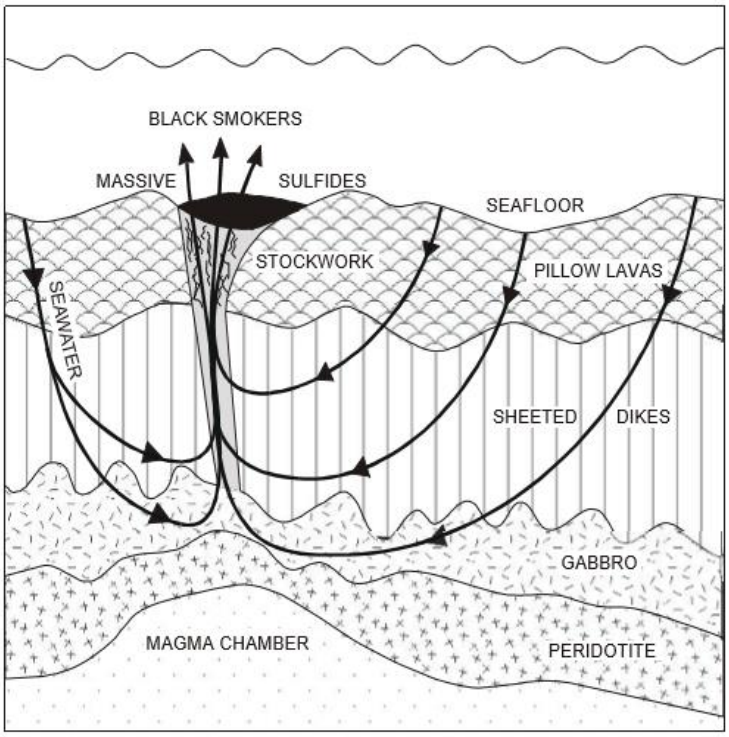

Figure 2: Fluid pathways taken as seawater seeps down from the seafloor, entering through pillow lavas and dyke networks. Hydrothermal fluids are heated by a magma source and elements dissolve in from the reacting crust. Hydrothermal fluids then percolate back up, precipitating out sulphide minerals containing high proportions of base metals as massive sulphides in black smoker vents (Herzig et al., 2002).

Metal sulphide minerals commonly formed in this process include: pyrite, marcasite, chalcopyrite, galena and sphalerite. White smokers are often found in association with black smokers, forming at cooler temperatures and away from the main venting; minerals such as barite, calcite and silica can be precipitated (Fallon, 2018). As hydrothermal systems evolve, the inactive vents become oxidised with time, forming a cap or crust known as a gossan which may still be of commercial value (Edwards, 2004; Fallon *et al.*, 2018).

The geochemistry of SMS deposits is highly variable both regionally and locally (Petersen and Hein, 2013). Variations arise from changes in host rock composition, changes in the input of magmatic volatiles and metals in hydrothermal circulation cells. However, tectonic setting and related lithology appears to be the biggest control on the subsequent geochemistry of SMS deposits (Figures 3 and 4).

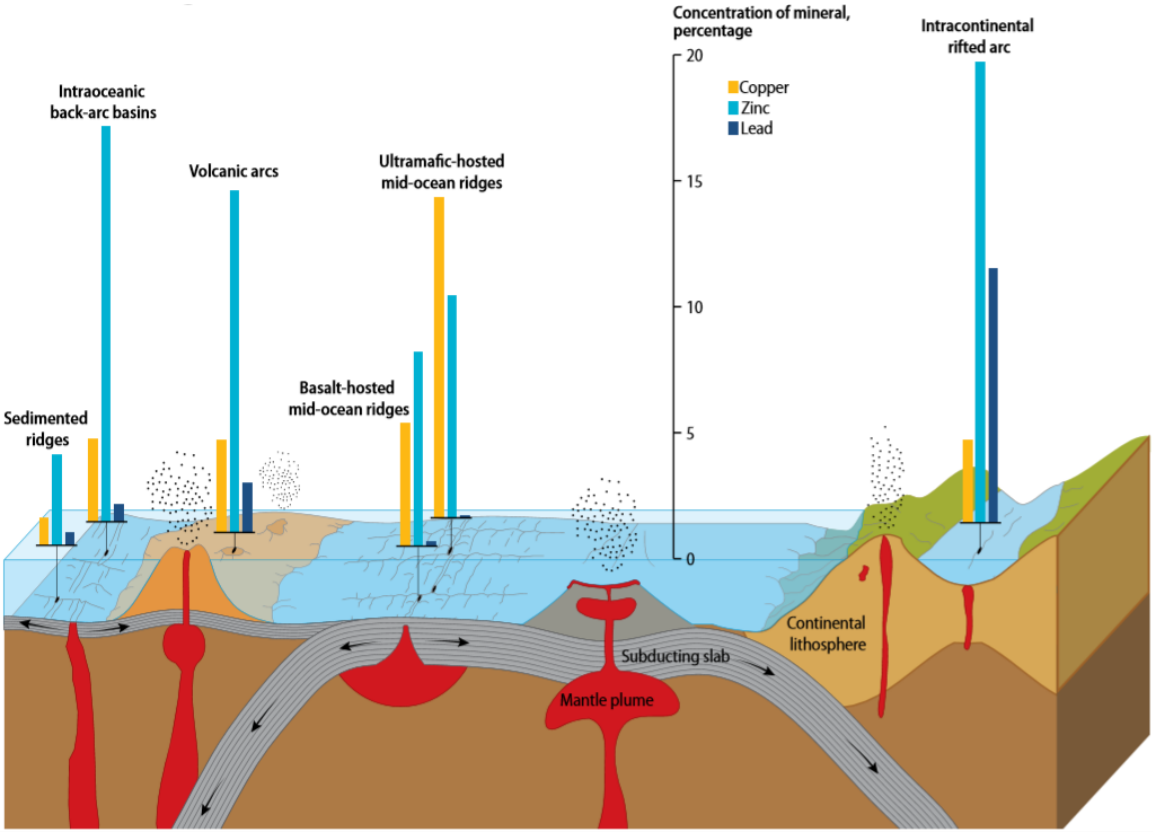

Figure 3: Displays the variation in SMS deposit geochemistry (%) across different tectonic settings; Ultramafic-hosted mid ocean ridges hold the highest concentration of copper (Cu) out of the different settings, with Intra-continental rifted arcs displaying the highest concentration of both lead (Pb) and zinc (Zn). Both volcanic arcs and intra oceanic back-arc basins exhibit higher concentrations of lead and zinc than mid-ocean ridges (Petersen and Hein, 2013).

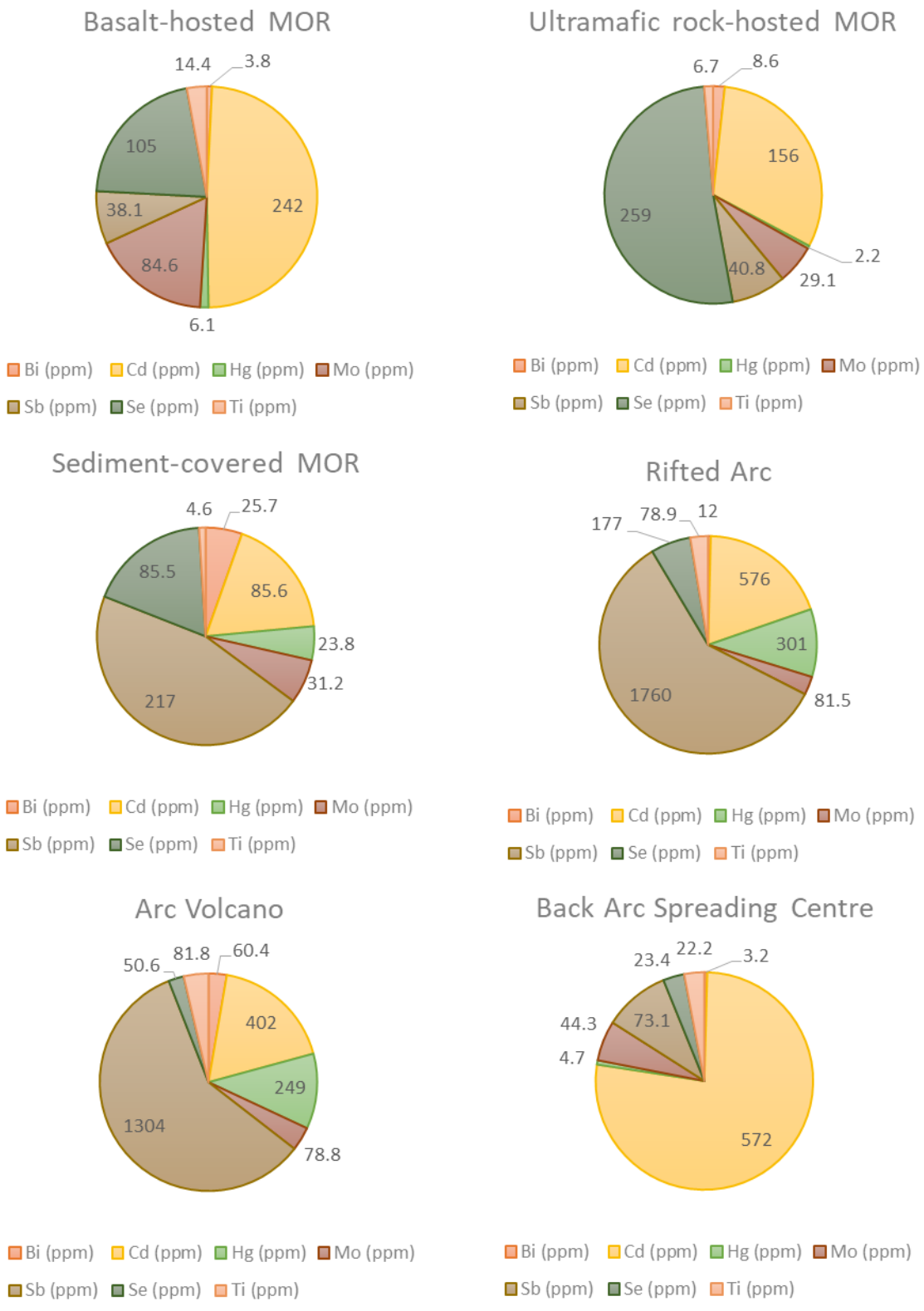

Figure 4: Pie charts displaying the average concentration (ppm) of various minor elements found in SMS samples across different tectonic settings. The data shows that host rocks at mid ocean ridges (MOR) have a strong control on the geochemistry of SMS formed. Generally MOR contain higher concentrations of selenium and molybdenum. However, sediment-covered MOR have antimony concentrations more similar to that of rifted arcs and volcano arcs. The geochemistry of back arc spreading centres has the highest cadmium concentration, making up >3/4 of its geochemistry. Data used from Monecke et al. (2016).

1.1.3 The Mining Process and Impact

Regulations specifically for SMS mining are not yet in place, however marine scientific research has 'high seas freedom' status, and for continental shelf only requires prior consent from adjacent coastal states that controls its own exclusive economic zone (EEZ) (Hoagland *et al.*, 2010). For more distant locations such as most spreading ridges The International Seabed Authority regulates exploration contracts (*Isa.org.jm,.* 2019).

Nautilus Minerals is the only company so far that has proposed a mining process; 'the code for environmental management of marine mining', released in 2000 outlines principles and operating guidelines for responsible and sustainable seafloor mining (Hoagland *et al.*, 2010). Nautilus Minerals is the first company to attempt recovery of high grade polymetallic SMS deposits within the Papua New Guinea EEZ, with the Solwara 1 project taking place at 1600m depth of the Bismarck Sea, New Ireland Province (Gwyther, 2008). Although Nautilus Minerals identifies potential hazards and proposes mitigation strategies within their own mining process, there are still many important environmental considerations that remain grey areas in both the mining process and current literature. These unknowns may potentially have negative consequences to seafloor ecosystems if not identified and addressed, highlighting the need for increased exploration and research.

Numerous potential environmental hazards are thought to be associated with the physical process of SMS mining, as presented in Figure 5. Potential hazards are thought to arise throughout the mining procedure from the SMS extraction itself, to the proposed mining equipment/machinery. As discussed by Weaver *et al*. (2018) , there are concerns for how seafloor habitats will be impacted in the extraction process of mining, with removal of crusts predicted to cause severe destruction of habitat for attached epifauna. Sediment laden plumes produced through mining are likely to negatively impact seabed animals via smothering, with the extent of spread being dependent on both the mining process and local currents. Recovery times for both these hazards is estimated to be slow, taking tens to hundreds of years (Weaver *et al*., 2018). Marine mammals could experience masking effects from the mining, and therefore change their migration routes, as low frequency noise from mining machinery could travel >600 Km, with the strongest impacts being felt <15 Km (Weaver *et al*., 2018). Recovery from some of these effects is thought to be immediate after mining is completed, but the effects to mammal migration paths in the long term is unknown (Weaver *et al*., 2018).

As well as the physical environmental hazards of SMS mining, there are also numerous geochemical risks related to sulphide oxidation, such as the release of toxic metals into the water column (Gwyther, 2008). eochemical hazards may arise through different mining practices including, the dewatering of ore rock and return waters; accidental spillage of ore material during transportation to the surface; extraction of ore at the seafloor; and through plume formations (Gwyther, 2008). Dewatering is a mining practice with potential to release metal toxicants into the water column for 100-1000s of Km,

as highlighted in Figure 6 (Hauton *et al.*, 2017). Fuchida *et al.* (2017), look at metal contamination that could be released through accidental spillage of hydrothermal ore particulates from mining vessels. Fine particulate matter of mined material, different chemical compositions found in hydrothermal ores, and the rapid release of ore leachates in accidental spills, all have the potential to damage primary production in surface waters (Fuchida *et al.*, 2017).

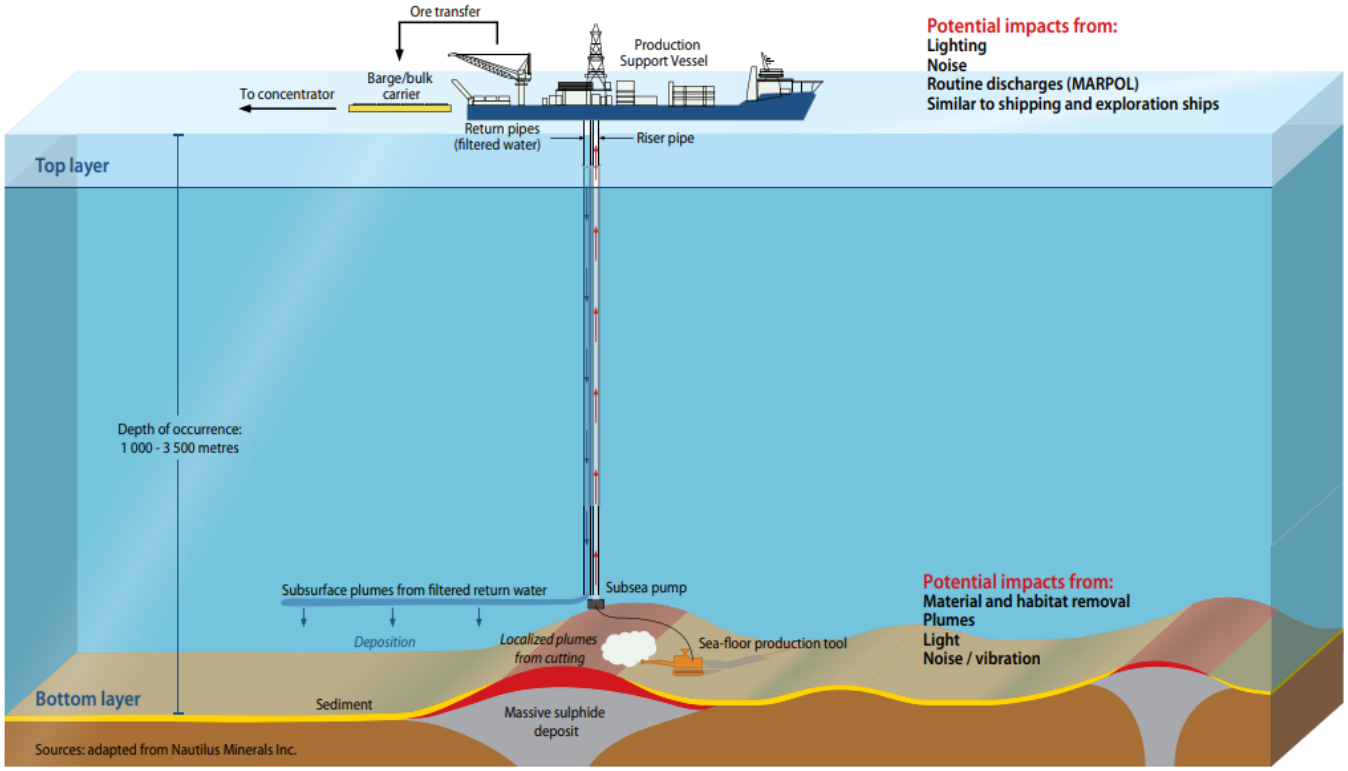

Figure 5: Highlights the different environmental hazards associated with each step in proposed plans for SMS mining (Weaver *et al.*, 2018).

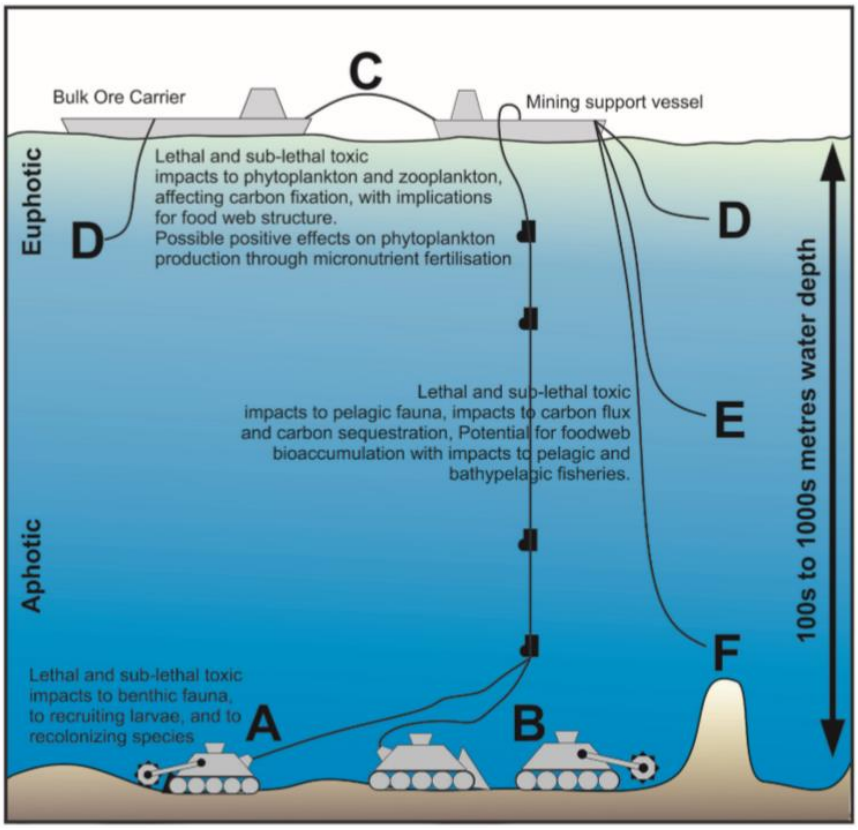

Figure 6: Schematic diagram illustrating the different stages which have potential to release heavy metals into the water column (both in solution and particulate phases), during deep sea mining practices; A – metals released in localised plumes from mining collectors; B – individually controlled mining tools; C – dewatering ore slurry at support vessel; D/E – mid-water discharge; F – discharge near seabed. (Hauton *et al*., 2017)

1.2 Anthropogenically Enhanced Oxidation of SMS Deposits

Geochemical hazards such as those listed previously in Fuchida *et al*. (2017), need to be considered further. These hazards include the enhanced oxidative dissolution of sulphide minerals through SMS mining and the associated release of toxic metals; the effect metal contamination may have on local ecosystems; as well as the effects of local acid generation (Gwyther, 2008; Bilenker *et al*., 2016; Fuchida *et al.,* 2017).

The release of heavy metals (and metalloids such as arsenic) through sulphide leaching, is particularly important as these elements accumulate in ecosystems, reducing productivity (Fuchida *et al.,* 2017). There is particular concern for the effect of toxic metals if they get transferred to coastal communities, including coral reefs, pelagic organisms, as well as the ubiquitous open sea fisheries which could lead to consumption by humans (Luick, 2012).

Oxidative dissolution of sulphide minerals occurs naturally on the seafloor, at active and inactive hydrothermal vents, due to chemical interaction between sulphide minerals and seawater (Fallon *et al*., 2018). The weathering of SMS deposits releases sulphate, soluble at low temperatures, and dissolved metals (Edwards, 2004). Leached metals such as Fe often produce insoluble oxy-hydroxide minerals, such as ferrihydrite, goethite and haematite, accumulating as crusts or caps on the surfaces of sulphide deposits, known as gossans on the seafloor (Edwards, 2004; Fallon *et al.,* 2018). However, some Fe and a whole host of metals can remain soluble in seawater at trace levels (Fallon *et al.,* 2018).

In terrestrial settings, oxidative dissolution of sulphide minerals brings about acid rock drainage (ARD). In these scenarios, exposed surfaces of sulphide ores react with moist air or oxygenated waters and oxidise rapidly (Akcil and Koldas, 2006; Bilenker *et al*., 2016). The process arises when sulphides interact with oxygenated surface waters during and/or after terrestrial mining activities, causing sulphide minerals to oxidise and release sulphur oxyanions and protons (Bilenker, 2011; Ridley *et al*., 2012; Romano, 2012). Sulphuric acid is a by-product of this reaction, and causes heavy metals to become more soluble in solution; minerals such as pyrrhotite, chalcopyrite, and pyrite are especially susceptible (Bilenker, 2011; Ridley *et al*., 2012; Romano, 2012). As these systems are often not well buffered and solutions are relatively confined, acidity can drastically increase and toxic elements can build up dramatically (Bilenker *et al*., 2016). Equations 1 and 2, demonstrate this process in pyrite dissolution, demonstrating how a continued decrease in pH can promote further sulphide dissolution, exacerbating the problem (Fallon *et al.,* 2018).

$$FeS_2 + 3.5O_2(aq) + H_2O \rightarrow Fe^{2+} + 2SO_4^{2-} + 2H^+ \quad (1)$$

$$FeS_2 + 14Fe^{3+} + 8H_2O \rightarrow 15Fe^{2+} + 2SO_4^{2-} + 16H^+ \quad (2)$$

The equivalent of terrestrial ARD is not expected to be observed in seafloor environments, as large-scale reductions in pH from sulphide oxidation processes will be buffered by the large volume of the ocean (Fallon *et al.*, 2018). Although low pH conditions may persist locally in pore waters and fractures, it is not considered to be as much of a threat as its terrestrial counterparts (Fallon *et al.*, 2018). However, the leaching of base metals, is of major concern when it comes to SMS leaching (Gwyther, 2008; Fallon *et al.*, 2018). The extent of toxicity risk that base metals pose to seafloor organisms remains unknown, as well as the degree in which SMS mining may increase the leaching of base metals.

SMS mining may anthropogenically enhance sulphide oxidative dissolution and therefore increase the leaching of base metals, as well as producing scenarios that are more susceptible to acid generation (Bilenker *et al*., 2016).

1.2.2 Variability of Mineral Dissolution Rates

Numerous studies have investigated various aspects of oxidative dissolution rates of different sulphide minerals in seawater (Morse, 1991; Edwards *et al.*, 2003a; Bilenker and McKibben, 2011; Romano, 2012; Fuchida *et al.*, 2018) and these have been reviewed by Fallon (2018). A summary is provided in Table 1 (1.1-1.4), and a representation of these data (as amended by Fallon, 2018) are plotted in Figure 7. This emphasises the high variability between dissolution rates of sulphide minerals in seawater, showing both temperature and grain size to be important controls. Studies by Bilenker (2011) and Romano (2012) are comparable due to similar grain sizes and temperatures being used in experiments runs. The results from these studies indicate that pyrrhotite oxidises at a significantly faster rate in seawater than chalcopyrite. Both Edwards *et al.* (2003) and Feely (1987) studies conduct their experiments at different grain sizes/temperatures, but their results show a similar pattern again in individual sulphide minerals oxidation rates. Both studies are in agreement with each other, showing sulphide minerals oxidising in order of slowest to fastest as follows: chalcopyrite < pyrite < sphalerite < marcasite.

Table 1.1: Calculated oxidation rates from various seawater dissolution studies Morse 1991; Edwards et al., 2003; Bilenker, 2011; Romano, 2012; Fuchida et al., 2018, using a range of different variables including, grainsize, pH, temperature, PO_2, pressure, and salinity. At pressure 1 bar (220 bars in Feely, 1987).

Mineral	Study	Field/Lab	Method	Salinity (‰)	pH	Temperature (°C)	O_2 (atm)	Grain Size (μm)	Oxidation Rate		Error
									mol/kg/sec	cm/sec	
Pyrrhotite	**Romano (2012)**	Lab	Solution analysis of Fe	~35	3.15	19.5	0.995	45-106	$3.7436x10^{-10}$	$6.6876x10^{-12}$	
Pyrrhotite		Lab	Solution analysis of Fe	~35	3.15	20.0	0.995	45-106	$4.7612x10^{-10}$	$8.5054x10^{-12}$	
Pyrrhotite		Lab	Solution analysis of Fe	~35	3.09	34.0	0.995	106-150	$6.7612x10^{-10}$	$4.3555x10^{-11}$	
Pyrrhotite		Lab	Solution analysis of Fe	~35	3.10	35.0	0.995	106-150	$5.5955x10^{-10}$	$3.6045x10^{-11}$	
Pyrrhotite		Lab	Solution analysis of Fe	~35	2.97	21.0	0.995	106-150	$2.0045x10^{-10}$	$9.3433x10^{-12}$	
Pyrrhotite		Lab	Solution analysis of Fe	~35	2.98	22.0	0.995	106-150	$2.5028x10^{-10}$	$9.0991x10^{-12}$	
Pyrrhotite		Lab	Solution analysis of Fe	~35	2.96	13.0	0.995	106-150	$1.4504x10^{-10}$	$7.6709x10^{-12}$	
Pyrrhotite		Lab	Solution analysis of Fe	~35	3.04	4.0	0.995	106-150	$1.4125x10^{-10}$	$1.2913x10^{-11}$	
Pyrrhotite		Lab	Solution analysis of Fe	~35	3.08	4.0	0.995	106-150	$1.1908x10^{-10}$	$1.6122x10^{-11}$	
Pyrrhotite		Lab	Solution analysis of Fe	~35	2.98	21.0	0.100	106-150	$1.9472x10^{-10}$	$8.9298x10^{-12}$	
Pyrrhotite		Lab	Solution analysis of Fe	~35	3.00	22.5	0.100	106-150	$1.6898x10^{-10}$	$9.6763x10^{-12}$	
Pyrrhotite		Lab	Solution analysis of Fe	~35	3.00	21.0	0.100	106-150	$6.7875x10^{-10}$	$1.2544x10^{-11}$	
Pyrrhotite		Lab	Solution analysis of Fe	~35	3.50	23.0	0.100	106-150	$4.6451x10^{-10}$	$1.0886x10^{-11}$	
Pyrrhotite		Lab	Solution analysis of Fe	~35	3.90	22.0	0.995	106-150	$1.3862x10^{-10}$	$4.3724x10^{-12}$	
Pyrrhotite		Lab	Solution analysis of Fe	~35	1.97	22.0	0.995	106-150	$1.5021x10^{-10}$	$2.9923x10^{-12}$	

Table 1.2: Calculated oxidation rates from various seawater dissolution studies Morse, 1991; Edwards et al., 2003; Bilenker, 2011; Romano, 2012; Fuchida et al., 2018, using a range of different variables including, grainsize, pH, temperature, PO_2, pressure, and salinity. At pressure 1 bar (220 bars in Feely, 1987).

Mineral	Study	Field/Lab	Method	Salinity (‰)	pH	Temperature (°C)	O_2 (atm)	Grain Size (μm)	Oxidation Rate		Error
									mol/kg/sec	cm/sec	
Chalcopyrite	**Bilenker (2011)**	Lab	Solution analysis of Cu	~35	3.00	9.5	0.995	45-106	3.3E-12		
Chalcopyrite		Lab	Solution analysis of Cu	~35	3.00	9.0	0.995	45-106	1.8E-12		
Chalcopyrite		Lab	Solution analysis of Cu	~35	3.00	8.5	0.995	45-106	1.44E-12		
Chalcopyrite		Lab	Solution analysis of Cu	~35	3.10	21.0	0.100	45-106	1.87E-13		
Chalcopyrite		Lab	Solution analysis of Cu	~35	3.00	21.0	0.100	45-106	4.9E-12		
Chalcopyrite		Lab	Solution analysis of Cu	~35	3.20	21.5	0.995	45-106	1.74E-12		
Chalcopyrite		Lab	Solution analysis of Cu	~35	4.50	22.0	0.995	45-106	1.11E-12		
Chalcopyrite		Lab	Solution analysis of Cu	~35	4.00	22.5	0.995	45-106	4.77E-13		
Chalcopyrite		Lab	Solution analysis of Cu	~35	8.20	23.5	0.100	45-106	-7.47E-13		
Chalcopyrite		Lab	Solution analysis of Cu	~35	8.20	23.5	0.100	45-106	-3.65E-14		
Chalcopyrite		Lab	Solution analysis of Cu	~35	2.20	21.0	0.995	45-106	5.55E-12		
Chalcopyrite		Lab	Solution analysis of Cu	~35	2.20	22.0	0.995	45-106	4.6E-12		
Chalcopyrite		Lab	Solution analysis of Cu	~35	2.20	22.0	0.995	45-106	5.12E-12		
Chalcopyrite		Lab	Solution analysis of Cu	~35	2.70	23.0	0.995	45-106	2.87E-12		

Table 1.3: Calculated oxidation rates from various seawater dissolution studies Morse, 1991; Edwards et al., 2003; Bilenker, 2011; Romano, 2012; Fuchida et al., 2018, using a range of different variables including, grainsize, pH, temperature, PO_2, pressure, and salinity. At pressure 1 bar (220 bars in Feely, 1987).

Mineral	Study	Field/Lab	Method	Salinity (‰)	pH	Temperature (°C)	O_2 (atm)	Grain Size (μm)	Oxidation Rate		Error
									mol/kg/sec	cm/sec	
Chalcopyrite	**Bilenker (2011)**	Lab	Solution analysis of Cu	~35	3.00	23.5	0.995	45-106	2.68E-12		
Chalcopyrite		Lab	Solution analysis of Cu	~35	4.10	23.0	0.995	45-106	-1.04E-09		
Chalcopyrite	**Feely (1987)**	Field	Sulphide mass change over time	~35	7.5	1.8	n/a	1000-3000		1.20E-12	
Pyrite		Field	Sulphide mass change over time	~35	7.5	1.8	n/a	1000-3000		5.30E-12	
Pyrite		Field	Sulphide mass change over time	~35	7.5	1.8	n/a	1000-3000		1.10E-11	
Sphalerite		Field	Sulphide mass change over time	~35	7.5	1.8	n/a	1000-3000		2.40E-11	
Marcasite		Field	Sulphide mass change over time	~35	7.5	1.8	n/a	1000-3000		5.10E-11	
Pyrrhotite		Field	Sulphide mass change over time	~35	7.5	1.8	n/a	1000-3000		1.10E-10	
Marcasite		Lab	Fe solution analysis	n/a	7.5	25	1.000	20-53		2.50E-10	1.00E-10
Pyrite		Lab	Fe solution analysis	n/a	7.5	25	1.000	20-53		6.70E-11	2.90E-11
Pyrite; Galveston Bay Texas	**Morse (1991)**	Lab	Pyrite solution analysis	10	7.5-8.4	22	n/a	<62		6.3203E-09	
Pyrite; Galveston Bay Texas		Lab	Pyrite solution analysis	10	7.5-8.4	22	n/a	<62		9.4805E-09	

Table 1.4: Calculated oxidation rates from various seawater dissolution studies Morse, 1991; Edwards et al., 2003; Bilenker, 2011; Romano, 2012; Fuchida et al., 2018, using a range of different variables including, grainsize, pH, temperature, PO_2, pressure, and salinity. At pressure 1 bar (220 bars in Feely, 1987).

Mineral	Study	Field/Lab	Method	Salinity (‰)	pH	Temperature (°C)	O_2 (atm)	Grain Size (µm)	Oxidation Rate		Error
									mol/kg/sec	cm/sec	
Pyrite; Galveston Bay Texas	**Morse (1991)**	Lab	Pyrite solution analysis	10	7.5-8.4	22	n/a	<62		1.8961E-09	
Pyrite; Texas Shelf		Lab	Pyrite solution analysis	34	7.5-8.4	22	n/a	<62		1.5801E-10	
Pyrite	**Edwards et al. (2003)**	Field	FISH analysis/Fe solution analysis	n/a	7.5	~4	n/a	10000-20000		2.12E-11	
Marcasite		Field	FISH analysis/Fe solution analysis	n/a	7.5	~4	n/a	10000		1.72E-10	
Chalcopyrite		Field	FISH analysis/Fe solution analysis	n/a	7.5	~4	n/a	250-500		1.46E-11	
Sphalerite		Field	FISH analysis/Fe solution analysis	n/a	7.5	~4	n/a	500-1000		1.13E-10	
Elemental Sulphur		Field	FISH analysis/Fe solution analysis	n/a	7.5	~4	n/a	125-500		1.24E-12	

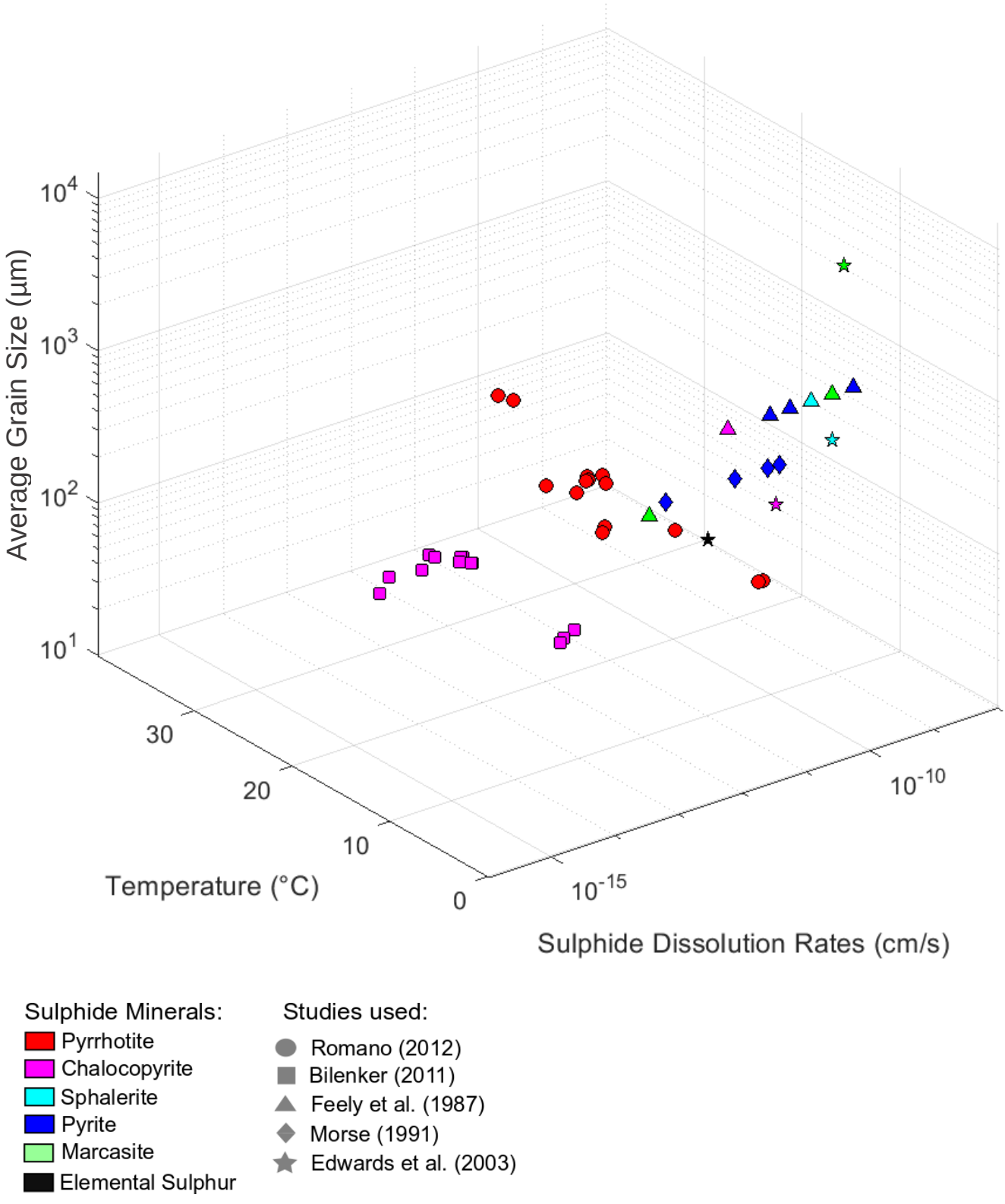

Figure 7: Dissolution rates (cm/s) of different sulphide minerals from a collection of different sulphide dissolution studies against both temperature (°C) and average grainsize (cm) (calculated from grainsize ranges provided in studies). The wide variety of dissolution rates can be observed across different studies, with the dissolution rates of different sulphide minerals showing a clear trend. Temperature and grainsize have an effect of sulphide dissolution rates, behaving as further controls. Unit conversions and rate calculations were provided by Fallon, 2018 and calculated from the referenced studies.

2.0 Current Literature

2.1 Controls on Sulphide Dissolution

2.1.1 Previous Studies on Sulphide Oxidative Weathering

Early studies on the dissolution of sulphide minerals at vent sites (as summarised in Figure 7) looked at natural sulphide oxidation, and vent particulate evolution through field and laboratory based studies. Feely (1987) results conclude that dissolution rates of minerals range >3 orders of magnitude, from $3.2x10^{-8}$ cm s^{-1} for sulphates such as anhydrite to $1.2x10^{-12}$ cm s^{-1} for chalcopyrite, not deliberating on what variables affect dissolution rates.

In a review by Chandra and Gerson (2010), studies of sulphide oxidation in aqueous (non-seawater) solutions, indicate that solution pH, Eh, oxidant, concentration, particle grain size, and surface area are all major factors in determining the rates of sulphide dissolution. Stressing that Eh of solution and surface area are the most influential factors effecting dissolution rates, referencing electrochemical properties of pyrite making it particularly susceptible to oxidative dissolution. Other studies contradict this, observing that pyrite is cathodically protected when in contact with other sulphides due to its high rest potential (Attia and El-Zeky, 1990). Sulphides minerals in contact with pyrite with lower resting potentials (chalcopyrite, galena, and sphalerite), are preferentially oxidised due to galvanic interactions (Attia and El-Zeky, 1990). This will be discussed further in Section 2.2 and forms the main focus for the experiments of this thesis. There have been numerous studies investigating individual sulphide minerals in seawater oxidation experiments, they are helpful in attempts to predict sulphide weathering behavior on the seafloor, especially if accelerated by SMS mining (Bilenker, 2011; Ridley, Shanks and Thurston, 2012; Romano, 2012).

Romano (2012), conducted synthetic seawater oxidation experiements with pyrrhotite grains crushed and sieved to 106-150 µm or 45-106 µm, keeping the system continously mixed. Dissolved Fe (mol/kg) increased steadily over 8 hours, and pH did not show estimated decreases, but instead slightly increased (Romano, 2012). Romano (2012) acknowledges SMS mining processes such as slurried sediment transport may create situations that accelerate sulphide oxidation and therefore local acidifcation. Steady increases in dissolved Fe over time highlights how pyrrhotite oxidation leaches soluble-Fe and mining practices may encourage further leaching of soluble metals from other sulphide minerals (Romano, 2012).

Bilenker *et al*. (2016), agree with Romano (2012) and determine through predicting maximum acid generation rate calculations, that acid production through in-situ SMS mining cannot exceed the buffering capacity of the ocean, and therefore will not result in large-scale reductions in pH. However, consider the possibility for SMS mining techniques to create scenarios that are much more susceptible to rapid acid generation, and may temporarily exceed the buffer capacity of the ocean (Bilenker *et al*., 2016). They also calculate residence times for crushed sulphides in seawater, "shrinking sphere

model", and determine mining waste, dependent on the grain size, could potentially persist on the seafloor for a number of years (Bilenker *et al*., 2016).

Fallon (2018) investigated sulphide mineral oxidative dissolution in high and low pressure seawater studies, using grain sizes of 2.5 μm and 45-50 μm. Low pressure experiments follow a semi-batch experiment design, at 1 atm pressure, 12°C, and 2g/L rock:fluid ratios. High pressure experiments follow a full batch experiment design, at 300 bar pressure, ~4°C and 6.35g/L rock:fluid ratio. Low pressure experiments saw rapid increases in metal leaching during the first 10 minutes, metals were then removed from solution. High pressure experiments displayed initial increases in metal leaching during the first hour, with consistent concentrations of leached metals between 60-1440 minutes. Zn, Cu, Fe, Mn, Co displayed the most significant rise in concentration (>1000 μmol/m^2) in both experiments. The low pressure experiments being more representative of early dissolution as mined material is returned to the ocean after ship-board processing. The high pressure experiments being more representative of sulphide dissolution over 24 hours in stagnant water columns and seabed.

Laboratory and field studies by Feely (1987) indicate that sulphide minerals settling from a buoyant plume could persist on the seafloor for days to years, dependent on grain size and mineral type. Rates of dissolution of sulphides was determined through weight changes for both type experiments (Feely, 1987). Large weight changes were observed for marcasite samples, and small but significant weight changes were seen in sphalerite, pyrite and chalcopyrite samples (Feely, 1987). Using a deposition model, they determined that for stable phases (pyrite and chalcopyrite), dissolution rates are slow, so dissolution processes are unlikely to occur in the water column (plume) before deposition (Feely, 1987). However, rapid dissolution observed in marcasite suggests that significant amounts of dissolution could take place during settling from a buoyant plume. Where mining activities may create a plume sulphide matter, or where accidental spillages occur in surface waters, sulphides with fast dissolution rates could potentially begin dissolving in the water column, effecting organisms here, as well as those on the seafloor.

Knight *et al*. (2018) conducted seawater sulphide dissolution studies, comparing monomineralic and polymineralic experiments for evidence of galvanic interactions. Using sulphide mixtures of pyrite, sphalerite and chalcopyrite, at 100-200 μm grain size, they saw evidence of accelerated dissolution and galvanic interactions taking place in the polymineralic studies. In mixtures containing pyrite, pyrite was always cathodically protected, and the mineral pair (chalcopyrite, sphalerite) preferentially dissolved. In the pyrite-chalcopyrite experiments, Cu was released up to 600% faster, than chalcopyrite monomineralic experiments. While in the pyrite-sphalerite experiments, Zn release increased 300% when compared with sphalerite monomineralic studies. Increased high rates in the polymineralic studies were not sustained, and metal release slowed over time; whereas in the monomineralic counterparts this slowing down of metal release was not observed. Knight *et al*.

(2018) identify chalcopyrite to be of the largest geochemical concern. Therefore, any increase in Cu release due to galvanic interactions needs to be considered in an environmental context when it comes to SMS mining scenarios.

Findings such as these are important as crushing/grinding during SMS mining is expected to expose sulphide surfaces to oxygenated seawater, encouraging further oxidation (Knight *et al*., 2018). The effect of galvanic interactions, coupled with factors such as: increases in temperature of return waters (~10ºC) and higher concentrations of dissolved oxygen in surface waters, have potential to increase metal leaching from sulphide minerals (Knight *et al*., 2018).

Furthermore, Fuchida *et al.* (2017), carried out metal leaching experiments on sulphide samples, sieved through 1/16 mm mesh, in artificial seawater. Finding that hydrothermal sulphides released Zn and Pb into solution (especially under oxic conditions), determining an array of leaching mechanisms are responsible; individual metal solubility, dissolution rates and galvanic interactions (Fuchida *et al.,* 2017). This is important because they highlight how metal leaching can occur independently of acid generation, therefore metal contamination must be seriously considered with the effects on deep-sea and surface water ecosystems (Fuchida *et al.,* 2017). The results also indicate how metal leaching could be accelerated under increased redox and temperature conditions, in cases where accidental leakage or spillages of SMS deposits occur in ocean surface waters (Fuchida *et al.,* 2017).

2.1.2 Controls on Oxidative Dissolution Rates

Temperature: It is generally agreed upon that increasing temperature, increases the rate of sulphide oxidation due to changes in the kinetics of the reaction (Fallon *et al.*, 2017). Table 2 summarises different sulphide mineral oxidation studies that investigate temperature amongst other variables as controls. The limitation of high-temperature studies such as; King and Lewis (1980) and Long and Dixon (2004) (Table 2) is that temperatures used are not representative of average seawater temperatures, so are not applicable to non-active vents, deposits formed some distance away, or indeed SMS mining activities.

Seafloor mining tools have operating temperature ranges of 0-35°C, mining cannot take place outside of this range; although material could be discharged into areas with warmer temperatures (Bilenker *et al*., 2016). Seafloor temperatures (1000-5000 m depths) are on average 2-4°C, while temperatures of fluids exiting hydrothermal vents are significantly higher at ~60-400°C, generally being restricted to active vents (cm's-m's) as mixing with cold seawater returns elevated temperatures to background levels (Bilenker *et al*., 2016; Fallon *et al.*, 2017). The majority of non-active sites that might be mined will be expected to be within the range of 0-35°C where mining equipment can operate, in some cases mining may take place near active vents (Bilenker *et al*., 2016). As the effect of temperature is well versed in the literature, future temperature studies may look towards the effect of rising global temperatures on sulphide oxidation.

Table 2: Studies investigating the effect temperature has on sulphide mineral oxidation rate.

Study	Variables investigated	Samples	Method	Result/Discussion
Bilenker et al. (2016)	pH; temperature; dissolved O2; surface area	Pyrrhotite; chalcopyrite	Sulphide dissolution experiments in seawater, using batch reactor set up. Flourescent In-Situ Hybridizations (FISH); Scanning Transmission Electron Microscopy (SEM, TEM); light analysis.	Increased temperature, surface area and dissolved oxygen all positively affect sulphide oxidative rates of reactions. Oxidation rates between 4-35°C increased linearly with higher temperatures on an Arrhenius plot. pH had a minimal effect over the investigated range.
Edwards et al. (2003)	Temperature; Microbes	Pyrite; marcasite; chalcopyrite, sphalerite, elemental sulphur; natural chimney, Main Endeavour Segment, Juan de Fuca Ridge	Incubation studies at low temperatures (~4°C)	High degree of variability in sulphide oxidation rates at lower temperatures (4°C). Surfaces were only colonised by bacteria, with colonisation densitites varying over an order of magnitude with: elemental sulfur > chimney sulfide > marcasite > pyrite > sphalerite > chalcopyrite; corresponding with the abiotic oxidation rates of these samples.
Gartman and Luther (2014)	Temperature; Oxygen conc.; total HCl-soluble Fe conc.; pH	Sub-micron pyrite	Seawater pyrite oxidation study	Decreasing temperature from 25°C to 9°C, decreased oxidation rates on average by a factor of 3. These findings are concordant with Arrhenius approximation. Nanoparticulate pyrite oxidises up to 2 orders of magnitude slower than previous studies using bulk pyrite (ground/sieved).
King & Lewis (1980)	Temperature (80 to 100 °C); Oxygen Pressure (0 to 120 psig); Intial ferric Fe conc. (concentration) (0 to 0.5 M)	Pyrite particles in aqueos slurry	Two methods to measure Fe conversion: 1. monitoring liquid samples for total Fe increases. 2. Light absorbance measurement	Temperature, oxygen pressure, and intial ferric Fe conc. all significantly affect pyrite oxidation, causing increased rates of reaction. Pyrite conversion increased ~25% to 60% when variables were set at 100°C, 30 psig and intial Fe conc. 0.5 M, and 20g/L ratio.
Long & Dixton (2004)	Temperatue (170 - 230°C); particle size (49-125 µm diameter); agitation speed (650 - 950 rpm); oxygen partial pressure (345 - 1035 kPa); pulp density (1 - 20 g/L)	High-grade massive pyrite specimens, Zacatccas, Mexico	Pyrite oxidation kinetics in sulphuric acid, under oxygen pressure.	Tempertaure significantly affected pyrite dissolution with almost all pyrite sample being dissolved at 230°C within 20 minutes. Agitation speed had no significant effect on intial pyrite oxidation rates when at or above 800 rpm. Particle size, oxygen partial pressure and pulp density were all found to affect pyrite oxidation.

Mineral surface area: Sulphide surface area is an important control on oxidative dissolution rates, as higher specific surface areas increase reaction volumes (Romano, 2012). Mining activities can increase sulphide surface area and expose fresh surfaces through; pulverisation, crushing, grinding and through the discharge of slurry waste (Bilenker *et al*., 2016). Smaller grain sizes equate to larger surface areas, illustrated in Figure 8. Surface area may be the most important control on sulphide oxidation in mining, as mining practices can actively reduce surface areas whereas other variables, temperature and dissolved oxygen remain relatively constant (Bilenker *et al*., 2016).

Bilemker *et al.* (2016) calculate surface area using B.E.T. gas adsorption on grain sizes 45-106µm-106-150µm for chalcopyrite and pyrrhotite to get 0.062 m2g-1 and 0.032 m2g-1 respectively. Finding samples with smaller surface areas oxidse more quickly, ~1.74x faster for pyrrhotite (Bilenker *et al*., 2016).

Some studies suggest that sulphide oxidation has a more complex relationship with surface area, observing that oxidant adsorption is non-uniform, taking place on grain edges, corners, defects and areas of high surface energy (de Haan, 1991; Chandra and Gerson, 2010; Bilenker *et al*., 2016). Determining 'reactive surface area' to be more important than 'bulk surface area'; these features vary between sulphide grains, introducing variations on spatial scales to observed rates of reactions (de Haan, 1991; Chandra and Gerson, 2010; Bilenker et al., 2016).

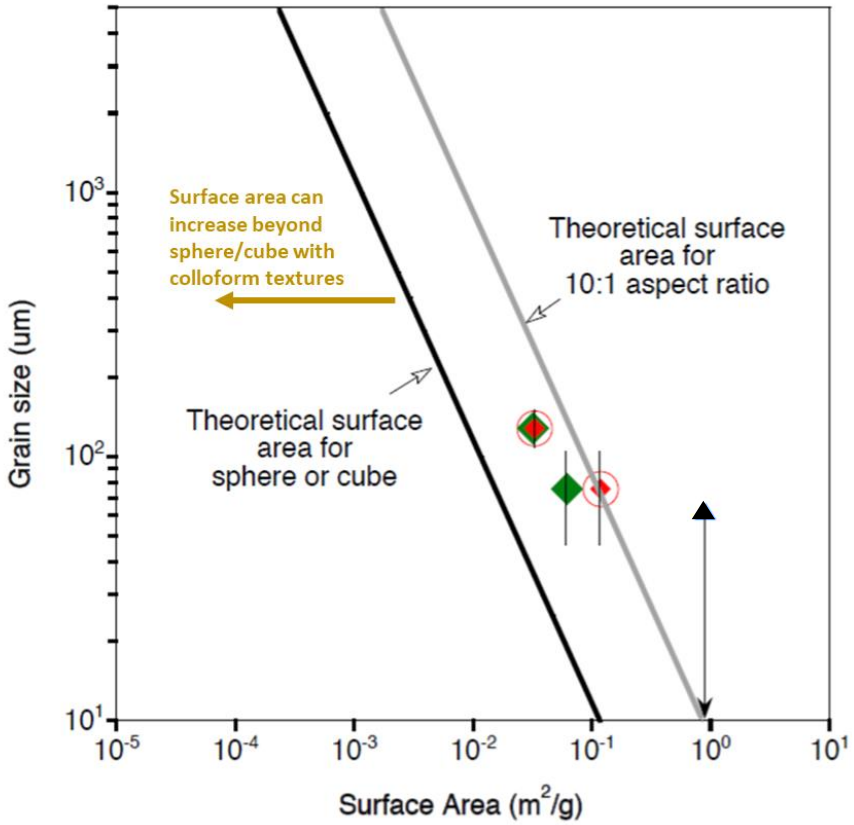

Figure 8: Comparison of grain size of measured surface area from literature. Theoretical lines are calculated using the density of pyrite, but other sulphides would be almost indistinguishable. The theoretical values for sphere or cube would be considered the minimum possible surface area values. Surface irregularities would increase this value as would porous grains. Colloform textures (most commonly seen in pyrite or marcasite) and hollow grains increase surface area beyond the theoretical surface area line for sphere or cube. Red = Pyrrhotite, Green = Chalcopyrite, Blue = Pyrite, Purple = Sphalerite, Orange = Marcasite. Circles = Romano, 2012; Diamonds = Bilenker, 2016; Squares = Morse, 1991. Arrow bar indicates reported grain size range with Morse only reported as <62 um.

Geochemistry: Chen and Chen (2010), found that 'perfect' sulphide surfaces were unable to adsorb oxygen, while natural surfaces (with impurities, vacancies, defects) were energetically favourable for oxygen adsorption and therefore oxidation. This may be important for sulphide oxidation, as perfect mineral surfaces are rare in natural deep-sea environments (Chen and Chen, 2010). Rimstidt and Vaughan (2003), also find that variations in exposed surface area of pyrite minerals has a stronger control on oxidation, than mineral composition or crystal structure (Rimstidt and Vaughan, 2003).

Dissolved Oxygen: Dissolved oxygen (DO) concentration is an important control on oxidative dissolution (van Hoorebeke and Alexander, 2016). DO and ferric iron both act as oxidants in sulphide weathering and increasing oxygen concentration results in increased reaction rates in low pH solutions (Romano, 2012; Heidel *et al*., 2013). van Hoorebeke and Alexander (2016) , discuss how at lower temperatures, initial concentrations of DO is a more important factor to the rate of pyrite oxidation than the initial pH of seawater, but only by a small margin. However, Romano (2012) observed that DO concentration is not linear with sulphide oxidation rates. Bilenker *et al*. (2016), discuss DO

dependence on seawater density, which is influenced by pressure finding seawater density has little influence on DO, concluding therefore pressure has an insignificant effect.

pH: The effect of pH on the rate of sulphide mineral oxidative dissolution is well established in the literature; with data demonstrating that at lower pH, the rate increases (Bilenker, 2011).

Fallon *et al.* (2017), discuss how water pH after mining affects the oxidation rates of sulphides, as well as speciation and solubility of heavy metals, determining toxicity and reactivity. Metal sensitivity in organisms can also be affected by pH, including bacteria (population numbers, species type), which in turn influences natural weathering processes (Fallon *et al.*, 2017).

Average seawater pH is 8.1, ranging pH 7.5-8.4 globally; inactive hydrothermal vents are typically more neutral, dependent on last activity and proximity to other active vents (Bilenker, 2011; Fallon *et al.*, 2017). The rate of sulphide oxidation is assumed to be near zero at average seawater pH (Bilenker, 2011; Fallon *et al.*, 2017). However, ocean acidification due to anthropogenic rises in carbon dioxide will likely increase SMS weathering when coupled with local pH increases through SMS mining (Bilenker, 2011). Furthermore, pH has been found to cause variations in sulphide rest potentials, which inadvertently influences which minerals are preferentially dissolved through galvanic interactions in sulphide mixtures (Attia and El-Zeky, 1990).

Ion concentration: The five major ions in seawater (~35‰ salinity) are Na^+, Ca^{2+}, Cl^-, SO_4^{2-}, and HCO_3^- , Cl^- being most frequently discussed in sulphide oxidation (Poisson and Papaud, 1983). Chandra and Gerson (2010), review highlights the uncertainty surrounding Cl^- concentration effect on dissolution rates. Dimitrijevic et al. (1996), found adding Cl^- or SO_2^{-4} to leachate solutions caused a reduction in pyrite oxidation rates, possibly from Cl^- or SO_2^{-4} adsorbing onto pyrite surfaces, inhibiting oxidation.

Other studies agree, discussing how Cl^- readily absorbing on sulphide surfaces uses up sites for Fe^{3+} or sulphur, preventing sulphur deposition and Fe-hydroxy coatings (Lehmann *et al.*, 2000; Chandra and Gerson, 2010). In relation to this, Dutrizac (1981), saw Cl^- media result in faster rates with higher metal leachates in solution than those conducted in SO_2^{-4} media. Another study noted that dissolution of pyrite occurred faster in Cl^- and SO_2^{-4} solutions as complexes with higher electrode potentials were formed (Sasaki *et al.*, 1995; Chandra and Gerson, 2010). Overall, it is clear that the effect of Cl^- and other ions on oxidation rates is not well understood and needs further research.

Biotic influence: The effect bacterial activity has on increasing dissolution rates and galvanic interactions was previously discussed by Berry *et al.* (1978). Studies on large grazing shrimp at a Mid-Atlantic Ridge hydrothermal vent site, revealed that grazing shrimp feed by scraping SMS deposit surfaces, exposing sulphide mineral surfaces, subsequently increase oxidation rates (Van Dover *et al.*, 1988; Polz *et al.*, 1998). Field incubation studies by Edwards *et al.* (2003), saw rapid

colonisation of bacteria on exposed sulphide surfaces; suggesting mineral-oxidising bacteria has an important role in SMS weathering. Sulphur reducing bacteria (SRB) and Fe-oxidising bacteria were indicated from the results and in part account for reaction rates, though reduction of $S^0 \rightarrow S^{2-}$ and promoting active oxidation of minerals (Edwards *et al.*, 2003). They also found that the rate at which sulphide minerals leach beneficial chemical species of chemolithoautotrophs, determines population size of colonising bacteria: marcasite > pyrite > sphalerite > chalcopyrite (this sequence shows some correlation with the dissolution rates in Figure 6.0) (Edwards *et al.*, 2003).

Seafloor mining sequences outlined by Gwyther (2008) do not give enough time for bacteria colonisation, as the transit time between in-situ pulverisation, surface processing and waste return is <30 minutes (Bilenker *et al*., 2016). However, fine sulphide particles and exposed surfaces left behind will experience bacteria colonisation, and elevated rates of oxidative dissolution.

2.2 Galvanic Interactions of Sulphide Mineral Pairs:

Few studies look at the effect of galvanic interactions in relation to SMS deposits on the seafloor and the subsequent environmental effects. Increased dissolution of sulphide minerals through galvanic interactions will increase metal leaching, if not balanced by precipitation of phases, soluble metals may accumulate in local ecosystems/disperse into ocean (Fallon *et al.*, 2017).

Galvanic cells arise when two sulphide minerals with different conductivities come into contact in an aqueous solution with an electrolyte present (Da Silva *et al*., 2003; Heidel *et al*., 2013). In natural seafloor environments seawater acts as an efficient electrolyte, and a current is set up between the two minerals, the mineral with the lower resting potential is preferentially dissolved (anode) and the mineral with the higher resting potential is cathodically protected, as seen in Figure 9 (Da Silva *et al*., 2003; Heidel *et al*., 2013). When more than two sulphide minerals come into contact, a galvanic series forms, with oxidation rate increasing with decreasing rest potentials (Attia and El-Zeky, 1990; Abraitis *et al.*, 2004). Galvanic interactions in sulphide minerals are generally accepted to increase the oxidative dissolution rates of sulphide minerals in seawater solutions (Fallon *et al.*, 2017). A variety of studies have observed evidence of galvanic interactions between sulphide mineral pairs (Berry *et al*., 1978; Da Silva *et al*., 2003; Abraitis *et al.*, 2004; Knight *et al*., 2018).

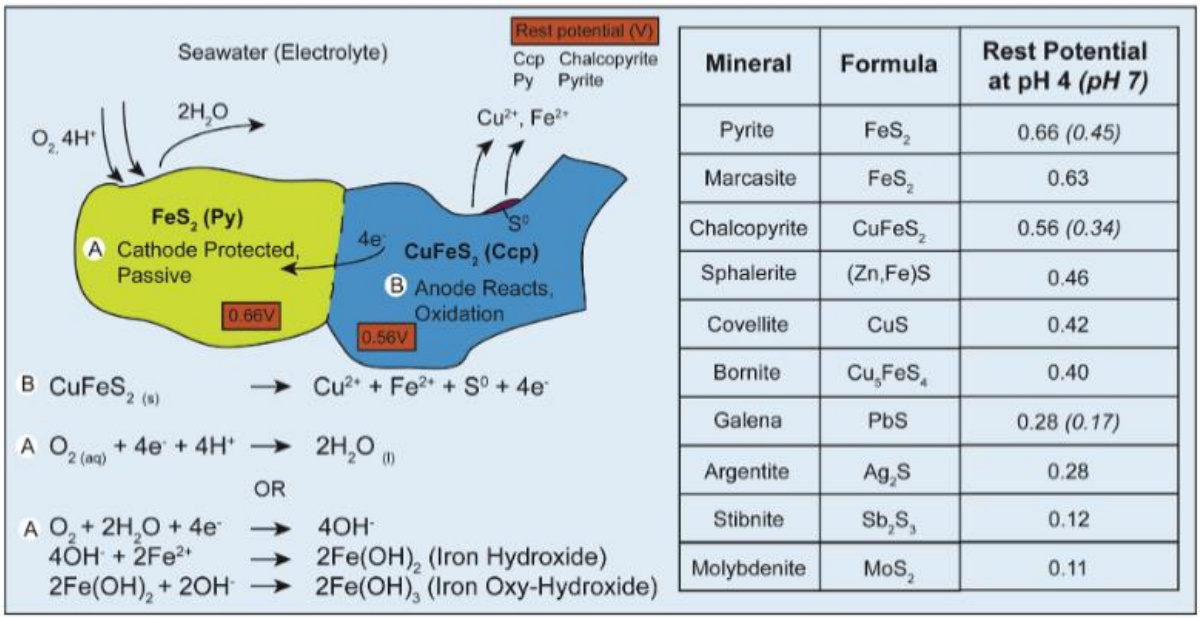

Mineral	Formula	Rest Potential at pH 4 *(pH 7)*
Pyrite	FeS_2	0.66 *(0.45)*
Marcasite	FeS_2	0.63
Chalcopyrite	$CuFeS_2$	0.56 *(0.34)*
Sphalerite	(Zn,Fe)S	0.46
Covellite	CuS	0.42
Bornite	Cu_5FeS_4	0.40
Galena	PbS	0.28 *(0.17)*
Argentite	Ag_2S	0.28
Stibnite	Sb_2S_3	0.12
Molybdenite	MoS_2	0.11

Figure 9: demonstrates a galvanic cell set up between Bornite and Pyrite in seawater (acting as electrolyte), with surface reactions taking place. Bornite behaves as an anode, due to its lower resting potential, preferentially dissolving and leaching trace metals (Cu^{2+}, Fe^{2+}). Pyrite has a higher resting potential so behaves as a cathode and is subsequently cathodically protected, so does not oxidise in this system (Fallon *et al.*, 2017).

Da Silva *et al*. (2003), measure rest potentials for galena and sphalerite at 0.325 V and 0.375 V, respectively (relative to a standard hydrogen standard). Although these rest potentials differ to those in Figure 9, they show the same order of rest potentials, and through leaching experiments show that galena persistently has higher oxidation rates than sphalerite (Da Silva *et al*., 2003).

Pyrite should have the highest rest potential in a series of typical SMS sulphides, so is galvanically protected in mixed sulphide solutions; long-term oxidation experiments confirm this with pyrite remaining intact, while galena and sphalerite show signs of dissolution (Heidel *et al*., 2013). This has also been observed in natural SMS deposits, where only accessory quantities of sphalerite and chalcopyrite remained in a studied mound after dissolution, due to preferential leaching, and assumed galvanic interactions when in contact with pyrite (Webber *et al.*, 2015). This is significant because it indicates that sulphide minerals of lower conductivities will preferentially leach at faster rates (Heidel *et al*., 2013).

Different studies have witnessed increased dissolution rates, Abraitis *et al.* (2004), observing leaching rates increased by factors of 31, 18, and 1.5 x for galena, chalcopyrite and sphalerite, when in solution with pyrite, during acid-leaching experiments. Other studies have observed similar increased rates of oxidation, for galena, sphalerite and covellite, at 8-20x faster when preferentially dissolved through galvanic interaction with pyrite (Attia and El-Zeky, 1990).

Biotic influences may be a problem in mining scenarios where fine mixed-sulphide particles settle after extraction/dewatering (Fallon *et al.*, 2018). Bioleaching experiments undertaken by Da Silva *et al*. (2003) show that rates of galvanic reactions are faster in lower oxidant ferrous (Fe^{2+}) experiments, than in ferric (Fe^{3+}) leaching experiments in which high concentrations of ferric iron are maintained.

Other factors may increase galvanic effects, such as sulphide grain/phase contacts. Berry *et al*. (1978) saw chalcopyrite dissolution was optimised when chalcopyrite grains/phases were surrounded by pyrite, increasing electrical contact regimes and subsequently rates of reactions.

2.3 Toxicity Effect and Transport/Transfer of Metal Leachate

There are few studies which investigate the effect of heavy metal leachates through sulphide oxidation on seafloor environments and associated ecosystems.

Hydrothermal-vent communities are thought to be adapted to high concentrations of heavy metals in their environment, so increased metal leachate through mining activities is thought to have little impact (Boschen *et al.*, 2013). However, background fauna, and fauna occupying inactive vents are much less adapted to heavy metals so may be vulnerable to mining wastes (Boschen *et al.*, 2013). Many vent-site microbes (heterotophic bacteria, thermaccales, thermophiles) display resistance to heavy metals including: cadmium, zinc, arsenate, silver, high amounts of copper, and mercury oxide (Hg(II)), this may indicate increased metal tolerance adaptations (Jeanthon and Prieur, 1990; Llanos *et al.*, 2000; Ando *et al.*, 2002; Vetriani *et al.*, 2005; Gadd, 2010). Van Dover (2014), suggest physical impacts such as smothering from sediment plumes, ore removal, degradation of habitat quality through re-shaping, and changes to the fluid flux regime, to be the biggest threat to these communities.

Fuchida *et al.* (2017) propose that toxic metals accumulate in ecosystems through food chains, from seawater leaching experiments using mixed sulphide samples and phytoplankton (primary producers in surface environments) proxy for deep-marine organisms. Finding growth was inhibited in S. marinoi-dohrnii complex (phytoplankton) by all ore sample leachates with large amounts of Mn, Fe, Cu, Zn, As, Cd, Sb, and Pb released, Fe-rich ore leachates being most toxic (lethal >1%) (Fuchida *et al.*, 2017). Brown and Hauton (2018), investigated ecotoxicological response of Palaemonvarians as a proxy for hydrothermal-vent shrimp to chalcopyrite exposure (<250µm grains), finding exposure to 2887.8 mgL^{-1} chalcopyrite (~37x lethal threshold of soluble Cu) did not result in death or significantly affect respiration rates, indicating Cu isn't bioavailable in its mineralic form. Boschen *et al.* (2013); Simpson and Spadaro (2016); Fuchida *et al.* (2017), highlight how studies often test metal toxicity on shallow water dwelling organisms which are not representative of deep marine environments.

Through metal toxicity experiments Simpson and Spadaro (2016), determine the form of metal/metalloids (e.g. particulate or dissolved) to be more important than the total concentration of metals/metalloids when considering toxicity. Metals associated with sulphide phases have low bioavailability, but through re-deposition can transform into more available forms, such as through mining leachate (Simpson and Spadaro, 2016). Different physical states of metals can affect organisms differently, with metals in solution more likely to cross permeable tissues (e.g. gills), and particulate/adsorbed metals more likely to be ingested by deposit feeders (Hauton *et al.*, 2017). There is potential for some metals (Cu, Zn, Fe) to have long term positive effects on pelagic communities, as they are known to be essential micronutrients in the open oceans (Hauton *et al.*, 2017)). Hauton *et al.*

(2017), further finds that lower temperatures decrease metal toxicity for Cu and Cd at 10ºC, this is generally positive for deep sea mining under normal seafloor conditions.

The Solwara 1 Project launched by Nautilus Minerals has discussed the potential negative effects of metal leachate in an Environmental Impact Statement (EIS) (Gwyther, 2008). The EIS recognises that there will be some toxicity from metals released in seawater, but has deemed this toxicity irrelevant to deep sea organisms which are already adapted to higher concentrations of metals (Gwyther, 2008). Nautilus Minerals committed to ensuring that mining wastes will be expelled 25-50m above the seafloor to avoid contact with more vulnerable surface organisms and plan a 600-fold dilution of contaminated water to meet ANZECC/ARMCANZ (2000) guidelines for 95% protection (Gwyther, 2008). Toxicity tests representative of water conditions and sediments discharged in shallow to mid-water depths, showed some toxicity to surface test organisms, but is not of concern as plans aim to discharge return waters close to the seafloor (Gwyther, 2008). Ocean currents and vertical movement were addressed in the EIS; both surface and deeper currents being dominated by wind, moving in a general N-E direction, with any 'upwelling's' dominated by a downwards motion (Gwyther, 2008)

Luick (2012), argues that the EIS data was 'questionable' with Nautilus neglecting to release heavy metal exposure models for the project, ignoring the potential impacts to marine ecosystems and humans. Likewise, Luick (2012) disputes Nautilus's ocean transport mechanism data arguing that there is periodic upwelling at Solwara 1 mound of ~1000 m/day, with currents actually flowing shoreward (towards New Ireland), resulting in serious implications regarding the dispersion and risk of heavy metals from Solwara 1 site. Hauton *et al.* (2017), discusses further the potential for heavy metal dispersion in the water column, describing how extraction will release metals in dissolved and particulate phases over large scales (100-1000s Km^2).

Overall, these studies show that metal toxicity can be influenced by both natural and anthropogenic factors, but mining is a key factor in both the release of heavy metals.

2.4 Adsorption of Trace Metals

Sulphide minerals are unstable at ambient seawater conditions and dissolve, releasing heavy metals including Fe, Zn and Cu (Dekov *et al.*, 2011; Knight *et al*., 2018). Metals can be sequestered from solution onto weathering products such as Fe-oxides/oxy-hydroxides forming gossans at SMS sites (Fallon *et al*., 2017). Adsorption, a process where molecules (the adsorbate) are transferred to a solid surface (the adsorbent) through physical forces or chemical bonds; of trace metals onto weathering products may be important in heavy metal dispersion/reducing toxicity and is used in terrestrial remediation (e.g. Blowes *et al*., 1997; Artioli, 2008; Naderi, 2015).

Some papers assume reacting sites on mineral surfaces to be heterogeneous, adsorption investigations on Ni, Zn and Cd onto synthetic-geothite found the affinity of MOH^+ ion sites logarithmically decreased as adsorbate logarithmically increased (Bruemmer et al., 1988; Benjamin and Lecki, 1981).

Knight *et al*. (2018), found the precipitation of Fe-oxyhydroxides to sequester Fe, Zn and potentially Cu from solution in dissolution experiments, and to form under alkaline conditions. While oxyhydroxides may reduce Fe in solution, soluble-Fe was still observed in pyrite, chalcopyrite and sphalerite dissolution experiments at lower concentrations, concluding that oxyhydroxides layers may eventually cease sulphide oxidation/metal adsorption take over as dominant process (Knight *et al*., 2018).

Öhlander *et al.* (2007) observed enrichment in As, Cd, Cu, and Zn on pyrite surfaces, with adsorption thought to be the main retention process as both Fe- and Al-oxyhydroxides have a high capacity for metals (Öhlander *et al.*, 2007).

2.5 Aims and Thesis Outline

This review highlights the lack of consensus in addressing the magnitude/relative importance of variables known to affect, and the environmental implications of mining SMS deposits.

It is well established that sulphides in SMS deposits oxidise naturally, leaching heavy metals into solution, the rate which this occurs depending on mineralogy, temperature, surface area and galvanic interactions. The latter of which is not as well understood.

Studies by (Berry *et al*., 1978; Da Silva *et al*., 2003; Abraitis *et al.*, 2004; Knight *et al*., 2018), have already demonstrated how galvanic interactions between sulphide mineral pairs can increase metal leaching through oxidation. However, more research is needed, to investigate the extent, conditions and duration that the effects become most apparent. As well as understanding the physical nature of grain contacts required for galvanic cells to arise. With the mining of SMS deposits likely to expose fresh surfaces of mineral pairs through extraction, crushing and pulverisation, the impact of galvanic

interactions on metal leaching needs to be well understood. Furthermore, the impact of heavy metal leaching on the local environment needs to be considered, previous studies indicating a risk of bioaccumulation in local ecosystems - with transport and dispersion of heavy metals through food chains and the water column.

A greater understanding of the role galvanic cells have in sulphide oxidation, and subsequent metal leaching, will be beneficial when it comes to producing future regulations for the mining of SMS deposits. In addition to predicting which mineral pairs in SMS deposits will be of higher risk of producing more undesirable environmental impacts associated with sulphide oxidation.

The aim of this Masters project is to investigate some of the parameters affecting galvanic cells and the relative reactivity (galvanic potential) of various natural SMS sulphide pairs. In addition, to investigate with some sulphide 'standards' (terrestrial sulphides) which were easier to characterise as homogeneous, gave a better guarantee of purity and were easier to handle in terms of obtainable grain size range etc. The original idea was to compare dissolution rates for; i) monomineralic single sulphides using 'standards' (terrestrial sulphides) and separated sulphides from SMS deposits, then ii) polymineralic pairs of mechanical mixtures, then iii) polymineralic pair of naturally intergrown sulphides selected SMS localities. However, this had to become more focused due to the nature of the natural samples and the limited access to the labs due to Covid-19 restrictions. The more specific objectives of this study are listed below:

- To use sulphide mineral pairs not yet investigated in the literature: sphalerite-galena, chalcopyrite-sphalerite, chalcopyrite-galena, chalcopyrite-secondary-Cu-sulphides, pyrite-secondary-Cu-sulphides, and pyrite-galena.
- To carry out both simple monomineralic dissolution experiments and polymineralic dissolution studies, to comparatively investigate the effect of galvanic interactions.
- To use natural intergrown sulphide samples from both Logatchev and Turtle Pits hydrothermal vent sites, to compare with mechanical mixtures made from off the shelf 'standard' sulphide mineral samples in seawater dissolution studies, to investigate the importance of the nature of mineral pair contacts.
- To execute an ICP-OES analysis of samples taken throughout the dissolution experiments, to investigate leached metal concentrations between experiment runs.
- To carry out some higher temperature experiments to investigate the effect temperature has on sulphide mineral pairs undergoing galvanic interactions, and the coupled effect on metal leaching concentrations.

The main themes and hypothesise evolved over the course of this study, but the original ideas and hypothesise of this project are listed below:

- Sulphide mineral pairs of different conductivities (rest potentials) will result in galvanic cells being set up when in contact in seawater.
- Galvanic cells in turn will give rise to increased metal concentrations in the seawater solution from preferential leaching of the anodic sulphide mineral, whilst the cathode mineral is protected.
- 'Mechanical' sulphide contacts where sulphide minerals of different conductivities are touching will be sufficient for galvanic cells to arise between them.
- Galena will preferentially leach Pb into solution when coupled with sulphide minerals of higher rest potential (e.g. pyrite).
- High temperature experiments will result in increased preferential leaching of anodic minerals in galvanic pairs, subsequently further increasing metal concentrations in solution.

3.0 Materials and Methods

3.1 Introduction

Natural SMS samples (LOG-11, LOG-13, TP-2L) used in this Masters project were sourced from GEOMAR, Helmholtz Centre for Ocean Research, Ocean Drilling Program from the slow spreading Mid Atlantic Ridge. Some high quality display specimen single sulphide crystals were obtained from classic terrestrial localities and will be referred to as 'Standards' or 'Std.' throughout this investigation. Sphalerite standard samples are from Trepca mine, Kosovo, and both the galena and chalcopyrite standards are from Morocco. The pyrite standard was sourced from Navajun La Rioja, Spain.

3.1.1 Geologic Setting of Hydrothermal Sample Sites

The natural samples used in seawater dissolution experiments, are sourced from two hydrothermal vent sites: LOG-11 (Logatchev, Mid Atlantic Ridge: Inactive chimney), LOG-13 (Logatchev, Mid Atlantic Ridge: inactive and multi-layered active chimney) and TP-2L (Turtle Pits, Southern Mid-Atlantic Ridge: Inactive mound) (Fallon, 2018).

3.1.2 Turtle Pits:

Turtle Pits, Mid-Atlantic Ridge, is a slow-spreading mid ocean ridge (MOR), with two main identified sites of active hydrothermal venting (German *et al.*, 2008). The latter of these sites being where TP-2L is sourced, coming from a more oxidised zone, located 4°48.19'S/12°22.30'W, at a depth of 2996 m, Figure 10 (Haase *et al.*, 2007; Fallon, 2018).

Turtle Pits hosts active and inactive black smokers within two major areas of hydrothermal sediment, Figure 10 (Haase *et al.*, 2007; Fallon, 2018). Characterised by recrystallised massive sulphide blocks, habitat to colonies of mussels, crabs, and shrimps, which are likely unique to this type of environment (Haase *et al.*, 2007). Chalcopyrite-pyrite-sphalerite assemblages dominate deposits here with Fe-oxyhydroxides found adjacent to active vents, evidencing sulphide oxidation (Haase *et al.*, 2007). Active vents experience frequent activity, with lava flows and high-temperature venting reaching 407°C (hydrothermal fluids) (German *et al.*, 2008). Active black smokers display pyrrhotite-chalcopyrite-isocubanite assemblages, with inactive vents displaying hematite-magnetite-pyrite assemblages, indicating higher oxidising conditions in the past (Haase *et al.*, 2007).

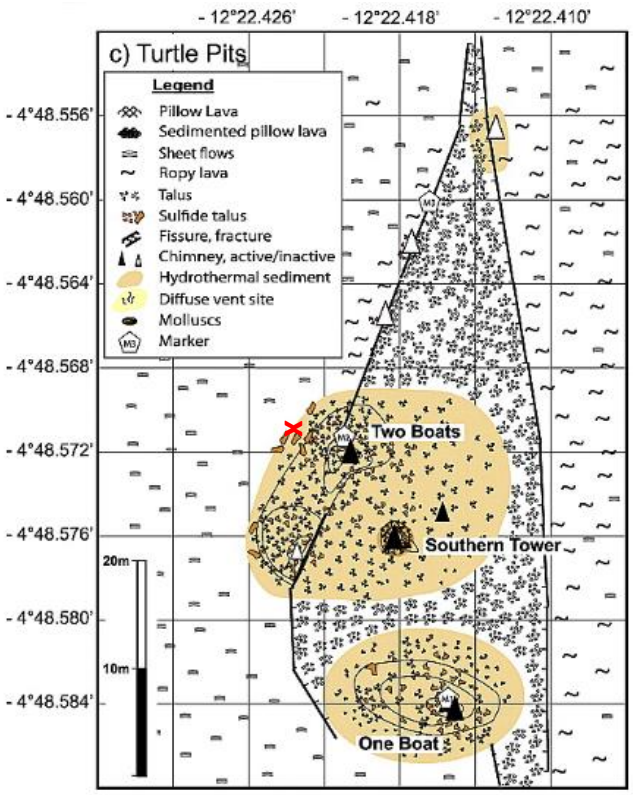

Figure 10: Sketch map illustrating the hydrothermal vent fields at Turtle Pits Field, **X** (red) approximately marks where sample TP-2L was taken on the inactive mound, location identified in Fallon, 2018. Figure (Haase et al., 2007).

3.1.3 Logatchev, Mid Atlantic Ridge:

Logatchev hydrothermal field located south of Turtle Pits on the Mid Atlantic Ridge (14°45'N, 44°59'W), is hosted in ultramafic lithology, demonstrated on Figure 11 (*Standard Definitions*, 2012; Augustin *et al.*, 2008; Petersen *et al.*, 2009). Activity takes place in depressions on the seafloor (smoking craters) and is characterised by high-temperature venting, >350°C (Augustin *et al.*, 2008).

Sulphide mineralisation occurs as two types: Cu-rich, consisting almost entirely of chalcopyrite with minor isocubanite, bornite, sphalerite, pyrite and pyrrhotite; and Zn-rich, characterised by sphalerite and pyrite-marcasite (Murphy and Meyer, 1998). Logatchev hydrothermal field is unusual as sulphide minerals are enriched in copper and gold, due to ultramafic host rocks (Murphy and Meyer, 1998). LOG-11 is collected from an inactive vent chimney at 'Candelabra', and LOG-13 is collected from the talus of an active, multi-layered, Cu-rich black smoker (Fallon, 2018).

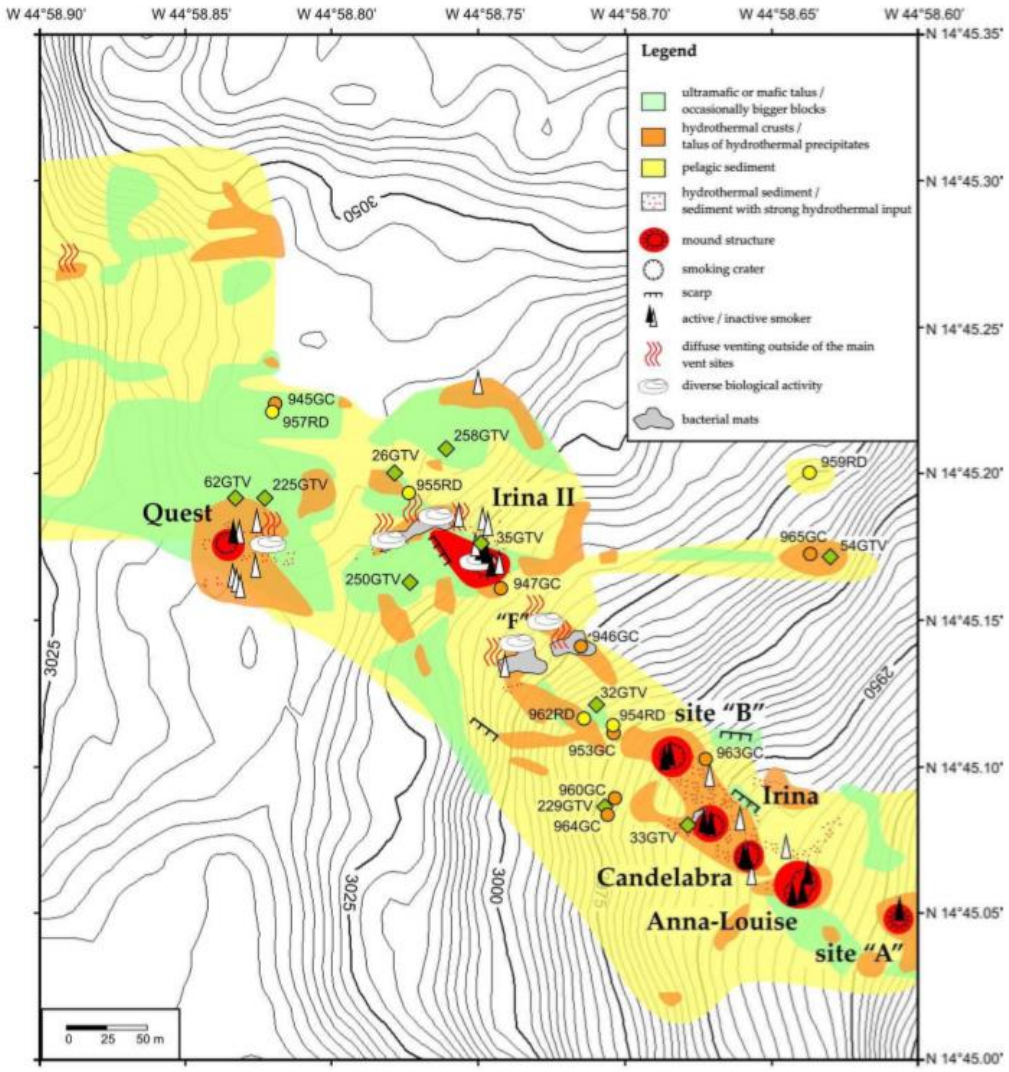

Figure 11: Sketch geologic map of the Logatchev hydrothermal field site; illustrating both the high-temperature and low-temperature hydrothermal vents, situated along a NW-SE strike. (Peterson et al., 2009)

3.2 Sample Preparation

The techniques applied to each sample in this study are summarised in Table 3. Natural samples were pre-crushed into grain size fractions, >500µm-1mm being the grain size fraction used. Standard samples required crushing and sieving prior to picking.

Table 3: Summarises the different analytical techniques applied to each sulphide sample.

Samples		Crushed	Sieved	Mounted	Polished	Reflective light microscopy	Reflective light photographs	Electron Micro Probe Analysis (EMPA)	X-Ray Diffraction Analysis (XRD)	Experiments
Pyrite (STD)		Y	Y	Y	Y	Y	Y	Y	Y	Y
Galena (STD)		Y	Y	Y	Y	Y	Y	Y	Y	Y
Sphalerite-1 (STD)		Y	Y	Y	Y	Y	Y	Y	N	Y
Sphalerite-2 (STD)		Y	Y	Y	Y	Y	Y	Y	N	Y
Chalcopyrite (STD)		Y	Y	Y	Y	N	N	N	N	N
LOG 11:		N	N	Y	Y	Y	Y	N	N	N
	Cp					Y	Y	N	N	N
	Secondary Cu Sulphides					Y	Y			N
	Cp & Secondary Cu Sulphides					Y	Y			N
LOG-13:		N	N	Y	Y	Y	Y	N	N	N
	Cp (+gange)					Y	Y			N
	Cp & Secondary Cu Sulphides					Y	Y			N
TP-2L:		N	N	Y	Y	Y	Y	N	N	N
	Py					Y	Y			N
	Py & Cp					Y	Y			N

Abbreviations used are as follows: Cp = Chalcopyrite, Py = Pyrite, Cu = Copper, N = No, Y = Yes

3.2.1 Mounting Samples for Characterisation

In order to prepare standard samples for the analytical methods and subsequent experiments, they were crushed and sieved to grain sizes: >2mm, >1mm, >500µm, >355µm, >255µm, >125µm, and >50µm. Each sample was handled separately and equipment was cleaned with ethanol to prevent cross-contamination. Crushing was conducted using a hammer and plate, with samples typically breaking along natural cleavages.

A random selection of natural sample grains (>1 mm) were selected to be representative of the entirety of each sample and to allow for multiple sulphide phases to be identified. Selected grains were mounted in 24.5mm Al-rings with Epofix epoxy resin and impregnated under vacuum. Once set, mounts were hand-sanded with SEALEY sandpapers to sizes: 240, 400, 600 and 1200µm. An oil based lubricant was used for all hand grinding and ethanol was used for all cleaning, to prevent dissolution of hydrous phases. Backfilling and further vacuum impregnation was conducted on all of the samples to account for their high porous nature. The final grinding/polishing was carried out by a

Buehler Ecomet 250 Grinder-Polisher using a polycrystalline diamond paste and an oil based lubricant: 6μm (for 10 minutes), 3μm (for 30 minutes), and 1μm (for 5 minutes).

A significant amount of time was spent on mineral picking for both natural and standard samples, as the success of this process was highly dependent on the purity separation. The natural samples required picking to ensure that the minerals in each individual grain were identified and separated for monomineralic and polymineralic experiments. In addition to this, standard samples also required picking, which had previously not been anticipated as gangue minerals present had to be removed to ensure the purity of the samples prior to experiments.

3.3 Sample Characteristics

Standard sulphides were used for monomineralic and polymineralic experiments through mechanical mixtures with controlled ratios, while natural sulphides were used for their natural physical contacts and natural textures/irregularities.

3.3.1 Sample Descriptions

Sulphide minerals in the natural SMS samples were identified under both normal reflective light and cross polarised microscopy, and cross referenced with their bulk chemistries, data provided from Fallon (2018) study.

3.3.2 LOG-11

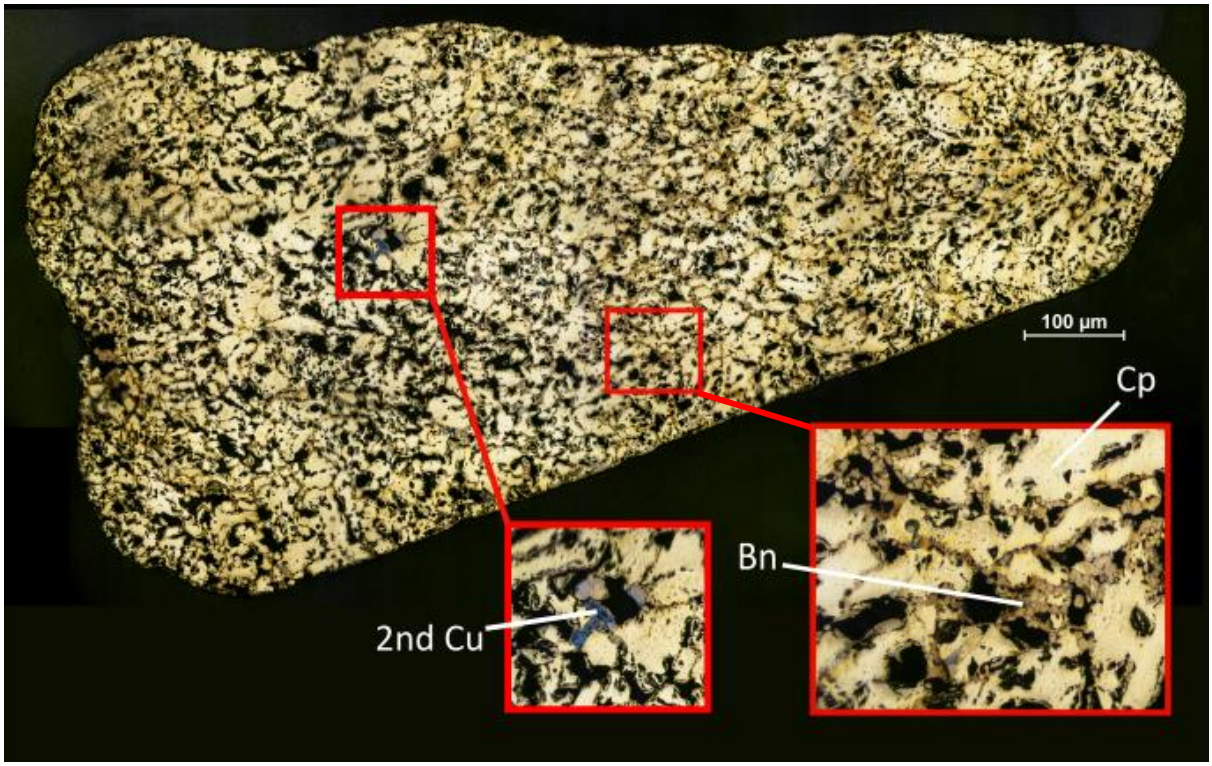

Figure 12: Reflective microscope photograph of LOG-11, showing porous to massive chalcopyrite, with minor bornite and secondary Cu minerals.

LOG-11, Figure 12, is largely composed of chalcopyrite identified under reflective microscopy, with trace amounts of bornite and secondary Cu minerals. Secondary Cu minerals couldn't be identified into individual minerals 100% of the time due to mixing of phases (bornite, covellite, chalcocite, sphalerite), but powdered XRD data from Fallon (2018), reveals that LOG-11 is: chalcopyrite (81%), isocubanite (11%), sphalerite (2.9%), and bornite (2.6%). Chalcopyrite exists in a porous to massive texture, with secondary Cu minerals exsolved along chalcopyrite edges. Bornite is observed within pore spaces and along fractures.

3.3.3 LOG-13

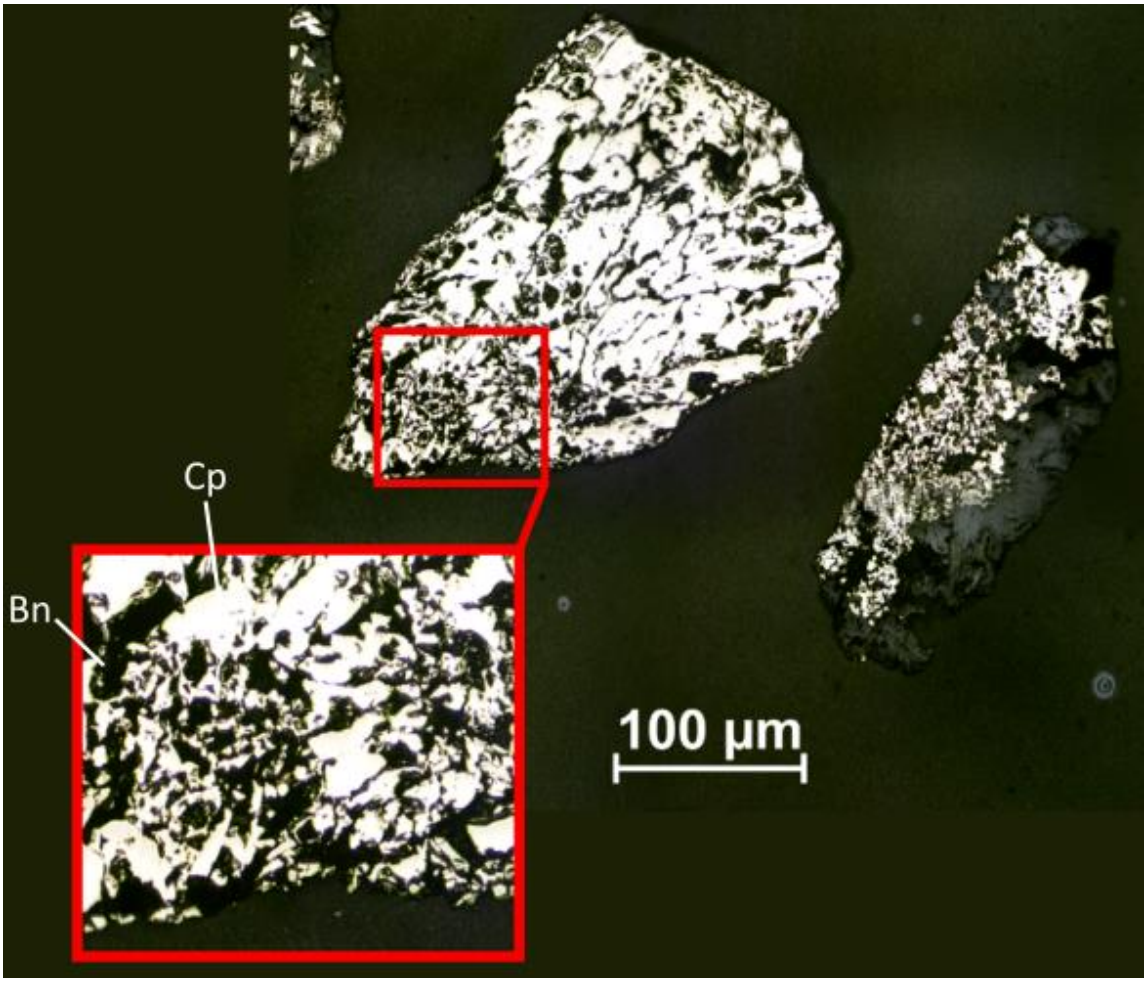

Figure 13: Reflective microscope photograph of LOG 13, showing massive to euhedral chalcopyrite, with minor bornite along fractures and pore spaces.

LOG 13 bulk composition is made up of chalcopyrite with trace bornite, identified under reflective microscopy as seen in Figure 13. XRD data from Fallon (2018), shows LOG-13 to be composed of: chalcopyrite (82%), bornite (0.9%), atacamite (10%), anhydrite (7.6%). Euhedral atacamite was observed under reflective microscope during the picking process, but was not present in high enough quantities required for experiments. Chalcopyrite in LOG-13 exists in euhedral massive textures with bornite occupying pore spaces and fractures.

3.3.4 TP-2L

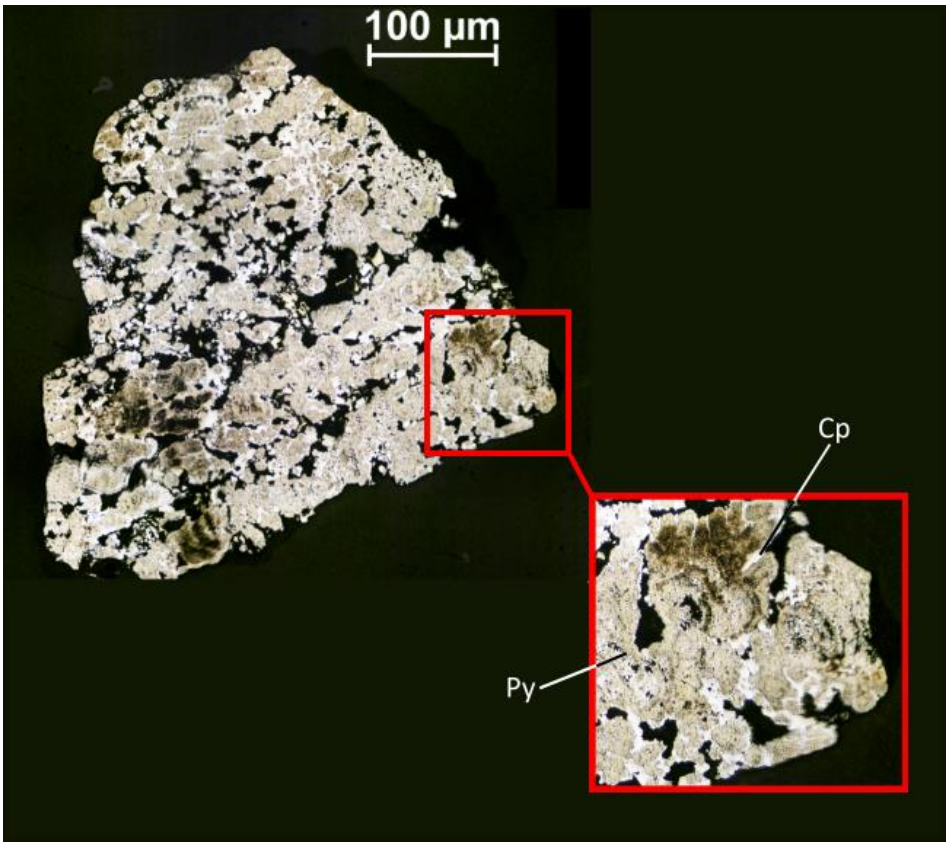

Figure 14: Reflective microscope photograph of TP-2L, colloform pyrite and/or marcasite with minor subhedral chalcopyrite grains occupying pyrite/marcasite grain boundaries.

TP-2L composition is dominated by pyrite and/or marcasite, Figure 14. It wasn't possible to distinguish between pyrite and marcasite in hand specimen when mineral picking, due to them having similar physical properties. However, XRD data of powdered TP-2L from Fallon (2018), shows that TP-2L consists of pyrite (73%), marcasite (13%), chalcopyrite (6.1%), atacamite (2.7%), anhydrite (0.7^{2}%), with other unknown minerals (3.4%). Pyrite (and/or marcasite) exhibits a classic colloform texture, with subhedral chalcopyrite occupying pyrite grain boundaries and pore spaces.

3.4 Experiment Design

Seawater dissolution experiments follow a semi-batch experiment design, where the system is continuously stirred within the reaction vessel, samples are taken at intervals and the vessel is open to equilibrate with outside air. This is an adaptation of a batch experiment design, with a closed system (Salmon and Malmström, 2006; Fallon, 2018). Trial experiments were run to establish rock:fluid ratios required to leach adequate metal concentrations above detection limits before the final experiments and allowed for pH, temperature and dissolved oxygen (DO) observations during sulphide oxidation. Monomineralic and polymineralic experiments with both mechanical mixtures of standard samples and natural contacts in natural samples were then carried out.

The experiment design included a round bottom flask with 3 outlet ports, for sampling and conditions monitoring (Figure 15). Artificial seawater was made initially for the trial experiments according to the ASTM D1141-98 (Reapproved 2013) international standard, and later bought in bulk. Experiments were continuously stirred using magnetic flea, the rate of stirring set to allow for samples to be heaped at base of the flask, ensuring 'mechanical' contacts between grains. Temperature was not controlled as it wasn't possible to have a magnetic flea in a temperature bath. The variation in room temperature was not expected to strong control on the results. Instead, temperature was monitored closely, so that any fluctuation could be recorded and cross-referenced with results. Samples were weighed prior to experiments at 2 decimal places. However, sample was lost throughout experiments on probes though sampling and condition monitoring.

Initial trial experiments ran with 500ml artificial seawater in 1L flask with continuous stirring, at room temperature (~25°C) and pH ~7.6-7.8. Different rock:fluid ratios were used between different runs, to gauge how much sample mass was needed to see clear results. After each run samples were filtered through Whatman 1 filter papers, dried under vacuum and re-weighed.

Later galvanic experiments ran in 500ml round bottom flask, with 250ml of artificial seawater, continuously stirred at room temperatures and pH of ~8.1. Temperature and pH were monitored throughout runs, but dissolved oxygen was not. This is because the outlet ports of the 500ml flask did not fit the dissolved oxygen instrument and based of the observations of the trial experiments (results of which can be found in Figure 23, in section 5.1.7), it wasn't deemed necessary. Standard sample experiments had a rock:fluid ratio of 5g:250ml, at a sample grain size fraction of 355-500µm; whilst natural sample experiments used a 8g:250ml ratio, with a sample grain size fraction of 500µm–1mm.

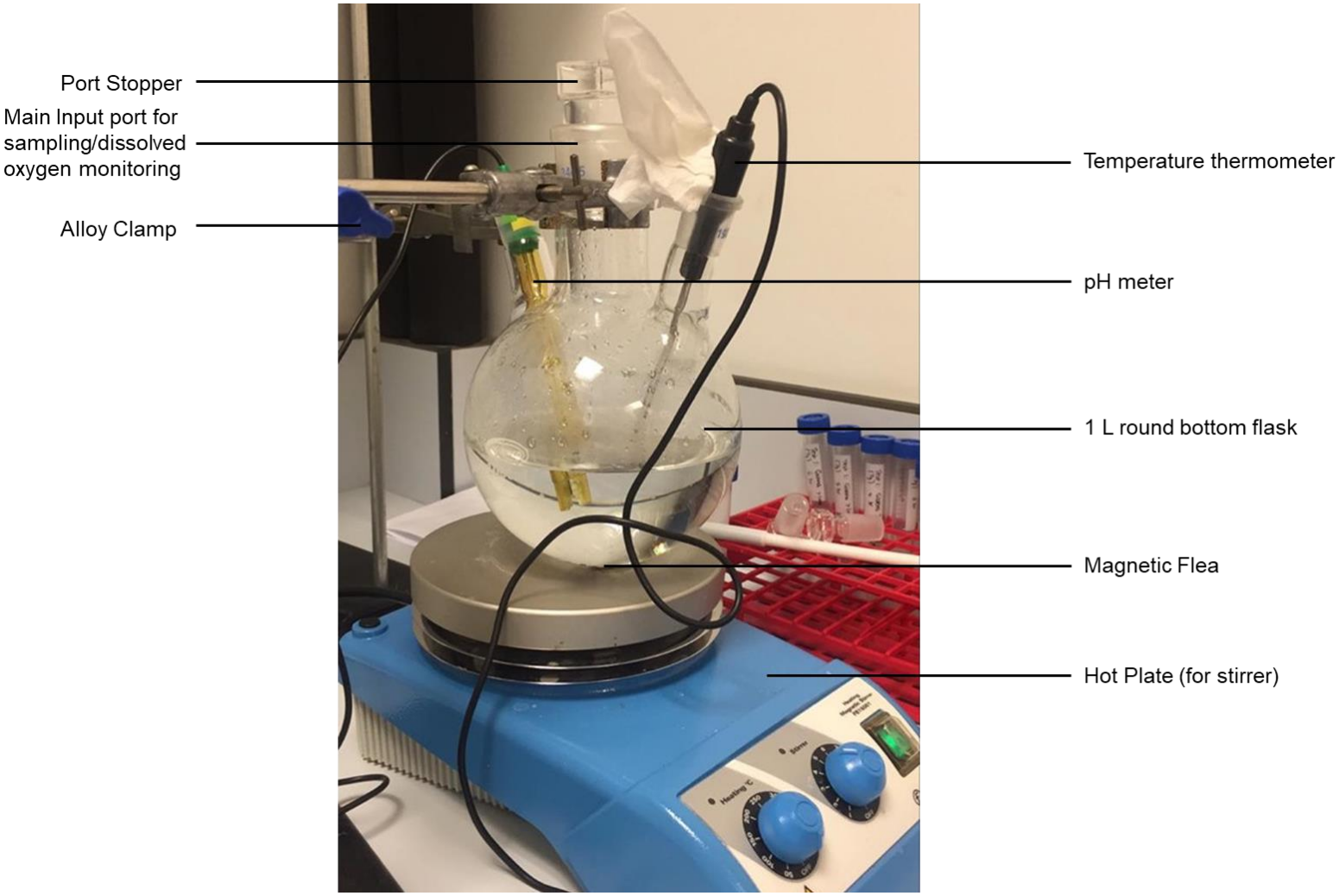

Figure 15: Trial experiment set up: semi-batch, room temperature (~25 °C), ~7.6-7.8 pH, 1 atm pressure. Experimental apparatus: 1 L round bottom flask, hot plate, pH meter, Temperature thermometer, Dissolved oxygen meter, 10 ml mechanical pipette, 5 ml syringe, 0.22 µm pore size filter, 250 ml volumetric flask (±0.15 ml at 20°C), Deionised water, 10 ml sample vials, magnetic flea, and Whatman 1 filter papers.

3.5 Sampling Protocol:

Samples (4.5ml) were taken at intervals (11 in trial experiments; 8 in later experiments) using 10 ml mechanical pipette (±0.28%). Fresh seawater was not added back into the system after each sampling, so a total of 49.5 ml of sample was removed during trial experiments, and 36 ml in later galvanic experiments. Samples were immediately filtered through 0.22 μm pore size filters to halt further sulphide leaching, and then diluted x4 in 1 molar HNO_3 for preservation and to prevent further oxidation.

To account for 49.5 ml and 36 ml volume reductions respectively in experiment runs, a correction was applied to account for any concentrated dissolved elements due to volume reductions. The correction used is sourced from (Salmon and Malmström, 2006), (eq. 3), which assumes that the accumulated amount (N) of element (j) up to sampling interval (k) can be calculated from the measured concentration (C_{meas}), as elements measured in previous elements remain in the system.

$$N_{kj} = [C_{kj,meas}(V_{0,total} - V_{k,ret)} + \sum_{s=1}^{k} C_{sj,meas}V_{s,sample}] \quad (3)$$

Where the total initial volume of solution in the reactor is $V_{0,total}$, the volume returned to reactor is V_{ret} (in this case 0 ml), and the volume of sample removed is V_{sample} (Salmon and Malmström, 2006).

3.5 Experimental Methods

3.5.1 Optical Observations of Natural Samples

Sulphide minerals were identified through hand specimen, cross polarised light and reflective light microscopy, identification relying on the optical and physical properties of each mineral. Pyrite was identified through its characteristic brass yellow-dull brass colour, metallic lustre, and often by its cubic habit. Chalcopyrite was distinguished by its golden yellow-orange colour, often occurring in massive textures. Sphalerite proved difficult to confidently identify, ranging from yellow-brown/black in hand specimen. Secondary-Cu-sulphide minerals were identified mainly by their colour in hand specimen, which ranged from light blue to dark night blue. These minerals appeared more tarnished in hand specimen than the other sulphide minerals, often exhibiting a sub-metallic lustre. Under reflective light both bornite (purple-pink) and covellite (bright blue) were observed, but it was often difficult to distinguish between them, so for this reason they were grouped together to prevent mis-identification. Atacamite was observed in LOG-11 in hand specimen, but not in high enough quantities to be used in experiments. Atacamite was distinguished from secondary-Cu-sulphides, due to its green colouring and dull-vitreous lustre, it also displayed well-formed short prismatic habits.

Polymineralic mineral grains, grain size >1 mm and >500 µm were investigated under reflective light microscopy. Once two different sulphide minerals were identified in individual sample grains, an estimated ratio between the mineral pairs was made and recorded. Once a representative quantity of grain sizes per sample had been recorded with their estimated ratios, an average ratio per sample group was calculated, shown below in Table 4.

Table 4: Average mineral pair ratios calculated from observed grains under reflective light for samples LOG-11 and TP-2L.

SAMPLE	MINERAL PAIR	RATIO
LOG-11	Chalcopyrite : Secondary-Cu-sulphides	3.6 : 6.4
TP-2L	Chalcopyrite : Pyrite	2.3 : 7.7

3.5.2 Electron Microscope Probe Analysis (EMPA)

Sample mounts were carbon coated to 10nm thickness prior to EMPA analysis on the Edwards Auto 306 carbon coater. EMPA was carried out on the sulphide samples and the analysis ran on a Cameca SX100 Electron Probe Micro Analyser, at the University of Bristol, School of Earth Sciences. The electron probe beam was set at 25 Kv, 10 nA for all samples. Detailed EMPA parameter set up can be found in the Appendix (Table 11.1-11.3). Analysed samples include: standard samples Pyrite, Galena, Sphalerite-1, and Sphalerite-2, to assess the major and trace element chemistry of the samples, and to help predict which trace metals will likely leach in the dissolution experiments. Due to access restrictions, EMPA was not carried out for Standard Chalcopyrite. Chalcopyrite in its purest form typically contains 34.5% Cu, 30.5% Fe and 35.0% S, although Au, Ni, and Co may exist in solid-solution, and only small amounts of SiO_2 and CaO (Haldar & Haldar, 2017; Wen *et al*., 2021). EMPA data for sulphides in the natural SMS samples (LOG-11, LOG-13 and TP-2L) is already published in Fallon (2018).

3.5.3 X-ray Tomography (XRT) Analysis

Galena (std) at grain sizes 500 µm and 355 µm and Pyrite (std) at grain size 500 µm were analysed using a Zeiss Xradia 520 Versa at the School of Life Sciences, University of Bristol, UK, to calculate surface area. Data TIFF stacks for analysis were processed on DragonFly software. Each sample TIFF stack was split into different regions of interest (ROI): mineral grain, pore space, and mineral inclusions, allowing for a multi-ROI to be created so that surface area could be calculated for each sample, removing pixels for pore space and mineral inclusions from the calculation. Surface area calculated can be seen in Table 5 and the ROI for each sample in Figure 16.

Table 5: Surface area calculated on DragonFly, using XRT analysis TIFF stacks for each mineral and grainsize.

Mineral	Density (g/cm³)	Grainsize (µm)	Volume (µm³)	Mass (g)	Surface Area (µm³/g)	Surface Area (m³/g)
Galena (PbS)	7.4	355	1.E+10	0.093	1.30E+09	1.30E-03
Galena (PbS)	7.4	500	3.E+10	0.250	1.83E+09	1.83E-03
Pyrite (FeS_2)	5.01	500	3.E+10	0.159	1.91E+09	1.91E-03

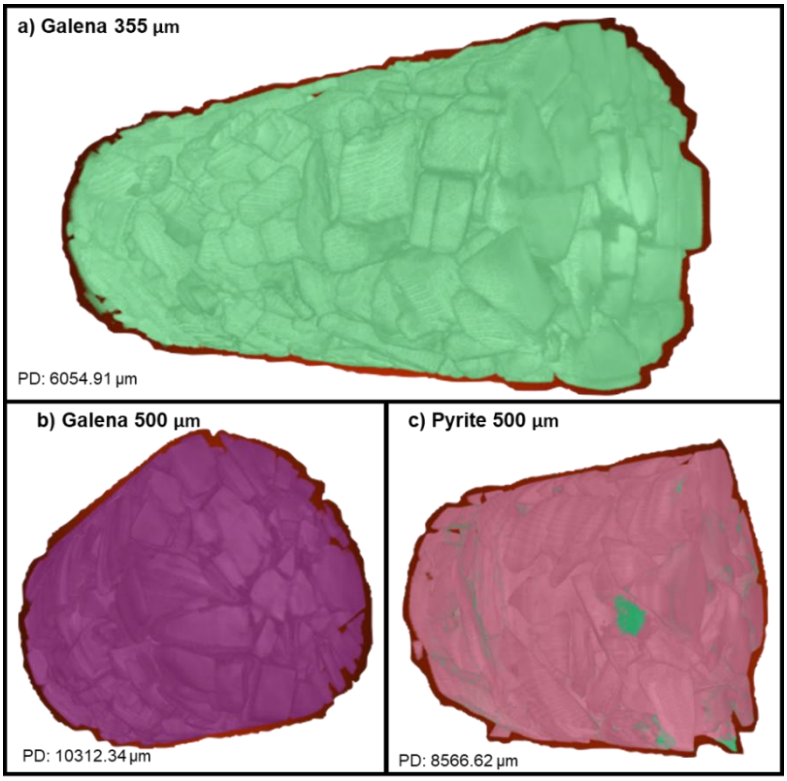

Figure 16: Shows the region of interest (ROI) for each sample in which surface area is calculated from. a) and b) samples don't contain any mineral inclusions so only one ROI is necessary. Whilst c) contains mineral inclusions within the pyrite sample. These inclusions are not incorporated into the pyrite grains surface area, and any grains which contain mineral inclusions or different mineral phases will be removed prior to experiments.

3.5.4 Seawater Analysis

The seawater used in experiments was according to the international standard (American Society For Testing and Materials-ASTM D1141, 2013).

Seawater metal detection limits by ICP-OES

Limits of detection (LOD) for target metals were measured, in order for the sample mass needed for each experiment to be estimated in the experimental design. To do this, synthetic seawater was doped with 50 ppb of the following metals: Cu, Zn, Fe, Mn, Ni, Cd, Co, Pb, As, Sb. The seawater solution was diluted x20 to prevent damage to the ICP-OES torch from the high levels of Na in the seawater. The metals added to the synthetic seawater were from standardised stock solutions in HNO_3. Artificial seawater according to ASTM D1141-98 standard metal concentration can be found in Table 6.

Table 6: Artificial seawater ASTM D1141-98 (2013) metal concentration.

Element	**Artificial seawater (ASTM D1141-98)**
	Concentration (ppb)
As	<1
Se	<1
Sb	<10
Co	<10
Mo	<30
Sn	<20
Cd	2.14
Cu	2.18
Pb	0.683
Ni	2.75
Zn	4.68
Ca	494
Fe	<100
Mn	27.5
Hg	0.39

Different standards were made up of the doped synthetic seawater solution to different concentrations and then put through the Inductively Coupled Plasma (ICP-OES) Spectroscopy machine. The LOD and limit of qualification (LOQ) were calculated from Equations 4 and 5, yielding the following results in Table 7.

$$\boldsymbol{LOD = (\Delta results + 3STD)} \quad (\mathbf{4})$$

$$\boldsymbol{LOQ = (\Delta results + 10STD)} \quad (\mathbf{5})$$

Table 7: Calculated limits of qualification (LOQ) and limits of detection (LOD) of ASTM D1141-98 synthetic seawater standard from ICP-OES analysis.

Element	LOQ (ppb)	LOD (ppb)
As 188.980	82.9	22.3
Cd 226.502	6.2	2.4
Co 228.615	9.5	3.3
Cu 224.700	19.8	7.7
Fe 238.204	3.7	2.3
Fe 259.940	4.1	1.7
Mn 257.610	2.7	1.4
Mn 259.372	3.2	1.7
Ni 216.555	7.0	1.9
Ni 230.299	9.9	3.4
Pb 217.000	204.4	69.6
Pb 220.353	36.7	12.1
Sb 217.582	93.0	10.8
Zn 213.857	37.3	13.9

3.5.5 Analytical Techniques

pH, Temperature, Dissolved Oxygen

pH, DO and temperature were recorded at the start and at sampling intervals during experiments, so that any changes could be accounted for. DO was recorded in trial experiments, but not in later galvanic experiments. pH and temperature were recorded using HQd Portable Meter, and DO using HI 9146. The pH meter probe was calibrated prior to use with pH buffer solutions: 4.01, 7.01, and 10.01, with uncertainty ±0.1-0.4, and ±0.3°C for temperature. The DO meter was calibrated prior to use at 100% saturation (ppm) with no salinity correction. A salinity correction was applied after calibration to 40 g/L, to correct for the effect high salinity in seawater has on dissolved oxygen readings.

3.5.6 ICP-OES Sample Analysis

Sample solutions in seawater dissolution experiments were analysed using an Agilent 710 inductively coupled plasma – optical electron spectrometer (ICP-OES) at the School of Earth Sciences, University of Bristol, UK. All samples were diluted prior to analysis in 1 molar HCl acid; samples were diluted x2 for initial trial experiment runs and x4 for later experiments.

The trial experiments allowed for the dilution factor of the remaining experiments to be calculated, as the large sample sets gave insight to how much sodium the ICP-OES torch could withstand in each analysis. Element concentration units are displayed in ppb (µg/L).

A range of element wavelengths were selected for each analysis run to increase the likelihood of an element being detected, and represented as element lines. The ICP-OES detects differences in wavelengths and recognises which element that energy belongs to from its signal. Post analysis the element lines with the best intensity (signal) and minimum interference are chosen for each element, as explained in Figure 17.

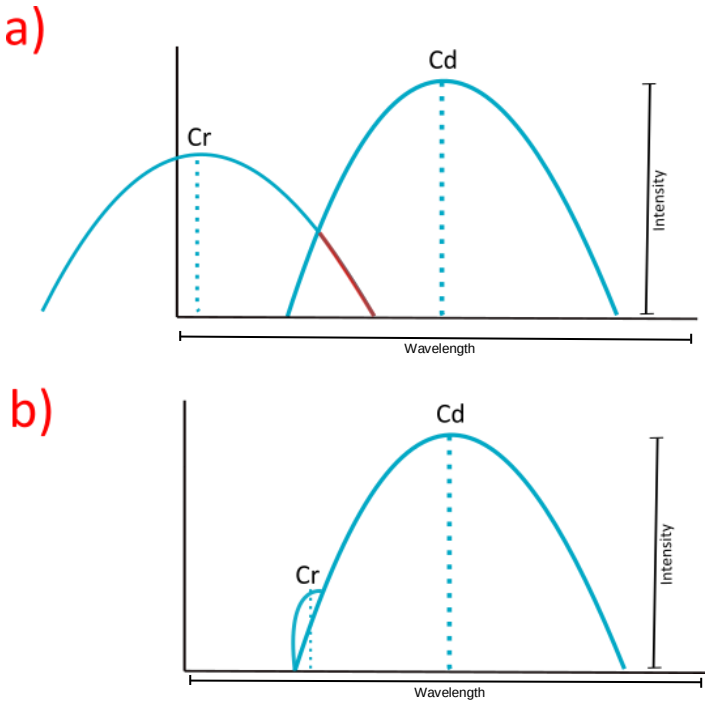

Figure 12: illustrates how intensity and interference influence which element wavelengths are picked for the data. Section (a) displays two lines with good intensity and low interference, so increases confidence that the energy signal detected comes from the desired element e.g. Cd or Cr. Section (b) shows how Cr with a lower intensity and high interference from Cd, reduces confidence in the signal detected to be Cr, as it may be a signal from the Cd interference. Therefore the lines in section (a) would be chosen to ensure no interference.

3.5.7 Corrections Applied

ICP-OES analysed samples were drift corrected, corrected for dilution factors (x2, x4, x20) with nitric acid, and corrected for volume reductions through sampling. Data below detection limits (bdl.) and negative values were removed from datasets, along with element wavelengths that did not produce acceptable lines.

4.0 Sample Characteristics Results

4.1 EMPA Results

EMPA analysis results are presented in Table 8, highlighting the trace chemistries for samples Pyrite (std.), Galena (std.), and Sphalerite-1/-2 (std.) for the given analysed elements: S, Pb, Cu, Ni, Fe, Mn, Zn, Co, As, Cd, Hg, Sn, and Sb.

As well as the expected major element components Pb and S, the interesting trace elements for Galena (std.) are iron, arsenic, mercury, and antimony. The low standard deviation (SD) for the elements detected in galena, particularly Pb, gives confidence in the purity of the sample for the dissolution experiments.

The main constituents found in Pyrite (std.) are sulphur and iron, with trace amounts of nickel, cobalt, and arsenic. The low SD for elements present in pyrite again gives confidence regarding the dissolution experiments and in predicting what elements will be leached.

Sphalerite-1 (std) contains bulk sulphur, zinc and iron; with traces of copper, arsenic, cadmium, mercury and antimony. Leached metals in experiments are expected to largely be of zinc and iron, along with trace metals, with the SD for elements being low.

Sphalerite-2 (std) is made up of high concentrations of sulphur, zinc, iron, and copper, and trace amounts of arsenic, antimony, mercury and cadmium. However, the SD for both iron and zinc is high decreasing confidence in the purity of sphalerite-2 and indicates that there is high variability between grains. Therefore, sphalerite-2 won't be used in dissolution experiments, as the uncertainty surrounding concentration may lead to confusion when analysing leachate concentrations.

The geochemistry of the above samples is also useful to know in terms of potential toxicity. It is well established that trace metals in high concentrations, can be harmful in many organisms. With Cu, Zn, Pb, Fe, As, hg, Ni, and Cd present in the analysed samples, being harmful to aquatic life (Wang, 1987; Simpson and Spadaro, 2016). Although as previously discussed the tolerance levels to trace metals across different organisms is variable, if metals leached from sulphide minerals are in high concentrations during sulphide oxidation (during mining), they will likely have negative impact on seafloor environments and ecosystems.

Table 8: EMPA results: Composition of standard sulphides (Pyrite, Galena and Sphalerite (1 & 2) in wt% for major elements and ppm for minor elements. Analysed elements S, Pb, Cu, Ni, Fe, Mn, Zn, Co, As, Cd, Hg, Sn, and Sb.

	S		Pb		Cu		Ni		Fe		Mn		Zn	
Sample	**mean (wt%)**	**SD**	**mean (wt%)**	**SD**	**mean (wt%)**	**SD**	**mean (ppm)**	**SD**	**mean (wt%)**	**SD**	**mean (ppm)**	**SD**	**mean (wt%)**	**SD**
Galena	14	0.14	87	0.46	0.01	0.02	135	0.50	0.03	0.00	133	0.61	0	0.00
Pyrite	54	1.08	0.00	0.02	0.00	0.00	103	0.45	46	1.03	91	0.58	0	0.00
Sphalerite-1	34	0.30	0.01	0.01	0.02	0.03	91	0.49	11	0.44	91	0.49	56	0.59
Sphalerite-2	34	0.73	0.01	0.01	10	16	92	8.39	12	12.23	90	0.74	45	27.97

	Co		As		Cd		Hg		Sn		Sb	
Sample	**mean (ppm)**	**SD**	**mean (ppm)**	**SD**	**mean (ppm)**	**SD**	**mean (ppm)**	**SD**	**mean (ppm)**	**SD**	**mean (ppm)**	**SD**
Galena	100	0.40	110	1.24	286	9.02	243	1.20	255	0.94	313	1.54
Pyrite	86	0.60	102	2.14	152	0.67	208	1.50	165	0.69	196	3.15
Sphalerite-1	70	0.51	151	3.40	160	1.28	254	1.76	174	3.87	207	0.88
Sphalerite-2	70	4.56	147	11	147	4.62	253	11.26	172	3.83	206	4.91

5.0 Results

5.1 Trial Experiment Results

5.1.1 Grain Size Effect

Different grain sizes (>1000-~2000 µm >500-1000 µm) of sphalerite-1 std. sample were experimented on to determine the best grain size for metal leaching for subsequent seawater dissolution experiments.

Grain size results are presented in Figure 18, the same trend is observed over all plots (abc) with >500-1000 µm consistently leaching higher concentrations of each element (Fe, Pb, Zn), than >1000-2000 µm. This is as expected due to the larger surface area for sulphide oxidation associated with smaller grain sizes, therefore more reactive to oxidation. While both grain size fractions produced concentrations above ICP-OES detection limits, concentrations remain relatively low. Therefore, for the galvanic dissolution experiments to follow, a smaller grain size fraction of >355-500 µm, was used to increase surface area and to ensure that any metal leaching is confidently detected by the ICP-OES. This is especially important as later experiments were diluted by a factor of x4, whilst trial experiments were only diluted x2.

Zn concentrations leached from sphalerite-1 are lower than anticipated for sphalerite. This may be due to the presence of silicates and other sulphide minerals in the sphalerite-1 sample, as mineral picking was not carried out prior to trial experiments. This issues surrounding the sphalerite-1 sample are discussed further in Sections 5.1.3 and 6.3.1.

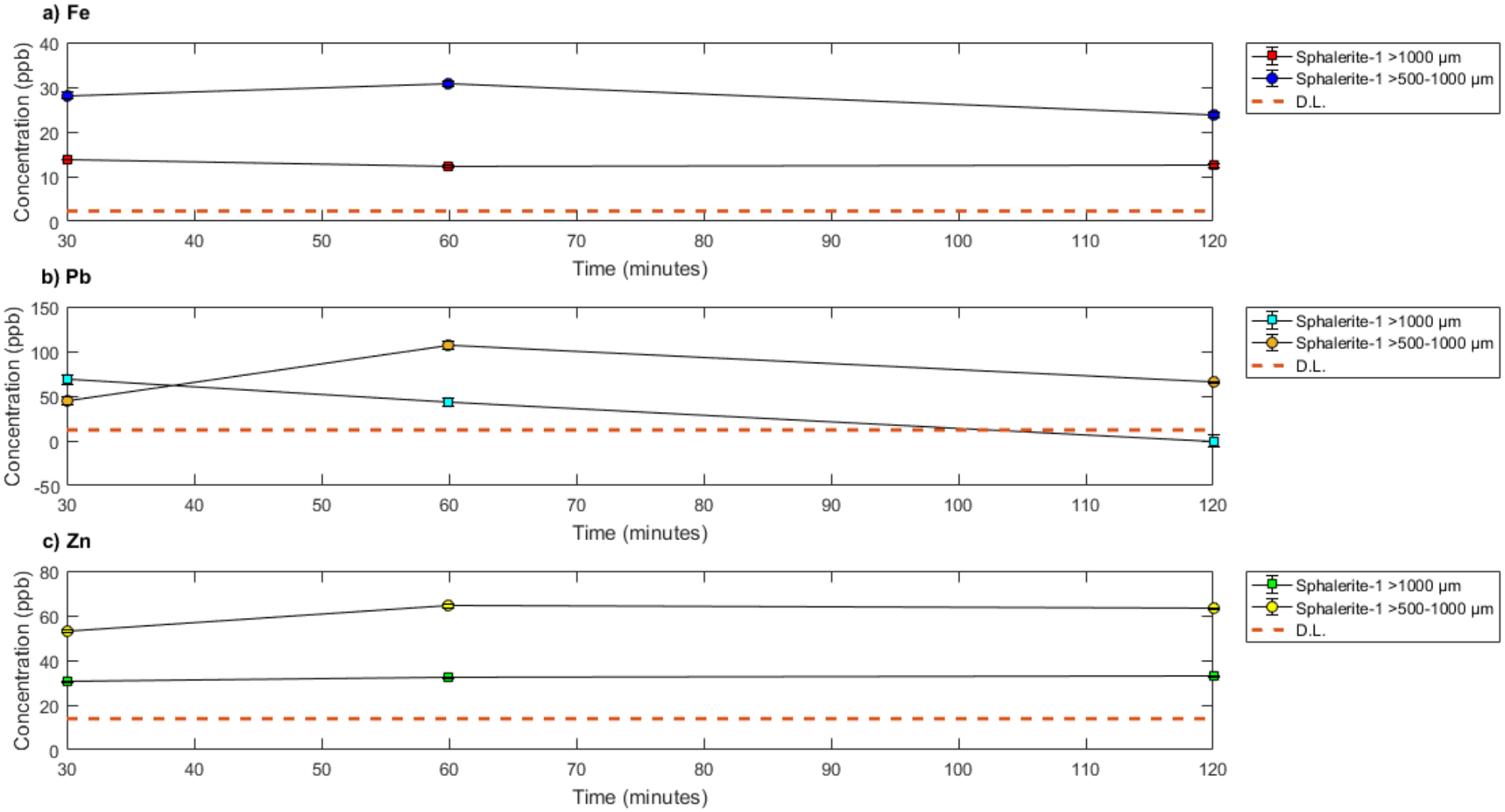

Figure 21: Concentration of Fe, Pb, and Zn for two grainsize fractions of sphalerite-1 (>1000 µm & >500-1000 µm). Data for sphalerite-1 >500-1000 µm experiment was normalised to 5g mass of sample for better comparison with sphalerite-1 >1000 µm experiment. **a)** Fe concentration leached from both experiments, show that the smaller grainsize fraction (>500-1000 µm) produces higher Fe concentration in solution by almost double that of the >1000 µm size fraction. **b)** Sphalerite-1 >1000 µm grainsize initially has a higher concentration of Pb at 30 minutes, before the >500-1000 µm grainsize fraction increases to higher Pb concentrations after an hour reaching a high of ~100 ppb. **c)** Shows a similar trend for Zn leaching, with the smaller grainsize fraction >500-1000 µm leaching significantly higher amounts of Zn than the >1000 µm size fraction, reaching a high of ~60 ppb. Abbreviation: D.L. = bdl.

5.1.2 Development of Mass:Fluid Ratios

Fluid ratios were investigated in trial experiments so that a minimum mass of sample that would leach high enough metal concentrations for the ICP-OES to detect could be determined, for the subsequent dissolution experiments. Standard galena was used for this, with different masses experimented with against 500 ml of artificial seawater, as can be seen in Table 13 (Appendix). The relationships between different mass:fluid ratios can be more clearly observed in Figure 19, where the elements with the highest concentrations from the galena trial experiments are plotted against each other for different masses. It is immediately clear from the results presented in Figure 19 that the leachate concentrations for Pb are not as expected for galena, indicating that something may have gone wrong whilst carrying out these experiments.

Despite the flaws in these experiments data, the process was still useful in the development of the dissolution experiments for later galvanic dissolution experiments. For instance, these trial experiments helped with the decision for smaller grain sizes (>355-500 μm) and therefore larger surface areas to be used in the later galvanic dissolution experiments. Fluid ratios were also developed so that 250 ml of seawater would be used instead of 500 ml, encouraging leachate in the experiment flask to be more concentrated, and well above detection limits for the ICP-OES, so that patterns could be identified with increased confidence.

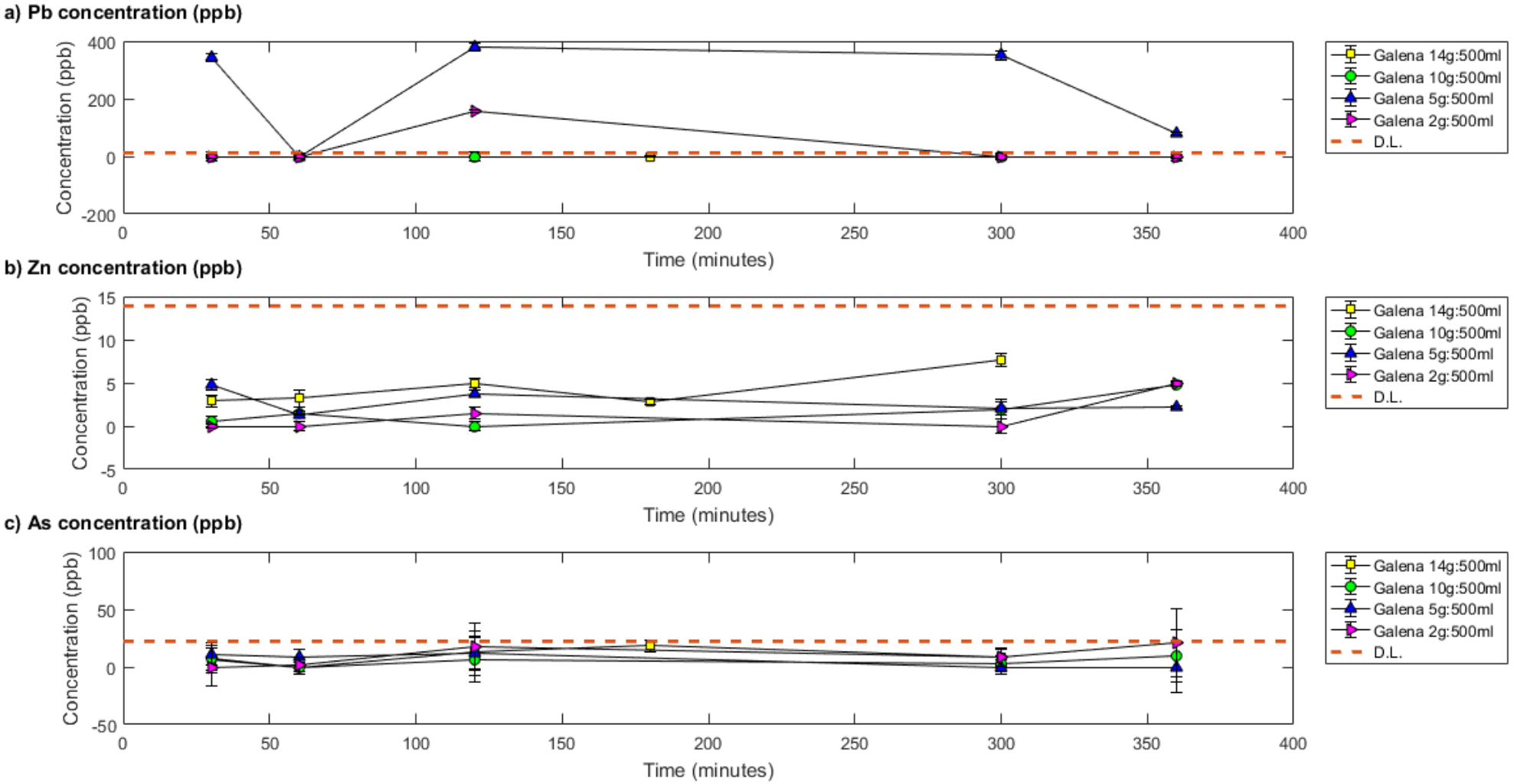

Figure 22: Pb, Zn and As concentrations (ppb) across trial experiments E2-E6 (experiment runs), showing the effect mass:fluid ratios (mass(g):seawater(ml)) has on metal leaching. **a)** Shows that for 14g and 10g of galena no Pb is leached across the duration of the experiment, while 2g of galena sees a small peak of Pb (ppb) at 2 hours, and substantially higher Pb concentrations when 5g of galena is used. **b)** Zn leachate concentration is highest when 14g of galena is used, with 5g showing the next highest increase. 10g and 2g both see the lowest Zn concentrations, 2g seeing a jump in concentration at 6 hours. **c)** As concentration behaves relatively the same across all masses, with 2g of galena leaching the most As by a small margin. Abbreviation: D.L. = bdl.

5.1.3 Trial Experimental Results For Standard Minerals

Standard Galena:

Trial experiments with galena see Pb (up to 380 ppb) to be the dominant dissolved element in solution from this lead sulphide, with the 5g:500ml ratio leaching the highest concentrations. Low/trace amounts of As (up to 20 ppb), Sn (up to 30 ppb), Zn (up to 7 ppb), Cr and Sb are also detected across standard galena experiments. This is concordant with previous EMPA data for galena that shows traces of As, Sn, Zn, Cr and Sb also present.

Standard Sphalerite-1:

Only two trial experiments using sphalerite-1 were analysed, with dominant concentrations of Pb (up to 68 ppb) and Zn (up to 46 ppb) observed. Moderate concentrations of Cu (up to 14 ppb), Fe (up to 13 ppb), and Sb (sporadically as high as 30 ppb) are also detected, along with low amounts of As and Mn.

Prior to trial experiments sphalerite-1 wasn't individually picked to separate out other sulphide minerals such as pyrite, galena and silicates as the presence of these minerals were unknown until an XRT analysis was carried out. Therefore, trial experiments with sphalerite-1 are not monomineralic, and galvanic cells between mineral pairs may have been set up. This would account for why Zn is observed during the trial experiments, and not in later monomineralic dissolution experiments with sphalerite-1. This also helps explain why the leached concentrations from dissolution experiments, are not concordant with EMPA data, where Zn makes up 56 wt% of sphalerite-1 and Fe makes up 12 wt%.

While these trial experiments are not helpful in revealing how sphalerite-1 behaves on its own, it does give an indication to what later polymineralic experiments may look like.

5.1.4 Mass Differences

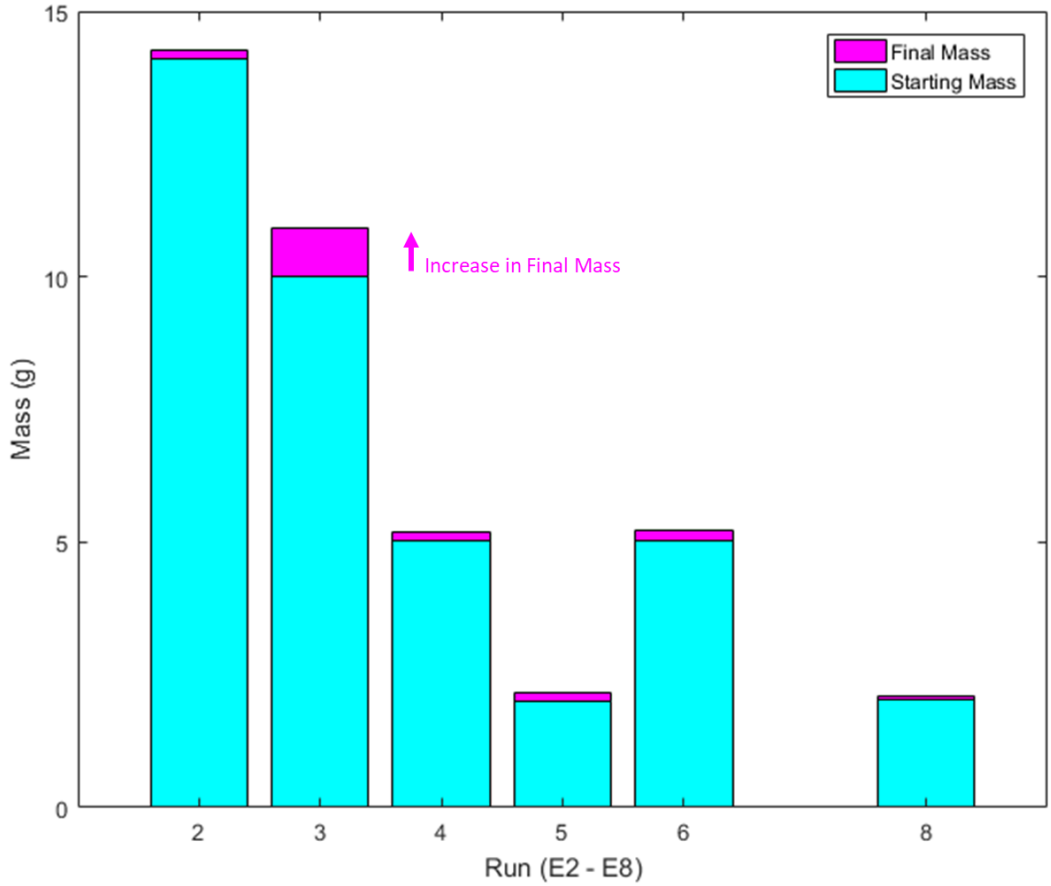

Figure 23*:* Displays the change in mass (g) from mass at the start of each experiment run (E2 – E8), compared to the mass at the end of each run. For all experiment runs the final mass is higher than the start mass. Experiment runs E2-E5 used galena std. (>1000 µm), E6 used sphalerite-1 std. (>1000 µm), and E8 used sphalerite-1 std. (>500-1000 µm).

Sample mass was measured at the start of each experiment to two decimal places, and again at the end. As seen above in Figure 20 for every trial run, final mass is higher than the start mass. The opposite might be expected due to sample loss occurring throughout the experiment process through sampling, measurements (pH, DO, temperature) being taken and post-experiment filtering. However, this increase in mass might suggest the presence of oxides forming or dissolved salts from the seawater precipitating onto sample grains and/or filter papers, increasing overall final mass. This is observed in Fallon (2018), with post-experimental analysis (XRD) of powdered sulphide ores, revealing the presence of a new halite-phase, indicating the precipitation of salt from the seawater solution.

Due to the ambiguity of mass changes in the trial experiments the decision was made that final mass would not be recorded in the dissolution experiments that followed.

5.1.5 Temperature Variation

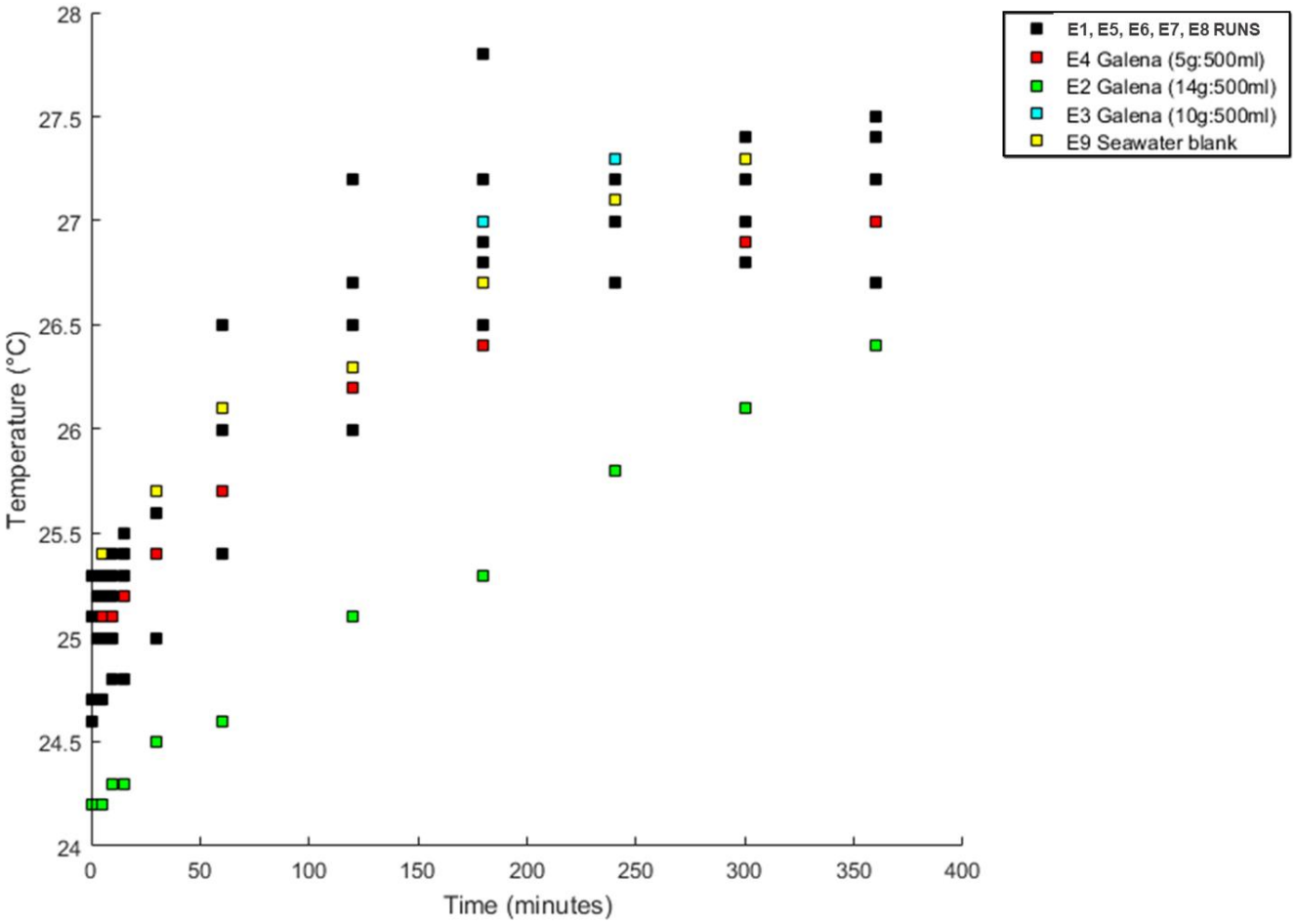

Figure 24: Temperature recordings across trial experiment runs E1, E5, E6, E7 and E8 (black) and seawater blank E9 (yellow), with E4 (Galena >1000 µm 5g:500ml) highlighted in red, E2 (Galena >1000 µm 14g:500ml) highlighted in green, and E3 (Galena >1000 µm 10g:500ml) highlighted in blue.

Figure 21 highlights the typical temperature fluctuations across trial experiments, with experiments typically increasing ~2 °C over the 6 hour experiments. Start temperatures vary depending on room temperature on the day. However, even with attempts to stabilise room temperature, heat generated by the motor used for magnetic flea, increased temperatures in the flask over the course of experiments. Although fluctuations in temperature are not ideal, it doesn't seem to have had much of an effect on the leaching of elements into solution. For example, Figure 21 shows the temperature fluctuations for E4, E2, and E3, where E3 has the highest temperatures recorded, E4 has a temperature in the middle, and E2 has the lowest temperatures. When compared to Figure 19 plot a) E4 (5g:500ml galena) has the highest concentration of Pb, while E2 (14g:500ml) and E3 (10g:500ml) both have no Pb leached. If small temperature fluctuations had a strong control on these experiments, E3 would be expected to leach the highest concentration of Pb out of all three experiments; it can be seen that this isn't the case.

5.1.6 pH Variation

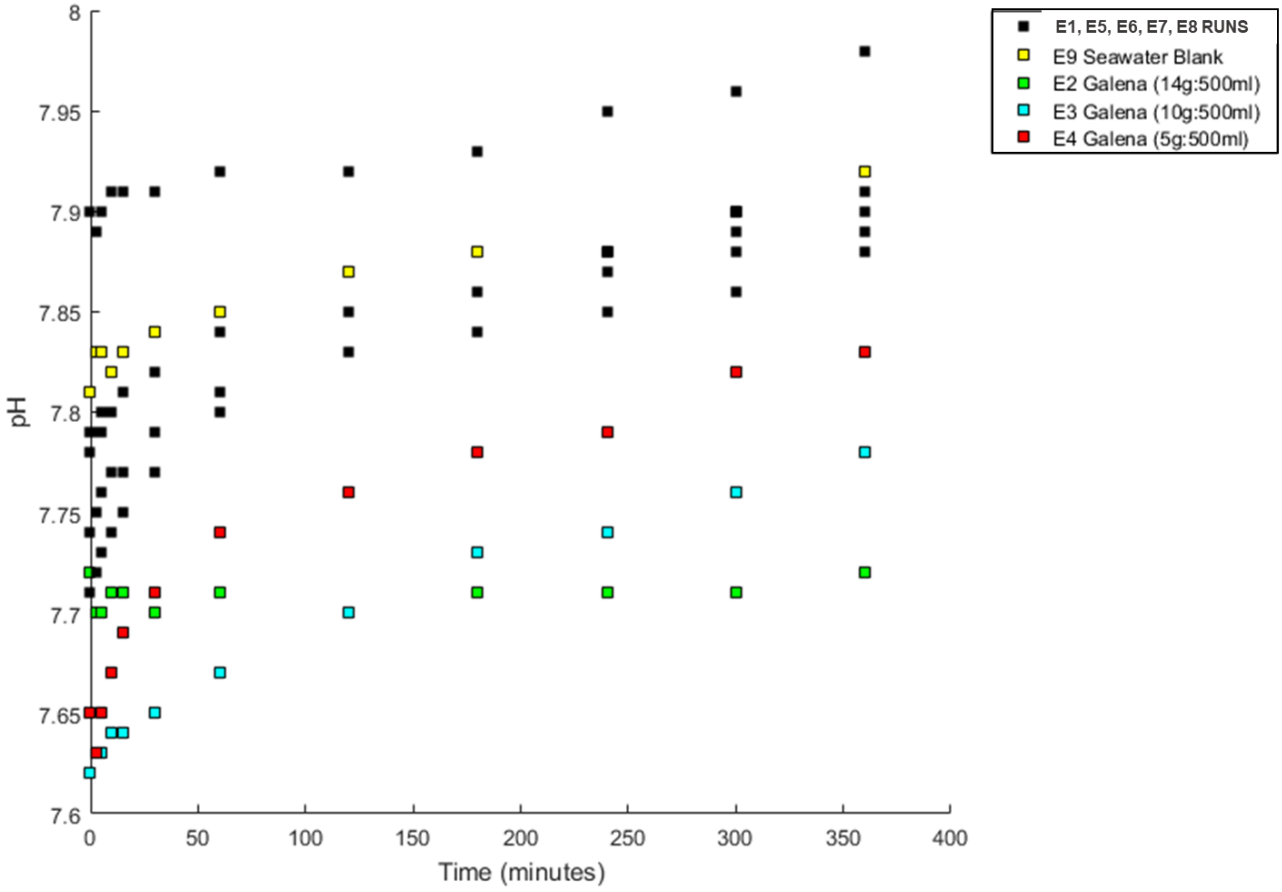

Figure 25: pH measurements across trial experiment runs E1, E5, E6, E7 and E8 (black) and seawater blank E9 (yellow), where E2 (Galena >1000 µm 14g:500ml) is highlighted in green, E3 (Galena >1000 µm 10g:500ml) in blue and E4 (Galena >1000 µm 5g:500ml) in red.

Figure 22 displays the fluctuations in pH across all trial experiments, and shows how starting pH varies from pH 7.6 to 7.9. Fluctuation of pH over the course of 6 hour experiments follows a relatively similar trend for all trial experiments, with an initial rapid increase in pH, developing into a more gentle increase after ~1 hour. Starting pH is important as it may influence the rate at which sulphide minerals dissolve, with more acidic conditions favouring increased metal leaching (Fallon, 2017). Although in these trial experiments all starting pH were neutral and the effect of starting pH does not seem to have had a strong control on metal leaching in the trial experiments over this pH range. With E4 in Figure 22 having a more alkaline starting pH than both E2 and E3, whilst still leaching higher concentrations of Pb. Nonetheless, the range of starting pH across the trial experiments was not desirable, therefore artificial seawater was purchased in bulk for the seawater dissolution experiments, eliminating such pH variation that seemed to occur in the lab made seawater.

5.1.7 Dissolved Oxygen Range

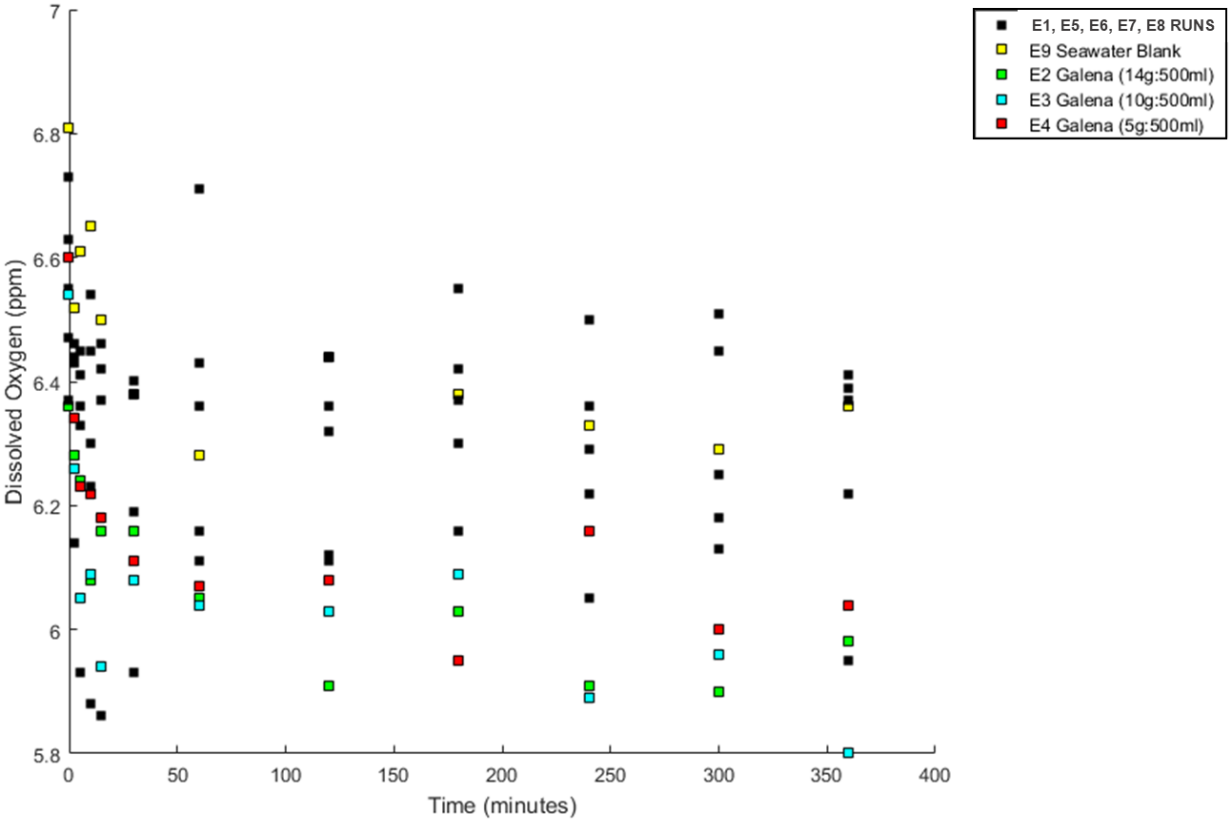

Figure 26: Dissolved oxygen (ppm) measurements across trial experiment runs E1, E5, E6, E7 and E8 (black) and seawater blank E9 (yellow), where E2 (Galena >1000 µm 14g:500ml) is highlighted in green, E3 (Galena >1000 µm 10g:500ml) in blue and E4 (Galena >1000 µm 5g:500ml) in red.

DO wasn't controlled and experiments were allowed to equilibrate with the air of the laboratory where they were conducted. Figure 23 shows that starting DO varies between 5.9–6.8 ppm across experiments, this likely being dependent on room conditions of the laboratory on set days. While starting DO varies, trends over the duration of experiments are relatively similar, with rapid decreases in DO being observed during the first 15 minutes of experiments, before they start to plateau. This initial rapid decrease could be due to addition of sample at the beginning of each experiment with sulphide oxidation using up DO. Alternatively, it could be due to the fact that prior to each experiment, the experiment flask was allowed to equilibrate with the room DO, with all valves open, and then upon experiments starting some of those valves were closed to create a semi-batch system. The latter being more likely, as this same trend with an initially rapid decrease in DO is seen in the seawater blank E9, where no sample was added.

DO does not seem to have a strong effect on the leaching of metals from trial experiments. For example, in Figure 23, E2, E3 and E4 all have different starting DO, but during an initially rapid decrease, DO values become more similar within the first hour, before later diverging once again.

6.0 Galvanic Effect Experiments

6.1 Monitored Temperature Differences

6.1.1 Standard Sample Experiments:

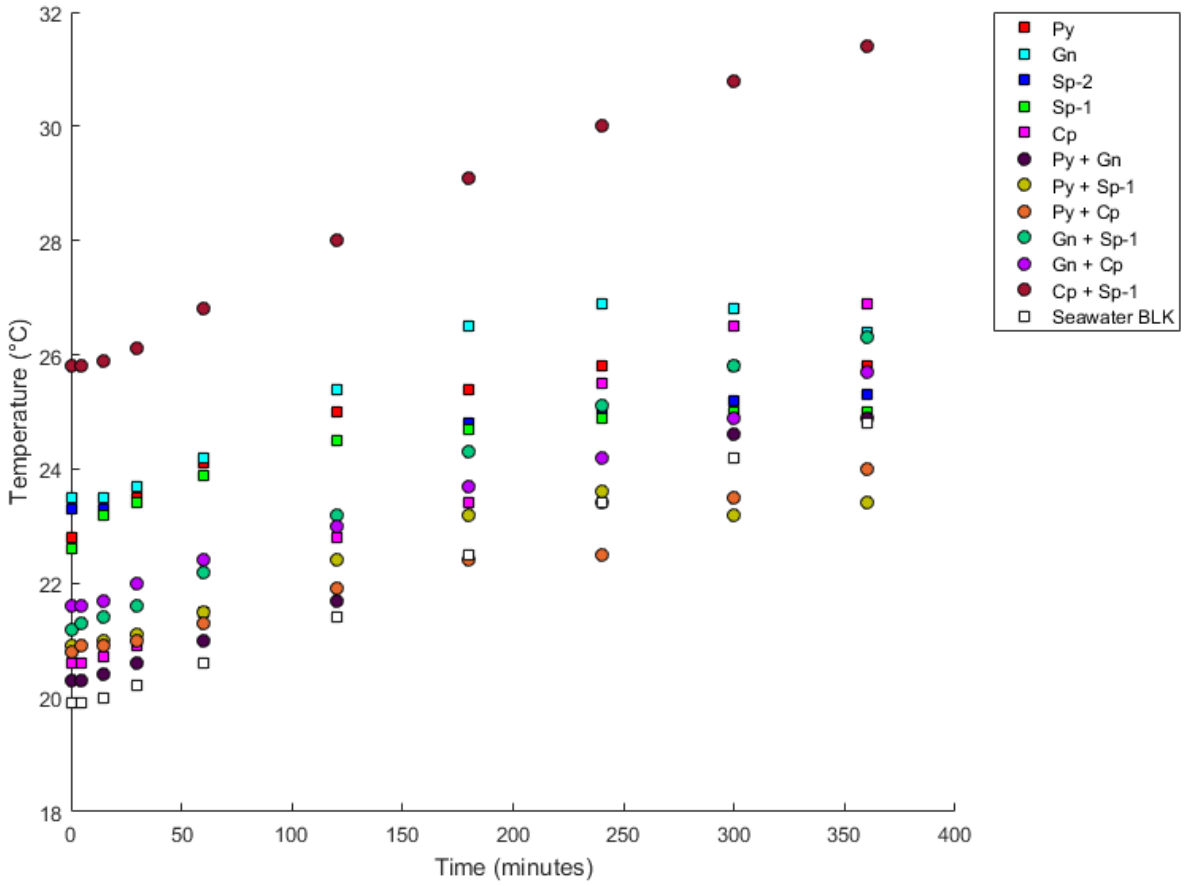

Figure 27: Temperature recordings across all standard mineral seawater dissolution experiments E1-E17 and seawater blank E25. Monomineralic experiments are represented by a square marker, whilst polymineralic is presented by a circle marker. Sample abbreviations are as follows: Py = pyrite, Gn = galena, Sp-2 = sphalerite-2, Sp-1 = sphalerite-1, Cp = chalcopyrite, and BLK = blank.

Start temperatures followed the same pattern as previously discussed for trial experiments (Section 5.1.5), varying significantly between experiments, with a range of ~6 °C observed, Figure 24. The majority of start temperatures fell between 20 °C and 23 °C. Cp + Sp-1 of Figure 24 has an anomalously high starting temperature as it was conducted during a heat wave in the summer months. This increase in temperature may have a small control on the results obtained, as sulphide oxidation rates increase under high temperatures.

Generally, experiments follow similar trends with temperature increases being observed until ~4 hours, coinciding with the hottest time of the day, before plateauing. On average temperature increases ~2 °C over experiment durations, as the experiment flasks got gradually heated by a hot plate, coupled with increasing background temperatures of the laboratory.

Although these fluctuations in temperature are not ideal, it can be assumed that the effect these temperature fluctuations (20 °C and 23 °C) has on sulphide leaching are negligible, as monomineralic experiments were on average conducted under hotter conditions, and still consistently leached lower concentrations of elements. While polymineralic experiments were generally conducted under cooler conditions and leached higher concentrations of elements. However, it should be noted that concentrations may have generally been lower in monomineralic experiments and any concentration increases from galvanic effects may be a minimum effect, as larger concentration differences may have been observed if monomineralic and polymineralic experiments were conducted at the same temperatures. This is the opposite of what would be expected if temperature (at room temperature) had a bigger control on the leaching of metals from sulphide minerals. This relationship changes when more extreme temperature differences are observed, as for the high temperature experiments conducted at 50°C, where temperature does then have a stronger control on metal leaching.

6.1.2 Natural Sample Experiments:

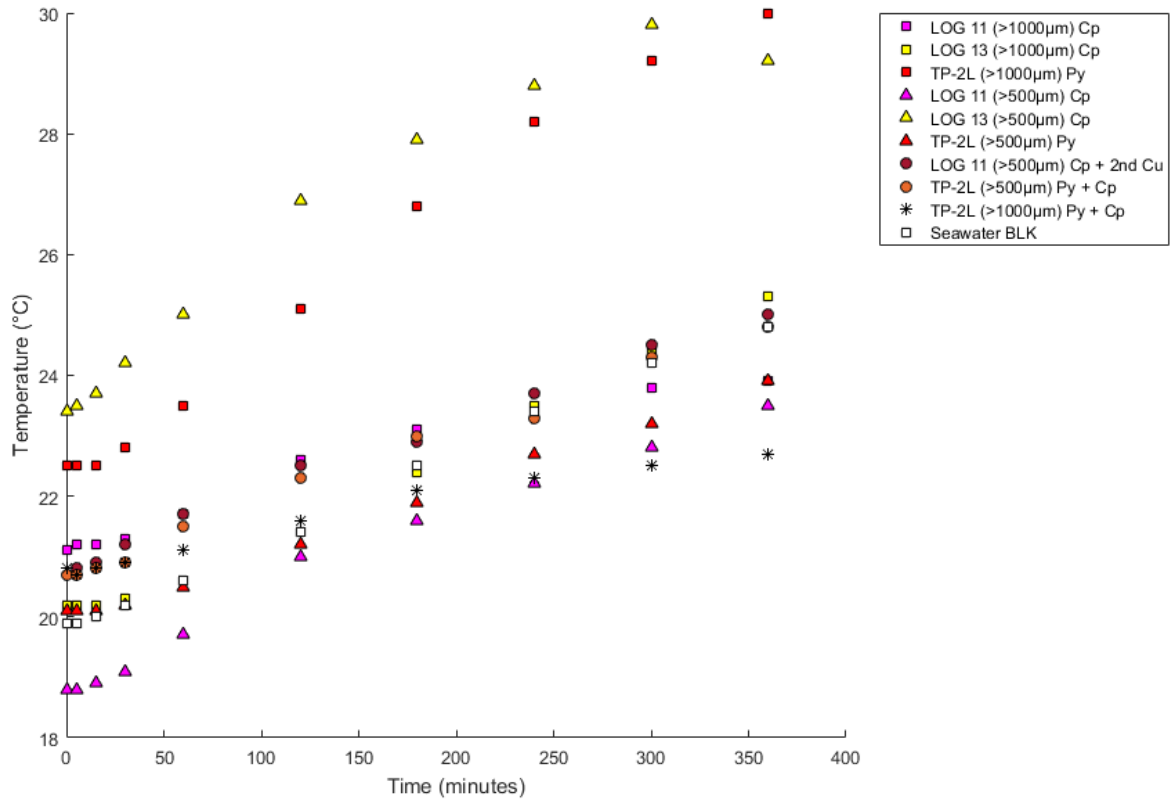

Figure 28: Temperature recordings across all natural sample seawater dissolution experiments E6-E24 and seawater blank E25. Monomineralic experiments are represented by a square marker (at >1000 µm) and triangle (at 500-1000 µm), whilst polymineralic is presented by a circle marker (at 500-1000 µm) and '*' (at >1000 µm). Mineral abbreviations are as follows: Py = pyrite, Cp = chalcopyrite, 2nd Cu = secondary-Cu-sulphides, and BLK = blank.

As seen previously, start temperatures vary across different experiments with the majority falling between 20 °C and ~21 °C, as seen in Figure 25. LOG-13 (>500 µm) Cp and TP-2L (>1000 µm) Py

both have higher start temperatures, as they were conducted during a heatwave in the summer months. These higher start temperatures may have increased the rate in which the sulphide samples oxidised effecting results, therefore these experiments were not discussed in comparison with the polymineralic counterparts.

Temperature fluctuations during experiment runs follow a similar trend to the standard samples, with a gentle increase in temperature observed over the 6 hours. Increasing on average ~3 °C, except for those with anomalously high start temperatures, which increased drastically across the duration of experiments ~8-9 °C.

6.2 Monitored pH Differences

6.2.1 Standard **Samples***:*

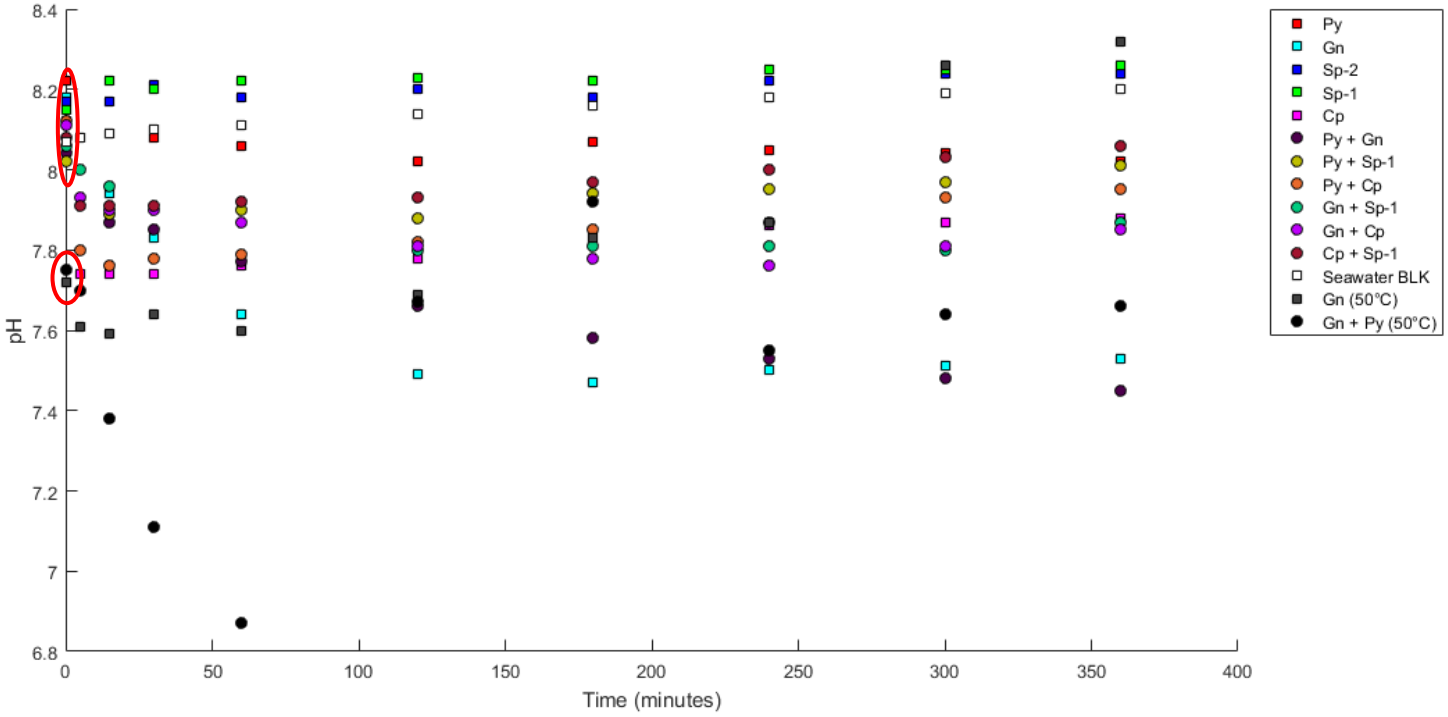

Figure 29: pH recordings across all standard mineral seawater dissolution experiments E1-E19 and seawater blank E25. Monomineralic experiments are represented by a square marker, whilst polymineralic is presented by a circle marker. Sample abbreviations are as follows: Py = pyrite, Gn = galena, Sp-2 = sphalerite-2, Sp-1 = sphalerite-1, Cp = chalcopyrite, and BLK = blank. Starting pH's circled in red.

Figure 26 presents all pH readings across the standard sample experiments. Start pH for the majority of standard sample experiments falls between a pH of ~8.0-8.2, this is a much smaller range than of that previously observed in the trial experiments. The high temperature (50 °C) experiments fall out of this range, with starting pH's in-between 7.7 and 7.8.

pH fluctuations follow a similar trend across all standard sample experiments at room temperature. With an initial decrease in pH observed in the first 30 minutes, before a plateau between 1-5 hours,

with a gentle increase observed after 5 hours. High temperature (50 °C) experiments behaved differently, with monomineralic galena (50 °C) showing an initial decrease in pH, before rising substantially for the remainder of the experiment. Polymineralic galena & pyrite (50 °C) display an initially drastic decrease in pH for up to an hour, before jumping back up to a pH close to its starting pH and plateauing for the remainder of the 6 hours.

6.2.2 Natural Samples:

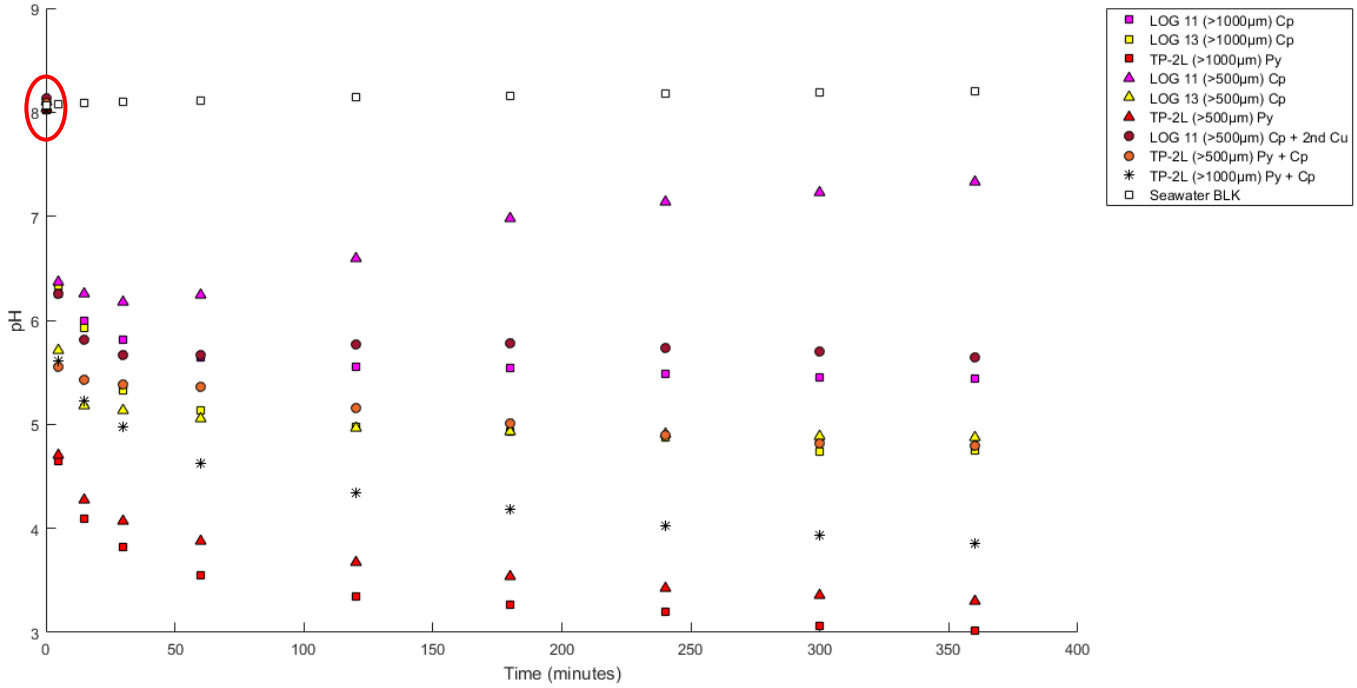

Figure 30: pH recordings across all natural sample seawater dissolution experiments E6-E24 and seawater blank E25. Monomineralic experiments are represented by a square marker (at >1000 µm) and triangle (at 500-1000 µm), whilst polymineralic is presented by a circle marker (at 500-1000 µm) and '*' (at >1000 µm). Mineral abbreviations are as follows: Py = pyrite, Cp = chalcopyrite, 2nd Cu = secondary-Cu-sulphides, and BLK = blank. All start pH are circled in red.

Start pH was between 8.0-8.1 for all experiments, circled in red on Figure 27. pH fluctuations throughout experiment runs were very different to those seen before with standard samples, with drastic decreases being observed within the first 5 minutes to as low as ~4.7 pH. The majority of samples' pH began to plateau after an hour, except for LOG-11 (>500 µm) Cp where instead the pH increased after 1 hour for the remainder of the experiment. Experiments with TP-2L again didn't plateau after the first hour, with less steep decreases in pH continuing.

Experiments with monomineralic TP-2L displayed the most drastic decreases in pH, reaching as low as pH 3. This is likely because TP-2L pyrite has a colloidal texture increasing surface area, allowing for faster rates of reaction, releasing more sulphuric acid as a by-product (Bilenker, 2011; Wilkin & Barnes, 1997). Polymineralic TP-2L did not see such drastic decreases in pH, as pyrite was paired with chalcopyrite. This is likely due to the chalcopyrite having massive textures with lower surface

areas than colloidal textures, decreasing the overall surface area of the sample. Logatchev samples (LOG-11 & LOG-13) decreased down to a similar pH range (~5-6 pH) with LOG-13 reaching a low of ~4.9 pH. Monomineralic LOG-11 (>500 μm) with chalcopyrite persistently displayed the highest pH, increasing back to a more neutral pH as time progressed, likely due to its massive textures and slower (chalcopyrite) oxidation rates. Whilst polymineralic LOG-11 (>500 μm) with both chalcopyrite and secondary-Cu-sulphides saw a more drastic decline in pH before plateauing after ~1 hour.

Samples with larger grain sizes (>1000 μm) consistently displayed lower pH's than smaller (>500 μm) counterparts. The reasons for this are unclear, but one hypothesis may be that crushing the samples to smaller grainsizes may remove some of the irregularities and porosity and therefore decrease the surface area.

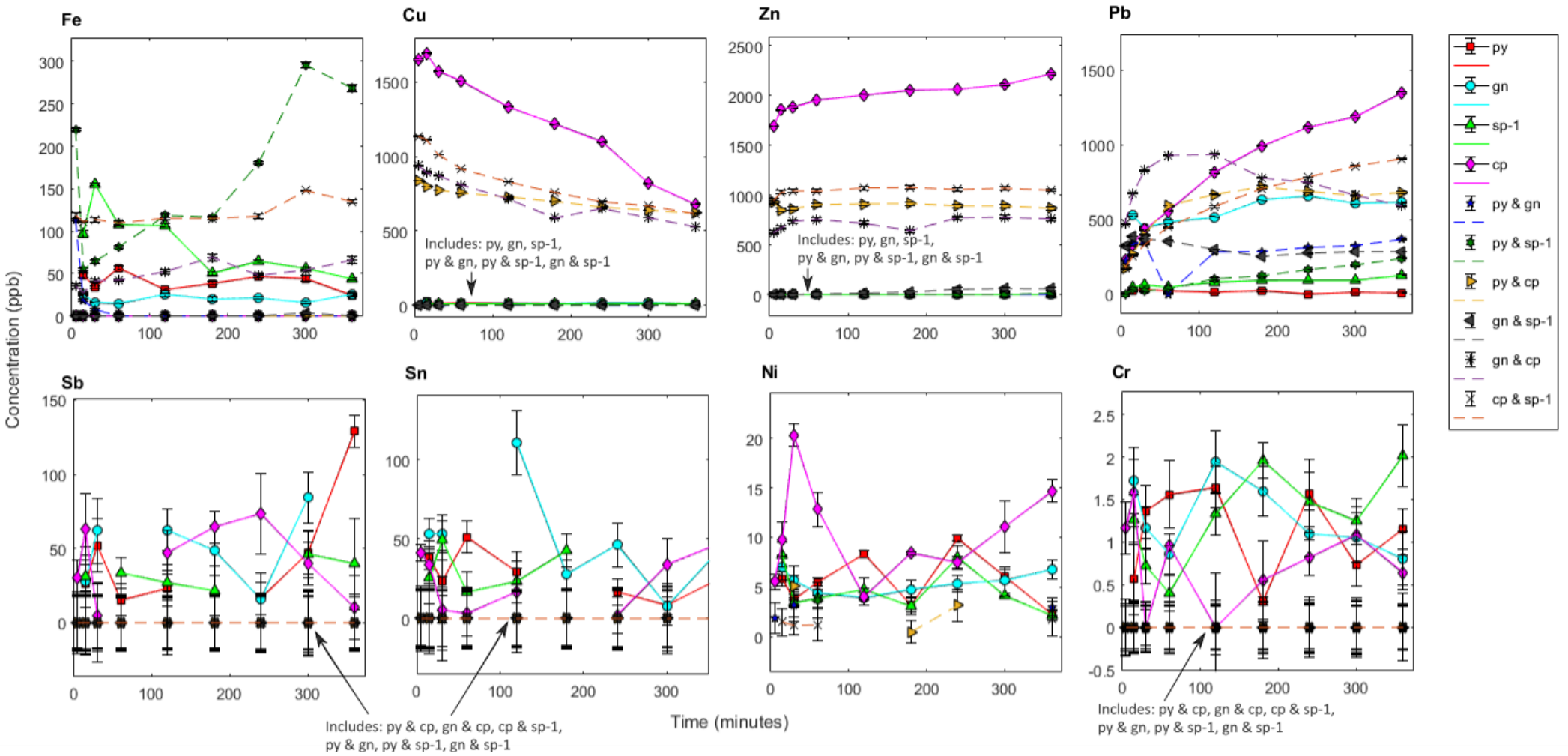

Figure 31: Standard mineral monomineralic and polymineralic seawater dissolution experiment concentrations (ppb) for Fe, Cu, Ni, Pb, Sb, Sn, Zn and Cr over 6 hour runs. Experiments were run at room temperature, ~8.1 pH, 355-500 µm grainsize and 5g:250ml rock:fluid ratio. Legend abbreviations: py = pyrite; gn = galena; sp-1 = sphalerite-1; cp = chalcopyrite. Mineral ratios for polymineralic experiments 2.5g:2.5g.

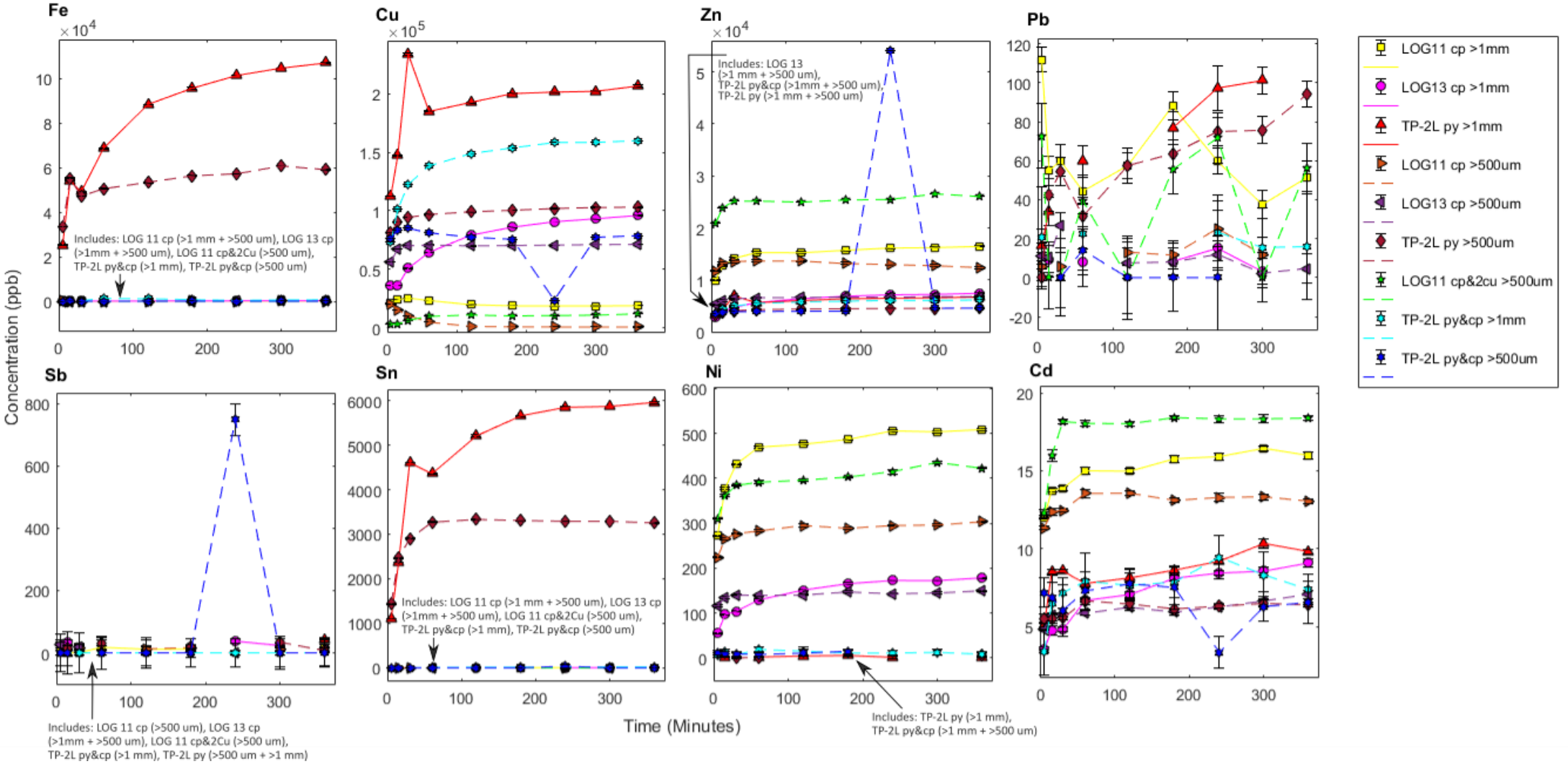

Figure 32: Natural samples (LOG11, LOG 13, TP-2L) monomineralic and polymineralic seawater dissolution experiment concentrations (ppb) for Fe, Cu, Ni, Pb, Sb, Sn, Zn and Cr over 6 hour runs. Experiments were run at room temperature, ~8.1 pH, 500-1000 µm grainsize and 5g:250ml rock:fluid ratio. Legend abbreviations: py = pyrite; gn = galena; sp-1 = sphalerite-1; cp = chalcopyrite.

6.3 ICP-OES Analysis Results For Galvanic Experiments

6.3.1 Dissolution Experiment Results

Concentration and standard deviations are presented in Table 13-16b (Appendix) for all dissolution experiments in ppb/ppm. Concentrations for both monomineralic and polymineralic experiments are displayed on Figure 28 for standard minerals, and Figure 29 for natural samples (LOG-11, LOG-13, TP-2L).

Both monomineralic and polymineralic experiments show substantial leaching of elements. The experiments using standard minerals show different leaching behaviours to those where natural samples (LOG-11, LOG-13 and TP-2L) were used. In standard sample experiments maximum leaching times vary dependent on which minerals were present. A general trend can be seen where, after an initial early leach in the first five minutes, leaching decreases within 5-30 minutes, and then slowly increases with maximum leaching concentration observed at around 3-4 hours. However, this trend is not observed in experiments where chalcopyrite was used, where maximum leaching concentrations peak at around 15 minutes, before a steady decline over the remaining duration of the experiment runs.

Both monomineralic and polymineralic experiments using natural samples show significantly higher concentrations of element release including Cu, Fe and Zn, than the standard mineral runs, as well as exhibiting lower concentrations of Pb. Leaching trends also differ to standard sample experiments, with elements generally following the same trend across experiments, where an initial rapid increasing concentration is observed within the first 5-30 minutes, before a slower increase or plateau in concentration takes over for the remainder of experiment runs. A possible explanation for this initial rapid increase in element concentrations may be due to the initial sample exposure to an oxygenated environment with increased agitation from mixing, before the settling of grains occurs.

Standard Chalcopyrite:

Standard chalcopyrite in monomineralic experiments shows very high concentrations of Cu (up to 1049 ppb), Pb (up to 1344 ppb), and Zn (up to 1763 ppb) being leached into solution. Moderate amounts of Mn (<21 ppb), Ni (<20 ppb), Sb (<73 ppb), and Sn (<46 ppb) were also detected in solution, with corrected values coming out as bdl ppb of Cd, Cr, Fe and Mg being found. Dominant elements observed in monomineralic chalcopyrite are seen in every experiment in which chalcopyrite is present.

High concentrations of Pb and Zn are unusual for pure chalcopyrite, and therefore may suggest the presence of another mineral, likely galena and sphalerite as unidentified inclusions which were not seen in reflected light or identified by EMPA (due to lack of access). Chalcopyrite is commonly found in association with sphalerite, which would account for the high concentrations of both Pb and Zn

(George *et al.*, 2018). The standard chalcopyrite sample used in these experiments is terrestrially sourced, where it is unusual to find pure chalcopyrite, with it often found paired with sphalerite (Galley et al., 2007). Therefore, it is highly likely that there is a mineral pair with sphalerite and perhaps galena within the standard chalcopyrite used; therefore monomineralic experiments with chalcopyrite were not in fact monomineralic. In seafloor massive sulphide environments pure chalcopyrite is more common, as is observed in LOG-11 and LOG-13, and the low Pb and Zn released by the natural chalcopyrite (below) is likely to be more representative of this minerals' dissolution behaviour.

The 'monomineralic' standard chalcopyrite data is still useful, as the high concentrations observed within "monomineralic" experiments is indicative of mineral pairs producing higher concentrations of metal leachate. As the amount of sphalerite and galena must be very minor (to avoid detection in reflected light) the higher concentrations than in galena or sphalerite standard monomineralic experiments suggest high dissolution rates for the inclusions consistent with a galvanic cell.

For these reasons discussed above, the monomineralic chalcopyrite experiment data will be discussed with that kept in consideration, and referred to as a "chalcopyrite mixed sulphide" for the remainder of this thesis.

Standard Sphalerite-1:

Monomineralic experiments with sphalerite-1 show that the main elements leached into solution are Fe (up to 155 ppb) and Pb (up to 124 ppb), with surprisingly no Zn being leached. Moderate amounts of Sn (<50 ppb), Sb (<46 ppb), and Cu (<13 ppb) are also present in sample solutions tested, with trace or corrected values <bdl ppb Cr, Cd, Mg, Mn, Ni and Zn being found. This is far from what is expected for sphalerite-1, with EMPA data confirming that Zn constitutes 57 wt% of sphalerite-1, Fe 12 wt%, Pb 0.01 wt%, and Cd ~166 ppm. Therefore, some other explanation for why there is a lack of Zn in sphalerite-1 leachate is needed.

Various studies observe sphalerite oxidation rates to be at its lowest in neutral pH solutions (Pan *et al.*, 2012; Scott & Barnes, 1972). As sphalerite experiments in this study were carried out at a pH around 8.1, slower oxidation rates may have affected the amount of Zn leached. Pan *et al.* (2012), also conclude sphalerite oxidation rates at pH 7.8 to be $2.56x10^{-10}$ mol/m^2/s. This is slower than previously thought with Edwards *et al.* (2003b) measuring sphalerites oxidation rate with the presence of bacteria colonies to be $7x10^{-8}$ mol/m^2/s. This reveals that sphalerite oxidation rates in this thesis are not as fast as previously thought.

Furthermore, it is possible that any Zn leached is being removed from solution via ferric oxyhydroxides formation, and/or that sphalerite requires longer reaction times for Zn leachate to be observed (Heidel et al., 2011; Gartman et al., 2020; Knight, 2018).

Alternatively, it possible that the sphalerite-1 used in experiments was not pure or had been contaminated with another mineral. The presence of Pb in the solution of monomineralic sphalerite-1 experiments is unusual despite Pb being detected in sphalerite-1 through EMPA analysis (~553 ppm Pb). Cook *et al.* (2009), discusses the presence of Pb in sphalerite samples of their study, existing mainly as micro inclusions of galena through LA-ICPMS analysis. It is possible that the Pb leached from monomineralic sphalerite-1 experiments, was preferentially leached from micro-inclusions of different minerals with lower rest potentials than sphalerite (potentially galena), at the same time cathodically protecting the sphalerite. Ideally this hypothesis would be tested through SEM probe of post-experiment sphalerite-1 material, to assess whether other minerals were present in the experiment runs, or for the presence of minerals such as Fe-oxyhydroxides sequestering Zn ions. Unfortunately, this analysis wasn't able to be carried out due to COVID-19 restrictions on lab access and travel. This post-material analysis would be highly recommended for any future work following up this study.

For these reasons covered above, sphalerite-1 will be referred to as sphalerite-mixed-sulphide when describing polymineralic experiments. All experiments involving the sphalerite-1 sample will not be discussed further in the discussion, instead being moved to the Appendix due to the uncertainty surrounding its mineralogy.

Standard Pyrite:

Monomineralic standard pyrite experiments show that dissolved elements with the highest concentration to be Fe (up to 55 ppb), Cu (>15 ppb), and Sb (>30 ppb). This is concordant with what is observed in the EMPA analysis, where Fe makes up 46 wt% of the standard pyrite, ~116 ppm Cu and ~196 ppm Sb, although more Fe leaching was expected. Whereas polymineralic pyrite experiments see higher leaching of different elements dependent on the mineral it is paired with.

The variations in concentration across pyrite polymineralic experiments, are indicative of the control sulphide mineralogy has on leaching, particularly on what elements are preferentially leached and supressed. These relationships between monomineralic standard pyrite experiments and polymineralic experiments can be seen in Figures 28.

Standard Pyrite & Galena:

When pyrite is paired with galena, there is significantly higher concentrations of Pb (>200 ppb) in the leachate, with initially higher Fe (>100 ppb) up to 30 minutes. In this pairing, lower concentrations are also observed, with Fe decreasing to ~0 ppb after 30 minutes, and with Cu, Sn and Sb all reducing to ~0 ppb as well.

Figure 28 shows this decrease in Fe, down to <bdl ppb for polymineralic pyrite & galena, while its monomineralic equivalents both leach moderate-low Fe concentrations (25-55 ppb pyrite and 15-25 ppb galena). This implies that something in the reaction is preventing Fe from being leached when

pyrite is coupled with galena, or that one or both minerals are being protected from oxidation. The same trend is observed for both Cu (decreases from ~10-25 ppb in both monomineralic pyrite and galena to ~0 ppb in polymineralic) and Sb (decreases from ~30-75 ppb in both monomineralic experiments to ~0 ppb polymineralic), while Pb in polymineralic pyrite & galena is ~half (~300-350 ppb) that of monomineralic galena (~500-650 ppb), which is likely the result of there being less galena in the experiment.

Standard Pyrite & Chalcopyrite-sulphide-mix:

Substantially higher concentrations of Cu (>700 ppb), Mn (>10 ppb), Pb (>600 ppb), and Zn (>800 ppb) are observed when pyrite is coupled with the chalcopyrite mixed sulphide. With Fe, Sb, and Sn being reduced to ~0 ppb.

Figure 28, shows this lack of dissolved Fe (bdl ppb) for polymineralic pyrite & chalcopyrite-sulphide-mix. As the chalcopyrite-sulphide-mix also leaches an unmeasurable amount of Fe, this implies that Fe leaching is being prevented in pyrite when coupled with chalcopyrite-sulphide-mix. While Cu for polymineralic pyrite & chalcopyrite-sulphide-mix initially starts low, it rapidly rises to higher concentrations, similar to those observed in the "monomineralic" chalcopyrite-sulphide-mix (CSM), despite there being less CSM in the experiment. As pyrite leaches negligible amounts of Cu, it is possible that when chalcopyrite-sulphide-mix is coupled with pyrite it preferentially leaches more Cu.

Pyrite & Sphalerite-mixed sulphide:

Polymineralic sphalerite-mixed sulphide and pyrite, has higher concentrations of Fe (up to 295 ppb) and Pb (up to 237 ppb), than in both monomineralic pyrite and sphalerite-mixed sulphide. Zn remains at ~0 ppb for the majority of the polymineralic experiment except at hour 6 where 12 ppb was recorded. Cd, Cr, and Ni remain low or ~0 ppb in solution, whilst Cu, Sb and Sn are also observed at ~0 ppb in this experiment. If the previous hypothesis of there being micro-inclusions of another mineral, possibly galena is true for the sphalerite-mixed sulphide, then the increase in Pb in the polymineralic experiment may suggest a galvanic cell with this micro-inclusion mineral. With the micro-inclusion then being completely preferentially dissolved, Zn may then be able to be leached from sphalerite at hour 6, when coupled with pyrite (next lowest rest potential). This hypothesis would need to be tested further, through post-experiment material analysis.

These relationships are visualised on Figure 28 along with Cu concentration, which is highest in monomineralic pyrite, and ~0 ppb in both "monomineralic" sphalerite-mixed sulphide and the polymineralic experiment. This may suggest that one or more of the minerals are protected from sulphide oxidation and therefore Cu leaching, most likely the pyrite as it is the only mineral present to previously show Cu release. When assessing all the relationships between pyrite and sphalerite-mixed

sulphide, it is likely that the sphalerite-mixed sulphide sample is being preferentially leached, with pyrite being protected when paired together.

Standard Galena:

Standard galena in monomineralic experiments show that the dominant dissolved element in solution is Pb with up to 650 ppb measured. Other elements with moderate concentrations are Fe (up to 25 ppb), Cu (up to 18 ppb), Sb (up to 62 ppb), and Sn (up to 110 ppb). Elements that weren't observed (~0 ppb) in monomineralic standard galena experiments include, Zn, Cd, Mg, as well as trace amounts of Mn, Ni, and Cr. EMPA data for galena is in agreement with these results, as Pb makes up 87 wt% of the galena, with 0.03 wt% Fe, 0.01% wt% Cu, ~313 ppm Sb and ~255 ppm Sn.

Galena & Sphalerite-mixed sulphide:

Polymineralic galena & sphalerite-mixed sulphide have Pb concentrations up to 385 ppb, and Zn leaching after 2 hours, up to 59 ppb. Unlike previous monomineralic galena and "monomineralic" sphalerite-mixed sulphide, no Fe (~0 ppb) release is detected in the polymineralic experiment. Other elements at low or negligible concentrations are Cd, Mn, Ni, Cr, Sb, and Sn.

Figure 28 shows the relationships between experiments, with after an initial increase in Pb in the polymineralic experiment, Pb decreasing to concentrations that are ~half of that in monomineralic galena. This is probably due to there being half the mass of galena present (2.5g) in polymineralic experiment. The presence of Zn being observed after 2 hours may suggest a few things; that perhaps a galvanic pair between galena and sphalerite-mixed sulphide is present preferentially leaching the lower rest potential mineral (galena), this being unlikely as more Pb leachate would be expected to be observed. Alternatively, it suggests that a galvanic pair isn't set up between galena and sphalerite-mixed sulphide, allowing Zn to be leached from the sphalerite-mixed sulphide. This however doesn't correlate with what has been previously observed with sphalerite-mixed sulphide not releasing Zn. Instead, it could suggest that any micro-inclusions present within sphalerite are dissolved within the first 2 hours, allowing sphalerite to begin oxidising and leach Zn. While this hypothesis cannot be tested without knowing the exact mineralogy of the sphalerite-mixed sulphide sample, the decrease in Pb in the polymineralic experiment after 2 hours may further suggest this.

Furthermore, no Fe (~0 ppb) being leached during the polymineralic experiment, despite both monomineralic experiments leaching Fe, may suggest that something is preventing the release of Fe from both minerals. Alternatively, it could indicate that something is removing Fe from solution, perhaps an oxide. This same trend is observed for Cu, with no Cu being detected in the polymineralic experiments, despite low concentrations being observed in both monomineralic equivalents.

The relationship between galena & sphalerite-mixed sulphide are unclear due to the sphalerite-mixed sulphides uncertain mineralogy; future work would have to ensure that sphalerite-mixed sulphide

samples were re-analysed to assess the purity of the sample and to ensure that no micro-inclusions are present affecting the results.

Standard Galena & Chalcopyrite-sulphide-mix:

Much higher concentrations of Cu (up to 940 ppb), Fe (up to 66 ppb), Pb (up to 930 ppb), and Zn (up to 585 ppb) are observed when galena is paired with chalcopyrite-sulphide-mix, when compared to monomineralic galena. With ~0 ppb of Cr, Ni, Sb, and Sn also observed in this polymineralic pair. However, overall concentrations of Cu, Pb and Zn are higher in "monomineralic" chalcopyrite-sulphide-mix, therefore higher concentrations of these elements in the polymineralic pairing can be attributed to the chalcopyrite-sulphide-mix.

In Figure 28, Fe leaching is highest in polymineralic mix of galena & chalcopyrite, while monomineralic galena has much lower concentrations of Fe and chalcopyrite-sulphide-mix displays close to 0 ppb. This implies that there may be preferential leaching of galena taking place when it is coupled with chalcopyrite, as much higher concentrations of Fe are observed for a lower mass of galena. For Cu, Pb and Zn leaching in Figure 23, the same relationships are observed, with "monomineralic" chalcopyrite-sulphide-mix persistently leaching higher concentrations of each element, and with polymineralic galena & chalcopyrite-sulphide-mix leaching lower concentrations for each. For the case of Zn leaching, this is likely due to there being less chalcopyrite-sulphide-mix present in the polymineralic experiment (2.5g) and this is probably where the Zn is coming from. For Cu leaching, the concentration of polymineralic galena & chalcopyrite-sulphide-mix is very similar to monomineralic chalcopyrite-sulphide-mix despite there being less sample mass present. This therefore might imply that there is some accelerated or preferential dissolution of chalcopyrite taking place. Polymineralic galena & chalcopyrite-sulphide-mix appears to follow a more similar leaching pattern of Pb to monomineralic galena. With after an initially rapid increase of Pb in galena & chalcopyrite-sulphide-mix, Pb decreases back down to more similar levels as that of galena, while "monomineralic" chalcopyrite-sulphide-mix sees a continuous increase of Pb throughout the experiment. This may suggest that either the Pb is being precipitated out of solution after 2 hours in polymineralic galena & chalcopyrite-sulphide-mix. Or that the Pb is being preferentially leached from galena when coupled with chalcopyrite-sulphide-mix, so more readily dissolves at the beginning of the experiment. When considering both Fe and Pb leaching across the three experiments, it is most likely that galena is being preferentially dissolved when in contact with chalcopyrite.

Sphalerite-mixed sulphide & Chalcopyrite-sulphide-mix:

Polymineralic sphalerite-mixed sulphide coupled with chalcopyrite sulphide mix sees high concentrations of Cu (up to 1112 ppb), Fe (up to 147 ppb), Pb (up to 905 ppb), and Zn (818 ppb). While Mn is observed at moderate concentrations (up to 14 ppb) and low/~0 ppb concentrations of Cd, Cr, Ni, Sb, Sn are seen. The high concentrations of Cu, Pb and Zn are likely due to the presence

of chalcopyrite-sulphide-mix in the experiment, as “monomineralic” chalcopyrite-sulphide-mix experiments also leach high concentrations of these elements.

Fe leaching in Figure 28, shows that “monomineralic” sphalerite-mixed sulphide initially leaches the highest concentration of Fe in the first 30 minutes. With polymineralic sphalerite-mixed sulphide and chalcopyrite-sulphide-mix having the highest sustained concentrations of Fe, despite no Fe being observed with monomineralic chalcopyrite-sulphide-mix. This implies that in the polymineralic experiment, increased leaching of Fe from one or both minerals is observed. As no Fe is observed in monomineralic chalcopyrite-sulphide-mix, the release of Fe is likely sourced from sphalerite-mixed sulphide, suggesting that the sphalerite-mixed sulphide may be being preferentially leaching Fe.

No Cu is leached during “monomineralic” sphalerite-mixed sulphide, with “monomineralic” chalcopyrite-sulphide-mix leaching higher Cu than the polymineralic experiment in the first 2 hours. After 2 hours “monomineralic” chalcopyrite-sulphide-mix decreases to lower Cu concentrations ending at similar Cu as the polymineralic equivalent, where ~half (2.5g) of chalcopyrite-sulphide-mix is present. The Cu concentration in the polymineralic experiment is likely due to there being less chalcopyrite-sulphide-mix present, the Cu decreases in both experiments perhaps being due to Cu being sequestered out of solution by an oxide.

Relationships between these two samples are unclear and confusing due to the uncertainties surrounding both samples mineralogy’s; further work must account and correct for this.

6.3.2 Natural LOG-11 (500- 1000 µm) Samples:

Monomineralic LOG-11 (500-1000 µm) experiments with separated chalcopyrite, show dominant elements leached into solution to be Cu (up to 20 ppm) in the first 30 minutes, before rapidly decreasing to ~0 ppb, as well as Zn (up to 13.6 ppm). Relatively high concentrations of Ni (up to 300 ppb) were also observed, along with moderate amounts of Fe (<70 ppb), Cd (<13 ppb), and Mn (<42 ppb). Low or ~0 ppb of Cr, Mg, Pb, Sn, and Sb were observed in sample solutions.

Polymineralic LOG-11 chalcopyrite + secondary-Cu-sulphides (500-1000 µm) see sustained high concentrations of Cu (up to ~12 ppm) for the whole duration of the experiment, with Zn (up to 26 ppm) and Ni (up to 435 ppb) also seeing a rise in concentration. Cd up to ~18 ppb and Mn up to ~100 ppb were detected; with moderate Pb (up to 72 ppb) observed; Fe was not detected (~0 ppb) in polymineralic LOG-11, despite up to 70 ppb being observed in monomineralic LOG-11. This may suggest that Fe release was prevented in the polymineralic experiment, possibly chalcopyrite being cathodically protected; alternatively Fe may have precipitated out of solution early on in polymineralic LOG-11 or Fe sequestering by an oxide. ~0 ppb of Cr, Sb and Sn were also observed in polymineralic LOG11.

Figure 29 better shows the relationships between monomineralic LOG-11 and polymineralic LOG-11 experiments, displaying how monomineralic chalcopyrite in LOG-11 initially has high concentrations of Cu before rapidly decreasing to 0 ppb after ~30 minutes. Polymineralic chalcopyrite and secondary-Cu-sulphides begin with lower concentrations of Cu before a rapid increase in Cu, plateauing after an hour. When considering the formulas of chalcopyrite ($CuFeS_2$) and secondary-Cu-sulphides, assuming bornite (Cu_5FeS_4) (from Fallon, 2018, XRD data of LOG-11) and the approximated ratios (3.6 cp: 6.4 bn) of each element in the polymineralic LOG-11 grains; polymineralic grains would be expected to contain ~52.9% Cu when compared to monomineralic LOG-11 (chalcopyrite) of 34.6% Cu. These simplified Cu % estimates further indicate that the increase of Cu observed in the polymineralic experiment is due to the presence of secondary sulphide minerals such as bornite. Alternatively, one or both minerals in the pair may be preferentially leaching more Cu as a part of a galvanic cell, possibly the secondary-Cu-sulphides as bornite has a lower rest potential to chalcopyrite.

Monomineralic chalcopyrite in LOG-11 has low-moderate (<70 ppb) amounts of Fe, while polymineralic LOG-11 with secondary-Cu-sulphides has no (~0 ppb) Fe present. Since chalcopyrite is present in both experiments, it suggests that the release of Fe is being prevented from one or both minerals when in a couple in the polymineralic experiment. Alternatively, Fe may be being removed from solution, as an oxide precipitate.

Monomineralic LOG-11 displays lower concentrations of both Zn and Ni, when compared to polymineralic LOG-11, both experiments following the same trend with initial rapid increases in Zn and Ni, but at much higher concentrations for polymineralic LOG-11. As bulk chemistry data from Fallon (2018) shows LOG-11 (unpicked polymineralic) to have 2 wt% Zn and 170 ppm Ni; one of the minerals present in LOG-11 (chalcopyrite, issocubinite, sphalerite, bornite) is potentially composed of more Zn and Ni than the other. As higher concentrations for both are observed in the polymineralic experiments (chalcopyrite and secondary-Cu-sulphides) of this study, it may be the secondary-Cu-sulphides. Fallon (2018) LA-ICP-MS data supports this hypothesis, showing bornite in LOG-11 to contain ~780 ppm Ni and ~2310 ppm Zn, higher than those in LOG-11 chalcopyrite, ~241 ppm Ni and ~562 ppm Zn. Another possibility is that Zn and/or Ni is leached at higher rates when chalcopyrite and secondary sulphides are in contact with each other, due to secondary-Cu-sulphides having faster oxidation rates or from galvanic interactions.

6.3.3 Natural TP-2L (500-1000 µm) Samples:

Monomineralic TP-2L (500-1000 µm) experiments involving pyrite and/or marcasite, leached high concentrations of: Cu (up to 100 ppm), Fe (up to 60 ppm), Sn (up to 3000 ppb), and Zn (up to 17 ppm). Moderate concentrations of Pb (up to 94 ppb) and Mn (up to 232 ppb) was also observed in sample solutions, with low concentrations of Cd, Cr, Ni, and Sb detected.

TP-2L polymineralic (500-1000 µm) experiments involved the natural pairing of pyrite/marcasite with chalcopyrite. In these experiments high concentrations of Cu is observed (up to 84 ppm), but at lower concentrations to monomineralic TP-2L (Figure 24). High values of Zn are also seen (up to 4.5 ppm), with an anomalously high concentration of 54 ppm observed at 4 hours. Moderate concentrations of Fe (up to 71 ppb) are observed, drastically lower than that of monomineralic TP-2L, and Mn (up to 204 ppb). Low concentrations of Cd, Cr, Ni, Pb, Sb and Sn are observed. Fallon (2018) XRD data for TP-2L (unpicked polymineralic), shows Fe to make up 40 wt% of TP-2L, with Cu making up 4 wt%, and Zn 0.2 wt% (~152 ppm), with more Zn being present in monomineralic TP-2L it is likely found mainly in pyrite/marcasite as there is no sphalerite in TP-2L bulk composition, but does exist within inclusions in pyrite, Fallon (2018) description, although sphalerite inclusions weren't observed under optical/reflective light when mineral picking in this study.

Figure 29 demonstrates these relationships more clearly. An initially rapid increase in Cu is observed in both monomineralic py/m and polymineralic py/m + cp, before py/m continues to steadily increase whilst Cu in py/m + cp gradually decreases. At 4 hours there are anomalously low concentrations of Cu in polymineralic TP-2L, the reason for which is unclear. Low Fe concentrations in polymineralic TP-2L compared to monomineralic TP-2L, may suggest that Fe leaching is prevented or that Fe is readily sequestered from solution. Anomalously high Zn concentrations observed at 4 hours for polymineralic TP-2L, along with a disappearance of Ni also at 4 hours are observed. Again the reason for this disruption at 4 hours is unknown, but could indicate a disruption to the experiment flask or potentially a break/or formation in galvanic contact between the two minerals.

Experiments with use of TP-2L show different trends when compared to other samples such as LOG-11. TP-2L polymineralic experiments do not show a higher increase in Cu and Zn, which is expected when two mineral pairs are in contact with each other due to galvanic interaction between minerals pairs. These results don't necessarily suggest that galvanic interactions are not happening between the two minerals (pyrite/marcasite + chalcopyrite), but that instead another process is more dominant in the experiment. When mineral habit of TP-2L is considered in context with the experiments, it is likely that surface area has a strong control on the leaching of both pyrite/marcasite and chalcopyrite. Pyrite/marcasite appears in a colloidal habit in TP-2L, this habit is typically formed from bacterial processes and creates high surface areas. Whilst the chalcopyrite appeared in a massive crystalline

habit, that typically has smaller surface areas. So, in the case of these experiments, pyrite/marcasite of TP-2L may simply just have much higher surface areas than chalcopyrite, and therefore leach elements more readily. This suggests that surface area is a more important control on metal leaching than galvanic cells. Furthermore, both minerals (pyrite/marcasite & chalcopyrite) may have similar Cu compositions, but different oxidation rates; Feely (1987) found chalcopyrite to have slower oxidation rates than pyrite, therefore pyrite may simply be oxidising more readily than chalcopyrite.

6.4 High Temperature 50°C Experiments:

High temperature experiments run at 50°C for monomineralic galena std. and polymineralic galena std.+pyrite std. were carried out so that the effect temperatures could be observed. Monomineralic galena at 50°C leached high concentrations of both Fe (up to 2112 ppb) and Pb (up to 1300 ppb), with moderate concentrations of Zn (up to 216 ppb) also observed (Figure 30). EMPA data for galena, shows it to be composed of 87 wt% Pb, 0.03 wt% Fe, ~62 ppm Zn and ~313 ppm Sb, therefore it is unexpected that more Fe has been released than Pb. The higher temperature may have affected the solubility limits for both Fe and Pb, with Fe having a higher solubility limit of 2.3 ppm in seawater at 25 °C and Pb having a solubility of 0.68 ppm in seawater at 22 °C, it is expected that solubility increases with increasing temperature (Liu and Millero, 2002; Angel *et al.*, 2016). If the relationship between solubility and temperature is assumed to be linear, then the solubility limit for Pb and Fe at 50 °C would be ~1.36 ppm and ~4.6 ppm respectively. Cr, Cu, Mn, and Ni appeared in low concentrations, with no (~0 ppb) Cd, Sb, and Sn detected.

Polymineralic galena+pyrite at 50°C saw Pb to again be leached in high concentrations (up to 1200 ppb), with Fe starting high at 675 ppb, before steadily decreasing down to ~0 ppb at hour 5. Zn also started in moderate concentration, before rapidly decreasing to ~0ppb after 15 minutes. Low concentrations of Mn, Ni, and Cu were again detected with ~0ppb Cd, Cr, Sb, and Sn. Pb concentrations are similar in both monomineralic and polymineralic experiments likely due to the solubility limit being reached based on the estimated limit from (REF) and concentrations observed (1200-1300 ppb).

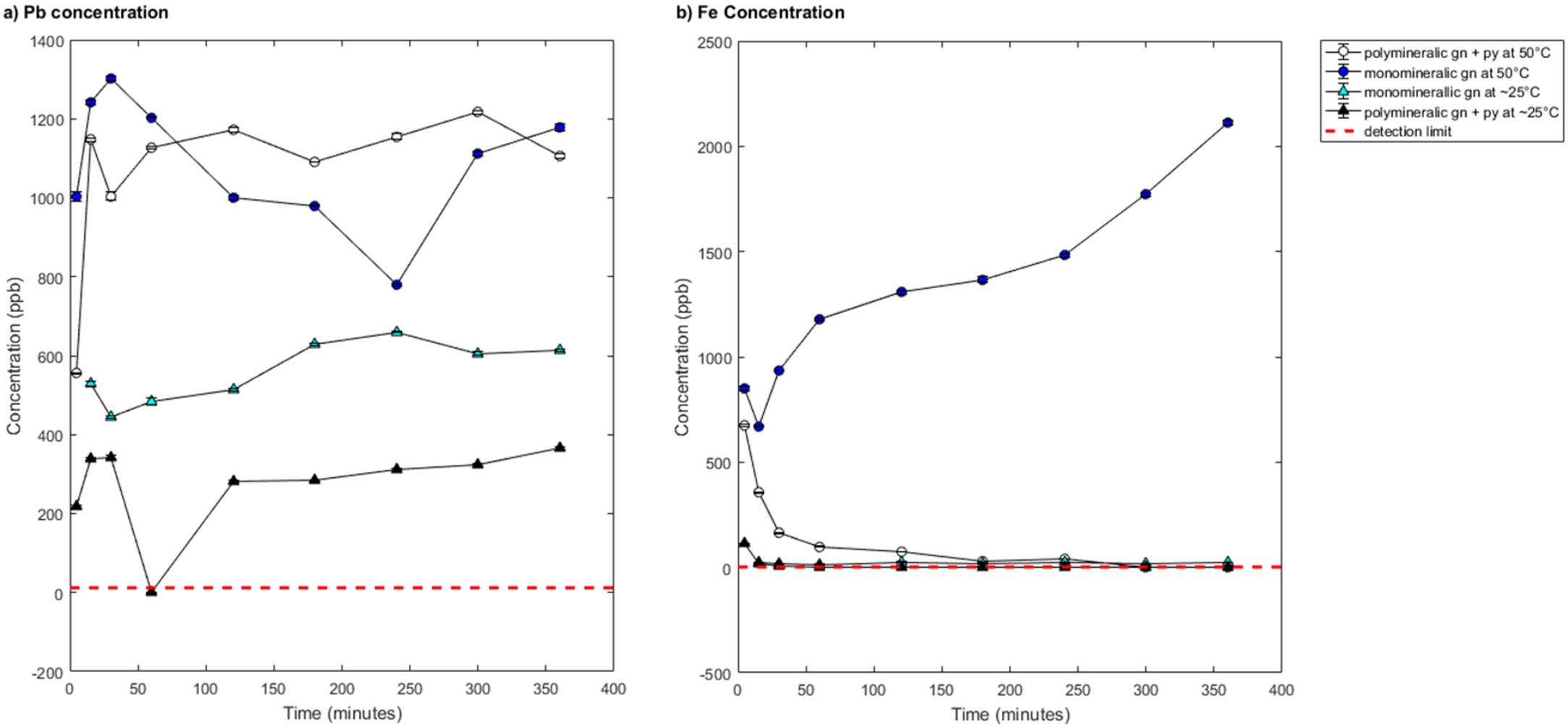

Figure 33: Comparison of Pb and Fe concentrations between high temperature (50 °C) and room temperature (~25 °C) monomineralic galena experiments and polymineralic galena and pyrite. Abbreviations: gn = galena; py = pyrite, D.L. = bdl.

6.5 Solubility Limits

Table 9: Known solubility limits for Pb, Cd, Cu, Fe, Mn, and Zn from literature (Mann and Deutscher, 1977, 1980; Baturin, 1987; Sadiq, 1989; Liu and Millero, 2002; Angel et al., 2016).

Element	Temperature (°C)	pH	Solubility Limit (ppm)	Medium	Source
Pb	22	8.15	2	Natural Seawater	Angel et al. (2016)
Pb	22	8.15	0.68	Artificial Seawater	Angel et al. (2016)
Cd	25	7.00	112.411	NaCl	Sadiq (1989)
Cu	25	5.00	1033	NaCl	Mann (1977)
Cu	25	6.00	10.6	NaCl	Mann (1977)
Cu	25	7.00	0.353	NaCl	Mann (1977)
Fe	5	8.10	0.0000195	NaCl	Liu (2002)
Fe	5	2.80	103	NaCl	Liu (2002)
Fe	25	3.41	193.65	NaCl	Liu (2002)
Fe	25	8.10	2.9	NaCl	Liu (2002)
Mn	0	8.00	1.7	0.2 M Na2SO4	Baturin (1987)
Mn	0	7.00	17	0.2 M Na2SO5	Baturin (1987)
Mn	0	6.00	170	0.2 M Na2SO6	Baturin (1987)
Zn	25	3-3.5	>10^6	NaCl	Mann (1980)
Zn	25	5.00	983000	NaCl	Mann (1980)
Zn	25	5.50	175000	NaCl	Mann (1980)
Zn	25	6.00	31000	NaCl	Mann (1980)
Zn	25	6.50	5530	NaCl	Mann (1980)

Table 9 displays solubility limits data from various sources (Mann and Deutscher, 1977, 1980; Baturin, 1987; Sadiq, 1989; Liu and Millero, 2002; Angel *et al.*, 2016), for elements Pb, Cd, Cu, Fe, Mn, and Zn. Figure 31 compares these solubility limits to the highest concentrations of each element detected across all seawater dissolution experiments. Concentrations of Cu, Fe and Zn leached from dissolution experiments are significantly lower than their relative solubility limits for those pH's and do not exceed at any point. Pb concentration from dissolution experiments at times crosses over the solubility limit for Pb at 0.94 ppm, but at a lower pH to that of the solubility limit. A trend observed for all solubility limits presented, is that with decreasing pH solubility increases. Therefore, it is likely that at lower pH the solubility limit for Pb is higher, and that the dissolution experiment concentrations recorded are within limits.

As solubility potential increases with decreasing pH, it is no surprise that the highest concentration values for each element (particularly Fe) are observed at lower pH's. The semi-batch nature of the experiment allows for pH to rapidly decline with sulphide oxidation in the experiment vessel, as no buffering solution was added throughout experiment runs. This decline in pH is unlikely to be observed in nature over long timeframes as the buffering capacity of the ocean is so large, therefore solubility limits for elements such as Fe would be expected to remain around 2.9 ppm at ~8.1 pH.

Therefore, in real circumstances it is probable that elements with lower solubility limits at pH 8.1 would precipitate out of solution. However, in some instances pH may remain low locally in pore spaces, fractures, or in plumes, where ocean mixing doesn't occur as readily, in these instances the solubility limits for Fe may increase (Romano, 2012).

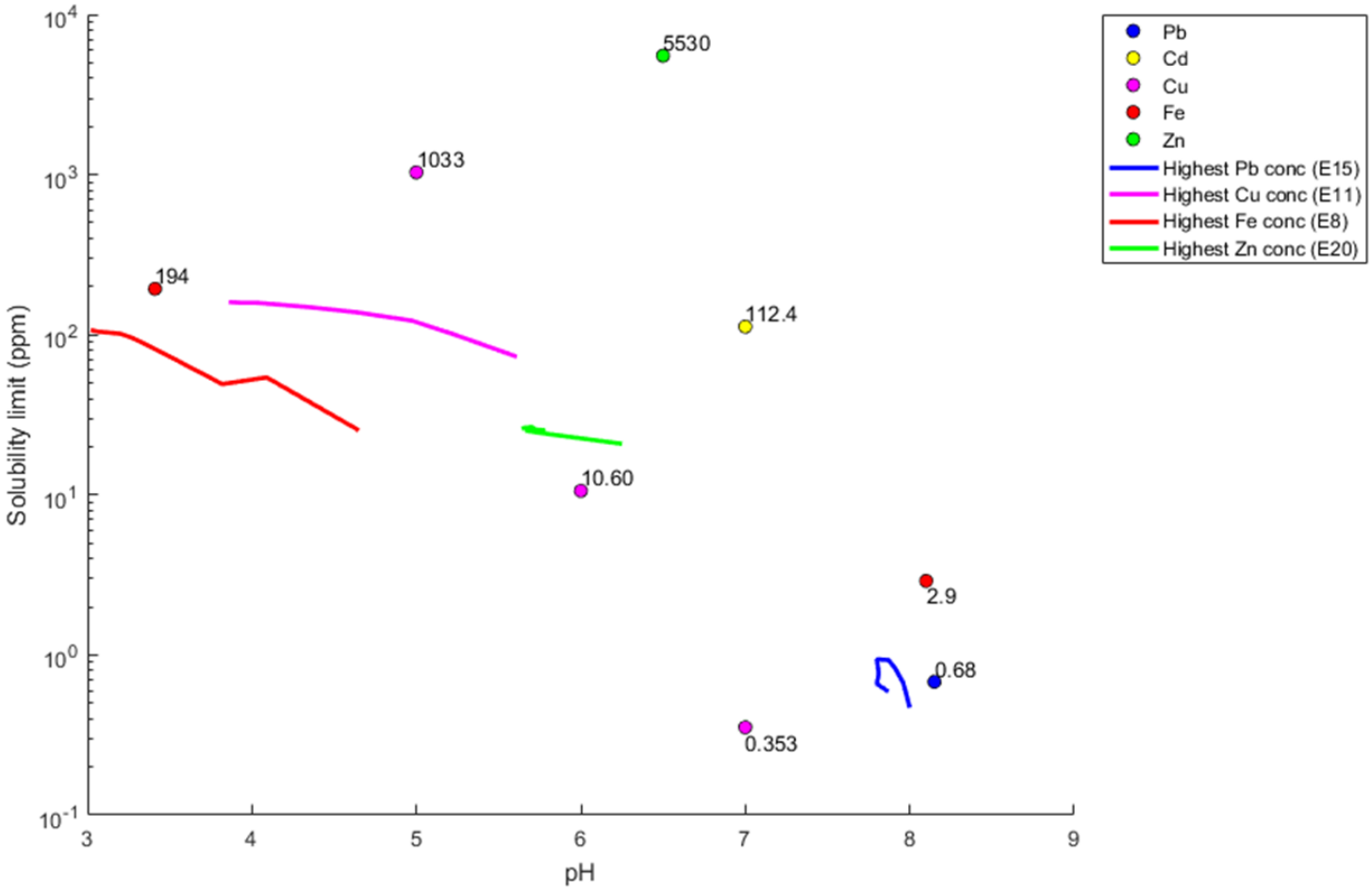

Figure 34: Solubility limits for elements Pb, Cd, Cu, Fe and Zn in artificial seawater (markers). Solubility limits for Cd, Cu, Fe and Zn at 25 °C, and Pb at 22 °C. References for values used: Angel et al., 2016, Sadiq, 1989, Mann, 1977, Liu, 2002, Mann, 1980. Plotted against the highest concentration for element from all experiments combined. E15 = Galena std. + Sphalerite-1 std. (>355 µm), E11 = TP-2L Pyrite + Chalcopyrite (>1000 µm) , E8 = TP-2L Pyrite (>1000 µm), and E20 = LOG-11 Chalcopyrite + secondary-Cu-sulphides (>500 µm).

7.0 Discussion

7.1 Experiments versus Mining Scenarios

With Nautilus Mineral's mining process, ore rock will be mined along the seafloor, and cut up into small fragments to be transported to surface vessels (Gwyther, 2008). The removal of ore rock from the seafloor by Nautilus Mineral's, although detrimental to benthic species, is not of major concern in regard to metal leaching. While small fragments of ore rock will likely be produced during the actual mining process, the coarser grain sizes in this stage are not expected to produce as much metal leaching or plume formations as finer grain sizes would, although both will likely still occur. The biggest risk for sulphide particle exposure for which oxidation can occur, comes from accidental spillages of slurried ore rock when being transported to surface vessels, and via return waters (Gwyther, 2008). After the dewatering of slurried ore, water containing fine (<8 μm) sulphide particles will be discharged back into the ocean as return water (Gwyther, 2008). The experiments conducted in this thesis are representative of accidental spillages of slurried ore material and crushed/exposed sulphide ores at the seafloor of the Nautilus Mineral's mining process or mine tailings left on the seafloor from dewatering plumes; because of the grain size fractions experimented on (355-1000 μm) and the continuous stirring exposing grains to oxygenated waters. Crushed ore rock of massive sulphides will be composed of a range of different grain sizes, where a mix of sulphide minerals and mineral pairs will be present. Exposure to seawater will allow oxidation and subsequent metal leaching to occur.

As seen in the natural sample dissolution experiments, pH reduction through sulphide mineral oxidation can occur rapidly, decreasing pH to acidic levels. As discussed in Bilenker et al. (2016), acid production produced through in-situ mining is unlikely to exceed the buffering and diluting capabilities of the ocean. However, with mining techniques such as pulverisation of SMS ores creating high reactive surface areas, the buffering capacity of the ocean could be temporarily exceeded by acid production (Bilenker *et al*., 2016). Temporary decreases in pH will increase the solubility limits of certain metals (as previously seen in Section 6.3.1), allowing metals to exist in solution for longer before being precipitated out.

One of the threats to marine habitats from SMS mining is the leaching of heavy metals. The disposal of waste ore rock and unconsolidated materials will create sediment plumes from the points of discharge (Gwyther, 2008). The Solwara 1 EIS states that these waste plumes will settle within 1 km of discharge points, covering an area just larger than 2.3 km^2, with any deposition beyond this occurring at a lower rate than natural sedimentation (Gwyther, 2008). Dewatering plumes are said to be discharged at 25-50 m above the seafloor, with particles <8 μm settling approximately 5-10 km W and NW of Solwara 1 (Gwyther, 2008). Exposure time for dewatered particles at surface temperature

and oxygenation is to be limited to 12 minutes (Gwyther, 2008) which, as observed in the seawater dissolution experiments of this thesis, is enough time for substantial metal leaching.

There is little information in the Solwara 1 EIS to how long a dewatering plume may be suspended in the water column at different particle sizes. Equations applied to TAG sediment plumes in (German & Sparks, 1993) using Stokes' Law indicates TAG particles with ~5 μm radius will achieve a terminal settling velocity of 4-8 m d^{-1}, and 0.2-0.3 m d^{-1} for fine grained particles with ~1 μm radius. If the assumptions are made that dewatering particles from Solwara 1 behave in a similar fashion, then it would take particles of 5 μm ~6.25-12.5 days to settle from 50 m height, while a particle of 1 μm would take approximately 166.7-250 days. During this time oxidation and metal leaching would be able to occur. When applying this equation to the 500 μm LOG-11 chalcopyrite, the settling velocity achieved is much faster of 0.274 m s^{-1}; so would only take a particle ~3 minutes to settle from a height of 50m. For a LOG-11 chalcopyrite particle of 8 μm, the settling velocity would be 6.07 m d^{-1}, taking ~8.24 days to settle from a height of 50m. Therefore, LOG-11 chalcopyrite sample particles experimented on in this thesis (500 μm) would be expected to settle within minutes, limiting exposure within the water column. However, for LOG-11 chalcopyrite particles at 8 μm, exposure in the water column could persist for days, with potential for metal leaching throughout. Since grain particles <8 μm are expected to be released in return waters from Nautilus Minerals Solwara 1 project (Gwyther, 2008), this is concerning in terms of potential metal leaching.

As return waters would be ~80% seafloor water and ~20% surface water, the lower salinities found in surface waters may also affect the buoyancy of any dewatering plumes, carrying plumes higher/further by currents (Luick, 2012).

With a limited understanding of the grain size range (<8 μm) in dewatering plumes from Solwara 1, it is not possible to know the way in which the plume will behave once in the water column. With sulphide minerals having the potential to leach metals over an unknown distances and times, it is worrisome for marine life, both at and downstream of vent sites. With the relationship of grain size on sulphide oxidation being well established in the literature and in the results of this study, smaller grain sizes will likely result in increased surface areas on which oxidation can occur. Therefore, it can be assumed that metal leaching observed from the experiments in this study would occur at higher rates on the smaller grain sizes presumed to be found in return waters if Nautilus Minerals mining process is followed.

A range of elements were observed in solution from seawater dissolution experiments, including Cd, Cr, Cu, Fe, Mn, Ni, Pb, Sb, Sn, and Zn, with the biggest concentrations observed in Cu, Fe, Pb, and Zn. Of these metals Cu, Ni, Cd, Zn, Cr, and Pb are thought to be toxic to aquatic life, whilst Fe, Zn in low concentrations may be of some bio-importance (Singh & Kalamdhad, 2011). Heavy metals

released into aquatic systems, in trace amounts, can potentially cause oxidative stress to organisms, negatively affecting the organisms within proximity, and indirectly effecting organisms through aquatic food chains (Singh & Kalamdhad, 2011).

7.2 Levels of Metal Release in Monomineralic Experiments

Standard mineral dissolution experiments saw on average much lower concentrations of metal leachate, when compared to natural sample dissolution experiments. Figure 32 highlights the difference in leachate concentration between monomineralic standard samples (355-500 μm) and monomineralic natural samples (500 and 1000 μm). For Cu, Fe, and Zn, natural samples consistently leach higher concentrations than standard samples, TP-2L leaching ~100x more Cu than standard chalcopyrite. Figure 32 shows that for Cu and Fe TP-2L comes out on top out of the natural samples; while LOG-11 leaches the highest concentrations of Zn. Natural samples likely leach higher metal concentrations due to mineral textures and habits that create higher surface areas on which oxidation can take place (refer to SA Figure 8). The colloform texture of TP-2L and massive/porous textures in LOG-11 and LOG-13, increases the surface area on the surface of each grain. In comparison, the smooth euhedral crystals in standard samples decreases surface area as they lack the textural impurities of the natural samples. The result which is apparent with the concentrations of leached metals being ~100s of times lower than the natural sample counterparts. These relationships are obvious in Figure 32 where concentrations leached from standard samples are visible much lower on a log ppm scale.

It is apparent through the results obtained, that experiments using standard samples to investigate the metal leaching potential of seafloor massive sulphides are not representative of these types of deposits. Experiments using samples from hydrothermal vent sites will bring about a better understanding to how mining activities may encourage sulphide oxidation, despite there being geological and mineralogical differences across different vent site locations.

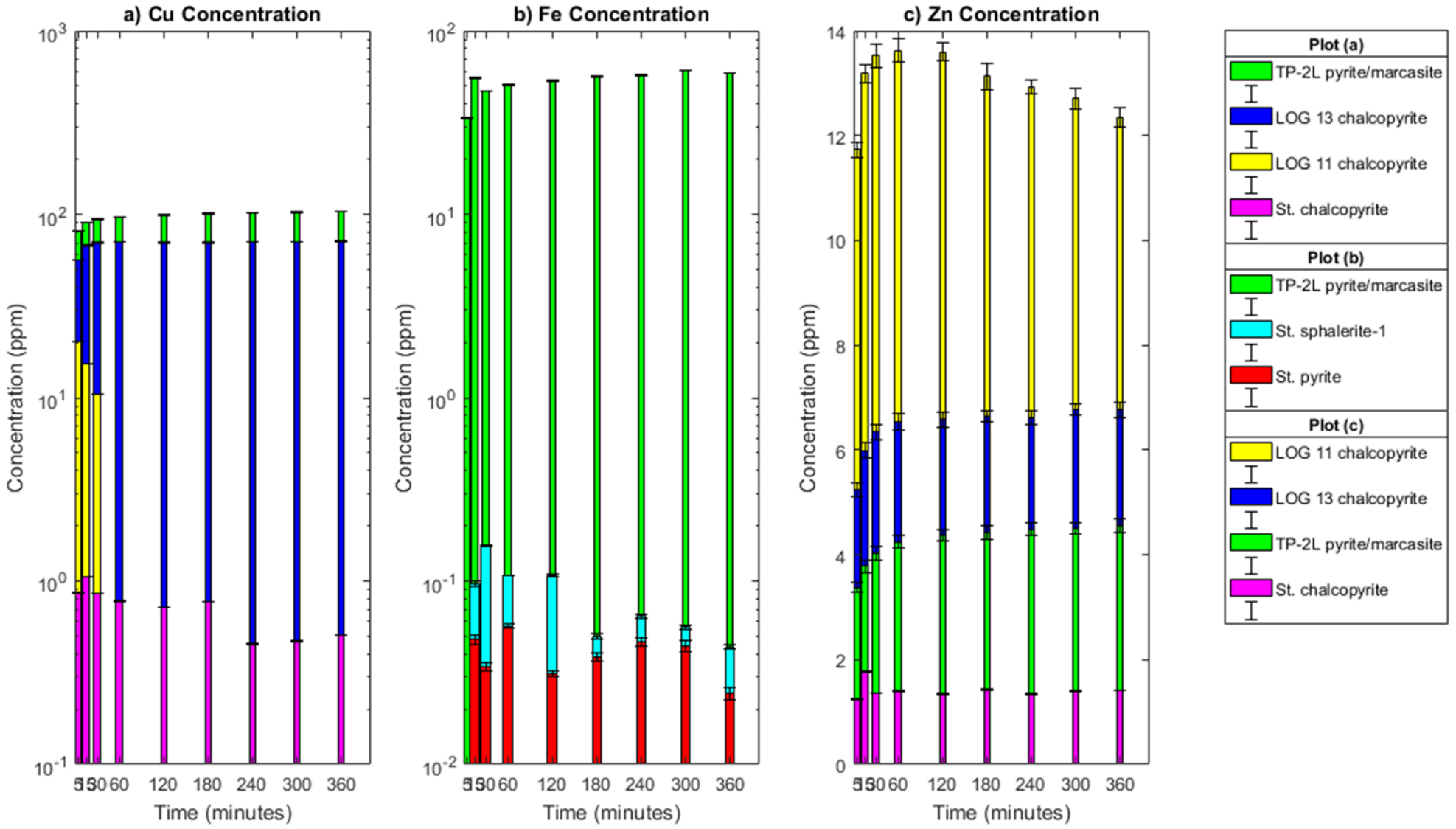

Figure 35: Plots a), b), and c) show the difference in metals leached (Cu, Fe, Zn) from natural sample experiments, compared standard sample experiments. Natural samples monomineralic >500-1000 µm, room temperature 5g:250ml (TP-2L, LOG 13), and 3g:250ml (LOG-11). Standard samples monomineralic >355-500 µm, room temperature 5g:250ml. Across all plots, natural sample experiments leach significantly higher concentrations of Cu, Fe, and Zn, than the standard sample experiments. St. = Standard samples.

Figures 33 and 34 compare the metal concentrations (Fe, Cu, Zn) leached from this study for pyrite/marcasite monomineralic experiments, with those from Fallon (2018); Fuchida *et al.* (2018); Knight *et al.* (2018). Fe concentrations in pyrite from Knight *et al.* (2018) (Figure 33), display similar values to the standard pyrite used in this study, despite being conducted at cooler temperatures (2.3 °C) and finer grain sizes (100-200 µm). Knight *et al.* (2018) pyrite samples are terrestrially sourced, like the pyrite used in this thesis's study, bought in polished and crushed, which may account for the similar concentrations being leached (both circled in red on Figure 33). Fuchida *et al.* (2018) pyrite samples are fresh hydrothermal sulphides, sourced from Okinawa Trough, Chikyu, and at both 5°C and 20°C leach a Zn concentration range within the same order of magnitude as the TP-2L pyrite(/marcasite) samples. These values are similar despite much finer grain sizes being used (mode 14 µm) and higher mass:fluid ratios (3g:150ml) in Fuchida's experiments (Fuchida *et al.*, 2018). Fe concentrations in Fuchida *et al.* (2018) pyrite unlike Zn, appear at lower concentrations to TP-2L

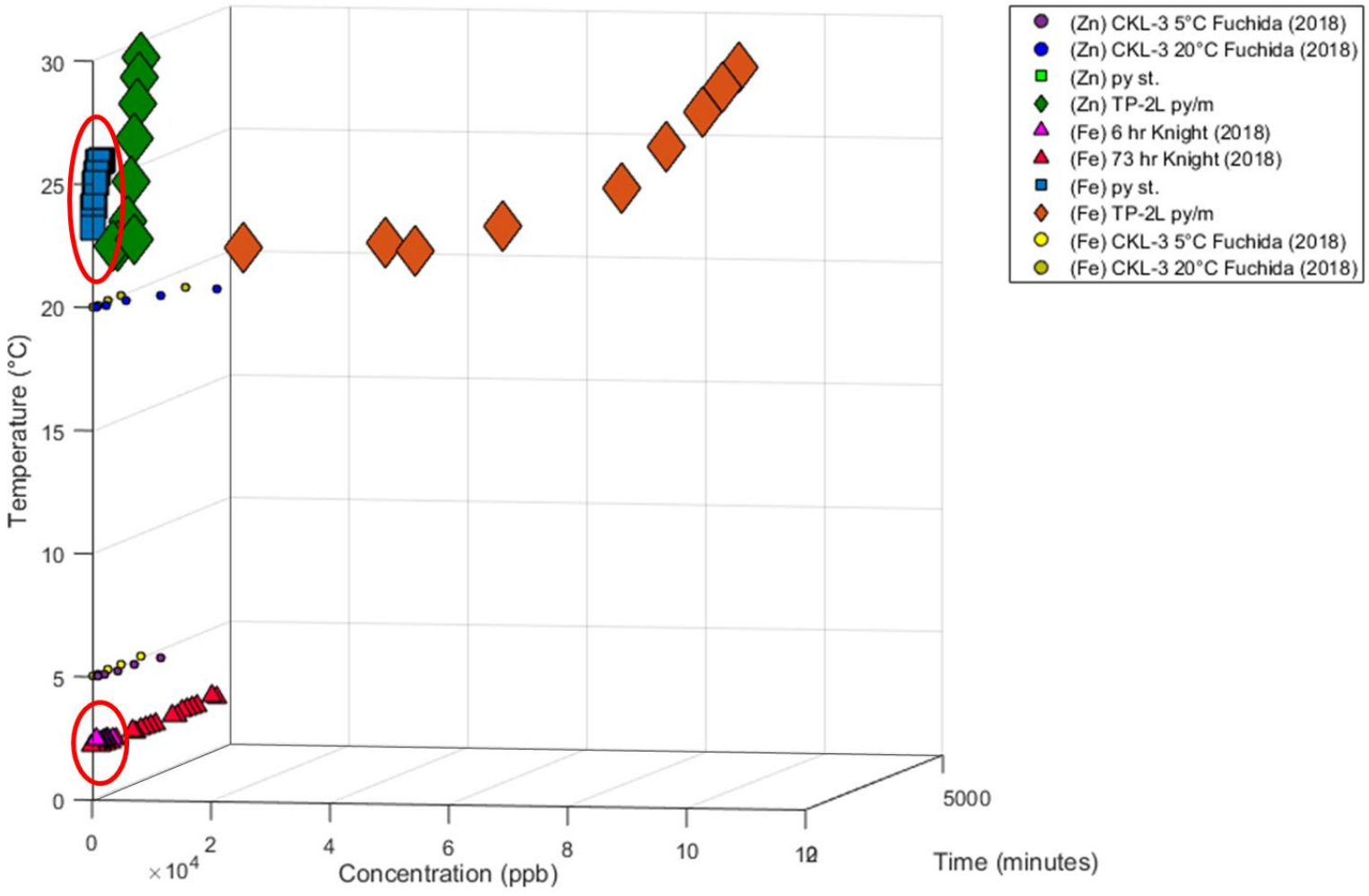

Figure 36: Concentration of Fe and Zn across pyrite samples in Knight (2018) and Fuchida (2018) against this projects standard pyrite and TP-2L. Different grainsizes are represented by marker size, Fe concentration in red, and Zn concentration in green. Conversions for Knight (2018) and Fuchida (2018) values to ppb were made on the assumption that 1kg = 980 ml of seawater. Grainsizes: Knight (2018) = 100-200 µm, Fuchida (2018) = mode 14 µm, standard pyrite = 355 µm, TP-2L py/m = 1000 µm. Rock:Fluid ratios in each study: Fuchida (2018) – 3g:150ml; Fallon (2018) - 0.55g:5.5ml; Knight (2018) – 0.6g:700ml.

pyrite(/marcasite). This may be due to the composition of the two samples or to the higher temperatures recorded in the TP-2L experiments. It could also be that the colloidal texture of TP-2L creates higher surface areas despite the larger grain sizes than the CKL-3 pyrite of Fuchida *et al.* (2018).

Cu concentrations in chalcopyrite (Figure 34) again show Knight *et al.* (2018) chalcopyrite (terrestrially sourced and crushed) to be within the same order of magnitude as the standard chalcopyrite of this study (circled red in Figure 34), seemingly uninfluenced by the temperature or grain size differences. Fallon (2018) uses the same LOG-13 chalcopyrite as this study, but at much finer grain sizes (2.5-50 µm). The lower concentrations observed in Fallon (2018) LOG-13 chalcopyrite when compared to this studies LOG-13 chalcopyrite, is likely due to the smaller mass used in experiments, and not the influence of temperature or grain size differences. If the ~0.55g:5.5ml of LOG-13 cp in Fallon (2018) is scaled up to the 5g:250ml that was used in this study, the Cu concentrations would be 5x higher, more similar to concentrations observed in this study.

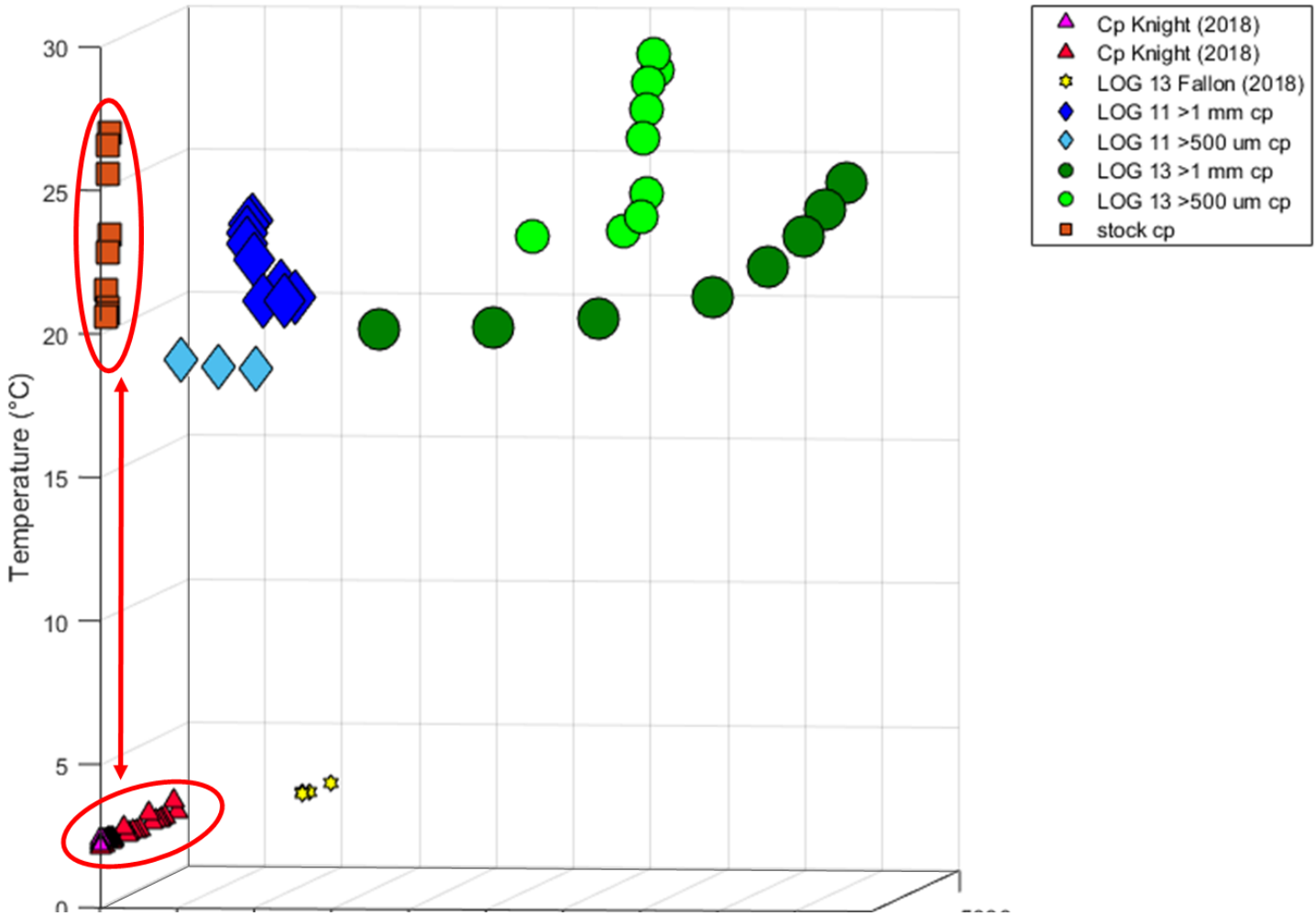

Figure 37: Concentration of Cu across chalcopyrite samples in Knight (2018) and Fallon (2018) against this projects standard chalcopyrite, LOG 13 and LOG-11. Different grainsizes are represented by marker size, and Cu concentration in pink. Conversions for Knight (2018) values to ppb were made on the assumption that 1kg = 980 ml of seawater. Grainsizes: Knight (2018) = 100-200 µm, Fallon (2018) = 2.5 – 50 µm, standard chalcopyrite = 355 µm, LOG-11 cp = 1000 µm and 500 µm, and LOG 13 cp = 1000 µm and 500 µm. Rock:Fluid ratios in each study: Fuchida (2018) – 3g:150ml; Fallon (2018) - 0.55g:5.5ml; Knight (2018) – 0.6g:700ml.

Across Figures 33 and 34 it is clear that for pyrite and chalcopyrite, the factors with the strongest effect on metal leaching are reactive surface area and mineral composition. Concentrations in Knight *et al.* (2018) are consistently higher for Fe, Cu, and Zn for pyrite and chalcopyrite as temperature appears to have a lesser effect on leaching potential than the smaller grain sizes used in Knight *et al.* (2018) and are likely the source for increased metal concentrations observed.

Natural hydrothermal samples such as the separated LOG and TP-2L mineral samples used in the study, as well as the CKL samples of Fuchida *et al.* (2018) and LOG-13 of Fallon (2018) are comparable. CKL-3 pyrite released Zn at higher concentrations to TP-2L, and Fe concentrations that were lower. The smaller grain sizes, 1 $m^2 g^{-1}$ surface area, used in Fuchida *et al.* (2018) may have had some influence on leaching rates, but then the colloidal textures of TP-2L give rise to high surface areas, making it hard to quantify which sample actually had the higher surface area, especially since Zn in Fuchida *et al.* (2018) had higher concentrations, while Fe in TP-2L was higher. This could be due to the geochemistry of both samples with the metal percentage in both being similar with 94% Fe and 4.6% Zn in Fuchida (2018), and 90.5% Fe and 0.45% Zn in TP-2L; Zn being higher in Fuchida (2018). While Fuchida (2018) CKL-3 sample is primarily pyrite with some trace barite, the picked TP-2L in this study is bulk pyrite, with some marcasite. Therefore, it is possible in this scenario that the mineralogy of both samples had the biggest control on the concentrations of elements leached. Fuchida *et al.* (2018) discusses the likelihood of Fe being sequestered from solution by the formation of insoluble oxyhydroxides due to its low solubility in seawater, while Zn has much higher solubility limits allowing it to remain in solution in highly soluble Zn-minerals. This could be a potential reason for why Fe in CLK-3 is lower in Fuchida *et al.* (2018), while Zn concentrations are higher. However, as this isn't also observed in the TP-2L results, this is unlikely to have a big effect on Zn and Fe concentrations in solution for TP-2L experiments.

The main control for LOG-13 chalcopyrite used in Fallon (2018) and LOG-13 chalcopyrite of this study, appears to be the difference in grain size and surface area, with Fallon (2018) LOG-13 leaching x5 more Cu when scaled up from 0.55g:5.5ml to the same mass:fluid ratio as what this study used (5g:250ml).

Overall, when you compare the monomineralic leaching ability of the natural samples discussed above with standard samples across different studies, it reinforces the idea that natural samples are clearly more representative of metal leaching from SMS, and therefore will be more revealing in the effects of SMS mining. While standard samples that are more accessible, convenient and pure, can be useful in showing the baseline relationships between factors such as surface area, temperature and mineralogy, the lower concentrations leached from these samples should be kept in consideration when applied to the potential effects of SMS mining and scaled up.

7.3 The Effect of Mineral Pairs on Elemental Leaching

To recap, galvanic cells arise between sulphide minerals with different rest potentials in a saline solution, the higher rest potential being cathodically protected from dissolution, and the lower being preferentially dissolved (Knight *et al.*, 2018).

The presence of galvanic cells can be alluded to in the polymineralic experiments of this study, from the difference in element leaching from individual monomineralic minerals when compared with their mineral pair comparisons. Galvanic cells are more likely in natural samples due to grain contacts, while standard samples possessed 'mechanical' contacts. However, galvanic cells may have arised through minerals touching in standard samples, this being observed in Knight et al. (2018) study which used similar techniques.

7.3.1 Standard Pyrite & Galena

Figure 35 shows the relationship between pyrite and galena for Fe, Cu and Pb leached during each experiment. In the first hour pyrite leaches high concentrations of Fe before stopping, this could be explained by a galvanic cell arising between pyrite & galena, cathodically protecting pyrite. Alternatively, if galvanic cells were present from the start, galena could have preferentially leached out all of its Fe content within the first hour. Cruz *et al.* (2005) looks at the potential for galvanic cells between pyrite and galena in a concentrate of pyrite, sphalerite and galena (105-150 μm at 10g/L, 20 °C in a CO_2 saturated water). Only the effects of galena coupled with pyrite were observed in this concentrate (lowest rest potential), finding that pyrite activity is greatly affected, with pyrite dissolution resuming only after the galena and sphalerite phases were removed (i.e. dissolved) (Cruz *et al.*, 2005). Abraitis *et al.* (2004) saw that when galena & pyrite were coupled, Pb leaching increased by a factor of 31, with no increases observed in Fe. The similarities between studies, may suggest that standard pyrite dissolution was prevented when paired with standard galena, preferentially releasing Fe from galena as it dissolved.

However, preferential leaching of Pb from galena is also expected in this pairing, with only ~half of Pb in polymineralic experiment being observed compared with monomineralic galena, likely due to there being half the mass of galena in polymineralic. EMPA data of galena used in both experiments % of Pb leached out of mass put in to each experiment was calculated: For monomineralic galena 5g of galena, (87 wt% of galena is Pb according to EMPA analysis, therefore ~14700 ppm of Pb) was put in to the experiment, with ~0.66 ppm of Pb leached out equalling ~$0.0038 \pm 2 \times 10^{-5}$% of the galena mass. For polymineralic galena & pyrite ~2.5g of galena (~8700 ppm Pb) was put into the experiment, with ~0.37 ppm leached out, equating to ~$0.0042 \pm 3.5 \times 10^{-5}$%. Therefore, the polymineralic experiment leached 10.9±1.5% more Pb than monomineralic galena. This isn't a huge increase in Pb and while a bigger increase would have been expected for it to be considered preferentially leaching, this coupled with the absence of Fe and Cu in the polymineralic

experiment, does suggest that only galena was oxidising in the mineral coupling. So overall there is evidence for galena protecting pyrite. Figure 35 is not normalised for concentration put in vs leached out of the experiments but instead shows the true concentrations leached during each experiment run.

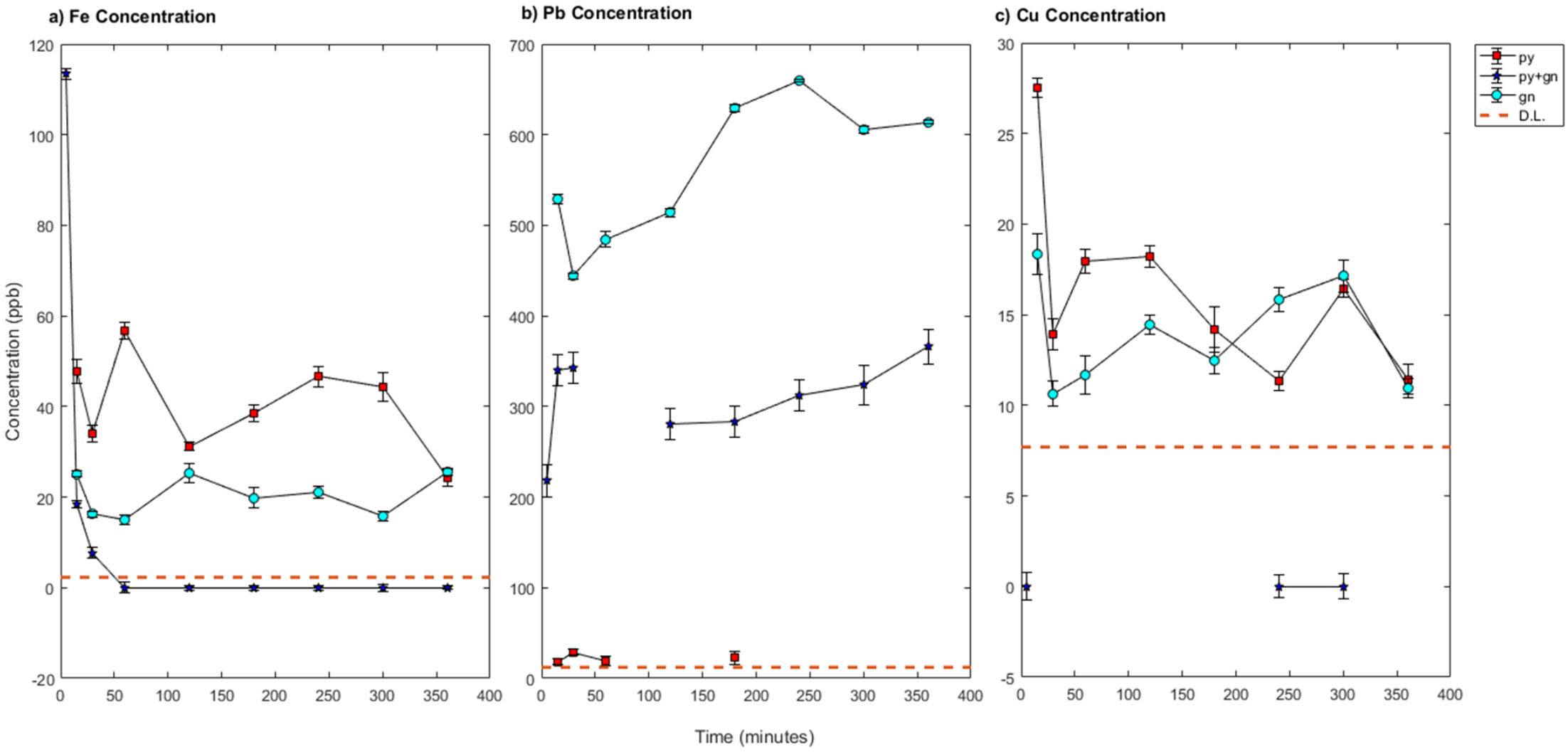

Figure 38: Polymineralic pyrite & galena experiment data presented against monomineralic pyrite and monomineralic galena, for Fe, Cu, Pb concentrations (ppb). Experiments run at room temperature, ~8.1 pH, 355 µm grainsize and 5g:250ml rock:fluid ratio. Legend abbreviations: py = pyrite, gn = galena, D.L. = detection limits **a)** Monomineralic pyrite leaches the highest concentration of Fe across the experiment, reaching a high of 60 ppb, while monomineralic galena contains lower concentrations, consistently around 20-25 ppb throughout. Polymineralic pyrite & galena initially has the highest concentration of Fe at ~118 ppb, before a rapid decrease to 0 ppb by 1 hour. **b)** Monomineralic galena displays the highest concentrations of Pb, with a high of ~670 ppb reached at 4 hours. Monomineralic pyrite contains negligible amounts of Pb, with polymineralic pyrite & galena having values somewhere in the middle of both, reaching a high of ~350 ppb at 6 hours. **c)** Monomineralic pyrite and monomineralic galena both leaching similar amounts of Cu throughout experiments, while polymineralic pyrite and galena leach <bdl. and 0 ppb of both Cu and Sb. Data points are absent where values were bdl, instead it can be presumed that concentrations at missing time intervals lie between bdl dashed line and 0 ppb.

7.3.2 Standard Pyrite & Chalcopyrite-sulphide-mix

Figure 36 presents the relationships for pyrite and chalcopyrite-sulphide-mix for Cu, Fe, Ni and Zn. Suspected mineral pairs existing in the form of inclusions within the chalcopyrite—sulphide-mix (e.g. +sphalerite) needs to be considered when discussing these experiments.

Absence of Fe and persistently high Cu concentrations observed in polymineralic pyrite & chalcopyrite-sulphide-mix, suggests galvanic interactions are occurring. With chalcopyrite-sulphide-mix likely being preferentially dissolved and pyrite cathodically protected, hence no Fe leaching. This is congruent with rest potentials, pyrite>chalcopyrite, however if sphalerite is present in the chalcopyrite-sulphide-mix then it may have a similar or lower rest potential to chalcopyrite (suggesting sphalerite and/or chalcopyrite would be anodically dissolving). The high Zn concentrations leached from both monomineralic chalcopyrite-sulphide-mix and the polymineralic experiment is indicative of sphalerite being present in the chalcopyrite-sulphide-mix sample and therefore adds further confusion surrounding what minerals are present and being anodically dissolved.

Cu concentrations in the polymineralic experiment do not surpass those observed in monomineralic chalcopyrite possibly due to Cu solubility limits being met. Therefore, it is possible that Cu above its solubility is removed from solution as precipitates or oxides. However, if assuming the formula for chalcopyrite $CuFeS_2$ (excluding any other minerals that may be present e.g. sphalerite) in the chalcopyrite-sulphide-mix, then 2.5g of chalcopyrite-sulphide-mix of which ~25% is Cu (~5000 ppm of Cu) went into the monomineralic experiment with <1.050 ppm leached out, ~0.00021±7x10^{-7}%. Using the same assumptions for the polymineralic experiment, 1.25g of chalcopyrite-sulphide-mix (~2500 ppm of Cu if assuming pure chalcopyrite) went in to the experiment, with ~0.7 ppm being leached out, equating to ~0.00028±1x10^{-6}%, an increase of 33.1±0.8% between both experiments. Therefore, it is possible that Cu leaching from the chalcopyrite-sulphide-mix could see a rise when paired with pyrite.

Knight (2018) also sees pyrite cathodically protected when coupled with chalcopyrite, but unlike this study, saw an increase in Cu at 600% faster rates from chalcopyrite. While Abraitis *et al.* (2004) observes Cu increases by a factor of 1.5 when pyrite is coupled with chalcopyrite, they go on to say that there was no clear evidence for galvanically promoted chalcopyrite leaching. The lack of Fe leaching in the polymineralic experiment of this study would strongly suggest the prevention of pyrite dissolution, based on the relationships between pyrite & chalcopyrite (sulphide mix) of other studies, it is probable that galvanic cells are at play here, with pyrite being cathodically protected, despite there being no definitive evidence for preferential chalcopyrite-sulphide-mix leaching. Future work for this pairing would need to require EMPA analysis of chalcopyrite to ensure mineral purity. Overall, there seems to be evidence for pyrite being protected by chalcopyrite.

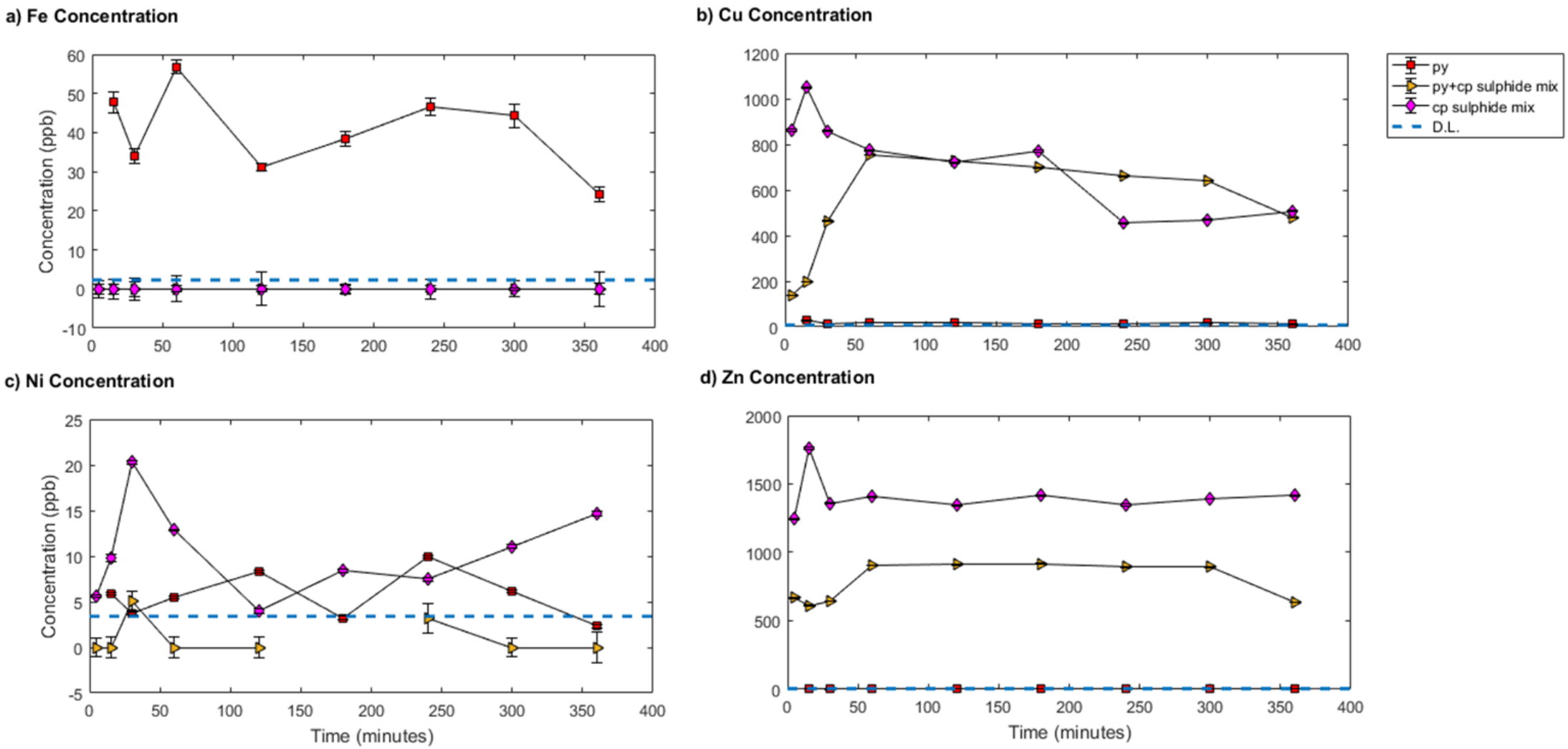

Figure 39: Polymineralic pyrite & chalcopyrite sulphide mix experiment data presented against monomineralic pyrite and monomineralic chalcopyrite, for Fe, Cu, Ni, Zn concentrations (ppb). Experiments run at room temperature, ~8.1 pH, 355 µm grainsize and 5g:250ml rock:fluid ratio. Legend abbreviations: py = pyrite, cp = chalcopyrite sulphide mix, D.L. = detection limits. **a)** Pyrite has the highest concentration of Fe in solution, reaching ~58 ppb at 1 hour, while both chalcopyrite sulphide mix and pyrite & chalcopyrite sulphide mix have no Fe leaching. **b)** Displays the opposite to a), where pyrite has negligible concentrations of Cu across the 6 hours. Chalcopyrite sulphide mix displays the most Cu leaching, with highs over 1000 ppb. Pyrite & chalcopyrite sulphide mix behave in a similar fashion to chalcopyrite sulphide mix, with an initially rapid increase of Cu, to concentrations matching those of chalcopyrite, before steadily decreasing, with chalcopyrite. **c)** monomineralic pyrite and chalcopyrite sulphide mix both leach variable amounts of both Ni over the 6 hours, while pyrite & chalcopyrite sulphide mix leaches negligible (~0 ppb) amounts of Ni. d) Monomineralic chalcopyrite sulphide mix leaches the highest concentration of Zn with polymineralic pyrite & chalcopyrite sulphide mix leaching approximately half of that, while monomineralic pyrite leaches ~) ppb Zn. Data points are absent where values were bdl, instead it can be presumed that concentrations at missing time intervals lie between bdl dashed line and 0 ppb.

7.3.3 Standard Galena & Chalcopyrite-sulphide-mix

Polymineralic galena & chalcopyrite-sulphide-mix demonstrate concentrations that suggest both galena being preferentially dissolved, as well as chalcopyrite-sulphide-mix dissolution still occurring, Figure 37. Surprisingly, Fe concentration in polymineralic galena and chalcopyrite-sulphide-mix is higher than in monomineralic galena, this may suggest that galena is being preferentially dissolved, leaching more Fe, as monomineralic chalcopyrite-sulphide-mix leaches no detectable Fe (bdl). Polymineralic galena & chalcopyrite-sulphide-mix sees an initially sharp Pb increase before decreasing back down to concentrations observed in monomineralic galena. This is in contrast to monomineralic chalcopyrite-sulphide-mix which continues to steadily increase in Pb over the duration of the experiment to levels higher than released by monomineralic galena (Figure 37). However, there is less chalcopyrite-sulphide-mix in the polymineralic experiment. This relationship is interesting as it may indicate that the Pb observed in polymineralic galena and chalcopyrite-sulphide-mix is being leached from galena. As after initially higher Pb concentrations in the polymineralic experiment, they decrease again, behaving in the same way as monomineralic galena, while the chalcopyrite-sulphide-mix in the pair would be expected to continue increasing like the monomineralic chalcopyrite-sulphide-mix. Alternatively, the presence of galena may result in Pb being removed from solution after the first 3 hours by other reactions taking place, such as sequestering of Pb by oxides. Cu in polymineralic galena & chalcopyrite-sulphide-mix is very similar to monomineralic chalcopyrite-sulphide-mix throughout the 6 hours, suggesting that Cu release from chalcopyrite-sulphide-mix continues when galena is present, but is not increased. Polymineralic galena & chalcopyrite-sulphide-mix has Zn leachate concentrations ~half of that in monomineralic chalcopyrite-sulphide-mix, while galena has ~0 ppb. This suggests that chalcopyrite-sulphide-mix in the polymineralic experiment is continuing to leach Zn, but at lower quantities due to less mass being present. Contradicting what is observed in this study, Fuchida *et al.* (2017) observed no Cu in leachate produced from a Zn-Pb (sphalerite-galena) rich ore containing chalcopyrite. Whether galvanic cells are set up between galena and chalcopyrite-sulphide-mix is unclear, with some evidence for galena being anodically dissolved through the increase in Fe and possibly also Pb leaching trends; but there's more evidence for chalcopyrite-sulphide-mix dissolution occurring as normal, which doesn't indicate a galvanic pair. In conclusion, based on standard terrestrial sulphides, it could be concluded that pyrite is galvanically protected by the other sulphides, but the order between the remaining sulphides remains unclear. This could be resolved in future work with samples like chalcopyrite-sulphide-mix being analysed for purity, so more confidence can go into the galvanic pairings.

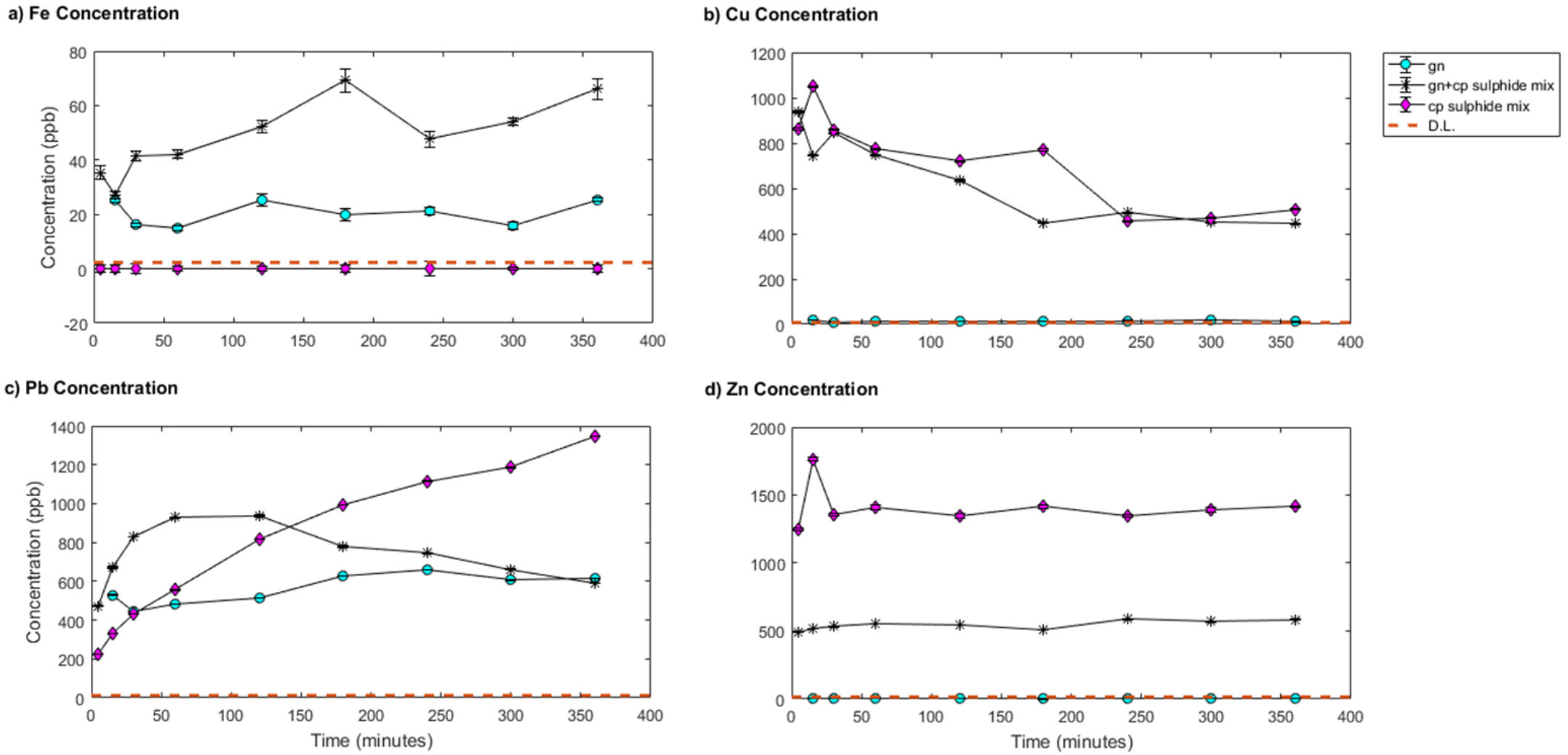

Figure 40: Polymineralic galena & chalcopyrite sulphide mix experiment data presented against monomineralic galena and monomineralic chalcopyrite sulphide mix, for Fe, Cu, Pb, Zn concentrations (ppb). Experiments run at room temperature, ~8.1 pH, 355 µm grainsize and 5g:250ml rock:fluid ratio. Legend abbreviations: gn = galena, cp = chalcopyrite sulphide mix, D.L. = detection limits. **a)** Galena sees an initial decrease in Fe before plateauing around 2 hours, with low-moderate concentrations of Fe observed across the 6 hours. Chalcopyrite sulphide mix doesn't display any Fe leaching across the experiment duration, while galena & chalcopyrite sulphide mix sees two main increases in Fe concentration after an initial dip, peaking at ~70 ppb at 3 hours. **b)** Galena leaches 0 ppb of Cu across the 6 hours, while both chalcopyrite sulphide mix and galena & chalcopyrite sulphide mix follow the same trend with similar Fe concentrations, with Fe decreasing over the duration of the experiments. **c)** Chalcopyrite sulphide mix leaches the highest concentration of Pb, up to ~1380 ppb, with rapid increases in concentration observed over the 6 hours. Galena leaches moderate concentrations of Pb plateauing around 3 hours after an initial increase. Galena & chalcopyrite sulphide mix sees an initially rapid increase of Pb, peaking at ~940 ppb at 2 hours, before decreasing down to monomineralic galena levels. **d)** Galena sees no Zn leaching over the course of the experiment, with chalcopyrite sulphide mix bringing about the highest concentrations, peaking at ~1750 ppb. Galena & chalcopyrite sulphide mix has Zn values just under half of those of monomineralic chalcopyrite sulphide mix (~500-600 ppb), following a similar trend. Data points are absent where values were bdl, instead it can be presumed that concentrations at missing time intervals lie between bdl dashed line and 0 ppb.

7.3.4 Natural LOG-11 Chalcopyrite & Secondary-Cu-sulphides

LOG-11 trends for Cu, Fe, Zn and Ni are presented on Figure 38.

Monomineralic LOG-11 has initially high Cu concentrations that sharply declines, possibly due to Cu removal from solution. The opposite occurs in polymineralic LOG-11, where perhaps prolonged release of Cu balances out the amount removed from solution. The lack of Fe in polymineralic LOG-11, suggests that any Fe release from chalcopyrite is prevented when coupled with secondary-Cu-sulphides; or that Fe is precipitated out of solution more rapidly. Higher concentrations of Zn and Ni in polymineralic LOG-11, may indicate that chalcopyrite is preferentially leaching Zn and Ni when paired with secondary-Cu-sulphides; or that secondary-Cu-sulphides are composed of higher Zn and Ni. The latter being more likely, Fallon (2018) LA-ICP-MS data shows bornite/covellite to be composed of higher Ni and Zn (~780/~1970 ppm and ~2310/~12500 ppm respectively) than chalcopyrite in LOG-11. This can be further supported if the amount of Ni and Zn going in to each experiment vs leaching out is approximated from Fallon (2018) LA-ICP-MS data and estimated mineral pair ratios: ~0.0012g of Ni went into monomineralic LOG-11 and ~$7.5x10^{-4}$g leached out equalling ~6.2±1.8% of the Ni leached into the seawater from the amount that went in. ~0.0048g Ni went into polymineralic LOG-11, with ~0.00011g leached out, only ~2.2±0.4% of Ni that went in, this is a decrease of 63.8±37% from monomineralic LOG-11. The same trend is seen for Zn with ~0.0032g Zn going in to monomineralic LOG-11 and ~0.0034g leaching out, leaching ~106.8±8.3% of Zn that went in; while polymineralic LOG-11 sees ~0.025g going in and ~0.0065g leaching out, only 26.3±0.3.8%, a decrease of 75.3±15.6% from monomineralic LOG-11. A key limitation of these calculations is the assumption that the probe data concentrations for LOG-11 in Fallon (2018) are the same for the LOG-11 used here, another limitation is the assumption that the proportion of bornite:covellite in secondary copper sulphides of LOG-11 are an averaged ratio. Therefore, these calculations are useful as a guide to how much Ni and Zn may have been used from LOG-11. However, large decreases in the % of Ni and Zn used from monomineralic LOG-11, may suggest that chalcopyrite dissolution has significantly decreased/prevented in polymineralic LOG-11 when coupled with secondary copper sulphides.

Fallon (2018) discusses how the presence of secondary-Cu-sulphides including covellite and atacamite may explain for increased dissolved Cu in TAG-J Cu-rich ore (chalcopyrite + pyrite). They also observe decreases in Cu overtime, as was seen in monomineralic LOG-11 of this study, speculating exhaustion of Cu source or isolation from seawater (Fallon, 2018). This may be an explanation for what was observed in monomineralic LOG-11, while polymineralic LOG-11 had multiple Cu sources. Fallon (2018) further discusses how galvanic cells in TAG-J (pyrite + chalcopyrite + secondary-Cu-sulphides) produced higher Cu concentrations later on in their experiments, when compared to TAG-B (a sample with less pyrite) which had initially higher Cu that decreased over time, attributing these observations to the potential for TAG-J to contain more

galvanic cells. This is similar to the trends observed between monomineralic LOG-11, which had an initially higher Cu leach, and polymineralic LOG-11 which had higher and more sustained Cu release later on. Based on the Cu leaching evidence discussed above and that Fe release was prevented in polymineralic LOG-11, it would suggest that there is some indication of galvanic coupling between chalcopyrite and secondary-Cu-sulphides, with the latter preferentially oxidising - although more evidence is needed in order for there to be confidence in the presence of these potential galvanic cells.

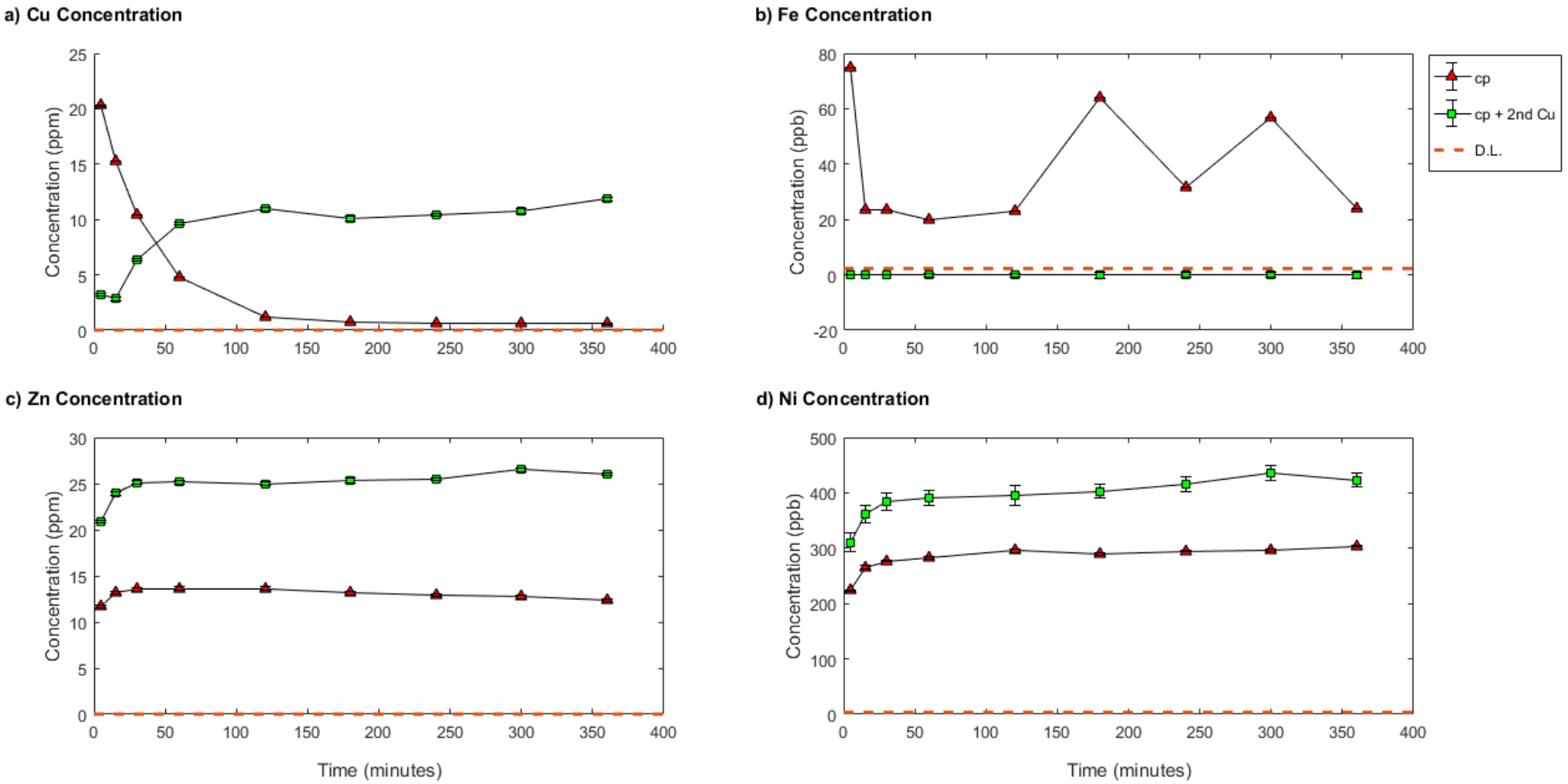

Figure 41: Cu, Fe, Zn and Ni concentrations (ppm/ppb) across E21 monomineralic LOG-11 (chalcopyrite) and E20 polymineralic (chalcopyrite & secondary Cu minerals) experiments. Abbreviations: cp = chalcopyrite, 2nd Cu = secondary copper sulphides, D.L. = detection limit. **a)** Cu (ppm) drastically declines over time in E21 (monomineralic: chalcopyrite (LOG-11)), plateauing after 240 minutes. The opposite is observed in E20 (polymineralic: chalcopyrite & secondary Cu minerals (LOG-11)), where Cu (ppm) concentrations overtakes that in E21 after 30 minutes. **b)** Fe concentration in E21 fluctuates over time but remains at relatively low concentrations. Whereas no Fe (ppm) was leached during E21. Fe error margins for monomineralic LOG-11 were removed so over-arching trends could be observed. **c)** Both E21 and E20 contain relatively high concentrations of Zn, with E20 containing substantially higher concentrations of Zn. **d)** Shows a similar trend as c), with E20 displaying higher concentrations of Ni (ppb) than E21. Data points are absent where values were bdl, instead it can be presumed that concentrations at missing time intervals lie between bdl dashed line and 0 ppb.

7.3.5 Natural TP-2L Pyrite(/Marcasite) + Chalcopyrite

There is no clear indication for galvanic interactions in polymineralic TP-2L, as monomineralic TP-2L persistently leaches higher concentrations of Cu, Fe, and Zn, Figure 39. If galvanic cells had a dominant effect on metal leaching, it would be expected that chalcopyrite would preferentially leach Cu in polymineralic TP-2L. This isn't observed - with Cu release being lower in polymineralic TP-2L. However, the lack of Fe from polymineralic TP-2L may suggest that pyrite dissolution is halted when coupled with chalcopyrite, or alternatively that Fe is precipitating out more quickly. As with Cu, Zn is higher in monomineralic TP-2L, this may indicate Zn concentrations being lower in chalcopyrite than in pyrite/marcasite, or it might reflect the smaller mass of pyrite/marcasite being put in. If galvanic coupling is present, then chalcopyrite could be leaching lower concentrations of Zn until chalcopyrite is fully dissolved in the pairing and pyrite/marcasite dissolution can resume, returning to higher Zn concentrations. Fallon (2018) LA-ICP-MS data reveals pyrite and chalcopyrite to have similar Zn concentrations, with pyrite (colloform) in TP-2L to have ~140 ppm Zn, whilst chalcopyrite (massive) has ~152 ppm Zn. It is possible that the high surface area associated with a colloform texture, as observed in TP-2L pyrite, allows for the pyrite to leach higher concentrations of Zn, and therefore it is more likely that the smaller mass of pyrite in polymineralic TP-2L is the cause for lower Zn leachate concentrations. A disruption in leaching trends for Cu, Zn and Ni in polymineralic TP-2L are observed at 4 hours. This could potentially be the result of chalcopyrite being used up in any galvanic coupling, and pyrite/marcasite oxidation resuming, or could simply just represent a shift in grains in the flask. Fallon (2018) compares bulk chemistry for TP-2L to dissolved elements detected from leaching experiments, finding that while there is high confidence in the bulk chemistry for the sample, there was considerable trace elements of Cu, Mn, Co, Zn, and Ni in the leaching experiments that were not anticipated by the bulk chemistry. Fallon (2018) attributes these trace element concentrations from leaching experiments to the large surface area that the TP-2L sample has due to pyrites colloform texture, where bulk chemistry doesn't take surface area of a sample as a whole into account. Therefore, the higher Cu, Zn and Ni dissolved concentrations observed from the monomineralic TP-2L experiment of this study, may be due to the high surface area of the colloform pyrite/marcasite. Where chalcopyrite present in polymineralic TP-2L doesn't have such high surface areas as pyrite, this may account for the lower Cu, Zn, and Ni concentrations leached. However, this doesn't account for the absence of Fe leaching in polymineralic TP-2L, which would be indicative of pyrite being cathodically protected from dissolution. It is hard to determine whether surface area or galvanic coupling is the dominant control on element leaching in TP-2L without further experimentation, but it could be that a combination of both are at play.

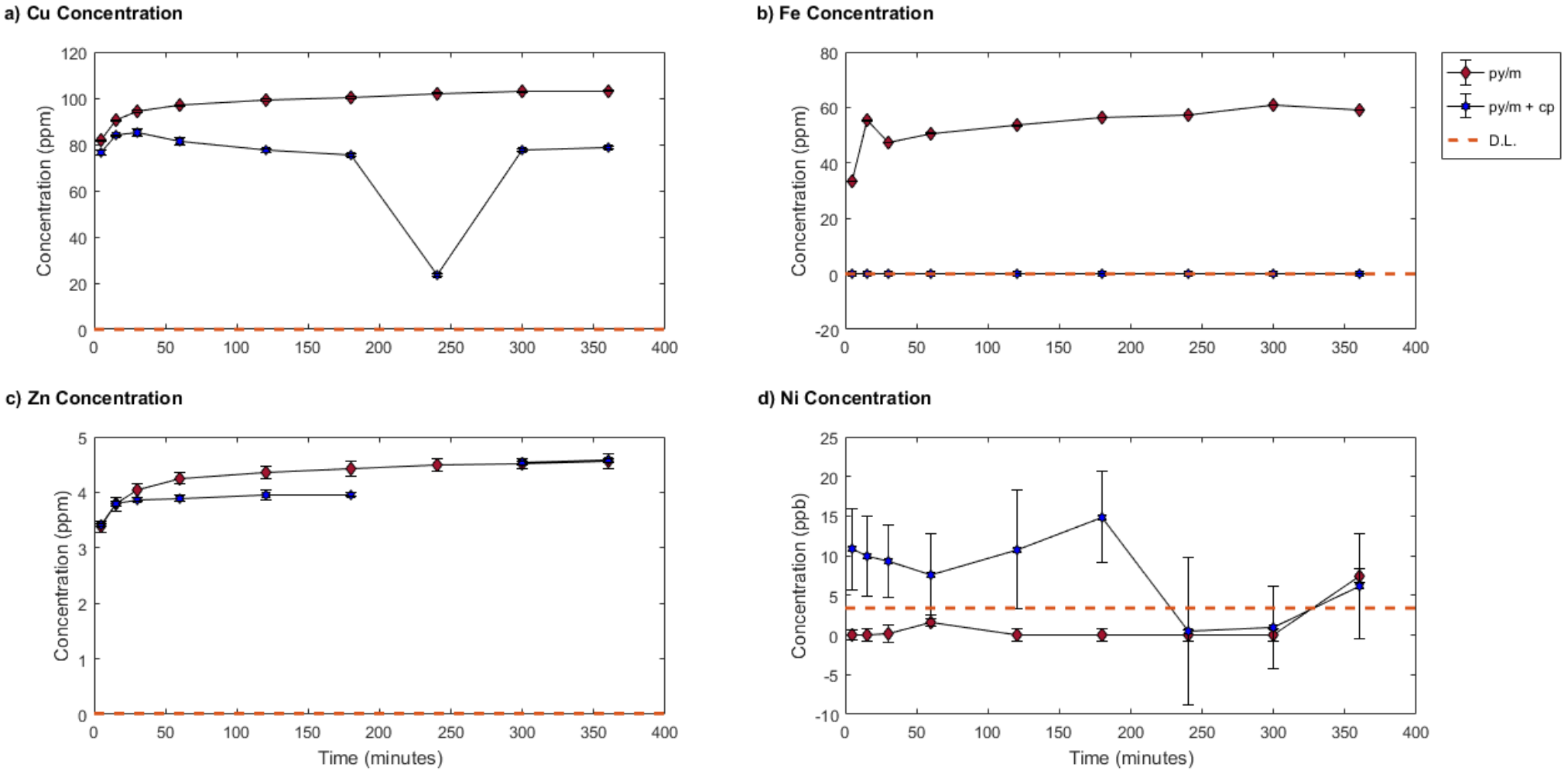

Figure 42: Cu, Fe, Zn and Ni concentrations (ppm/ppb) across E23 monomineralic TP-2L (pyrite) and E24 polymineralic (pyrite & chalcopyrite) experiments. Abbreviations: py/m = pyrite/marcasite, Cp = Chalcopyrite, D.L. = detection limit. **a)** Cu concentrations (ppm) are higher in E23 (monomineralic: pyrite/marcasite) than in E24 (polymineralic: pyrite/marcasite + chalcopyrite). **b)** Shows the same trend to a), with E23 containing much higher concentrations of Fe (ppm) than E24 with has ~0 ppb of Fe. **c)** E24 initially contains lower concentrations of Zn (ppm) than E23, before increasing and ending with the same/slightly higher concentrations at 5-6 hours. **d)** The opposite trend is observed than in a) and c), with Ni (ppb) in E24 having initially higher concentrations of Ni than E23, before decreasing to similar concentrations as E23. Data points are absent where values were bdl, instead it can be presumed that concentrations at missing time intervals lie between bdl dashed line and 0 ppb.

The effect of galvanic coupling on hydrothermal sulphide deposits during SMS mining, is an overall increase the concentrations of metals being released into solution through the preferential leaching of anodic minerals. SMS deposits in mining scenarios, such as the Solwara 1 project, will likely behave in a similar fashion to the natural sulphide samples investigated in this study. Where mineral pairs are present within the mined samples and exist even in smaller crushed grain fractions. There is also potential for galvanic cells to arise when accidental ore rock spillages or waste rock return of certain sulphide minerals are deposited on top of SMS deposits with different sulphide minerals, a scenario similar to the standard sulphide experiments. Metal release associated with galvanic coupling is dependent on the mineralogy of the hydrothermal sulphide deposits. Therefore, it is important that the effect of mineral pairs and galvanic interactions are considered in the context of SMS mining to fully evaluate potential hazards such as metal leaching in risk assessment studies. As the Solwara 1 deposit has a rough composition of ~30% pyrite, ~24% chalcopyrite, and ~6 sphalerite (Knight *et al.*, 2018), it may be that galvanic cells contribute to higher concentrations of Cu and Zn in metal leachates in reality than what has been previously predicted.

7.4 High Temperature (50 °C) Galvanic Experiments

The effect of galvanic interactions on sulphide leaching under high temperatures (50 °C) is not obvious, whilst the effect of high temperature is very clear with increased Pb concentrations in the 50 °C experiments. Pb leachate concentrations in Figure 40 shows trends between monomineralic and polymineralic galena experiments at 50°C and at 25°C. Monomineralic galena (50°C) begins and maintains higher Pb concentrations throughout the 6 hour run, while polymineralic galena + pyrite (25°C) have consistently lower Pb concentrations to monomineralic galena (25°C) across the 6 hours. While polymineralic galena + pyrite (50°C) again starts with lower Pb concentrations to monomineralic galena (50°C), before steadily increasing to overtake and maintain similar concentrations to monomineralic galena (50°C), this may be due to solubility limits preventing further Pb in solution. This estimated solubility limit at 50 °C is roughly the maximum Pb leaching observed in both monomineralic and polymineralic experiments at 50 °C. These comparisons between the 50°C and 25°C experiments, show that high temperature differences do have an effect on sulphide leaching, indicating that large temperature differences are a more dominant control on sulphide leaching than galvanic pairs alone, and on smaller temperature fluctuations as previously seen in the room temperature experiments. Whilst the effect of galvanic pairs under high temperatures are not obvious in these experiments, they are potentially indicated through the sustained higher concentrations of Pb and suppression of Fe leaching in the 50 °C polymineralic experiment. The combined effect of high temperatures and galvanic pairs may allow for higher concentrations of sulphide leachates for longer durations, this may have implications on SMS mining in the scenario that sulphide waste/return waters fall close to active hydrothermal vents.

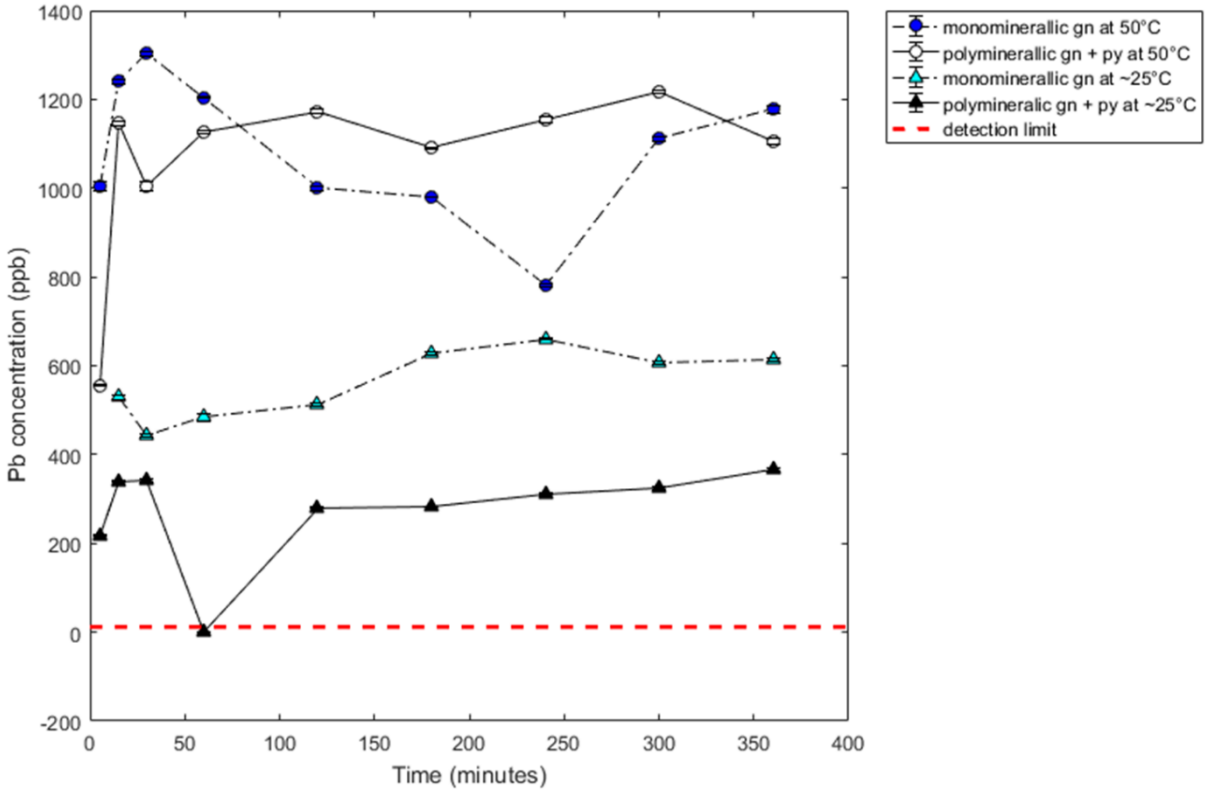

Figure 43: Comparison of Pb concentrations between high temperature (50 °C) and room temperature (~25 °C) monomineralic galena experiments and polymineralic galena and pyrite. Abbreviations: gn = galena; py = pyrite D.L. = detection limits.

7.5 Solubility Limits and Precipitate Formation

The formation of precipitates from leached sulphide metal products, may be a means of sequestering and removing dissolved metals from solution. Whole evidence for were not specifically identified in the seawater dissolution experiments, their presence may have been indicated by: increases in mass of samples after trial experiment runs, yellowing of solution in the TP-2L experiments, and the subsequent decreases in element concentrations in seawater dissolution experiments over time after initial increases.

Increases in mass were observed in the trial experiments for standard galena and sphalerite-1 post runs. Samples were weighed prior to each experiment run, then filtered and dried under vacuum conditions before being re-weighed post experiment. On average there was an increase in sample mass of ~0.15g, this small increase in mass occurred despite there being probable sample loss during experiment runs and may indicate salt or weathering product precipitation .

Experiments in which TP-2L was used, saw cloudy yellowing of the solution, darkening as the experiment progressed. A similar phenomena was observed LOG-11 and LOG-13 experiments, with solutions darkening over time to cloudy grey. While it is possible that these colour changes were due to sample grains being broken up forming a fine sediment; it is more likely that colour changes were the formation of precipitates such as iron oxide.

The biggest indication for dissolved metals being sequestered out of solution by the formation of precipitates, is the decreases in element concentrations observed over time. This is most commonly observed in Cu and Fe for standard experiments, and Cu in monomineralic LOG-11 and polymineralic TP-2L. Fallon (2018) observes a similar Cu decrease during TAG samples leaching experiments, finding larger Cu drops in TAG-B, than in TAG-J, suspecting the presence of Fe-oxides and oxy-hydroxides observed in TAG-B (prior to experimentation) to be responsible.

Fuchida *et al.* (2018) states that any ferrous iron (Fe^{2+}) released into oxidised solutions will likely be immediately oxidised to ferric iron (Fe^{3+}) and precipitate out of solution due to its low solubility in seawater to oxy-hydroxides. While this may explain decreases in Fe observed during the standard mineral experiments, this isn't observed in the natural sulphide experiments (no Fe decreases). pH decreases observed in the natural experiments, may have allowed Fe to remain in solution at higher concentrations due to an increased solubility.

As previously discussed in *Section 6.3.1,* Zn has a high solubility in seawater. Fuchida *et al.* (2018) assumes the presence of Zn and Pb to be higher in seawater due to their high solubility limits, and also the high solubility's of any secondary Zn-minerals that may form. This is in-line with Zn and Pb concentrations observed during the seawater dissolution experiments of this study, where decreases in Zn and Pb were not seen over time.

The formation of oxides and oxy-hydroxides may be beneficial in terms of SMS mining, as a means of removing dissolved Fe and Cu from solution. Multiple studies agree on the theory that Fe is readily taken out of solution by oxide/oxy-hydroxide formation (Fallon *et al.*, 2018; Fallon, 2018; Fuchida *et al.*, 2018; Knight *et al.*, 2018). With the lack of Fe decrease observed in the natural mineral experiments likely being from major decreases in solution pH. These pH decreases are unlikely to be an issue overtime in SMS mining scenarios as the large volume of the ocean will offset any pH change, so it is relatively safe to assume that dissolved Fe will largely be precipitated out of solution. However, low pH may be able to persist temporarily in plumes, rock pore spaces and fractures, making them highly toxic and allowing for higher solubility's of certain metals to exist. While it is possible for Cu decreases to occur, it isn't always the case as seen for the polymineralic LOG-11 and monomineralic TP-2L experiments. While Fallon (2018) considers that the presence of Fe oxides/oxy-hydroxides already to be advantageous for mining as they result in significant Cu sequestering, not all sulphide deposits will have oxides/oxyhydroxides present prior to mining. The formation of oxides/oxyhydroxides are unlikely to have an effect on Zn and Pb concentrations in solution within the time frame of the experiments.

7.6 Toxicity Potential to Seafloor Environments and Vent Species

Solwara 1 projects plan to release <8 μm grain size of sulphides in return waters, 25-50 m above the seafloor (Gwyther, 2008) may result in higher metal leachate concentrations than anticipated. Depending on the mineralogy of sulphide ores, 600-fold dilutions as proposed in the Solwara 1 EIS (Gwyther, 2008) to achieve ANZECC/ARMCANZ (2000) guidelines for 95% protection may be a major underestimation. Even 5000-fold dilutions as proposed for suspended sediment plumes in return waters may not be enough to meet water quality guidelines (Gwyther, 2008).

The EIS for Solwara 1 (Gwyther, 2008), discusses how return waters will be limited to surface temperatures and oxygenation to 12 minutes. However, as seen throughout the seawater dissolution experiments of this study, substantial metal leaching can occur from sulphide samples within the first 15 minutes of exposure.

Organisms associated with hydrothermal vents include crustaceans, molluscs and polychaete worms (Hauton *et al.*, 2017). These environments naturally experience higher concentrations of heavy metals, with many studies having discussed the likelihood for vent species to display high tolerances to metals, a 'metal resistance', although these tolerance concentrations are unknown (Jeanthon and Prieur, 1990; Llanos *et al.*, 2000; Ando *et al.*, 2002; Vetriani *et al.*, 2005; Gadd, 2010; Simpson & Spadaro, 2016; Fuchida *et al.*, 2017). Despite vent species likely already having high tolerances to metals, it is important that the effect SMS mining will have on dissolved metal concentrations, doesn't exceed those tolerance levels causing toxicity.

Metal tolerance available from Llanos *et al.* (2000) and Edgcomb *et al*. (2004) for active vent species is plotted against AZMECC/ARMCANZ guidelines (2000) for 95% protection in Figure 41, where the average metal leachate concentration from the dissolution experiments is given for comparison. Tolerance level data was available for metals Cu, Zn, Co, Ni and Cd (Llanos *et al.*, 2000; Edgcomb *et al*., 2004). Edgcomb *et al*. (2004) includes tolerance data for free-metals and metal-sulphide complexes (+ 2mM H_2S), where it is clear that tolerance in vent species improves significantly when metal-sulphide complexes are present, compared to when only free-metal were present. This can be observed in Figure 41, where for both Cu and Zn, vent species can tolerate up to 1 μM free-metal forms, increasing to 100 μM and 1000 μM respectively, one reason for this may be that the bioavailability of metals is reduced in metal-sulphide complexes (Edgcomb *et al*., 2004). Heavy metals are more bioavailable when in solution, with the ability to pass across permeable membranes (gills or gut tissues), whilst solid forms need to be ingested (Hauton *et al.*, 2017). Hydrothermal fluids from active vents are enriched in H_2S, therefore metal tolerance for active vent species will be increased, with the formation of metal-sulphide complexes in the presence of H_2S (Fisher *et al*., 2007).

While there isn't H_2S release at inactive vents and throughout the water column, H_2S is associated with sulphide mineral oxidation (Erickson et al., 2009; Fallon, 2018). Therefore, any metals released through sulphide oxidation, will likely form metal-sulphide complexes with H_2S, increasing tolerance levels for vent species. However, average metal concentrations from the natural seawater dissolution experiments in this study, persistently exceed Cu, Zn concentrations for both AZMECC/ARMCANZ guidelines (2000) for 95% protection and the vent species metal tolerance levels.

Cu concentrations released from LOG-13 and TP-2L, are higher than vent species tolerance with 2 mM of H_2S present, indicating that these minerals have toxic potential. Standard minerals generally do not produce enough Cu to be toxic to vent species, although std. chalcopyrite-sulphide-mix and LOG-11 do exceed tolerance levels when H_2S is not present. A similar trend is seen for Zn, where natural samples (LOG-11, LOG-13 and TP-2L) produce high enough quantities of Zn to be toxic to vent species even with H_2S present, while Zn without the presence of H_2S is highly toxic, only requiring 1 µM to be fatal (Edgcomb *et al*., 2004). Ni leached from dissolution experiments does not exceed tolerance thresholds for vent species for any of the samples, although both LOG-13 and TP-2L exceed AZMECC/ARMCANZ guidelines (2000) for 95% protection, meaning that toxicity may occur to other species aside from vent species. Cd concentrations from leaching experiments are again typically lower than vent species tolerance, but exceeds AZMECC/ARMCANZ guidelines (2000) for 95% protection, so although vent species may be able to tolerate these Ni concentrations, toxicity may still occur in different environments.

While the concentration of metals released does depend strongly on a number of variables that are not considered in Figure 41 (grain size, galvanic pairings, mineralogy, mass, etc.), it is clear from these results that there is a high likelihood that SMS mining activities will produce metal concentrations greater than safety thresholds, with large amounts of buffering required to bring concentrations down to adequate levels. Furthermore, the safety AZMECC/ARMCANZ guidelines are general guidelines for all marine environments and there currently aren't any appropriate tolerance guidelines specifically for hydrothermal environments. Therefore the guidelines being used may be under or over estimating the metal tolerance of these environments species.

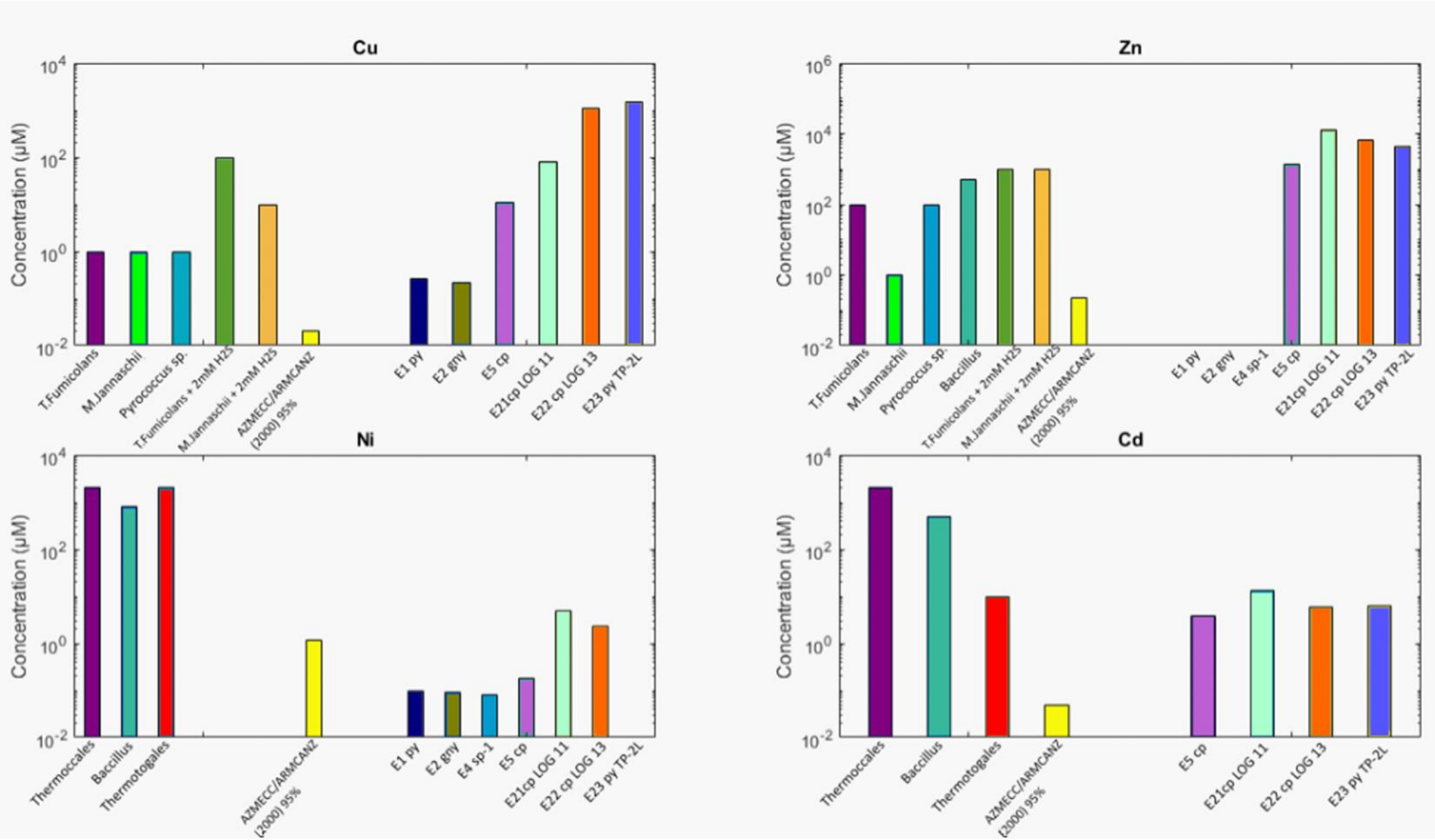

Figure 41: Available tolerance levels data from Edgcomb et al., 2004 and Llanos et al., 2000 studies for different species, plotted against AZMECC/ARMCANZ guidelines, 2000 for 95% protection and average leached metal concentrations from monomineralic seawater dissolution experiments. Ppb → µMol conversions made with assumptions that 1 Kg of seawater is the same as 1 Kg of freshwater, not taking density differences into account. Abbreviations: py = pyrite, gny = galena, sp-1 = sphalerite-1, cp = chalcopyrite sulphide mix.

Figure 41 also shows how tolerance to metals deviates between species, with Thermococcales studied in Llanos *et al.* (2000) showing higher resistances to Cd than Thermotogales, highlighting that despite one species showing resistance to high metal concentrations, other species may not be able to tolerate such concentrations. Therefore, further studies on vent species metal tolerance levels are needed, to fully understand the impact of increased metal concentrations in these environments. While vent species may naturally have a higher resistance to metals, the effect of increased metals in solution on species throughout the water column and through food chain transport needs to be considered (Fuchida *et al.*, 2017). This is where AZMECC/ARMCANZ guidelines (2000) for 95% protection, gives a general safety threshold for metal concentrations in seawater, with Figure 41, illustrating how vent species tolerance to metals drastically exceeds those recommended in the guideline.

Steiner (2009) states that the expected discharge rate of dewatered return waters from the Solwara 1 project, will be 0.3 m^3/sec, equating to >$10x10^6$ tonnes/year. Table 10 shows what that number may look like for the monomineralic dissolution experiment concentrations over a 6 hour period (g/6 hour converted). Projected concentrations show that much higher dilution factors would be required for the samples in this study, compared to the 600x dilution factor presented in the Solwara 1 EIS (Gwyther, 2008). For example, monomineralic std. galena would leach an estimated $7.7x10^{11}$ ppb Pb and monomineralic TP-2L an estimated $1.3x10^{14}$ ppb of Cu over a 6 hour period if scaled up to 7x10+09 g/6hr, requiring dilution factors of $1.7x10^{11}$ and $1.0x10^{14}$ respectively to reach safe levels as according to AZMECC/ARMCANZ guidelines. These concentration projections are only based on the increase in mass for the grain sizes used in experiments (355-500 μm, 500-1000 μm), not taking into account the range of grain sizes expected to be present in the return waters (<8 μm), that will further increase metal leaching potential. Therefore, the dilution and buffering required to bring metal concentrations down to appropriate levels, is likely much higher than first thought, meaning that dangerous concentrations of metals may exist for much longer during and after the mining process.

Table 10: Average metal concentration (ppb) for 6 hour experiments scaled up from 5g mass to projected $7x10^{+09}$ g/6hr for dewatered return plume (Steiner, 2009). >10 million tonnes/year of dewatered return plume, converted to g/6 hour from Steiner, 2009. Dilution factors required calculated to bring projected seawater dissolution results within AZMECC/ARMCANZ, 2000 guideline for 95% protection limits.

	Cd (ppb)	Dilution factor	Cr III (ppb)	Dilution factor	Cr VI (ppb)	Dilution factor	Co (ppb)	Dilution factor	Cu (ppb)	Dilution factor	Pb (ppb)	Dilution factor	Hg (ppb)	Dilution factor	Ni (ppb)	Dilution factor	Ag (ppb)	Dilution factor	Zn (ppb)	Dilution factor
AZMECC/ARMCANZ (2000) 95%	5.5E+00		2.7E+01		4.4E+00		1.0E+00		1.3E+00		4.4E+00		4.0E-01		7.0E+01		1.4E+00		1.5E+01	
E1 py	0.0E+00	0.0E+00	1.1E+00	4.1E-02	1.1E+00	2.5E-01	/	/	1.6E+01	1.3E+01	2.2E+01	5.0E+00	/	/	5.6E+00	8.0E-02	/	/	0.0E+00	0.0E+00
E1 py scaled 7E+09 g/6hr plume	0.0E+00	0.0E+00	1.5E+09	5.6E+07	1.5E+09	3.5E+08	/	/	2.2E+10	1.7E+10	3.0E+10	6.9E+09	/	/	7.7E+09	1.1E+08	/	/	0.0E+00	0.0E+00
E2 gn	0.0E+00	0.0E+00	1.3E+00	4.7E-02	1.3E+00	2.9E-01	/	/	1.4E+01	1.1E+01	5.6E+02	1.3E+02	/	/	5.5E+00	7.8E-02	/	/	0.0E+00	0.0E+00
E2 gn scaled 7E+09 g/6hr plume	0.0E+00	0.0E+00	1.8E+09	6.4E+07	1.8E+09	4.0E+08	/	/	1.9E+10	1.5E+10	7.7E+11	1.7E+11	/	/	7.5E+09	1.1E+08	/	/	0.0E+00	0.0E+00
E4 sp-1	0.0E+00	0.0E+00	1.3E+00	4.7E-02	1.3E+00	3.0E-01	/	/	1.2E+01	8.9E+00	7.7E+01	1.8E+01	/	/	4.7E+00	6.7E-02	/	/	0.0E+00	0.0E+00
E4 sp-1 scaled 7E+09 g/6hr plume	0.0E+00	0.0E+00	1.8E+09	6.5E+07	1.8E+09	4.0E+08	/	/	1.6E+10	1.2E+10	1.1E+11	2.4E+10	/	/	6.5E+09	9.2E+07	/	/	0.0E+00	0.0E+00
E5 cp	3.9E+00	7.1E-01	9.7E-01	3.6E-02	9.7E-01	2.2E-01	/	/	7.2E+02	5.5E+02	7.8E+02	1.8E+02	/	/	1.0E+01	1.5E-01	/	/	1.4E+03	9.4E+01
E5 cp scaled 7E+09 g/6hr plume	5.4E+09	9.7E+08	1.3E+09	4.9E+07	1.3E+09	3.0E+08	/	/	9.8E+11	7.6E+11	1.1E+12	2.4E+11	/	/	1.4E+10	2.0E+08	/	/	1.9E+12	1.3E+11
E21 cp LOG 11	1.3E+01	2.3E+00	1.1E+00	4.0E-02	1.1E+00	2.5E-01	/	/	5.1E+03	3.9E+03	4.3E+03	9.7E+02	/	/	2.8E+02	4.0E+00	/	/	1.3E+04	8.7E+02
E21 cp LOG 11 scaled 7E+09 g/6hr plume	1.8E+10	3.2E+09	1.5E+09	5.5E+07	1.5E+09	3.5E+08	/	/	7.0E+12	5.4E+12	5.8E+12	1.3E+12	/	/	3.8E+11	5.5E+09	/	/	1.8E+13	1.2E+12
E22 cp LOG 13	6.0E+00	1.1E+00	1.3E+00	4.9E-02	1.3E+00	3.0E-01	/	/	6.9E+04	5.3E+04	3.0E+03	6.7E+02	/	/	1.4E+02	2.0E+00	/	/	6.4E+03	4.3E+02
E22 cp LOG 13 scaled 7E+09 g/6hr plume	8.3E+09	1.5E+09	1.8E+09	6.7E+07	1.8E+09	4.2E+08	/	/	9.4E+13	7.2E+13	4.1E+12	9.2E+11	/	/	1.9E+11	2.7E+09	/	/	8.8E+12	5.8E+11
E23 py/m TP-2L	6.1E+00	1.1E+00	1.5E+00	5.4E-02	1.5E+00	3.4E-01	/	/	9.7E+04	7.4E+04	5.5E+04	1.2E+04	/	/	8.3E-01	1.2E-02	/	/	4.2E+03	2.8E+02
E23 py/m TP-2L scaled 7E+09 g/6hr plume	8.4E+09	1.5E+09	2.0E+09	7.4E+07	2.0E+09	4.6E+08	/	/	1.3E+14	1.0E+14	7.5E+13	1.7E+13	/	/	1.1E+09	1.6E+07	/	/	5.8E+12	3.8E+11

8.0 Conclusions

Monomineralic and polymineralic seawater dissolution experiments at room temperature and 50 °C, show the relationship between select mineral pairs, with compelling evidence for the presence of galvanic interactions. The presence of oxide precipitates were not investigated in this study as potential sinks to dissolved metals, with increased metal concentrations being detectable despite the potential oxide formation and subsequent metal sequestering. The results of this study give contradictory results with the presence of galvanic cells being indicated in some but not all mineral pairs. Evidence for galvanic interactions were observed for mineral pairs: pyrite & galena, pyrite & chalcopyrite-sulphide-mix and polymineralic LOG-11 (chalcopyrite & secondary-Cu-sulphides); with Fe leaching (pyrite) being supressed in all. ~10% more Pb was leached from galena when paired with pyrite, with ~33% more Cu leached from chalcopyrite-sulphide-mix when paired with pyrite, than in monomineralic equivalents. Polymineralic LOG-11 (chalcopyrite + secondary-Cu-sulphides) saw a reduction of ~75% Zn and ~63% Ni when compared to monomineralic LOG-11 (chalcopyrite). Sustained Cu leaching was also observed in polymineralic LOG-11, indicating that chalcopyrite dissolution was cathodically protected, while secondary-Cu-sulphides dissolution resumed. These results are concordant with previous rest potentials established for sulphide minerals, with leaching series following: pyrite>chalcopyrite>covellite>bornite>galena (See Figure 9). Increased leaching in mineral pairs was shown to be exasperated when combined with increased temperatures in 50 °C experiments; but room temperature experiments were seemingly unaffected by small temperature fluctuations (<5 °C), suggesting that mineralogy and galvanic cells have a stronger effect on sulphide oxidation than small temperature fluctuations at room temperatures.

Surface area and textures were confirmed to exert a strong control on leaching trends, with TP-2L dissolution experiments, showing higher metal leaching in monomineralic experiment, presumed to be due to the colloform textures of the pyrite. The increased surface area brought about by textures in TP-2L saw higher metal leaching, despite mineral pairs in polymineralic experiment between pyrite and chalcopyrite being present. Surface area and texture is therefore, likely a more important control for sulphide leaching than galvanic interactions.

High temperature experiments (50 °C) indicated that high seawater temperatures are also likely to be a more dominant control on sulphide leaching than galvanic pairs. Galvanic pairs exposed to higher temperatures resulting in higher concentrations of leachate. This may have implications for the mining of SMS deposits, in the scenario that extraction takes place too close to active hydrothermal vents or in the case where waste rock/return water particles settle near active vents (or inactive vents that later become active), metal concentrations may be elevated through increased leaching of dissolved sulphide minerals.

Natural samples (LOG, TP-2L) were shown in this study to leach much higher metal concentrations than the standard mineral experiments. Metal concentrations for Cu, Fe and Zn increased ~3 orders of magnitude between standard and natural experiments. Therefore, while experiments using standard samples are useful for investigating the different variables effecting sulphide oxidation; experiments in which samples from hydrothermal vent sites are used will give a truer representative insight into what metal concentration ranges can be expected.

In summary, not one variable on its own is responsible for metal leaching, but instead a range of controls such as surface area, texture, galvanic interactions, temperature and mineralogy, are all at play affecting sulphide oxidation rates and leaching concentrations.

In terms of seafloor mining, this study highlights how sulphide mineral pairs found within seafloor massive sulphides can bring about galvanic interactions where the preferential leaching from one mineral can occur, while suppressing the other. The effect of this is dependent on the minerals present, with pyrite being the most likely to be cathodically protected in a pair, the leaching of Fe from pyrite may be halted – but as Fe is already readily precipitating out of solution, this won't have a significant effect. However, if minerals such as chalcopyrite, sphalerite and galena are preferentially leaching Cu, Zn and Pb in a mineral pair, this could bring about more negative consequences associated with SMS mining such as metal toxicity.

This study has found that for the natural samples, metal concentrations released are much higher than previously anticipated in the Solwara 1 EIS, exceeding ANZECC/ARMCANZ safety guidelines by >1000x. While the ocean is expected to quickly buffer and dilute any increased metal leachates, the dilution factors required to do so for the natural samples of this study are ~an order of magnitude higher than those in Nautilus Minerals proposed mining plan (Gwyther, 2008). Therefore, toxic concentrations of metal leachate is likely to exist for longer in the water column and in vent environments. Furthermore, while Nautilus Minerals mining plan has stated that the exposure time for return water particles to be limited to 12 minutes at ocean surface conditions (Gwyther, 2008), the results of this study are clear in that substantial metal leaching can occur in this time window (~15 minutes).

Current SMS mining and mining proposals vastly underestimate the geochemical risks associated with sulphide oxidation and metal leaching. To avoid irresponsible mining in the future, the impact of metal leaching and subsequent toxicity must be fully understood and evaluated in future risk assessments with adequate plans to mitigate and counteract potential metal toxicity that may occur. In addition, future studies investigating metal leaching from sulphide minerals should aim to use natural samples like the ones used in this study, to more accurately assess the leaching potentials observed with natural mineralogy's and textures.

9.0 Future Work

To build upon the work carried out in this study, an EMPA analysis of chalcopyrite-sulphide-mix should be performed to ensure the exact mineralogy of the sample instead of relying on speculation from leaching results – this wasn't able to be completed in this study due to time restrictions as a result of the COVID-19 pandemic. Further post-experiment material analysis should also be carried out on samples, particularly sphalerite-mixed-sulphide, to identify any changes to samples mineralogy, to identify any micro-inclusions of other minerals, but also to detect the presence of oxides and precipitates that may have been sequestering dissolved metals from solution. In addition to this, a further analysis into the surface areas and textures of samples could be investigated, identifying the key differences between standard mineral and natural samples and pin-pointing the difference in surface area between the two types of sample.

As the effect of bacteria colonies on sulphide oxidation rates has previously been investigated in Edwards et al. (2003); the bacterial effect on galvanic interactions may be significant in terms of SMS mining, and therefore could be incorporated in any future studies. Alternatively, the effect bacteria has on metal adsorption and removal from solution could also be investigated, looking for any possible connections.

With there being gaps in the literature for metal toxicity on different vent species, with limited investigations (Edgcomb *et al*., 2004; Llanos *et al*., 2000). Any future studies regarding the metal tolerance of individual vent species (active/inactive/weathering sites) to add to the current knowledge would be beneficial in assessing the risks involved with increased metal leaching from SMS mining. Further studies could also incorporate metal pathways through food-chains to assess potential risks throughout the water column.

Furthermore, with the threat of climate change bringing about the worry of rising sea temperatures and ocean acidification, the effect of both could be investigated, possibly through modelling, to evaluate the extent that they will increase the oxidation of SMS deposits and subsequent metal leaching.

References

Abraitis, P. K. *et al.*, 2004, 'Acid leaching and dissolution of major sulphide ore minerals: processes and galvanic effects in complex systems', *Mineralogical Magazine*. doi: 10.1180/0026461046820191.

Akcil, A.; Koldas, S., 2006, 'Acid Mine Drainage (AMD): causes, treatment and case studies', *Journal of cleaner production*, 14(12–13), pp. 1139–1145.

American Society For Testing and Materials - ASTM D1141, 2013, 'Standard Practice for the Preparation of Substitute Ocean Water', *ASTM International*, 98(Reapproved 2013), pp. 1–3. doi: 10.1520/D1141-98R13.2.

Ando, T. *et al.*, 2002, 'Bioaccumulation of mercury in a vestimentiferan worm living in Kagoshima Bay, Japan', *Chemosphere*. doi: 10.1016/S0045-6535(02)00291-6.

Angel, B. M. *et al.*, 2016, 'Lead solubility in seawater: An experimental study', *Environmental Chemistry*. doi: 10.1071/EN15150.

Antonijević, M. M., Dimitrijević, M. and Janković, Z., 1997, 'Leaching of pyrite with hydrogen peroxide in sulphuric acid', *Hydrometallurgy*. doi: 10.1016/s0304-386x(96)00096-5.

Artioli, Y., 2008, 'Adsorption', in *Encyclopedia of Ecology, Five-Volume Set*. doi: 10.1016/B978-008045405-4.00252-4.

Attia, Y. A. and El-Zeky, M., 1990, 'Effects of galvanic interactions of sulfides on extraction of precious metals from refractory complex sulfides by bioleaching', *International Journal of Mineral Processing*. doi: 10.1016/0301-7516(90)90068-A.

Augustin, N. *et al.*, 2008, 'Mineralogical and chemical mass changes in mafic and ultramafic rocks from the Logatchev hydrothermal field (MAR 15°N)', *Marine Geology*. doi: 10.1016/j.margeo.2008.09.004.

Baturin G. N., 1987, 'The Geochemistry of Manganese and Manganese Nodules in the Ocean', *Springer Netherlands*. Available at: ISBN 9400937318.

Beaulieu, S. E., Graedel, T. E. and Hannington, M. D., 2017, 'Should we mine the deep seafloor?', *Earth's Future*. doi: 10.1002/2017EF000605.

Benjamin, M. M. and Leckie, J. O., 1981, 'Multiple-site adsorption of Cd, Cu, Zn, and Pb on

amorphous iron oxyhydroxide', *Journal of Colloid And Interface Science*. doi: 10.1016/0021-9797(81)90063-1.

Berry, V. K., Murr, L. E. and Hiskey, J. B., 1978, 'Galvanic interaction between chalcopyrite and pyrite during bacterial leaching of low-grade waste', *Hydrometallurgy*. doi: 10.1016/0304-386X(78)90036-1.

Bierens de Haan, S., 1991, 'A review of the rate of pyrite oxidation in aqueous systems at low temperature', *Earth Science Reviews*. doi: 10.1016/0012-8252(91)90039-I.

Bilenker, L. D., Romano, G. Y. and McKibben, M. A., 2016, 'Kinetics of sulfide mineral oxidation in seawater: Implications for acid generation during in situ mining of seafloor hydrothermal vent deposits', *Applied Geochemistry*. doi: 10.1016/j.apgeochem.2016.10.010.

Bilenker, L. and McKibben, M. A., 2011, 'Abiotic oxidation rate of chalcopyrite in seawater; implications for seafloor sulfide mining', *Abstracts with Programs - Geological Society of America*.

Birney, K. *et al.*, 2008, 'Potential deep-sea mining of seafloor massive sulfides: A case study in Papua New Guinea', *Donald Bren School …*.

Boschen, R. E. *et al.*, 2013, 'Mining of deep-sea seafloor massive sulfides: A review of the deposits, their benthic communities, impacts from mining, regulatory frameworks and management strategies', *Ocean and Coastal Management*. doi: 10.1016/j.ocecoaman.2013.07.005.

Brown, A. and Hauton, C., 2018, 'Ecotoxicological responses to chalcopyrite exposure in a proxy for deep-sea hydrothermal vent shrimp: implications for seafloor massive sulphide mining', *Chemistry and Ecology*. doi: 10.1080/02757540.2018.1427231.

BRUEMMER, G. W., GERTH, J. and TILLER, K. G., 1988, 'Reaction kinetics of the adsorption and desorption of nickel, zinc and cadmium by goethite. I. Adsorption and diffusion of metals', *Journal of Soil Science*. doi: 10.1111/j.1365-2389.1988.tb01192.x.

Chandra, A. P. and Gerson, A. R., 2010, 'The mechanisms of pyrite oxidation and leaching: A fundamental perspective', *Surface Science Reports*. doi: 10.1016/j.surfrep.2010.08.003.

Chen, J. and Chen, Y., 2010, 'A first-principle study of the effect of vacancy defects and impurities on the adsorption of O2 on sphalerite surfaces', *Colloids and Surfaces A: Physicochemical and Engineering Aspects*. doi: 10.1016/j.colsurfa.2010.04.013.

Company, R. *et al.*, 2006, 'The effect of cadmium on antioxidant responses and the susceptibility to oxidative stress in the hydrothermal vent mussel Bathymodiolus azoricus', *Marine Biology*. doi: 10.1007/s00227-005-0116-0.

Cook, N. J. *et al.*, 2009, 'Trace and minor elements in sphalerite: A LA-ICPMS study', *Geochimica et Cosmochimica Acta*. doi: 10.1016/j.gca.2009.05.045.

Cruz, R. *et al.*, 2005, 'An experimental strategy to determine galvanic interactions affecting the reactivity of sulfide mineral concentrates', *Hydrometallurgy*. doi: 10.1016/j.hydromet.2005.03.006.

DEGENS ED ET and ROSS ED DA, 1969, 'HOT BRINES AND RECENT HEAVY METALS DEPOSITS IN THE RED SEA. A GEOCHEMICAL AND GEOPHYSICAL ACCOUNT', *Springer-Verlag New York Inc*.

Dekov, V. *et al.*, 2011, 'Atacamite and paratacamite from the ultramafic-hosted Logatchev seafloor vent field (14°45'N, Mid-Atlantic Ridge)', *Chemical Geology*. doi: 10.1016/j.chemgeo.2011.05.002.

Dimitrijevic, M., Antonijevic, M. M. and Jankovic, Z., 1996, 'Kinetics of pyrite dissolution by hydrogen peroxide in perchloric acid', *Hydrometallurgy*. doi: 10.1016/0304-386X(95)00094-W.

Van Dover, C. L. *et al.*, 1988, 'Feeding biology of the shrimp Rimicaris exoculata at hydrothermal vents on the Mid-Atlantic Ridge', *Marine Biology*. doi: 10.1007/BF00391196.

Van Dover, C. L., 2014, 'Impacts of anthropogenic disturbances at deep-sea hydrothermal vent ecosystems: A review', *Marine Environmental Research*. doi: 10.1016/j.marenvres.2014.03.008.

Dutrizac, J. E., 1981, 'The dissolution of chalcopyrite in ferric sulfate and ferric chloride media', *Metallurgical Transactions B*. doi: 10.1007/BF02654471.

Edgcomb, V. P. *et al.*, 2004, 'Sulfide Ameliorates Metal Toxicity for Deep-Sea Hydrothermal Vent Archaea', *Applied and Environmental Microbiology*. doi: 10.1128/AEM.70.4.2551-2555.2004.

Edwards, K. J. *et al.*, 2003a, 'Seafloor bioalteration of sulfide minerals: Results from in situ incubation studies', *Geochimica et Cosmochimica Acta*, 67(15), pp. 2843–2856. doi: 10.1016/S0016-7037(00)00089-9.

Edwards, K. J. *et al.*, 2003b, 'Seafloor bioalteration of sulfide minerals: Results from in situ incubation studies', *Geochimica et Cosmochimica Acta*. doi: 10.1016/S0016-7037(00)00089-9.

Edwards, K. J., 2004, 'Formation and degradation of seafloor hydrothermal sulfide deposits', in *Special Paper of the Geological Society of America*. doi: 10.1130/0-8137-2379-5.83.

Erickson, K. L., Macko, S. A. and Van Dover, C. L., 2009, 'Evidence for a chemoautotrophically based food web at inactive hydrothermal vents (Manus Basin)', *Deep-Sea Research Part II: Topical Studies in Oceanography*. doi: 10.1016/j.dsr2.2009.05.002.

Fallon, E. K. *et al.*, 2017, 'Oxidative dissolution of hydrothermal mixed-sulphide ore: An assessment of current knowledge in relation to seafloor massive sulphide mining', *Ore Geology Reviews*. doi: 10.1016/j.oregeorev.2017.02.028.

Fallon, E. K. *et al.*, 2018, 'Experimental leaching of massive sulphide from TAG active hydrothermal mound and implications for seafloor mining', *Marine Pollution Bulletin*. doi: 10.1016/j.marpolbul.2017.10.079.

Fallon, E. K., Scott, S. T. B. and Brooker, R. A., 2018, 'The oxidative dissolution of seafloor massive sulphide (SMS) deposits and implications for future mining activity'.

Feely, R. A., 1987, 'Composition and dissolution of black smoker particulates from active vents on the Juan de Fuca Ridge.', *Journal of Geophysical Research*. doi: 10.1029/jb092ib11p11347.

Fisher, C. R., Takai, K. and le Bris, N., 2007, 'Hydrothermal vent ecosystems', *Oceanography*. doi: 10.5670/oceanog.2007.75.

Francheteau, J. *et al.*, 1979, 'Massive deep-sea sulphide ore deposits discovered on the East Pacific Rise', *Nature*. doi: 10.1038/277523a0.

Fuchida, S. *et al.*, 2017, 'Leaching of Metals and Metalloids from Hydrothermal Ore Particulates and Their Effects on Marine Phytoplankton', *ACS Omega*. doi: 10.1021/acsomega.7b00081.

Fuchida, S. *et al.*, 2018, 'Onboard experiment investigating metal leaching of fresh hydrothermal sulfide cores into seawater', *Geochemical Transactions*. doi: 10.1186/s12932-018-0060-9.

Furness, R. W. and Rainbow, P. S., 2018, *Heavy metals in the marine environment*, *Heavy Metals in the Marine Environment*. doi: 10.1201/9781351073158.

Gadd, G. M., 2010, 'Metals, minerals and microbes: Geomicrobiology and bioremediation', *Microbiology*. doi: 10.1099/mic.0.037143-0.

Galley, Alan G., Hannington, Mark D., Jonasson, I. R., 2007, 'Volcanogenic massive sulphide deposits', *Geological Association of Canada, Mineral Deposits Division*, pp. 141–161.

Gartman, A., Whisman, S. P. and Hein, J. R., 2020, 'Sphalerite Oxidation in Seawater with Covellite: Implications for Seafloor Massive Sulfide Deposits and Mine Waste', *ACS Earth and Space Chemistry*. doi: 10.1021/acsearthspacechem.0c00177.

George, L. L. *et al.*, 2018, 'Trace elements in hydrothermal chalcopyrite', *Mineralogical Magazine*. doi: 10.1180/minmag.2017.081.021.

German, C. R. *et al.*, 2008, 'Hydrothermal activity on the southern Mid-Atlantic Ridge: Tectonically- and volcanically-controlled venting at 4-5°S', *Earth and Planetary Science Letters*. doi: 10.1016/j.epsl.2008.06.048.

German, C. R. and Sparks, R. S. J., 1993, 'Particle recycling in the TAG hydrothermal plume', *Earth and Planetary Science Letters*. doi: 10.1016/0012-821X(93)90049-F.

Gwyther, D., 2008, *Environmental Impact Statement: Nautilus Minerals Niugini Limited, Solwara 1 Project Volume A - Main Report, Nautilius Minerals Niugini*.

Haase, K. M. *et al.*, 2007, 'Young volcanism and related hydrothermal activity at 5°S on the slow-spreading southern Mid-Atlantic Ridge', *Geochemistry, Geophysics, Geosystems*. doi: 10.1029/2006GC001509.

Haldar, S. K. and Haldar, S. K., 2017, 'Chapter 1 – Introduction', in *Platinum-Nickel-Chromium Deposits*.

Hannington, M.D.; de Ronde, C.E.J.; Peterson, S., 2005, 'Modern seafloor tectonics and submarine hydrothermal systems', *Economic Geology*, 100, pp. 111–141. doi: doi:10.1029/GM091p0115.

Hannington, M. D., Jamieson, J. and Petersen, S., 2015, 'Seafloor massive sulfide deposits: Continuing efforts toward a global estimate of seafloor massive sulfides', in *MTS/IEEE*

OCEANS 2015 - Genova: Discovering Sustainable Ocean Energy for a New World. doi: 10.1109/OCEANS-Genova.2015.7271526.

Hauton, C. *et al.*, 2017, 'Identifying toxic impacts of metals potentially released during deep-sea mining-A synthesis of the challenges to quantifying risk', *Frontiers in Marine Science*. doi: 10.3389/fmars.2017.00368.

Heidel, C., Tichomirowa, M. and Breitkopf, C., 2011, 'Sphalerite oxidation pathways detected by oxygen and sulfur isotope studies', *Applied Geochemistry*. doi: 10.1016/j.apgeochem.2011.08.007.

Heidel, C., Tichomirowa, M. and Junghans, M., 2013, 'Oxygen and sulfur isotope investigations of the oxidation of sulfide mixtures containing pyrite, Galena, And sphalerite', *Chemical Geology*. doi: 10.1016/j.chemgeo.2013.01.016.

Herzig, P.M.; Peterson, S.; Hannington, M. D., 2002, 'Polymetallic massive sulphide deposits at the modern seafloor and their resource potential', *In Polymetallic Massive Sulphides and Cobalt-rich Ferromanganese Crusts: Status and Prospects*, pp. 7–35.

Herzig, P. M., 1999, 'Economic potential of sea-floor massive sulphide deposits: Ancient and modern', *Philosophical Transactions of the Royal Society A: Mathematical, Physical and Engineering Sciences*. doi: 10.1098/rsta.1999.0355.

Herzig, P. M. and Hannington, M. D., 1995, 'Polymetallic massive sulfides at the modern seafloor a review', *Ore Geology Reviews*. doi: 10.1016/0169-1368(95)00009-7.

Hoagland, P. *et al.*, 2010, 'Deep-sea mining of seafloor massive sulfides', *Marine Policy*. doi: 10.1016/j.marpol.2009.12.001.

van Hoorebeke, Alexander, T., 2016, *Oxidation kinetics of pyrite in synthetic seawater: Implications for seafloor mining operations*. University of California, Riverside.

Isa.org.jm., 2019, *International Seabed Authroity*. Available at: https://www.isa.org.jm/deep-seabed-minerals-contractors/overview (Accessed: 5 February 2020).

J.L., L., 2012, 'Physical oceanographic assessment of the Nautilus EIS for the Solwara 1 project', *Deep sea Mining Campaign*, p. 26.

Jeanthon, C. and Prieur, D., 1990, 'Susceptibility to heavy metals and characterization of heterotrophic bacteria isolated from two hydrothermal vent polychaete annelids, Alvinella

pompejana and Alvinella caudata', *Applied and Environmental Microbiology*. doi: 10.1128/aem.56.11.3308-3314.1990.

King, W. E. and Lewis, J. A., 1980, 'Simultaneous Effects of Oxygen and Ferric Iron on Pyrite Oxidation in an Aqueous Slurry', *Industrial and Engineering Chemistry Process Design and Development*. doi: 10.1021/i260076a037.

Knight, R. D., Roberts, S. and Cooper, M. J., 2018, 'Investigating monomineralic and polymineralic reactions during the oxidation of sulphide minerals in seawater: Implications for mining seafloor massive sulphide deposits', *Applied Geochemistry*. doi: 10.1016/j.apgeochem.2017.12.027.

Lehmann, M. N. *et al.*, 2000, 'The Effect of Chloride Ions on the Ambient Electrochemistry of Pyrite Oxidation in Acid Media', *Journal of The Electrochemical Society*. doi: 10.1149/1.1393893.

Liu, X. and Millero, F. J., 2002, 'The solubility of iron in seawater', *Marine Chemistry*. doi: 10.1016/S0304-4203(01)00074-3.

Llanos, J. *et al.*, 2000, 'Susceptibility to heavy metals and cadmium accumulation in aerobic and anaerobic thermophilic microorganisms isolated from deep-sea hydrothermal vents', *Current Microbiology*. doi: 10.1007/s00284431056.

Long, H. and Dixon, D. G., 2004, 'Pressure oxidation of pyrite in sulfuric acid media: A kinetic study', *Hydrometallurgy*. doi: 10.1016/j.hydromet.2003.07.010.

Macdonald, K. C. *et al.*, 1980, 'Hydrothermal heat flux of the "black smoker" vents on the East Pacific Rise', *Earth and Planetary Science Letters*. doi: 10.1016/0012-821X(80)90163-6.

Mann, A. W. and Deutscher, R. L., 1977, 'Solution geochemistry of copper in water containing carbonate, sulphate and chloride ions', *Chemical Geology*. doi: 10.1016/0009-2541(77)90018-3.

Mann, A. W. and Deutscher, R. L., 1980, 'Solution geochemistry of lead and zinc in water containing carbonate, sulphate and chloride ions', *Chemical Geology*. doi: 10.1016/0009-2541(80)90026-1.

Miller, K. A. *et al.*, 2018, 'An overview of seabed mining including the current state of development, environmental impacts, and knowledge gaps', *Frontiers in Marine Science*.

doi: 10.3389/fmars.2017.00418.

Monecke, T. *et al.*, 2016, 'The minor element endowment of modern sea-floor massive sulfide deposits and comparison with deposits hosted in ancient volcanic successions', *In: Rare Earth and Critical Elements in Ore Deposits. , ed. by Verplanck, P. L. and Hitzman, M. W. Reviews in Economic Geology, 18 . Society of Economic Geologists, Knoxville, Tenn., pp. 245-306.*

Morse, J. W., 1991, 'Oxidation kinetics of sedimentary pyrite in seawater', *Geochimica et Cosmochimica Acta*. doi: 10.1016/0016-7037(91)90064-C.

Murphy, P. J. and Meyer, G., 1998, 'A gold-copper association in ultramafic-hosted hydrothermal sulfides from the Mid-Atlantic Ridge', *Economic Geology*. doi: 10.2113/gsecongeo.93.7.1076.

Naderi, M., 2015, 'Surface Area: Brunauer-Emmett-Teller (BET). In Progress in filtration and separation', *Academic Press*, pp. 585–608.

NOAA. What is eutrophication?, 2017, *National Ocean Service website*. Available at: https://oceanservice.noaa.gov/facts/eutrophication.html.

NOAA, 2018, 'How much of the ocean have we explored?', *US Department of Commerce, National Oceanic and Atmospheric Administration*.

Öhlander, B. *et al.*, 2007, 'An attempt to use LA-ICP-SMS to quantify enrichment of trace elements on pyrite surfaces in oxidizing mine tailings', *Journal of Geochemical Exploration*. doi: 10.1016/j.gexplo.2006.06.001.

Pan, Z. *et al.*, 2012, 'A simulation experimental study on oxidative kinetics of sphalerite under hypergene condition', *Chinese Journal of Geochemistry*. doi: 10.1007/s11631-012-0597-8.

Petersen, S. *et al.*, 2009, 'The geological setting of the ultramafic-hosted Logatchev hydrothermal field (14°45′N, Mid-Atlantic Ridge) and its influence on massive sulfide formation', *Lithos*. doi: 10.1016/j.lithos.2009.02.008.

Petersen, S. *et al.*, 2016, 'News from the seabed – Geological characteristics and resource potential of deep-sea mineral resources', *Marine Policy*. doi: 10.1016/j.marpol.2016.03.012.

Petersen, S. and Hein, J. R., 2013, *The Geology of Sea-Floor Massive Sulphides, Deep Sea*

Minerals; Sea-Floor Massive Sulphides.

Poisson, A. and Papaud, A., 1983, 'Diffusion coefficients of major ions in seawater', *Marine Chemistry*. doi: 10.1016/0304-4203(83)90002-6.

Polz, M. F. *et al.*, 1998, 'Trophic ecology of massive shrimp aggregations at a Mid-Atlantic Ridge hydrothermal vent site', *Limnology and Oceanography*. doi: 10.4319/lo.1998.43.7.1631.

Ridley, W.I.; Shanks, W.C.P.; Thurston, R., 2012, *Weathering processes in volcanogenic massive sulfide occurrence model*.

Rimstidt, D. D. and Vaughan, D. J., 2003, 'Pyrite oxidation: A state-of-the-art assessment of the reaction mechanism', *Geochimica et Cosmochimica Acta*. doi: 10.1016/S0016-7037(02)01165-1.

Romano, G. Y., 2012, *Kinetics of Pyrrhotite Oxidation in Seawater: Implications for Mining Seafloor Hotsprings*. University of California: Riverside.

Sadiq, M., 1989, 'Marine chemistry of cadmium: A comparison of theoretical and field observations', *Environmental Technology Letters*. doi: 10.1080/09593338909384827.

Salmon, S. U. and Malmström, M. E., 2006, 'Quantification of mineral dissolution rates and applicability of rate laws: Laboratory studies of mill tailings', *Applied Geochemistry*. doi: 10.1016/j.apgeochem.2005.09.014.

Sasaki, K. *et al.*, 1995, 'Effect of anionic ligands on the reactivity of pyrite with Fe(III) ions in acid solutions', *Colloids and Surfaces A: Physicochemical and Engineering Aspects*. doi: 10.1016/0927-7757(95)03142-Z.

Scott, S. D. and Barnes, H. L., 1972, 'Sphalerite-wurtzite equilibria and stoichiometry', *Geochimica et Cosmochimica Acta*. doi: 10.1016/0016-7037(72)90049-X.

Da Silva, G., Lastra, M. R. and Budden, J. R., 2003, 'Electrochemical passivation of sphalerite during bacterial oxidation in the presence of galena', *Minerals Engineering*. doi: 10.1016/S0892-6875(03)00010-4.

Simpson, S. L. and Spadaro, D. A., 2016, 'Bioavailability and Chronic Toxicity of Metal Sulfide Minerals to Benthic Marine Invertebrates: Implications for Deep Sea Exploration, Mining and Tailings Disposal', *Environmental Science and Technology*. doi:

10.1021/acs.est.6b00203.

Singh, J. and Kalamdhad, A. S., 2011, 'Effects of Heavy Metals on Soil, Plants, Human Health and Aquatic Life', *International Journal of Research in Chemistry and Environment*.

Standard Definitions, 2012, *CRIRSCO, Committee for mineral, reserves international reporting standards*. Available at: http://www.crirsco.com/news_items/CRIRSCO_standard_definitions_oct2012.pdf.

Steiner, R., 2009, *Independent Review of the Environmental Impact Statement for the proposed Nautilus Minerals Solwara 1 Seabed Mining Project, Papua New Guinea, Bismarck-Solomon Seas Indigenous Peoples Council*.

Vetriani, C. *et al.*, 2005, 'Mercury adaptation among bacteria from a deep-sea hydrothermal vent', *Applied and Environmental Microbiology*. doi: 10.1128/AEM.71.1.220-226.2005.

Vidal, O., Goffé, B. and Arndt, N., 2013, 'Metals for a low-carbon society', *Nature Geoscience*. doi: 10.1038/ngeo1993.

Wang, W., 1987, 'Factors affecting metal toxicity to (and accumulation by) aquatic organisms - Overview', *Environment International*. doi: 10.1016/0160-4120(87)90006-7.

Weaver, P. P. E., Billett, D. S. M. and Van Dover, C. L., 2018, 'Environmental Risks of Deep-sea Mining', in *Handbook on Marine Environment Protection*. doi: 10.1007/978-3-319-60156-4_11.

Webber, A. P. *et al.*, 2015, 'Geology, sulfide geochemistry and supercritical venting at the Beebe Hydrothermal Vent Field, Cayman Trough', *Geochemistry, Geophysics, Geosystems*. doi: 10.1002/2015GC005879.

Weiss, R. F. *et al.*, 1977, 'Hydrothermal plumes in the Galapagos Rift [4]', *Nature*. doi: 10.1038/267600a0.

Wen, S., Liu, J. and Deng, J., 2021, 'Interactions among components of fluid inclusions in sulfide mineral, mineral surfaces, and collectors', in *Fluid Inclusion Effect in Flotation of Sulfide Minerals*. doi: 10.1016/b978-0-12-819845-2.00007-7.

Wilkin, R. T. and Barnes, H. L., 1997, 'Formation processes of framboidal pyrite', *Geochimica et Cosmochimica Acta*. doi: 10.1016/S0016-7037(96)00320-1.

Appendix

EMPA Parameter Set Up

Table 11.1: EMPA parameter set up for Standard Galena displaying analysed elements, lines, spectrometers, crystals, peaks, background positions, peak count times, calibration standards, and intensities. Calibration was set at 150 nA to avoid a high deadtime on Pb. Beam conditions were set to 25 kV, 150 nA, at a spot size of 5 µm.

Element	Line	Spectrometer	Crystal	Peak	Bg -ve Offset	Bg +ve Offset	Peak Count Time (s)	Calibration standard	Intensity (cps/nA)
S	Kα	2	PET	61421	-600	800	20	Pyrite	351.1
Pb	Lβ	3	LLIF	24371	-600	600	20	Galena	215.8
Cu	Kα	5	LLIF	38261	-400	1000	30	Cu metal	1652.2
Ni	Kα	5	LLIF	41178	-450	800	30	Ni metal	1661.0
Fe	Kα	5	LLIF	48081	-1000	1000	30	Pyrite	651.1
Mn	Kα	5	LLIF	52198	-1000	800	30	Mn metal	1383.6
Zn	Kα	3	LLIF	35634	-500	800	120	Zn metal	2085.5
Co	Kα	3	LLIF	44434	-200	200	30	Co metal	223.6
As	Lα	4	TAP	37626	-600	500	180	GaAs	181.3
Cd	Lα	2	PET	45211	-300	500	180	Cd metal	245.0
Hg	Mα	1	LPET	64480	-800	1500	60	HgTe	144.6
Sn	Lα	1	LPET	41082	-400	800	60	Sn metal	741.3
Sb	Lα	1	LPET	39246	-500	250	60	Sb metal	648.3

Table 11.2: EMPA parameter set up for Standard Pyrite displaying analysed elements, lines, spectrometers, crystals, peaks, background positions, peak count times, calibration standards, and intensities. Beam conditions were set at 25 kV, 10 nA, at spot size 5 µm.

Element	Line	Spectrometer	Crystal	Peak	Bg -ve Offset	Bg +ve Offset	Peak Count Time (s)	Calibration standard	Intensity (cps/nA)
S	Kα	2	PET	61421	-600	800	20	Pyrite	351.1
Fe	Kα	5	LLIF	48081	-1000	1000	20	Pyrite	651.1
Cu	Kα	5	LLIF	38261	-400	1000	30	Cu metal	1652.2
Ni	Kα	5	LLIF	41178	-450	800	30	Ni metal	1661.0
Mn	Kα	5	LLIF	52198	-1000	800	30	Mn metal	1383.6
Co	Kα	3	LLIF	44434	-200	200	30	Co metal	2223.6
Zn	Kα	3	LLIF	35634	-500	800	60	Zn metal	2085.5
As	Lα	4	TAP	37626	-600	500	180	GaAs	181.3
Cd	Lα	2	PET	45211	-300	300	180	Cd metal	245.0
Hg	Mα	1	LPET	64474	-800	500	60	HgTe	134.7
Sn	Lα	1	LPET	41082	-400	800	60	Sn metal	741.3
Sb	Lα	1	LPET	39246	-500	250	60	Sb metal	648.3
Pb	Lβ	3	LLIF	24371	-200	300	60	Galena	215.8

Trial Experiment Parameters

Table 12: Trial experiment parameters

Run	Experiment	Mineral	Temperature (start) (ºC)	Temperature (finish) (ºC)	pH (start)	pH (Finish)	Dissolved Oxygen Start (ppm)	Dissolved Oxygen Finish (ppm)	Grainsize (µm)	Start mass (g)	Final mass (g)	Seawater volume (ml)
1	Monominerallic	Galena	24.6	26.7	7.9	7.98	6.55	6.39	>1000	7.04	7.14	500
2	Monominerallic	Galena	24.2	26.4	7.72	7.72	6.36	5.98	>1000	14.1	14.27	500
3	Monominerallic	Galena	25.3	27.2	7.62	7.78	6.54	5.8	>1000	10.02	10.93	500
4	Monominerallic	Galena	25.1	27	7.65	7.83	6.6	6.04	>1000	5.04	5.18	500
5	Monominerallic	Galena	24.7	27.2	7.71	7.9	6.47	6.22	>1000	2.01	2.15	500
6	Monominerallic	Sphalerite	25.1	27.4	7.79	7.91	6.37	5.95	>1000	5.02	5.21	500
7	Monominerallic	Sphalerite	25.3	27.5	7.74	7.88	6.73	6.37	>1000	2	2.1844	500
8	Monominerallic	Sphalerite	25.3	27.5	7.78	7.89	6.63	6.41	>500-1000	2.02	2.11	500
9	Monominerallic	Seawater BLK	25.3	27.5	7.81	7.92	6.81	6.39				500

Trial Experiment Results

Table 13: Concentration (ppb/ppm) results for 6 hour trial experiments. Elements presented represent leachate concentration at different time intervals. ~0 is given where negative values were returned from ICP-OES analysis, and <bdl is given where concentration values were below the detection limit for that element on the ICP-OES instrument. 5g of sample was used in each experiment at 355 µm grainsize in 250 ml of artificial seawater. Gn = Galena, Sp-1 = Sphalerite-1. All trial experiments were run at 500 ml artificial seawater.

Run	Sample	Grainsize (µm)	Mass (g)	Time (minutes)	As	SD	Cd	SD	Cr	SD	Cu	SD	Fe	SD	Mn	SD	Ni	SD	Pb	SD	Sb	SD	Sn	SD	Zn	SD
					ppb		ppb		ppb		ppb		ppb		ppb		ppb		ppb		ppb		ppb		ppb	
E2	Gn	>1000	14	30	6.44	11.98	0.00	0.39	0.72	0.15	0.00	0.46	0.00	0.55	0.00	0.14	115.14	2.55	0.00	3.94	2.84	31.98	1.77	33.86	2.89	0.73
				60	0.00	3.46	0.00	0.17	0.21	0.51	0.00	1.18	2.91	1.03	0.00	0.16	1.46	2.85	0.00	6.92	0.00	34.45	17.25	2.85	3.25	0.99
				120	12.85	14.07	0.00	0.14	0.49	1.17	0.00	1.64	0.00	1.65	0.00	0.08	0.00	1.94	0.00	4.35	0.00	19.19	33.18	26.50	4.98	0.53
				180	18.42	5.44	0.00	0.19	0.73	0.78	0.00	0.68	0.00	0.47	0.00	0.21	0.00	0.84	0.00	1.91	0.00	52.59	1.67	5.75	2.80	0.32
				300	8.17	6.75	0.00	0.12	0.54	0.42	0.00	1.11	0.00	0.80	0.00	0.07	0.00	0.18	0.00	1.19	0.00	60.67	17.79	15.84	7.69	0.77
E3	Gn	>1000	10	30	7.24	9.60	0.00	0.16	0.69	0.79	1.01	0.63	0.00	1.36	0.00	0.19	0.00	1.42	0.00	15.85	0.00	5.54	0.13	37.75	0.47	0.60
				60	0.00	6.79	0.00	0.14	0.20	0.04	0.00	0.34	0.00	0.45	0.00	0.14	0.00	1.54	0.00	11.16	0.00	16.68	0.00	6.89	1.46	0.23
				120	6.66	19.23	0.00	0.10	0.86	0.33	0.00	1.18	0.00	0.02	0.00	0.23	0.00	2.33	0.00	14.27	0.00	13.86	14.31	26.17	0.00	0.56
				300	2.57	6.76	0.00	0.12	0.22	0.02	0.00	1.13	0.00	0.24	0.00	0.31	0.00	0.58	0.00	5.94	0.00	30.63	11.74	40.57	1.93	1.11
				360	9.25	22.67	0.81	0.22	0.24	0.17	1.03	1.32	0.00	0.82	0.00	0.10	0.00	0.51	0.00	13.80	0.00	35.25	0.00	19.01	4.79	0.22
E4	Gn	>1000	5	30	11.11	9.60	0.00	0.27	0.56	0.61	0.00	1.02	0.00	1.10	0.00	0.29	0.00	3.28	342.89	15.51	0.00	40.52	0.00	15.55	4.81	0.57
				60	8.37	6.79	0.00	0.09	0.00	0.47	0.00	1.05	0.00	0.41	0.00	0.11	0.00	0.81	0.00	3.19	0.00	18.85	0.00	21.00	1.34	0.10
				120	12.16	19.23	0.00	0.38	0.73	1.01	0.00	0.90	0.00	0.11	0.00	0.08	0.00	2.30	379.60	15.55	0.00	9.42	0.00	8.07	3.74	0.40
				300	0.00	6.76	0.00	0.23	0.07	0.28	0.00	2.57	2.28	2.26	0.00	0.50	0.00	1.27	350.08	15.53	0.00	38.90	0.00	12.30	2.08	0.72
				360	0.00	22.67	0.00	0.10	0.68	0.13	0.58	1.94	0.00	1.28	0.00	0.08	0.00	0.14	80.13	4.92	0.00	36.25	9.95	29.00	2.25	0.14
E5	Gn	>1000	2	30	0.00	17.03	0.00	0.08	0.80	0.15	0.00	0.76	0.00	1.03	0.05	0.35	0.00	2.77	0.00	7.84	0.00	21.07	0.00	27.25	0.00	0.28
				60	2.24	6.35	0.00	0.21	0.89	0.88	0.00	1.30	0.00	0.60	0.00	0.13	0.00	1.03	0.00	7.56	0.00	19.85	14.46	30.75	0.00	0.54
				120	17.30	20.46	0.00	0.06	0.52	0.37	0.00	0.34	0.00	0.64	0.12	1.43	0.00	0.95	157.05	6.17	11.80	51.93	0.00	13.50	1.48	0.68
				300	8.37	7.56	0.00	0.34	0.51	0.29	0.00	0.68	0.00	0.38	0.00	0.16	0.02	1.07	0.00	10.51	2.11	31.94	0.00	7.90	0.00	0.78
				360	20.88	29.26	0.00	0.29	0.16	0.62	0.00	0.36	0.00	0.53	0.00	0.12	0.00	1.70	0.00	9.09	0.00	14.81	0.00	24.24	4.90	0.31
E6	Sp-1	>1000	5	30	9.65	5.64	0.04	0.03	0.05	0.07	14.50	0.59	13.79	0.09	7.40	0.07	0.00	0.70	68.49	5.33	31.83	9.97	0.00	9.74	30.46	0.27
				60	3.90	9.41	0.04	0.03	0.00	0.16	13.37	0.29	12.20	0.31	7.62	0.17	0.00	1.23	43.45	4.44	0.00	15.91	0.00	1.09	32.22	0.30
				120	0.00	5.91	0.12	0.06	0.72	0.30	10.02	0.39	12.50	0.51	7.28	0.04	0.00	0.41	0.00	6.51	16.98	24.30	0.00	11.85	33.00	0.28
				300	0.00	1.06	0.07	0.05	0.60	0.07	7.07	0.03	12.28	0.38	7.56	0.11	0.00	0.48	65.30	5.96	0.00	6.57	2.28	8.81	46.40	0.48
				360	0.00	1.01	0.00	0.04	0.41	0.18	6.48	0.46	12.51	0.59	8.09	0.53	0.00	1.11	19.45	6.25	31.23	31.54	0.00	6.47	39.77	0.67
E8	Sp-1	500-1000	2	30	0.00	8.65	0.00	0.06	0.62	0.17	5.98	0.22	11.24	0.74	4.14	0.20	0.94	0.84	17.94	4.02	0.00	5.50	0.00	8.86	21.27	0.72
				60	3.26	13.70	0.00	0.15	0.70	0.19	6.99	0.39	12.27	0.57	4.43	0.10	0.00	0.40	42.60	4.21	5.27	24.29	0.00	11.27	25.70	1.14
				120	0.00	1.15	0.12	0.04	0.60	0.54	6.57	0.21	9.51	0.66	4.29	0.04	0.00	0.24	26.25	0.88	0.00	22.08	6.56	9.93	25.29	0.24

ICP-OES Galvanic Experiments Analyses Results

Table 14: Concentration (ppb/ppm) results for monomineralic standard minerals over the duration of 6 hour experiment runs. Elements presented represent leachate concentration at different time intervals. ~0 is given where negative values were returned from ICP-OES analysis, and <bdl is given where concentration values were below the detection limit for that element on the ICP-OES instrument. 5g of sample was used in each experiment at 355 µm grainsize in 250 ml of artificial seawater.

Run	Sample	Time (minutes)	Cd	SD	Cr	SD	Cu	SD	Fe	SD	Mg	SD	Mn	SD	Ni	SD	Pb	SD	Sb	SD	Sn	SD	Zn	SD
			ppb		ppb		ppb		ppb		ppm		ppb		ppb		ppb		ppb		ppb		ppb	
B2 E1	Pyrite	15	<bdl	0.23	0.57	0.42	27.54	0.54	47.79	2.62	~0	3.61	1.78	0.16	5.85	0.73	17.95	3.31	26.40	16.15	37.97	7.08	~0	0.79
		30	<bdl	0.13	1.36	0.31	13.92	0.86	33.99	1.89	~0	2.95	2.05	0.15	3.74	0.77	28.83	3.64	52.16	17.69	23.73	19.15	~0	1.15
		60	<bdl	0.11	1.56	0.40	17.94	0.67	56.75	1.75	~0	3.73	2.38	0.13	5.50	0.43	19.25	5.11	15.32	10.87	51.22	10.00	~0	0.80
		120	<bdl	0.12	1.65	0.24	18.21	0.58	31.18	0.86	~0	3.49	2.18	0.16	8.34	0.36	<bdl	3.49	23.18	11.88	29.28	12.98	~0	1.01
		180	<bdl	0.19	0.31	0.24	14.16	1.26	38.49	1.94	~0	3.07	2.31	0.21	3.19	0.89	22.79	7.09	~0	15.25	~0	7.46	~0	0.77
		240	<bdl	0.15	1.57	0.39	11.33	0.52	46.66	2.25	~0	4.20	2.49	0.15	9.89	0.30	<bdl	1.32	16.32	10.91	16.81	8.40	~0	0.89
		300	<bdl	0.13	0.73	0.24	16.45	0.51	44.24	3.12	~0	3.97	2.36	0.14	6.10	0.68	<bdl	4.07	46.98	14.34	8.25	5.67	~0	0.71
		360	<bdl	0.08	1.15	0.23	11.43	0.84	24.29	1.86	~0	4.45	2.16	0.17	2.31	0.27	<bdl	5.90	128.88	10.47	24.28	3.81	~0	0.74
B2 E2	Galena	15	<bdl	0.12	1.72	0.39	18.33	1.12	25.15	0.61	~0	3.53	~0	0.14	6.98	1.23	529.06	5.80	27.79	17.76	53.42	9.76	~0	1.39
		30	<bdl	0.16	1.17	0.25	10.65	0.71	16.21	0.68	~0	3.03	<bdl	0.10	5.71	1.39	443.89	3.34	62.00	22.10	53.19	11.85	~0	0.71
		60	<bdl	0.12	0.86	0.24	11.69	1.06	15.01	0.94	~0	2.91	<bdl	0.18	4.45	0.26	484.68	8.86	~0	11.12	~0	5.93	~0	0.99
		120	<bdl	0.19	1.94	0.36	14.46	0.51	25.31	2.17	~0	2.76	<bdl	0.18	3.98	0.11	513.83	4.04	62.34	13.96	110.68	20.05	~0	0.70
		180	<bdl	0.14	1.59	0.30	12.47	0.73	19.84	2.25	~0	3.56	<bdl	0.12	4.81	0.84	629.34	3.42	48.43	16.97	27.71	9.39	~0	1.57
		240	<bdl	0.12	1.10	0.27	15.84	0.68	21.17	1.32	~0	3.18	<bdl	0.14	5.40	0.84	659.55	1.58	15.63	18.17	46.16	13.54	~0	0.86
		300	<bdl	0.08	1.05	0.29	17.13	0.89	15.78	1.17	~0	4.04	<bdl	0.19	5.66	1.31	605.90	3.75	84.21	17.08	7.87	11.94	~0	1.17
		360	<bdl	0.20	0.81	0.31	10.95	0.54	25.47	0.80	~0	2.95	1.36	0.14	6.76	0.98	614.07	2.14	~0	19.70	41.54	12.93	~0	1.13
B2 E3	Sphalerite-2	15	<bdl	0.33	0.08	0.29	10.98	0.60	82.75	1.82	~0	3.79	3.76	0.20	7.55	0.41	184.01	1.43	92.10	19.49	48.40	13.35	~0	0.97
		30	<bdl	0.10	0.73	0.29	18.38	0.82	115.14	1.82	~0	3.34	6.16	0.19	3.43	0.54	181.11	1.54	21.62	16.85	~0	5.00	~0	0.80
		60	<bdl	0.08	0.63	0.25	14.12	0.46	84.90	2.18	~0	3.86	4.66	0.10	6.77	1.34	198.04	4.63	~0	10.50	~0	5.45	~0	1.52
		120	<bdl	0.09	1.67	0.21	10.94	0.81	101.36	1.28	~0	4.35	5.55	0.12	4.64	0.48	240.98	1.89	~0	13.91	50.23	13.44	~0	1.36
		180	<bdl	0.09	1.35	0.34	24.89	0.50	94.72	2.34	0.62	4.28	6.40	0.28	3.90	0.38	269.01	5.83	52.03	23.03	36.72	13.65	~0	2.28
		240	<bdl	0.31	1.20	0.24	11.67	0.82	115.09	0.74	5.35	4.11	7.04	0.34	4.12	0.75	223.37	4.76	~0	19.83	44.20	14.88	<bdl	1.99
		300	<bdl	0.09	1.93	0.28	11.35	0.53	145.75	0.52	~0	3.07	6.23	0.12	4.87	0.50	265.31	5.83	~0	22.23	17.14	6.42	29.66	0.72
		360	<bdl	0.09	1.91	0.23	14.21	0.63	106.81	0.65	~0	2.98	5.93	0.16	10.90	1.62	275.16	2.55	77.37	19.01	~0	9.58	54.23	1.91
B2 E4	Sphalerite - 1	15	~0	0.20	1.26	0.30	11.94	0.68	96.55	3.76	~0	3.61	<bdl	0.16	8.27	1.20	45.56	1.96	30.73	20.03	25.31	16.32	~0	0.96
		30	<bdl	0.09	0.72	0.21	11.64	0.95	155.77	1.13	~0	3.47	<bdl	0.14	3.40	0.30	58.57	4.66	~0	15.46	49.25	12.26	~0	1.39
		60	<bdl	0.10	0.41	0.21	10.75	0.49	107.36	0.65	~0	4.47	<bdl	0.15	3.86	0.89	44.51	2.84	33.60	10.58	16.63	12.43	~0	1.15
		120	<bdl	0.17	1.33	0.25	10.51	0.50	106.71	1.99	~0	4.47	<bdl	0.11	4.80	1.13	79.39	4.73	26.74	12.00	23.23	13.10	~0	0.98
		180	<bdl	0.12	1.96	0.21	9.35	0.63	50.00	1.98	~0	5.09	1.75	0.26	3.05	0.56	87.96	2.90	21.64	16.77	42.57	10.29	~0	1.82
		240	<bdl	0.19	1.47	0.35	11.50	0.46	64.34	1.28	~0	3.51	<bdl	0.19	8.02	1.18	88.53	1.21	~0	12.87	~0	17.13	~0	1.21
		300	<bdl	0.07	1.24	0.27	12.90	0.74	55.96	1.66	~0	3.63	1.49	0.20	4.10	0.07	88.13	4.26	46.14	16.25	~0	7.20	~0	0.97
		360	<bdl	0.20	2.01	0.36	13.61	0.57	43.68	1.15	~0	3.45	<bdl	0.17	2.19	0.58	124.55	4.85	39.63	30.63	~0	0.86	~0	0.98
B2 E5	Chalcopyrite	5	3.50	0.08	1.17	0.31	861.87	3.01	~0	1.20	~0	3.65	15.38	0.12	5.58	0.78	225.00	1.18	30.18	12.39	41.20	5.22	1246.46	4.67
		15	3.37	0.18	1.58	0.40	1049.83	3.38	~0	1.32	~0	3.62	16.27	0.40	9.78	1.74	331.45	3.55	62.95	23.74	33.46	15.26	1763.92	7.51
		30	3.40	0.10	~0	0.21	859.45	1.82	~0	1.91	~0	3.67	16.95	0.21	20.31	1.09	432.25	3.37	<bdl	21.72	5.69	8.52	1359.34	2.75
		60	3.89	0.08	0.96	264.51	775.14	2.81	~0	0.81	~0	3.70	18.29	0.11	12.84	1.74	555.84	6.82	~0	14.50	2.93	14.10	1409.07	4.26
		120	3.57	0.16	~0	0.64	719.57	3.13	~0	0.74	~0	4.75	18.14	0.25	4.02	0.84	818.15	8.66	47.33	14.59	17.01	14.85	1345.96	4.70
		180	4.10	0.10	0.56	0.46	771.53	4.28	~0	1.34	~0	3.31	19.69	0.18	8.41	0.21	991.53	4.77	64.22	10.87	~0	14.58	1416.61	6.08
		240	3.82	0.15	0.82	0.21	455.71	2.63	~0	2.57	~0	3.39	19.29	0.20	7.47	0.65	1116.15	5.43	73.60	27.04	2.12	11.56	1348.02	7.41
		300	4.86	0.14	1.09	0.32	468.88	1.70	~0	0.31	~0	4.51	19.54	0.15	11.07	2.63	1185.72	7.84	39.96	14.17	33.96	16.53	1391.16	3.76
		360	4.67	0.23	0.64	0.21	507.08	2.24	~0	1.43	~0	5.08	21.23	0.28	14.66	1.13	1344.91	8.12	10.32	21.71	46.48	6.93	1415.29	5.41

Table 15a: Concentration (ppb/ppm) results for polyminerallic standard minerals over the duration of 6 hour experiment runs. Elements presented represent leachate concentration at different time intervals. ~0 is given where negative values were returned from ICP-OES analysis, and <bdl is given where concentration values were below the detection limit for that element on the ICP-OES instrument. 5g of sample (2.5g of each mineral pair) was used in each experiment at 355 µm grainsize in 250 ml of artificial seawater.

Run	Sample	Time (Minutes)	Cd ppb	SD	Cr ppb	SD	Cu ppb	SD	Fe ppb	SD	Mn ppb	SD	Ni ppb	SD	Pb ppb	SD	Sb ppb	SD	Sn ppb	SD	Zn ppb	SD
B2 E12	Pyrite + Galena	5	~0	0.28	~0	0.17	~0	0.76	113.40	1.31	<bdl	0.17	1.88	1.58	218.26	3.21	~0	17.63	~0	19.58	~0	1.10
		15	~0	0.28	~0	0.34	<bdl	0.55	18.43	0.80	<bdl	0.19	~0	1.16	339.77	2.76	~0	17.42	~0	18.89	~0	1.17
		30	<bdl	0.30	~0	0.14	<bdl	0.61	7.70	1.26	<bdl	0.22	3.15	1.58	342.64	3.96	~0	17.65	~0	20.05	~0	1.15
		60	~0	0.30	~0	0.30	<bdl	0.72	~0	1.14	<bdl	0.18	~0	1.32	~0	0.88	~0	17.07	~0	18.47	~0	1.19
		120	<bdl	0.25	~0	0.23	<bdl	0.95	~0	0.59	1.31	0.15	~0	1.50	280.87	2.42	~0	17.41	~0	18.01	~0	1.27
		180	~0	0.26	~0	0.22	<bdl	0.57	~0	0.50	<bdl	0.24	~0	0.87	283.11	1.20	~0	17.59	~0	17.66	~0	1.21
		240	~0	0.28	~0	0.33	~0	0.62	~0	0.53	<bdl	0.13	~0	0.96	312.23	2.57	~0	17.34	~0	19.93	~0	1.12
		300	~0	0.35	~0	0.15	~0	0.69	~0	0.76	<bdl	0.20	~0	0.94	323.59	3.80	~0	22.24	~0	18.22	~0	1.14
		360	<bdl	0.27	~0	0.22	<bdl	0.57	~0	0.45	1.58	0.15	3.03	0.85	366.28	2.27	~0	18.96	~0	18.48	~0	1.35
B2 E13	Pyrite + Sphalerite-1	5	<bdl	0.33	~0	0.28	<bdl	0.70	219.71	1.58	<bdl	0.15	~0	1.51	~0	5.48	~0	18.26	~0	17.50	~0	1.13
		15	~0	0.25	~0	0.38	~0	0.57	54.83	0.97	<bdl	0.19	~0	1.80	26.05	2.82	~0	18.43	~0	17.63	~0	1.11
		30	~0	0.26	~0	0.19	<bdl	0.66	64.43	2.01	1.78	0.21	~0	0.95	17.55	2.43	~0	19.46	~0	19.13	~0	1.47
		60	~0	0.31	~0	0.30	<bdl	0.73	81.34	0.86	2.19	0.24	3.65	1.81	32.65	4.91	~0	18.69	~0	17.57	~0	1.11
		120	<bdl	0.25	~0	0.16	<bdl	0.57	118.59	1.66	2.33	0.22	~0	1.52	100.06	6.24	~0	16.88	~0	21.42	~0	1.17
		180	~0	0.36	~0	0.19	~0	0.80	116.58	1.02	2.71	0.13	~0	0.93	120.92	2.24	~0	19.22	~0	17.78	~0	1.17
		240	~0	0.26	~0	0.24	<bdl	0.63	180.81	1.43	3.10	0.13	~0	0.98	162.59	1.29	~0	18.08	~0	18.34	~0	1.32
		300	~0	0.30	~0	0.26	<bdl	0.56	295.60	3.80	3.16	0.18	~0	1.28	192.89	4.22	~0	18.28	~0	22.91	<bdl	1.40
		360	~0	0.27	~0	0.14	<bdl	0.60	267.92	4.22	3.48	0.14	~0	1.16	237.30	3.59	~0	19.30	~0	18.21	12.97	1.58
B2 E14	Pyrite + Chalcopyrite	5	<bdl	0.33	~0	0.27	137.86	0.71	~0	2.21	11.95	0.22	~0	1.07	168.17	3.03	~0	20.47	~0	17.80	665.93	1.64
		15	<bdl	0.30	~0	0.42	196.49	1.65	~0	2.46	12.91	0.23	~0	1.11	268.54	1.45	~0	19.21	~0	17.86	609.88	3.78
		30	<bdl	0.28	~0	0.20	464.48	2.35	~0	2.77	12.57	0.24	5.06	1.10	397.32	1.53	~0	17.32	~0	17.84	644.17	3.44
		60	<bdl	0.29	~0	0.36	755.29	1.33	~0	3.31	13.35	0.13	~0	1.14	591.36	0.84	~0	18.95	~0	18.12	903.51	3.17
		120	<bdl	0.32	~0	0.24	728.80	2.44	~0	4.21	13.98	0.16	~0	1.12	667.33	3.62	~0	18.12	~0	18.38	912.35	3.32
		180	<bdl	0.29	~0	0.18	698.58	2.13	~0	0.87	14.49	0.25	<bdl	1.11	717.20	6.33	~0	17.21	~0	17.73	915.91	5.33
		240	<bdl	0.30	~0	0.27	660.79	3.93	~0	0.77	13.36	0.20	3.17	1.65	687.07	5.91	~0	19.96	~0	17.80	892.23	6.24
		300	<bdl	0.31	~0	0.37	639.42	1.13	~0	2.02	13.61	0.21	~0	0.97	659.11	5.02	~0	17.32	~0	18.45	891.89	1.99
		360	<bdl	0.25	~0	0.37	477.68	1.59	~0	4.42	13.57	0.16	~0	1.75	679.52	5.70	~0	17.19	~0	20.85	632.58	2.33
B2 E15	Galena + Sphalerite-1	5	<bdl	0.09	~0	0.15	<bdl	0.70	~0	1.97	<bdl	0.21	~0	1.59	325.30	5.39	~0	18.91	~0	19.20	~0	1.29
		15	2.65	0.19	~0	0.36	~0	0.72	~0	2.72	<bdl	0.14	~0	1.57	384.25	1.10	~0	17.34	~0	21.15	~0	1.16
		30	2.75	0.10	~0	0.40	<bdl	1.15	~0	3.50	<bdl	0.15	~0	0.94	369.26	2.46	~0	26.31	~0	17.59	~0	1.13
		60	~0	0.25	~0	0.19	~0	0.71	~0	2.90	1.42	0.13	~0	1.47	356.48	3.62	~0	17.69	~0	22.19	<bdl	1.14
		120	~0	0.25	~0	0.29	<bdl	0.76	~0	1.53	<bdl	0.20	~0	1.18	298.72	2.81	~0	16.85	~0	17.92	13.55	1.48
		180	~0	0.30	~0	0.21	<bdl	0.73	~0	2.44	<bdl	0.21	~0	1.30	250.95	1.97	~0	18.22	~0	17.25	23.60	2.13
		240	~0	0.28	~0	0.16	<bdl	0.91	~0	1.40	<bdl	0.27	~0	0.87	272.18	4.61	~0	18.90	~0	18.00	52.61	2.07
		300	2.47	0.12	~0	0.25	<bdl	0.60	3.73	1.35	1.51	0.18	~0	1.56	282.73	1.15	~0	17.56	~0	18.16	59.51	1.38
		360	2.82	0.22	~0	0.17	~0	0.61	~0	1.99	2.07	0.15	~0	1.04	282.83	1.22	~0	18.74	~0	19.17	57.44	1.47
B2 E16	Galena + Chalcopyrite	5	<bdl	0.20	~0	0.21	938.72	4.80	35.36	2.43	7.68	0.21	~0	1.44	472.02	3.42	~0	17.13	~0	18.78	489.52	1.85
		15	<bdl	0.09	~0	0.33	744.92	3.09	27.13	1.24	8.22	0.26	~0	1.14	672.44	4.68	~0	20.53	~0	17.53	516.74	2.03
		30	2.39	0.09	~0	0.32	845.23	3.20	41.32	1.81	9.64	0.24	~0	0.96	829.17	2.96	~0	17.94	~0	17.70	530.55	1.63
		60	<bdl	0.12	~0	0.25	746.17	3.58	42.12	1.49	9.64	0.15	~0	1.33	929.61	3.66	~0	18.35	~0	19.77	552.02	2.09
		120	2.64	0.16	~0	0.23	635.86	3.99	52.30	2.47	8.47	0.17	~0	1.29	935.10	4.74	~0	21.54	~0	17.86	543.30	2.86
		180	2.32	0.20	~0	0.32	447.67	1.17	69.31	4.23	8.23	0.21	~0	1.29	777.94	4.73	~0	18.35	~0	18.50	509.38	0.77
		240	<bdl	0.14	~0	0.15	492.51	1.58	47.68	3.02	9.28	0.20	~0	1.30	746.14	3.02	~0	18.25	~0	18.91	585.43	1.47
		300	<bdl	0.10	~0	0.18	449.10	2.66	54.11	3.23	9.31	0.14	~0	1.26	662.14	4.30	~0	21.87	~0	19.36	569.22	4.11
		360	<bdl	0.16	~0	0.45	443.89	1.04	66.09	3.94	9.76	0.13	~0	0.99	589.65	2.18	~0	17.60	~0	17.72	584.32	0.63

Table 15b: Concentration (ppb/ppm) results for polymineralic standard minerals over the duration of 6 hour experiment runs. Elements presented represent leachate concentration at different time intervals. ~0 is given where negative values were returned from ICP-OES analysis, and <bdl is given where concentration values were below the detection limit for that element on the ICP-OES instrument. 5g of sample (2.5g of each mineral pair) was used in each experiment at 355 µm grainsize in 250 ml of artificial seawater. B2 E25 is a seawater blank experiment run with no sample.

Run	Sample	Time (Minutes)	Cd ppb	SD	Cr ppb	SD	Cu ppb	SD	Fe ppb	SD	Mn ppb	SD	Ni ppb	SD	Pb ppb	SD	Sb ppb	SD	Sn ppb	SD	Zn ppb	SD
B2 E17	Chalcopyrite + Sphalerite-1	5	2.43	0.13	~0	0.31	755.59	3.31	118.79	3.59	11.21	0.19	~0	1.03	171.64	2.27	~0	18.12	~0	21.68	686.63	2.90
		15	3.17	0.10	~0	0.19	1112.02	3.50	111.24	0.70	11.15	0.24	<bdl	1.33	252.71	6.15	~0	21.74	~0	17.88	784.49	2.45
		30	3.23	0.21	~0	0.17	858.75	1.20	113.88	2.88	12.31	0.15	<bdl	0.89	328.95	1.30	~0	17.59	~0	18.10	792.60	1.69
		60	3.50	0.20	~0	0.25	853.92	4.74	109.67	2.92	11.73	0.16	<bdl	1.62	448.04	4.39	~0	19.33	~0	17.44	807.51	3.71
		120	3.18	0.13	~0	0.49	702.05	1.54	115.36	1.53	12.69	0.15	~0	1.35	586.96	7.08	~0	17.28	~0	18.01	793.35	2.56
		180	3.03	0.14	~0	0.21	678.93	3.78	115.31	1.78	13.82	0.28	~0	0.85	704.88	2.29	~0	17.15	~0	19.35	810.69	4.07
		240	4.00	0.11	~0	0.18	660.28	2.49	117.51	2.87	13.64	0.27	~0	1.02	783.71	2.76	~0	17.83	~0	17.82	818.93	3.26
		300	3.15	0.10	~0	0.25	580.71	1.95	147.71	0.86	14.45	0.13	~0	1.16	856.81	2.21	~0	20.31	~0	17.59	810.83	3.36
		360	3.37	0.14	~0	0.34	670.71	3.51	134.91	2.43	14.80	0.14	<bdl	1.74	905.94	6.00	~0	17.53	~0	17.30	802.18	3.30
B2 E18	Galena	5	<bdl	0.28	4.52	0.23	7.60	0.58	850.52	9.89	2.16	0.17	~0	0.88	1003.11	10.66	~0	17.99	~0	17.98	84.06	1.12
		15	<bdl	0.25	2.50	0.25	<bdl	0.99	671.28	3.35	<bdl	0.25	~0	0.85	1240.91	5.33	~0	18.94	~0	17.60	30.62	1.57
		30	~0	0.29	10.34	0.16	<bdl	0.71	934.92	2.43	<bdl	0.13	<bdl	0.91	1302.55	5.95	~0	17.89	~0	17.57	62.93	1.12
		60	<bdl	0.27	16.22	0.20	7.35	0.59	1176.38	6.43	1.50	0.13	~0	1.14	1203.55	1.67	~0	17.45	~0	18.45	76.58	2.09
		120	<bdl	0.34	19.01	0.24	<bdl	0.80	1307.96	8.46	1.67	0.19	~0	1.56	999.40	5.65	~0	17.54	~0	17.87	84.69	1.65
		180	~0	0.27	18.77	0.21	<bdl	1.03	1366.20	13.41	2.68	0.24	~0	1.40	979.88	1.01	~0	17.58	~0	21.34	87.59	2.42
		240	<bdl	0.25	19.39	0.25	9.10	0.77	1481.27	6.07	4.23	0.20	~0	1.13	780.45	3.67	~0	17.92	~0	19.60	110.98	1.94
		300	<bdl	0.29	24.41	0.13	9.77	0.94	1770.38	6.74	4.18	0.20	~0	1.08	1111.75	5.04	~0	18.47	~0	18.42	117.02	2.00
		360	<bdl	0.30	30.82	0.33	9.82	0.71	2112.29	11.90	5.34	0.13	5.26	1.04	1178.06	8.72	~0	17.15	~0	19.78	216.00	2.19
B2 E19	Galena + Pyrite	5	<bdl	0.25	~0	0.18	<bdl	0.72	675.97	6.87	2.93	0.15	<bdl	0.98	556.14	1.56	~0	18.07	~0	17.88	118.30	1.66
		15	~0	0.31	~0	0.37	<bdl	0.86	355.17	0.86	3.80	0.26	~0	1.01	1146.70	5.68	~0	21.39	~0	19.92	~0	1.41
		30	<bdl	0.36	~0	0.35	<bdl	0.59	163.20	1.35	2.95	0.18	~0	1.05	1003.86	10.05	~0	19.05	~0	19.30	~0	1.35
		60	<bdl	0.25	~0	0.30	<bdl	0.91	99.35	0.89	2.33	0.14	~0	0.85	1125.97	2.61	~0	20.43	~0	21.26	~0	1.21
		120	<bdl	0.27	~0	0.33	<bdl	0.84	74.98	0.69	3.07	0.16	~0	2.70	1171.85	5.38	~0	17.96	~0	24.75	~0	1.89
		180	<bdl	0.25	~0	0.15	<bdl	0.79	30.19	0.48	3.59	0.16	13.53	2.71	1090.52	0.88	~0	21.10	~0	17.32	~0	1.65
		240	<bdl	0.27	~0	0.17	7.73	0.73	38.46	0.56	3.05	0.17	~0	0.97	1154.11	7.64	~0	18.51	~0	18.13	~0	1.37
		300	<bdl	0.25	~0	0.16	<bdl	0.85	~0	0.61	3.00	0.15	3.40	1.49	1216.75	4.83	~0	17.26	~0	18.24	~0	1.17
		360	<bdl	0.28	~0	0.29	<bdl	0.95	~0	0.57	3.20	0.20	<bdl	1.55	1105.88	6.54	~0	17.32	~0	18.05	~0	1.53
B2 E25	Seawater Blank	5	~0	0.26	~0	0.23	<bdl	0.89	~0	0.59	~0	0.21	~0	0.89	~0	2.16	~0	20.75	~0	18.39	~0	1.18
		15	~0	0.27	~0	0.43	~0	0.73	~0	0.48	~0	0.13	~0	0.91	~0	2.56	~0	19.29	~0	19.64	~0	1.31
		30	~0	0.29	~0	0.36	<bdl	1.06	~0	0.59	~0	0.16	~0	1.02	~0	3.42	~0	17.92	~0	19.67	~0	1.13
		60	~0	0.25	~0	0.24	<bdl	0.74	~0	0.55	~0	0.19	~0	0.88	~0	0.74	~0	17.32	~0	18.70	~0	1.43
		120	~0	0.25	~0	0.39	<bdl	0.73	~0	0.70	~0	0.21	<bdl	1.19	~0	3.63	~0	18.58	~0	20.57	~0	1.40
		180	~0	0.25	~0	0.26	<bdl	0.71	~0	0.58	~0	0.20	~0	0.87	~0	3.82	~0	20.17	~0	21.74	~0	1.11
		240	~0	0.29	~0	0.31	<bdl	0.93	~0	0.39	~0	0.17	~0	1.09	~0	0.71	~0	17.17	~0	19.45	~0	1.12
		300	~0	0.30	~0	0.16	~0	0.56	~0	0.65	~0	0.20	~0	0.85	<bdl	4.09	~0	17.08	~0	17.45	~0	1.15
		360	~0	0.29	~0	0.32	<bdl	0.59	~0	9.73	2.00	0.13	~0	1.05	~0	1.97	~0	18.38	~0	20.14	~0	1.16

Table 16a: Concentration (ppb/ppm) results for monomineralic natural sample minerals (LOG-11, LOG 13 & TP-2L) over the duration of 6 hour experiment runs. Elements presented represent leachate concentration at different time intervals. ~0 is given where negative values were returned from ICP-OES analysis, and <bdl is given where concentration values were below the detection limit for that element on the ICP-OES instrument. 5g of sample was used in each experiment at 500-1000µm and >1000 µm grainsize in 250 ml of artificial seawater.

Run	Sample	Grainsize (µm)	Time (Minutes)	Cd	SD	Cr	SD	Cu	SD	Fe	SD	Mg	SD	Mn	SD	Ni	SD	Pb	SD	Sb	SD	Sn	SD	Zn	SD
				ppb		ppb		ppm		ppm		ppm		ppb		ppb		ppb		ppb		ppb		ppm	
B2 E6	LOG 11 Chalcopyrite	>1000	5	12.02	0.14	1.02	0.13	21.24	0.05	0.11	0.00	~0	4.21	21.44	0.23	272.66	1.54	111.85	6.46	15.10	8.86	~0	6.60	9.90	0.15
			15	13.75	0.14	1.01	0.21	23.86	0.07	0.07	0.00	~0	5.30	27.54	0.25	377.51	3.73	54.81	7.38	1.22	10.65	~0	6.29	12.68	0.17
			30	13.87	0.15	0.00	0.26	25.28	0.05	0.07	0.00	~0	4.29	31.41	0.18	431.45	1.66	60.07	8.13	~0	7.28	~0	6.48	14.13	0.18
			60	15.00	0.23	2.02	0.28	23.26	0.03	0.08	0.00	~0	4.54	34.76	0.11	469.51	2.89	44.33	6.93	17.64	6.58	~0	8.22	15.23	0.16
			120	14.97	0.16	0.00	0.14	19.66	0.07	0.08	0.00	~0	4.99	34.11	0.26	476.02	2.63	57.49	6.72	11.55	11.63	~0	7.16	15.21	0.23
			180	15.77	0.23	1.15	0.32	18.70	0.01	0.08	0.00	~0	4.50	34.84	0.06	486.80	1.56	88.11	7.20	12.48	9.14	3.03	6.29	15.69	0.13
			240	15.91	0.24	2.20	0.17	18.59	0.04	0.13	0.00	~0	4.93	36.64	0.14	505.84	1.87	59.73	6.76	~0	6.57	4.39	7.10	16.12	0.14
			300	16.44	0.14	1.70	0.24	18.61	0.03	0.09	0.00	~0	5.20	36.08	0.09	503.65	3.13	37.47	7.31	~0	8.93	6.14	8.34	16.20	0.11
			360	15.98	0.20	1.24	0.15	18.84	0.02	0.17	0.00	~0	4.84	37.08	0.10	508.76	2.88	51.48	8.57	15.49	11.48	~0	6.95	16.42	0.11
B2 E7	LOG 13 Chalcopyrite	>1000	5	3.54	0.18	1.59	0.36	36.19	0.15	0.06	0.00	~0	5.03	16.20	0.15	54.77	2.12	~0	7.04	~0	5.58	~0	5.58	2.86	0.12
			15	4.76	0.27	0.74	0.17	36.10	0.07	0.06	0.00	~0	4.87	23.74	0.13	96.57	2.28	<bdl	8.98	34.64	7.14	~0	7.14	3.85	0.11
			30	4.81	0.16	1.91	0.21	50.81	0.27	0.10	0.00	~0	4.72	28.76	0.32	103.74	1.09	~0	6.87	~0	7.18	~0	7.18	4.72	0.16
			60	6.68	0.13	1.58	0.14	64.51	0.19	0.10	0.00	~0	4.41	33.92	0.33	129.25	1.74	<bdl	6.78	~0	8.92	~0	8.92	5.61	0.16
			120	7.06	0.17	0.52	0.23	79.11	0.21	0.15	0.00	~0	4.18	39.63	0.35	151.26	1.67	~0	6.79	<bdl	7.52	4.34	7.52	6.38	0.18
			180	8.11	0.21	1.85	0.44	86.03	0.35	0.17	0.00	~0	4.64	42.24	0.18	165.47	1.73	<bdl	6.66	~0	6.02	~0	6.02	6.85	0.14
			240	8.44	0.15	1.54	0.39	90.59	0.19	0.22	0.00	~0	5.50	44.02	0.10	172.60	1.48	15.03	6.58	37.35	6.89	4.09	6.89	7.12	0.13
			300	8.56	0.29	1.44	0.28	93.22	0.45	0.28	0.00	~0	5.79	44.39	0.21	172.29	2.24	<bdl	6.69	23.44	6.23	2.85	6.23	7.20	0.14
			360	9.09	0.24	~0	0.11	95.96	0.23	0.26	0.00	~0	3.72	46.20	0.31	178.43	1.35	~0	6.57	~0	6.14	~0	6.14	7.41	0.14
B2 E8	TP-2L Pyrite/Marcasite	>1000	5	5.08	0.19	1.68	0.36	112.45	0.17	25.30	0.05	~0	4.12	110.50	0.46	~0	1.24	16.78	8.16	~0	6.74	1103.29	7.54	3.32	0.13
			15	8.49	0.20	0.55	0.15	147.34	0.45	54.15	0.24	~0	4.05	139.62	0.33	2.17	1.19	34.01	7.42	~0	8.13	2362.93	7.56	4.36	0.10
			30	8.56	0.14	1.14	0.15	234.02	0.63	49.17	0.13	7.99	4.11	219.45	0.26	~0	1.07	~0	7.64	16.11	14.28	4604.91	6.63	6.89	0.11
			60	7.77	0.20	1.85	0.17	185.00	0.60	68.70	0.24	~0	4.10	178.36	0.13	2.09	1.37	60.13	7.31	~0	7.58	4357.33	8.30	5.61	0.10
			120	8.13	0.28	2.16	0.34	192.74	0.48	88.44	0.16	~0	5.10	192.50	0.10	4.43	1.03	~0	8.00	~0	8.39	5208.61	22.93	6.01	0.07
			180	8.63	0.18	1.81	0.14	200.27	0.72	95.73	0.38	3.70	5.17	204.84	0.79	5.56	1.76	76.76	8.33	11.61	7.13	5658.17	14.17	6.34	0.13
			240	9.20	0.15	1.79	0.13	201.54	0.55	101.44	0.17	11.02	4.60	211.43	0.48	<bdl	2.70	97.30	11.64	~0	12.79	5848.29	14.20	6.46	0.12
			300	10.34	0.32	1.45	0.21	202.25	0.63	104.74	0.14	2.44	4.15	212.09	0.35	~0	1.38	101.16	6.96	~0	18.41	5868.57	6.19	6.54	0.08
			360	9.82	0.16	1.57	0.10	206.70	0.80	107.05	0.43	~0	5.61	217.08	1.03	<bdl	1.03	~0	7.71	40.40	7.64	5959.50	22.88	6.67	0.16
B2 E21	LOG 11 Chalcopyrite	>500	5	11.33	0.13	1.94	0.27	20.31	0.04	0.07	0.00	9.44	3.90	33.91	0.12	223.43	1.28	<bdl	7.24	~0	11.30	~0	10.02	11.73	0.14
			15	12.36	0.23	0.42	0.09	15.28	0.03	0.02	0.00	~0	3.52	38.26	0.17	265.65	2.41	~0	6.55	~0	9.89	3.49	10.71	13.19	0.17
			30	12.47	0.13	~0	0.44	10.40	0.03	0.02	0.00	~0	5.44	39.70	0.22	276.70	1.72	<bdl	7.08	15.95	8.02	0.76	6.28	13.53	0.22
			60	13.54	0.27	1.03	0.41	<bdl	0.02	0.02	0.00	~0	4.19	40.34	0.36	282.90	2.33	~0	6.65	~0	12.83	~0	5.87	13.63	0.23
			120	13.56	0.16	~0	0.31	<bdl	0.01	0.02	0.00	~0	5.07	41.08	0.20	295.13	3.47	13.10	6.97	12.61	7.29	~0	9.91	13.60	0.18
			180	13.10	0.16	0.90	0.35	<bdl	0.01	0.06	0.00	~0	6.40	41.82	0.32	288.83	1.76	<bdl	7.17	16.60	9.60	~0	8.93	13.13	0.24
			240	13.29	0.25	0.86	0.11	<bdl	0.01	0.03	0.00	~0	6.93	42.10	0.19	294.97	1.41	25.24	9.11	~0	6.79	0.73	5.59	12.93	0.13
			300	13.33	0.19	1.46	0.19	<bdl	0.01	0.06	0.00	~0	5.30	42.78	0.23	296.16	2.55	<bdl	8.57	<bdl	6.79	~0	6.44	12.71	0.20
			360	13.05	0.17	1.16	0.29	<bdl	0.01	0.02	0.00	~0	4.13	42.85	0.20	303.43	1.60	~0	8.29	~0	11.83	~0	6.92	12.35	0.18

Table 16b: Concentration (ppb/ppm) results for monomineralic natural sample minerals (LOG-11, LOG 13 & TP-2L) over the duration of 6 hour experiment runs. Elements presented represent leachate concentration at different time intervals. ~0 is given where negative values were returned from ICP-OES analysis, and <bdl is given where concentration values were below the detection limit for that element on the ICP-OES instrument. 5g of sample was used in each experiment at 500-1000µm and >1000 µm grainsize in 250 ml of artificial seawater.

Run	Sample	Grainsize (µm)	Time (Minutes)	Cd	SD	Cr	SD	Cu	SD	Fe	SD	Mg	SD	Mn	SD	Ni	SD	Pb	SD	Sb	SD	Sn	SD	Zn	SD
				ppb		ppb		ppm		ppm		ppm		ppb		ppb		ppb		ppb		ppb		ppm	
B2 E22	LOG 13 Chalcopyrite	>500	5	4.86	0.14	0.74	0.17	56.14	0.07	0.02	0.00	~0	4.50	33.95	0.32	116.33	2.94	<bdl	6.64	25.35	10.44	~0	7.98	5.24	0.13
			15	5.72	0.13	1.19	0.35	67.70	0.07	0.02	0.00	~0	5.21	38.72	0.32	134.27	2.49	<bdl	7.56	~0	11.50	~0	10.35	5.99	0.15
			30	5.77	0.14	2.41	0.44	70.07	0.19	0.02	0.00	~0	7.58	40.64	0.28	140.41	1.37	26.62	6.51	19.20	8.41	~0	5.90	6.34	0.14
			60	5.86	0.16	0.38	0.17	70.68	0.38	0.03	0.00	~0	6.01	43.07	0.32	139.20	1.51	~0	6.52	~0	6.47	4.47	9.55	6.54	0.15
			120	6.24	0.23	1.48	0.21	70.00	0.32	0.12	0.02	~0	8.36	43.90	0.21	140.21	1.58	<bdl	7.77	~0	13.16	~0	7.22	6.58	0.14
			180	5.93	0.22	0.77	0.18	70.32	0.30	0.04	0.00	~0	8.84	44.63	0.18	146.99	1.89	<bdl	7.00	~0	11.48	~0	6.08	6.65	0.11
			240	6.27	0.13	1.19	0.50	70.63	0.12	0.07	0.00	~0	4.12	44.38	0.26	143.13	1.62	<bdl	6.96	<bdl	6.82	~0	6.27	6.62	0.14
			300	6.65	0.31	2.50	0.18	71.09	0.16	0.05	0.00	~0	5.13	45.48	0.14	144.67	2.64	<bdl	7.43	~0	13.44	3.17	5.86	6.77	0.11
			360	7.08	0.27	~0	0.21	71.30	0.11	0.06	0.00	~0	3.78	45.82	0.23	149.66	1.53	<bdl	7.54	11.00	6.85	~0	7.92	6.77	0.15
B2 E23	TP-2L Pyrite/Marcasite	>500	5	5.51	0.27	1.25	0.11	81.69	0.14	33.41	0.09	~0	3.99	168.68	0.69	~0	1.28	<bdl	6.53	~0	8.57	1436.76	9.36	3.38	0.10
			15	5.50	0.30	1.73	0.30	90.34	0.20	55.28	0.15	~0	3.97	193.19	0.74	~0	1.01	42.45	8.30	14.99	7.79	2465.17	14.15	3.78	0.11
			30	5.55	0.14	1.54	0.25	94.40	0.45	47.24	0.10	~0	4.57	206.67	1.08	<bdl	2.00	54.57	7.12	~0	8.31	2897.72	12.19	4.03	0.13
			60	6.66	0.24	1.12	0.19	96.84	0.21	50.56	0.22	~0	4.45	218.59	0.51	<bdl	1.00	31.39	6.69	31.62	8.91	3268.60	9.97	4.25	0.11
			120	6.45	0.23	1.46	0.21	99.17	0.41	53.45	0.18	~0	4.25	224.95	0.75	~0	1.28	57.51	9.08	~0	8.53	3331.16	8.86	4.37	0.11
			180	6.14	0.25	2.07	0.28	100.45	0.46	56.38	0.18	~0	4.78	225.60	0.74	~0	1.01	63.60	7.39	19.25	7.62	3307.60	17.44	4.43	0.13
			240	6.31	0.15	1.72	0.26	101.95	0.27	57.29	0.06	~0	3.87	227.95	0.71	~0	1.31	74.97	7.36	~0	9.16	3288.81	10.06	4.49	0.11
			300	6.49	0.20	1.68	0.43	102.79	0.37	60.81	0.10	~0	5.32	230.87	0.82	~0	1.26	75.66	6.88	34.22	10.36	3290.11	11.69	4.51	0.10
			360	6.41	0.14	0.78	0.38	103.19	0.42	59.11	0.12	~0	7.78	232.17	0.79	7.50	2.80	94.21	6.85	<bdl	8.19	3252.44	7.47	4.56	0.13

Table 17: Concentration (ppb/ppm) results for polymineralic natural sample minerals (LOG-11, LOG 13 & TP-2L) over the duration of 6 hour experiment runs. Elements presented represent leachate concentration at different time intervals. ~0 is given where negative values were returned from ICP-OES analysis, and <bdl is given where concentration values were below the detection limit for that element on the ICP-OES instrument. 5g of sample was used in each experiment at 500-1000µm and >1000 µm grainsize in 250 ml of artificial seawater.

Run	Sample	Grainsize (µm)	Time (Minutes)	Cd	SD	Cr	SD	Cu	SD	Fe	SD	Mn	SD	Ni	SD	Pb	SD	Sb	SD	Sn	SD	Zn	SD
				ppb		ppb		ppm		ppb		ppb		ppb		ppb		ppb		ppb		ppm	
B2 E20	LOG 11 Chalcopyrite + Secondary Cu Sulphides	>500	5	12.26	0.26	~0	0.41	3.21	0.14	~0	0.08	75.73	0.70	310.30	1.37	72.55	16.55	~0	7.56	~0	9.39	20.84	0.01
			15	15.96	0.36	~0	0.40	2.82	0.12	~0	0.00	90.04	0.35	361.78	1.58	~0	16.31	~0	6.85	~0	10.18	23.93	0.02
			30	18.16	0.13	~0	1.24	6.38	0.12	~0	0.00	96.87	0.81	384.26	2.19	~0	15.16	~0	6.92	~0	13.74	25.12	0.03
			60	18.04	0.21	~0	0.96	9.64	0.15	~0	0.64	99.19	1.12	391.37	3.24	39.53	13.09	~0	7.95	~0	4.39	25.16	0.03
			120	18.02	0.17	~0	0.98	10.94	0.21	~0	0.64	99.41	0.56	396.01	2.64	~0	18.40	~0	7.01	~0	9.38	24.96	0.15
			180	18.41	0.12	~0	1.33	10.03	0.23	~0	1.11	100.61	1.28	403.02	1.73	55.45	12.64	~0	13.78	~0	3.86	25.37	0.13
			240	18.33	0.24	~0	1.51	10.41	0.15	~0	0.98	100.36	0.99	415.15	5.26	71.67	12.90	~0	8.71	~0	11.89	25.47	0.16
			300	18.33	0.26	~0	1.12	10.76	0.23	~0	0.99	99.71	1.10	435.61	2.54	~0	12.67	~0	7.38	~0	4.56	26.55	0.03
			360	18.38	0.13	~0	0.70	11.83	0.17	~0	1.15	108.00	1.32	422.39	1.47	56.50	12.45	<bdl	8.17	~0	13.64	26.03	0.09
B2 E11	TP-2L Pyrite/Marcasite + Chalcopyrite	>1000	5	3.37	1.46	9.92	2.29	72.99	0.61	~0	0.62	106.18	2.33	5.27	5.42	20.99	25.47	~0	39.93	1.99	9.39	3.62	0.07
			15	6.52	1.34	22.16	2.98	101.19	0.75	167.37	0.94	127.16	1.46	14.43	4.67	<bdl	26.31	~0	68.63	1.38	10.39	4.33	0.05
			30	7.18	1.00	26.15	3.60	122.66	1.79	353.73	4.10	144.59	3.97	6.78	4.77	<bdl	20.30	~0	64.21	0.29	11.39	4.98	0.11
			60	7.91	1.83	29.57	2.08	138.42	1.14	1287.43	3.84	157.79	0.52	18.79	5.31	22.43	18.52	~0	52.26	9.94	12.39	5.44	0.01
			120	7.65	1.00	38.93	2.65	148.96	2.07	1164.41	4.59	166.82	3.57	15.24	9.87	<bdl	18.45	~0	41.83	13.76	13.39	5.76	0.08
			180	7.86	0.99	33.35	2.64	153.85	1.97	739.57	3.01	172.68	2.11	11.05	6.23	<bdl	26.43	~0	45.65	16.35	14.39	5.89	0.07
			240	9.46	1.40	40.27	2.24	158.37	3.36	394.68	1.07	180.54	3.85	10.89	4.74	23.28	19.30	~0	43.75	18.52	15.39	6.04	0.08
			300	8.32	1.50	35.06	2.34	158.55	1.46	625.16	4.63	179.73	2.06	12.65	5.60	15.49	20.58	~0	50.97	20.27	16.39	6.02	0.04
			360	7.38	1.00	39.18	2.14	160.01	2.00	695.72	1.77	183.49	2.71	8.39	6.26	15.90	27.14	~0	40.44	22.03	17.39	6.12	0.07
B2 E24	TP-2L Pyrite/Marcasite + Chalcopyrite	>500	5	7.18	0.95	13.80	2.53	76.46	1.18	40.08	0.01	157.44	1.14	10.86	5.15	<bdl	18.74	~0	60.90	~0	2.07	3.42	0.03
			15	6.86	1.53	15.47	2.96	83.80	0.45	51.30	0.01	180.01	2.63	9.87	5.04	<bdl	15.98	~0	41.86	~0	2.17	3.79	0.05
			30	6.06	1.66	15.99	2.29	84.94	1.57	45.50	0.01	185.95	2.51	9.28	4.54	~0	19.83	<bdl	47.15	~0	2.39	3.87	0.03
			60	7.29	1.22	16.66	1.99	81.18	1.54	33.80	0.01	190.51	3.57	7.61	5.11	14.15	18.88	~0	50.82	~0	1.01	3.89	0.06
			120	7.75	0.98	13.09	3.45	77.40	0.76	42.14	0.01	196.00	4.72	10.79	7.54	~0	21.28	~0	47.83	0.93	3.50	3.95	0.09
			180	7.51	1.41	16.19	2.97	75.61	0.53	50.25	0.01	195.78	1.19	14.87	5.79	~0	17.53	~0	45.68	~0	1.32	3.96	0.03
			240	3.35	1.02	0.80	2.09	23.60	0.69	6.66	0.01	9.65	0.32	<bdl	9.31	~0	39.15	747.82	50.42	34.39	16.71	54.18	33.72
			300	6.29	0.97	14.18	3.30	77.37	0.55	71.11	0.01	201.09	1.72	<bdl	5.20	<bdl	16.98	~0	46.84	~0	1.00	4.53	0.03
			360	6.56	1.36	15.43	2.52	78.68	0.64	49.07	0.01	204.85	1.30	<bdl	6.68	<bdl	16.55	~0	44.21	~0	1.67	4.57	0.03

Discussion for Sphalerite-1 (Sphalerite-mixed-sulphide)

Standard Pyrite & Sphalerite-mixed-sulphide

Polymineralic pyrite & sphalerite-mixed-sulphide leached higher concentrations of both Fe and Pb, than both monomineralic pyrite and sphalerite-mixed-sulphide, highlighted in Figure 42. While polymineralic pyrite & sphalerite-mixed-sulphide leached ~0 ppb of Cu and Sb, despite both monomineralic sphalerite-mixed-sulphide and pyrite producing low concentrations of both. The high concentrations of Fe and Pb present in the polymineralic experiment would suggest that some process is going on to exasperate leaching of these elements. Both monomineralic sphalerite-mixed-sulphide and pyrite leach Fe during their experiments, with sphalerite-mixed-sulphide leaching initially higher amounts. While only sphalerite-mixed-sulphide leaches clear amounts of Pb over the 6 hours, with pyrite initially leaching very low Pb concentrations before reducing to 0 ppb after the first hour. Therefore, this would imply that the increased concentrations of Fe and Pb in polymineralic pyrite & sphalerite-mixed-sulphide are the result of the sphalerite-mixed-sulphide in the mineral pair. It is possible that a galvanic cell between the two was set up, preferentially dissolving sphalerite-mixed-sulphide. This is consistent with rest potentials, as sphalerite has a lower rest potential than pyrite. Knight (2018) also investigates the galvanic potential between pyrite and sphalerite, finding that pyrite is galvanically protected when coupled with sphalerite, seeing Zn release from sphalerite occur at 300% faster rates. Fuchida *et al.* (2018) found similar trends again, with large amounts of Zn and Pb released from galvanic interactions occurring between pyrite and sphalerite (CKL-4 ore), when compared to CKL-1 ore experiments, a sphalerite & galena rich ore. Fuchida *et al.* (2018) also describes there being significant galvanic couples between pyrite and sphalerite in CKL-2 ore, but that the release of metal may have been suppressed by a silicate coating on the samples, reducing reactive surface areas. Abraitis *et al.* (2004) sees a similar relationship, with Zn leaching increasing by a factor of 18 when sphalerite was coupled with pyrite, but that pyrite dissolution was indicated alongside through a decrease in pH that was also observed in individual pyrite experiments. The trends across these studies gives confidence to that galvanic cells were likely present between pyrite and sphalerite-mixed-sulphide in this study, with sphalerite-mixed-sulphide being preferentially dissolved.

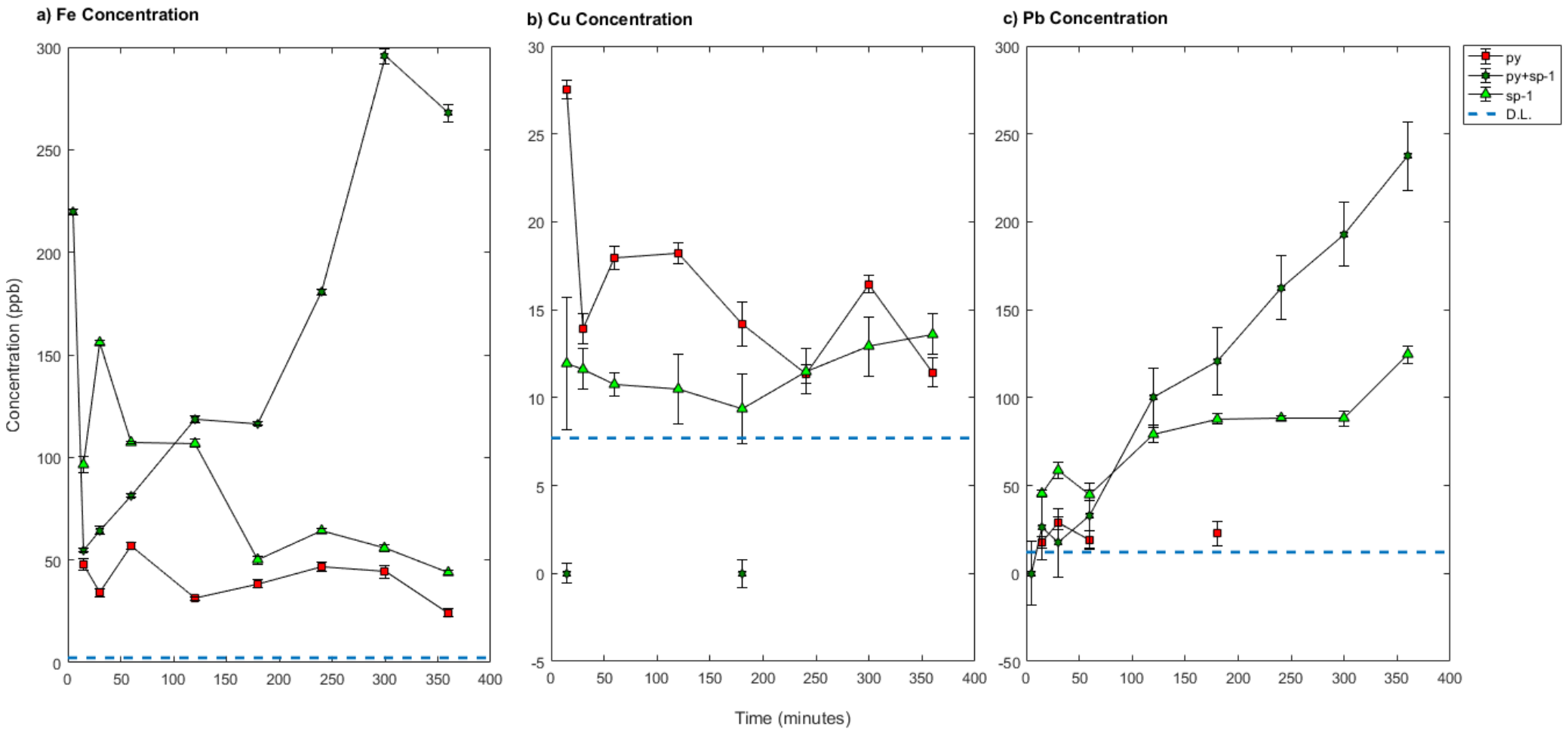

Figure 42: Polymineralic pyrite & sphalerite mixed sulphide experiment data presented against monomineralic pyrite and monomineralic sphalerite mixed sulphide, for Fe, Cu, Pb, Sb concentrations (ppb). Experiments run at room temperature, ~8.1 pH, 355 µm grainsize and 5g:250ml rock:fluid ratio. Legend abbreviations: py = pyrite, sp-1 = sphalerite mixed sulphide, D.L. = detection limits. **a)** Pyrite leaches the lowest concentration of Fe across the 6 hour run, with sphalerite mixed sulphide initially leaching the highest concentration, with ~220 ppb of Fe. Pyrite & sphalerite mixed sulphide initially starts with a similar Fe concentration to pyrite, before rapidly increasing in Fe over the duration of the experiment, reaching a high of ~300 ppb at 5 hours, before starting to decrease. **b)** While both monomineralic pyrite and sphalerite mixed sulphide leach moderate-low amounts of Cu, with pyrite leaching the most, pyrite & sphalerite mixed sulphide doesn't leach any Cu over the duration of the experiment. **c)** Pyrite leaches low-negligible amounts of Pb, with sphalerite mixed sulphide producing moderate concentrations of Pb that steadily increase over time. While pyrite & sphalerite mixed sulphide begins with the lowest concentration of Pb, before rapidly increasing over the duration of the experiment, overtaking sphalerite mixed sulphide at 2 hours, reaching a high of ~240 ppb. Data points are absent where values were bdl, instead it can be presumed that concentrations at missing time intervals lie between bdl dashed line and 0 ppb.

Standard Galena & Sphalerite-mixed-sulphide:

No clear relationships in polymineralic galena & sphalerite-mixed-sulphide were observed to indicate the presence of galvanic interactions, as seen in Figure 43. Polymineralic galena & sphalerite-mixed-sulphide leached negligible concentrations of Fe, despite monomineralic galena leaching low concentrations, and sphalerite-mixed-sulphide producing moderate quantities. The same trend is seen again for Cu concentrations, while Pb concentrations do not indicate any preferential leaching in the polymineralic experiment, with monomineralic galena leaching the highest Pb concentrations. No Zn is leached during either monomineralic experiments, but 2 hours in to the polymineralic experiment Zn concentration steadily increases. This increase in Zn and drop in Fe in polymineralic galena & sphalerite, are the only suggestions that one of the minerals in the couple is being preferentially dissolved. While some studies have looked at the effects of galena and sphalerite when both are coupled with pyrite, to find that pyrite is cathodically protected and galena and sphalerite are both preferentially leached, the relationship between galena and sphalerite is not so well studied (Cruz *et al.*, 2005; Heidel *et al*., 2013; Fuchida *et al.*, 2018). Fuchida *et al.* (2017) discusses leaching from a Zn-Pb rich ore (dominantly sphalerite & galena, although trace marcasite, chalcopyrite and pyrite also present), finding that both Pb and Zn are leached from this ore, predominantly Zn, with Fe being significantly low in the leachate. They propose that the high concentration of Zn and Pb in the leachate is due to ion exchange reactions occurring on the surface of the minerals (Fuchida *et al.*, 2017). Where metal ions adsorbed on mineral surfaces are replaced by hydrogen ions, releasing the metal ions into solution between the pHs of 4-7 (Fuchida *et al.*, 2017). As the pH of the polymineralic experiments of this study remained >7, it is unlikely that ion exchange is responsible for metal release, but is useful to keep in mind for experiments where pH decreased further. Based off the evidence discussed above it is possible that galvanic cells were set up between galena and sphalerite-mixed-sulphide in this study, resulting in a release of Zn and decrease in Fe. However, as there isn't any significant evidence that this is the case it remains speculation.

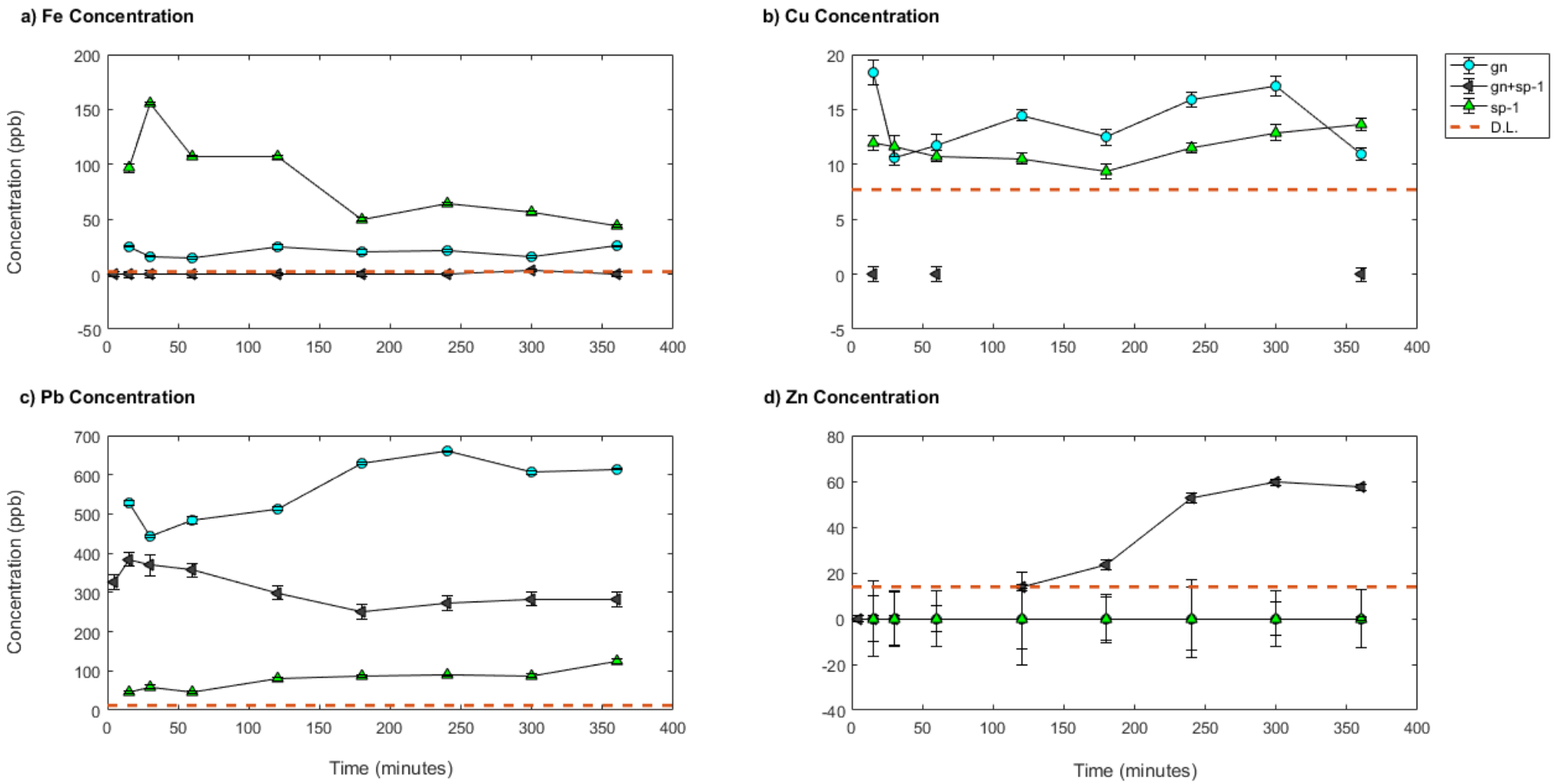

Figure 43: Polymineralic galena & sphalerite mixed sulphide experiment data presented against monomineralic galena and monomineralic sphalerite mixed sulphide, for Fe, Cu, Pb, Zn concentrations (ppb). Experiments run at room temperature, ~8.1 pH, 355 µm grainsize and 5g:250ml rock:fluid ratio. Legend abbreviations: gn = galena, sp-1 = sphalerite, D.L. = detection limits. **a)** Sphalerite mixed sulphide contains the highest concentrations of Fe, with a peak of ~155 ppb at 30 minutes. Galena leaches consistently low concentrations of Fe throughout the experiment, while galena & sphalerite mixed sulphide has negligible-0 ppb of Fe. **b)** While galena has the highest concentration of Cu, sphalerite-1 leaches similar concentrations throughout. Galena & sphalerite mixed sulphide in comparison leaches 0 ppb or concentrations below detection limits. **c)** Galena consistently leaches the highest concentrations of Pb, with a peak at 4 hours of ~650 ppb. Sphalerite leaches low-moderate concentrations <100 ppb of Pb, steadily increasing over the 6 hours. Galena & sphalerite mixed sulphide has an initial increase in Pb reaching ~400 ppb Pb, before decreasing again and plateauing at around 3 hours, it persistently leaches lower concentrations than monomineralic galena. **d)** Both galena and sphalerite mixed sulphide leach 0 ppb Zn throughout the duration of each experiment. Galena & sphalerite mixed sulphide however, sees an increase in Zn from 0 after 2 hours, reaching a peak of ~60 ppb at 5 hours before it begins to level off. Data points are absent where values were bdl, instead it can be presumed that concentrations at missing time intervals lie between bdl dashed line and 0 ppb.

Standard Sphalerite-mixed-sulphide & Chalcopyrite-sulphide-mix

Similarly to the previous, polymineralic sphalerite-mixed-sulphide and chalcopyrite-sulphide-mix has leachate concentrations which suggest both the preferential dissolution of sphalerite-mixed-sulphide and the continued dissolution of chalcopyrite-sulphide-mix, refer to Figure 44. Polymineralic sphalerite-mixed-sulphide and chalcopyrite-sulphide-mix has the highest sustained Fe concentrations, while monomineralic sphalerite-mixed-sulphide after having initially the highest Fe decreases after 30 minutes, while chalcopyrite-sulphide-mix has ~0 ppb. This may suggest the presence of galvanic coupling, with sphalerite-mixed-sulphide anodically dissolving, accounting for the high Fe leachate. Monomineralic sphalerite-mixed-sulphide produces negligible amounts of Cu, while both monomineralic chalcopyrite-sulphide-mix and polymineralic sphalerite-mixed-sulphide & chalcopyrite-sulphide-mix leach similar concentrations of Cu throughout their respective experiments. As monomineralic sphalerite-mixed-sulphide concentrations are so low, it's more likely that chalcopyrite-sulphide-mix is dissolving and releasing Cu within the polymineralic experiment. Zn leachate concentrations doesn't suggest that any galvanic interactions are occurring, with polymineralic sphalerite-mixed-sulphide & chalcopyrite-sulphide-mix leaching Zn concentrations roughly half of that in monomineralic chalcopyrite-sulphide-mix, whilst monomineralic sphalerite-mixed-sulphide doesn't produce any Zn leachate. Knight *et al.* (2018) also conducted polymineralic experiments with sphalerite and chalcopyrite, where sphalerite was expected to be preferentially dissolved due to its lower rest potential than chalcopyrite, this was not observed. Similarly to the polymineralic experiment of this study, Knight *et al.* (2018) did not observe any clear evidence for galvanic reactions, although initial faster reaction rates in the polymineralic experiment were observed compared to the monomineralic counterparts. While there is no definite proof of galvanic interactions between sphalerite-mixed-sulphide & chalcopyrite, Fe concentrations may suggest that sphalerite-1 is being anodically dissolved when coupled with chalcopyrite-sulphide-mix, but that chalcopyrite-sulphide-mix dissolution does not stop in this pairing.

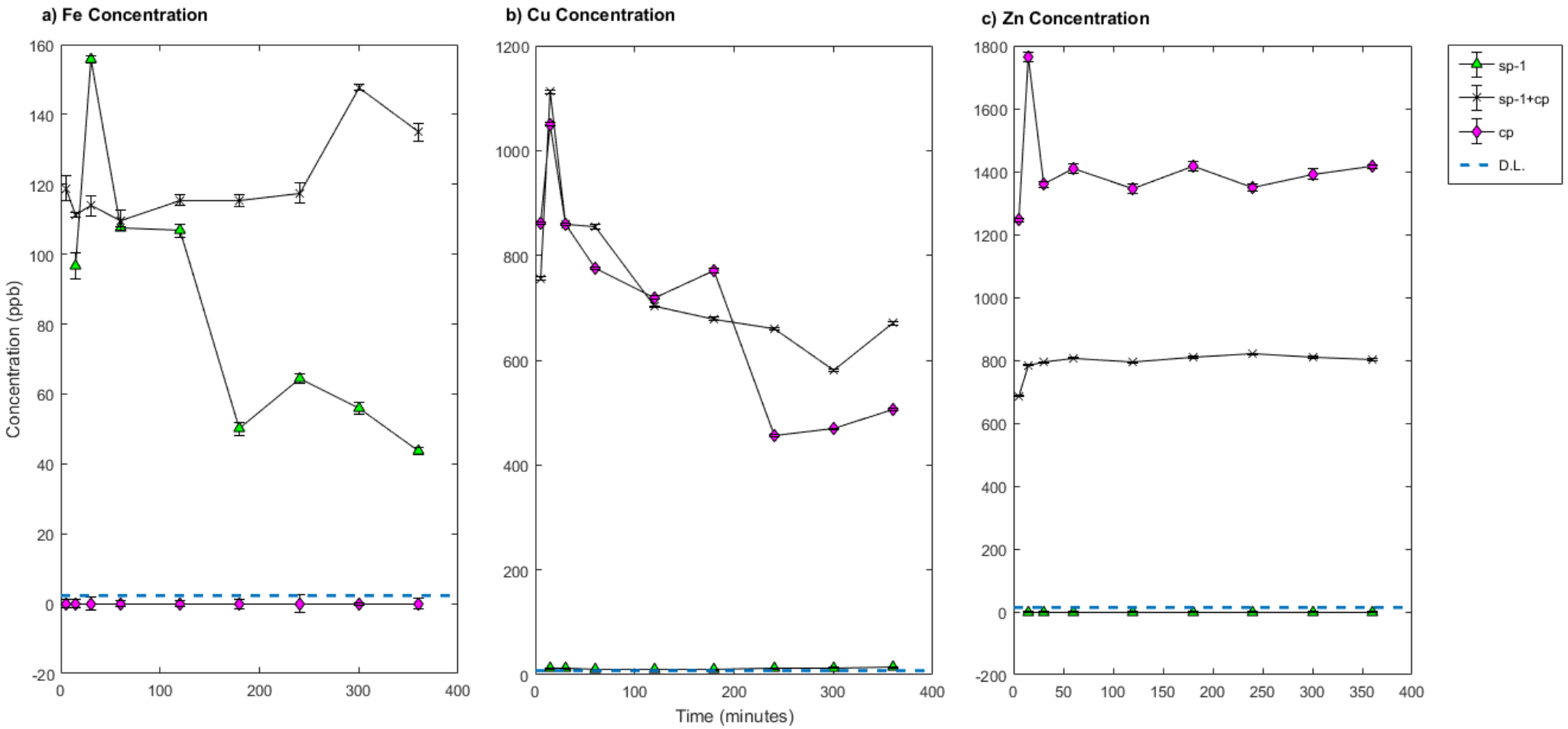

Figure 44: Polymineralic sphalerite mixed sulphide & chalcopyrite experiment data presented against monomineralic chalcopyrite sulphide mix and monomineralic sphalerite mixed sulphide, for Fe, Cu, Pb, Zn concentrations (ppb). Experiments run at room temperature, ~8.1 pH, 355 µm grainsize and 5g:250ml rock:fluid ratio. Legend abbreviations: sp-1 = sphalerite mixed sulphide, cp = chalcopyrite sulphide mix, D.L. = detection limits. **a)** Chalcopyrite sulphide mix displays no Fe leaching across the 6 hours, while sphalerite mixed sulphide leaches moderate concentrations of Fe peaking at ~155 ppb at 30 minutes before steadily decreasing for the remainder of the experiment. Sphalerite mixed sulphide & chalcopyrite sulphide mix, although starting at lower concentrations to sphalerite mixed sulphide, remains at moderate concentrations, before increasing after 5 hours to ~150 ppb. **b)** While no Cu is observed with sphalerite mixed sulphide, chalcopyrite sulphide mix and sphalerite mixed sulphide & chalcopyrite sulphide mix have very similar Cu concentrations during the first 3 hours of each experiment, peaking at ~1130 ppb. Before both decrease in concentration, with chalcopyrite sulphide mix decreasing to lower levels. **c)** The highest Zn concentration is observed in chalcopyrite sulphide mix, peaking at ~1750 ppb Cu, with sphalerite mixed sulphide & chalcopyrite sulphide mix leaching persistently lower concentrations of Cu, just over half of chalcopyrite sulphide mix's. No Zn is observed in sphalerite mixed sulphide. Data points are absent where values were bdl, instead it can be presumed that concentrations at missing time intervals lie between bdl dashed line and 0 ppb.